SOIL RESPONSE FROM DYNAMIC ANALYSIS AND MEASUREMENTS ON PILES

by

Frank Rausche

Submitted in partial fulfillment of the requirements
for the Degree of Doctor of Philosophy

DIVISION OF SOLID MECHANICS, STRUCTURES
AND MECHANICAL DESIGN

June 1970

SOIL RESPONSE FROM DYNAMIC ANALYSIS AND MEASUREMENTS ON PILES

by Frank Rausche

ABSTRACT

An automated prediction scheme is presented which uses both measured top force and acceleration as an input and computes the soil resistance forces acting on the pile during driving. The distribution of these resistance forces acting along the pile is also determined. Shear and dynamic resistance forces are distinguished such that a prediction of total static bearing capacity is possible. Using the shear force prediction a static load versus penetration curve is computed for comparison with the result from a corresponding field static load test.

The method of analysis uses the traveling wave solution of the one-dimensional, linear wave equation. As a means of calculating the dynamic response a lumped mass pile model is used and solved by the Newmark β-method.

Using stress wave theory two simplified methods are developed for predicting static bearing capacity from acceleration and force measurements. These methods can be used during field operations for construction control when incorporated in a special purpose computer. The automated prediction scheme and simplified methods are applied to 24 different sets of data from full scale piles. The piles were all of 12 inches diameter steel pipe with lengths ranging from 33 to 83 feet. Also, 24 sets of data from reduced

scale piles are analyzed by the simplified methods. All predictions are compared with results from static load tests. Correlation is very good for piles driven into non-cohesive soils. For cohesive soils better agreement with static load measurements are obtained than from existing methods.

As a check on the assumed soil response to both pile displacement and velocity results from measurements taken at the pile tip are investigated and discussed. Further, an approach to pile and hammer design is described using the results of stress wave theory.

ACKNOWLEDGEMENTS

The author wishes to express his appreciation and gratitude to:

Associate Professor Fred Moses, the author's thesis advisor, for contributing with ideas and stimulating discussions to this work.

Professor G.G. Goble, the author's co-advisor, for his guidance in both academic and experimental matters.

John J. Tomko, the author's friend, for his valuable suggestions to both theory and experiment.

The Ohio Department of Highways and the Bureau of Public Roads for the sponsorship of the research project. In particular, thanks to Mssrs. C.R. Hanes, R.M. Dowalter and R.A. Grover all of the Ohio Department of Highways for their assistance.

All the students of Case Western Reserve University who helped to obtain the data and to digitize and process dynamic records.

Miss Carol Green for typing this manuscript skillfully and patiently.

Yolita, the author's wife, for carefully drawing many of the figures and for helping with her thoughtfulness and encouragement.

LIST OF SYMBOLS

Symbol	Meaning
A	Pile cross sectional Area
a(t)	Acceleration
a_i	Least square coefficient
b	Intercept
C	Shear resistance matrix
CR_i	Difference criterion
c	Speed of wave propagation
$c_{i,j}$	Element of shear resistance matrix
D(t)	Damping force
d_i	Damping coefficient
E	Young's Modulus, damping matrix
E_i	Error number
$e_{i,j}$	Element of damping matrix
F(t)	Force
f	Wave traveling in negativ x-direction, Frequency
f_j	Force on top element
g	Gravitational acceleration, wave traveling in positive x-direction
H(t-x)	Heaviside Step Function
k	Stiffness of pile element
k_i, $k_{s,i}$	Soil stiffness at $x=x_i$
L	Pile length

LIST OF SYMBOLS (cont'd)

Symbol	Meaning
M	Mass of pile or pile element
m	Slope of straight line
n	Number of elements
P	Pile top force (ststic)
p_i	Soil parameter at i-th element
q	quake
$R_i(t)$	Resistance force at $x=x_i$
R_i	Coefficient of Pncelet's resistance law
r	Ratio of Masses, time interval counter
$r_{i,j}$	Resistance force at i-th element and $t=t_j$
S(t)	Shear resistance force
$S_{i,o}$	Ultimate shear resistance force at $x=x_i$
t	Time variable
u(t), u(x,t)	Pile particle displacement
$u_{i,j}$	Displacement of i-th element at time $t=t_j$
$\dot{u}_{i,j}$, $\ddot{u}_{i,j}$	Velocity, acceleration of i-th element at time $t=t_j$
v(t)	Pile particle velocity
W	Weight of pile
w(t)	Weighting function
x	Length variable
α	Damping coefficient
β	Newmark's parameter

LIST OF SYMBOLS (cont'd)

Symbol	Meaning
$\Delta(t)$	Measured Delta curve
$\Delta_e(t)$	Error Delta curve
$\Delta_i(t)$	Resistance Delta curve
$\Delta_{mod}(t)$	Modified Delta curve
$\Delta_{red}(t)$	Reduced Delta curve
ΔD	Difference in damping force
ΔT	Time difference
Δt	Time increment
Δv	Velocity Difference
$\delta(t-x)$	Dirac Delta function
ε	Small number
$\varepsilon(x,t)$	Strain in pile
ϕ	Ratio of critical time to time increment
η,μ	Independent variables
ρ	Pile mass density
σ	Standard deviation
$\sigma(t)$	Stress in pile

Subscripts

Symbol	Meaning
A	Applied at pile top
a	Arriving

LIST OF SYMBOLS (cont'd)

Subscripts

Symbol	Meaning
d	At maximum dynamic deflection, Due to damping
down	In downwards traveling wave
f	Due to f-wave, final, free, fixed.
g	Due to g-wave
i,h	At $x = x_i$, x_h
j	At time t_j
m	At maximum velocity
n	At pile toe
o	At time of zero velocity, at ultimate
r	Due to resistance force
s	Due to shear force
top	Resulting at pile top
up	In upwards traveling wave

Superscripts

Symbol	Meaning
a	From analysis
f	Final result
n	New value
*	Fixed value

LIST OF TABLES

LIST OF FIGURES

LIST OF FIGURES (Continued)

LIST OF FIGURES (Continued)

LIST OF FIGURES (Continued)

LIST OF FIGURES (Continued)

LIST OF FIGURES (Continued)

LIST OF FIGURES (Continued)

TABLE OF CONTENTS

TABLE OF CONTENTS (Continued)

TABLE OF CONTENTS (Continued)

CHAPTER I

Introduction

With the recent development of electronic measuring devices for short time phenomena it becomes feasible to record force and acceleration at the top of a pile during the impact driving operation. Measurements of this kind provide information about pile and soil behavior under hammer impact. A method to exploit these record properties is presented in this thesis. The method yields information about magnitude and locations of external soil forces resisting the motion of the pile.

The prediction of such soil forces during pile driving is complex due to the variation of soil properties over time and space. Investigations are difficult because only the pile top is easily accessible for measurements and the usual static and dynamic measurements do not provide enough information about external forces acting on the pile below grade. Modern measuring techniques, however, are shown herein to yield the data necessary to predict forces below grade from information obtained at the pile top.

1. Problem Description and Related Investigations

A foundation usually is sensitive to deformations occurring during and after the loading process. It is, therefore, not only necessary to obtain knowledge about the bearing capacity of the pile but also to predict the deformations associated with the load. The static load test of a pile after driving provides the most

reliable source of information. However, due to often rapidly changing soil properties within relatively short distances many static load tests have to be performed for different piles, a procedure that is not economical.

Good analytical results, i.e., a prediction of the deformations of a pile under load, can be obtained from so-called static formulae if extended information of soil properties is given in the neighborhood of all piles analyzed. Poulos and Mattes (1), (2) presented a realistic analysis by considering both pile and soil deformations. More work done in the area can be found in LaPay (3) and Coyle and Sulaiman (4). Besides the fact that it is not possible to determine soil properties at a sufficiently large number of locations errors will also arise from applying laboratory measured soil properties which are, in general, different from those encountered around the pile after driving.

To avoid the difficulties encountered in the use of the above static formulae, a commonly employed method relates bearing capacity of the pile to the rated hammer energy and to the pile permanent set under a blow. Thus, each pile can be tested individually during driving. Energy or dynamic formulae have been developed which will provide good predictions on the static bearing capacity of the pile, provided, hammer energy and certain soil properties are sufficiently well known. The Michigan Highway Commission (5) performed extensive experimental research in order to answer questions about hammer output cushion properties and the energy delivered to the pile, but the

question still remains as to what energy a hammer actually delivers to the pile since hammer and cushion are subject to wear. Discussions of dynamic formulae can be found in LaPay (3).

Hammer and soil properties alone are not sufficient to draw conclusions regarding the ultimate bearing capacity of a pile. Other important factors are the hammer impact velocity, and the flexibility of cushion and pile. This means that pile dynamics or wave theory have to be applied as a means of analysis. First attempts were made by Isaacs (6) and Fox (7) using the traveling wave solution which St. Venant had introduced. (A summary of St. Venant's method is given in (8)). The object of all these studies was to find the resistance force acting on a pile during driving when hammer energy and pile permanent set were given. Assumptions regarding resistance force distribution and its variation with time limited the applicability and accuracy of these methods.

With the introduction of high speed computers a numerical integration of the wave equation became possible. Smith (9) developed such a solution commonly referred to as "Pile Driving Analysis by the Wave Equation". A major advantage of using such a numerical method is the unlimited choice of a soil resistance law. This method of analysis was also used by Samson, Hirsch and Lowery (10) and Forehand and Reese (11) for parameter studies. Basically, these investigations "by the wave equation" used the approach introduced by Isaacs (6) and Fox (7), wherein namely, hammer energy and pile set were employed for predicting pile bearing

capacity.

In order to overcome one of the major sources of error in both dynamic formulae and wave equation methods, Goble, Scanlan and Tomko (12) proposed to take acceleration and force measurements at the pile top during driving. To compute the static bearing capacity of the pile they used a simplified model. It was assumed that the soil resistance R(t), acting along the pile could be approximated by Poncelet's Law:

$$R(t) = \sum_{i=0}^{\infty} R_i (v(t))^i \qquad (1.1)$$

where R_i are constant and v(t) is the velocity of the pile which is thought to act as a rigid body. Applying Newton's Second Law at the time t_o, the time when the velocity becomes zero, leads to

$$R_o = F(t_o) - Ma(t_o) \qquad (1.2)$$

where R_o is interpreted as being the static bearing capacity, $F(t_o)$ is the force and $a(t_o)$ is the acceleration, both measured at the pile top. M is the total mass of the pile. This prediction scheme, referred to as the Phase I method, is simple enough to be programmed in a special purpose field computer to display the static bearing capacity, R_o, under every blow in the field.

The results obtained from Equation (1.2) were compared with a static load test which was performed within a short time before or after the dynamic measurement was taken. Soils change their physical properties in response to driving operation. It was, therefore, proposed to delay the load test for a waiting period

after driving had been completed and then only to restrike the pile and take dynamic measurement.

Tomko (13) performed a study on how to obtain pile static bearing capacity by using the measured force as an analysis input and compare the output, i.e., top acceleration, with the measured one. As a mathematical model a continuous pile was used. A few parameters describing the soil resistance were adjusted to yield a match between theoretical and measured acceleration. The cases treated in this study showed encouraging results. Also an improvement of the Phase I method was recommended, by time averaging the second term in Equation (1.2) over some time before the time of zero velocity. A disadvantage, however, of the continuous pile model used by Tomko was that only simple soil resistance laws could be utilized in the analysis.

A large portion of Tomko's work was concerned with data acquisition on both full and reduced scale piles. Since his work is essential to the study reported in this paper a short review will be given.

His experiments on reduced scale piles involved static load tests and dynamic measurements under different soil conditions and with varying pile length. Two different static load tests were reported, a Constant Rate of Penetration (C.R.P.) and a Maintained Load (M.L.) test. The C.R.P. test yielded good results with significant time savings. Full scale pile tests were performed on actual construction sites. One test was reported which had

been conducted on a special test pile (referred to as F-30, F-50, F-60). Here additional instrumentation was used also for obtaining force records on locations other than the pile top.

Most of the piles tested were in coarse grained soils and agreement was good when using either the matching technique or the Phase II method. Results from reduced scale piles driven into cohesive soils, however, showed very poor correlation. The question as to the effects which soil properties and pile length had on the rigid body simplified models could not be answered.

2. Preliminary Experimental Work

Experimental data are the basis of the method discussed in this paper. Since much of the experimental work was performed in a manner as reported by Tomko (13) only a few special results are discussed in this Chapter.

A complete set of data consists of force and acceleration measured at the pile top. Analytical results from such dynamic data have to be compared with a static load test. The load test has to be performed within a short time of the dynamic measurements. Complete data sets were obtained from a number of actual construction piles and from reduced scale piles. The recording and signal conditioning equipment was essentially the same as in (13) also the types of force and acceleration transducers were the same as reported. Modifications had to be applied where special measurements were undertaken. Two full scale pile tests deserve special comment. In the first a site in Toledo was selected because of its clayey

soil conditions (see Table (1.1) for the soil profile). It was decided to drive two test piles one of 50 feet length (To-50) and one of 60 feet length (To-60). Further physical characteristics are given in Table (3.1). Both piles were instrumented along their length with strain gages. Two complete sets of data were obtained from each pile by testing the piles immediately after driving and after a waiting period. Both C.R.P. and M.L. tests were performed and their outcomes compared. Particularly interesting findings will be discussed using To-60 as an example.

(i) Dynamic strain records were obtained from various locations along the pile. As an illustration of this result see Figure (1.1) which is a three-dimensional plot of force in the pile as a function of time and pile length. Such results give further information for correlation with analytical predictions.

(ii) The static load test showed a very low ultimate bearing capacity (43 kip) immediately after driving but a strength increase of 100 percent during the waiting period. This change is due to high pore water pressures which build up during driving and which are only slowly released during the waiting period. In such soils highly viscous driving resistance forces can be expected.

(iii) The main static resistance was encountered at the pile skin. Figure (1.2) shows the load versus penetration curves of four locations along the pile. Also the forces in the pile are plotted for different penetrations.

The second special full scale pile test was conducted in

Rittman, Ohio. Table (1.2) shows the soil profile encountered at the site. Organic clays and silts of about 55 feet depth overlie a hard layer of gravel and sand. Hence, it was decided to drive a pile first to a depth of 50 feet to obtain two complete sets of data and then to extend the pile by driving it until the hard layer was reached. Thereafter, two more complete sets of data were to be obtained. Results of these tests are discussed in more detail later in this paper. However, two plots of the forces in the pile (before and after the pile hit the hard soil layer) are presented in Figure (1.3 and 4). Forces in the pile were again plotted as a function of time and pile length. A special feature of these tests in Rittman was an accelerometer placed in the pile toe. Physical pile characteristics are given in Table (3.1); the pile is referred to, either as Ri-50 or Ri-60, according to the length at which it was tested.

Further work was performed on reduced scale piles such as described by Tomko (13). Additional strain records from several locations and an acceleration record from the pile tip were obtained on piles driven into coarse sand (Table 1.3). It was observed that a shortcoming of tests on short piles was the relatively slow rise time of the pile top force at impact. Thus, cushioning properties were changed in order to make the reduced scale piles a better model of full scale piles.

3. General Description of Analytical Work

The force and acceleration of the pile top recorded under a hammer blow establish redundant information. In the usual dynamic problem only one of these variables is prescribed together with the external forces acting along the sides or at the other end of the pile. Pile driving, however, complicates the problem in that information can only be obtained at the pile top while the soil forces acting along the pile are unknown. Thus, the usual analysis process cannot be applied. Generally, the top force and acceleration of the pile are dependent on the external forces so that an inverse process of the usual dynamic analysis will yield information about these unknowns.

In this paper a method is presented which predicts the soil resistance force distribution along the pile by using both as input the acceleration and the force measured at the top of the pile. As an introduction to the analysis the traveling wave solution is applied. A detailed investigation of wave propagation in a pile under impact is discussed in Chapter II, wherein the development of an external force prediction scheme is also reported. It was found that the Phase I and II simplified methods derived from a rigid pile model can be studied on the basis of wave considerations and that an insight in their actual meaning can be obtained. This, together with proposals for improvement (Phase II-A) and the development of a new - Phase III - simplified prediction scheme, is presented at the end of Chapter II.

Chapter III summarizes the analytical results from both the external force prediction scheme and from the simplified methods. Special consideration will be devoted to the predicted force distribution along the pile and to comparisons of predicted load vs. penetration curve compared with that measured during a field static load test.

In Chapter IV limitations and shortcomings of the proposed method are critically investigated. Chapter V, finally, summarizes the present work and includes suggestions about possible extensions of the method and further necessary research.

Appendices contain the mathematical derivations along with additional material related to Chapter II. Appendix A1 deals with a lumped mass analysis based on Smith (9) and Newmark (14). This lumped mass analysis is a convenient tool for checking the validity of dynamic predictions from wave theory. Appendix A2 presents the static analysis used for computing a theoretical load test by use of the predicted external resistance forces. In Appendix A3 the traveling wave analysis is developed as discussed in Chapter II. Appendix B is a summary of studies required to interpret properly force and acceleration records. Appendix C discusses validity and limitations of the soil model used in the present prediction method. Simplified computation schemes which can be used in a special purpose computer are given in Appendix D. Finally, the computer program used for the prediction of the external forces along the pile is described in Appendix E by means of a block diagram.

CHAPTER II

Analysis by the Traveling Wave Solution

1. Introduction

Already in the nineteenth century a stress solution for a uniform and elastic rod struck by a mass had been derived by Saint-Venant, see Reference (8). The method of analysis used the solution of the one-dimensional, linear and homogeneous wave equation Superposition of suitable waves yielded results for rods with either prescribed end forces or displacements. Donnell (15) also used this method and extended it for investigating various problems of one-dimensional wave propagation including conical rods, nonlinear material properties and problems where impact forces were applied on locations other than the ends of the rod. The results of these investigations were applicable to problems where the external forces along the bar were known and stresses or velocities of rod particles were to be predicted.

Another approach of studying wave propagation in rods became a convenient method with the use of high speed digital computers. This approach which breaks up the rod into several elements - lumped masses - was introduced for pile driving analysis by Smith (9) and applied by Samson, et al. (10) and LaPay (3) among others. In these studies it was attempted to find out about certain pile, hammer and soil characteristics by using pile set and hammer energy as an input. In the present approach for using acceleration and force records measured at the pile top both methods, wave and lumped

mass analysis, will be used for devising a scheme in order to find out about the external forces acting on the pile during the motion of the pile. In this chapter relations will first be discussed which exist between stresses and particle velocities in a stress wave traveling through a rod with various boundary conditions. Then conclusions will be drawn on the effects which soil resistance forces have on the hammer applied stress waves. For this a spring-damper soil model will be used. It then will be attempted to describe a prediction scheme for determining the magnitude of these soil passive forces which are initiated by the motion of the pile under the hammer blow. This method will make use of the two records measured at the pile top: force and acceleration. The acceleration will be applied as an input, i.e. as a sensor wave. Soil reaction forces initiated by this sensor wave also produce stress waves which can be separated from the hammer input by means of the measured force. Knowledge of the mechanics of wave propagation will now give a tool for locating the source of these soil resistance forces and computing their magnitudes.

Finally, again using wave considerations existing approximation schemes for predicting static bearing capacity will be critically investigated and a new method will be developed.

2. Fundamentals of Wave Propagation in a Uniform and Elastic Rod

A continuous rod under impact having non-zero force or displacement end conditions and external forces acting along its length

can best be analyzed by use of a lumped mass system. In such an analysis the rod is divided into connected elements whose elastic and inertial properties are represented by springs and lumped masses, respectively. Since it is necessary herein to check predictions from wave theory the lumped mass analysis is a necessary and convenient tool. It is described in detail in Appendix A1. A few remarks are appropriate.

The method as developed by Smith (9) uses a so-called Euler integration scheme. This method computes the displacements of all rod elements at a certain time by means of linear extrapolation from values computed for an earlier time. This way an approximation error is made and carried through the subsequent computations. The results can be only a good approximation to the behavior of the discrete system if the time increments are chosen small enough. This, however, can introduce numerical errors due to the limited number of figures carried in the computations and will certainly add to the amount of computation time. In order to overcome this difficulty an improved numerical integration was proposed by Newmark (14). At every time step the Newmark method uses the result obtained from the Euler method as a prediction and computes a correction by checking on the dynamic balance of the whole system. Prediction and correction are then considered a new prediction and new corrections computed until the process converges. Then only, the computation proceeds to add the next time increment. By use of this method both accuracy and stability of the solution

is essentially improved without increasing excessively the computation time. Studies on accuracy, stability and computation time of the solution are investigated in Appendix A1 together with the question as to the necessary number of pile elements for a good representation of the continuous system.

For deriving qualitative results and for obtaining an insight into the propagation of hammer applied stresses the wave theory treatment of the continuous pile is of great help. Appendix A3 shows how the stress or particle velocity can be computed at a point along the pile even if the pile is subjected to complicated external force conditions.

A stress wave is due to a difference in stress between neighboring cross sections, so that no static equilibrium exists. The stress gradient causes accelerations of particles. Therefore, a dynamic balance exists between inertia forces of particles and stresses in such a wave. In a uniform and elastic pile where no external forces act the stress gradient will travel through the rod without being changed in magnitude so that particle velocity or acceleration are predictable for a point along the rod if they were known for some time at another location. The speed of propagation, commonly denoted by c, depends only on the material properties of the rod. It is equal to $\sqrt{E/\rho}$ where E is Young's modulus and ρ is the mass density of the material. In a uniform rod the stress gradient will cause the same particle velocities independent of the location at the rod. An important result of

this fact is the proportionality which exists between stress and velocity in a stress wave, providing a convenient means of calculating the one if the other one is known.

When the stress wave arrives at an end the stress gradient will be changed. For example at a free end the particles will be subjected to higher accelerations (twice as high in a uniform rod) since no further material is strained in front of the wave. However, due to the higher acceleration a new stress gradient builds up between particles next to the end. The dynamic balance can be maintained only if another wave travels away from the end. This stress wave will be called a reflection wave. At a free end a reflection wave changes the sign of the stresses. At a fixed end where the stresses build up to twice their original magnitude and no acceleration of particles is possible the particle velocity in the reflection wave will point in a direction opposite to that in the arriving wave. A more detailed discussion with quantitative results is given in Appendix A3.

If a load is applied at some point along the rod then a tension and a compression wave will be built up on both sides of the loaded section causing two stress waves to travel away from the load. In a uniform rod these two waves will have the same stress magnitude equal to one half of the applied stress. This is necessary to satisfy the condition of equilibrium at the loaded point and in order to satisfy the condition of continuity the particle velocities in both waves have to be the same.

For no internal damping or external forces present stress waves will continue to travel along the rod always generating reflection waves at the ends. If stresses are observed at a particular cross section after the impact forces ceased to vary then the stresses will oscillate about the static value. Velocities observed this way would oscillate about zero if the rod is fixed at one end or about the value obtained from Newton's Second Law for a rigid body in case of the unsupported rod.

In the present analysis two records, continuous over time, are available. The first question is as to which is more convenient to use as an input. Because of the proportionality connecting stress to velocity in a wave in an infinitely long rod both the force or the velocity (acceleration integrated over time) seem to be equally well suited. Comparing the measured force with velocity obtained from the measured acceleration shows that this proportionality exists only in the beginning of the record. This can be observed in Figure (2.1). Deviations from this proportionality can be due either to the finite pile length and reflection waves or the action of the soil, resisting the motion of the pile particles. If the pile is of finite length and no forces are assumed to act along the pile then by accounting for reflection waves generated at either end of the pile the velocity can be calculated from the force or vice-versa. The output from the calculation can be compared with the other measured quantity.

Suppose that the velocity were derived from the measured force for a free pile of actual length L. If this solution would

agree with the measured velocity then this would indicate that the actual pile had indeed no resistance forces acting. In general, this will not be true. A difference between the actual and the thus derived velocity could be interpreted as a top velocity effect due to the soil resistance forces.

The other alternative is to compute the force on top of the free pile of length L using the velocity as an input. The difference between measured and computed force at the top is the force effect due to the soil action. Since it is intended to predict forces along the pile it seems natural to select the second way of analysis. This yields a top force effect versus time relation due to the resistance forces. The advantage of this choice will become apparent when such difference curves are analyzed.

To understand the meaning of the above described top force effect the boundary conditions have to be examined. The free pile solution is defined to have the prescribed measured velocity at the top and zero forces along its length and bottom end. The actual pile has the same velocity at the top and the real resistance forces acting along its length and the bottom end. Thus, the difference between the measured top force of the actual pile and that of the free pile will be the top force for a pile whose top has fixed end conditions being subjected to the actual resistance forces. This difference will be referred to as the Measured Delta Curve.

The advantage of dealing with the Measured Delta curve rather than with either measured force or acceleration is the fact that the effect of the actual resistance forces on the force at the pile top

has been separated from the forces due to the applied velocity. The measured velocity or force show very different characteristics depending on the hammer properties. Properties of the Measured Delta curves are independent of these hammer characteristics and, therefore, can be compared even if obtained under different driving conditions.

It is next supposed, that the resistance forces acting on the actual pile can be represented by concentrated equivalent forces. The Measured Delta curve can then be thought of being the result of a superposition of top force effects from each of these concentrated forces. Each of these top force effects is due to the action of only the one particular force acting on the pile with fixed top. Such a top force effect will be called a Resistance Delta curve. In case of a pile having only a resistance force acting at one station, the Measured Delta curve would be equal to the Resistance Delta curve for this station if the resistance force versus time relation is the same in both cases.

The Resistance Delta curve is a theoretical force versus time relation. It can be obtained for each force acting on the pile as a function of time. Since resistance forces acting on the pile depend on displacement and velocity at the point of action the Resistance Delta curve is to be computed by first computing the top force for a pile with the actual top velocity and the considered resistance force acting. Then the free pile solution has to be subtracted as in the case of the Measured Delta curve. It must be kept in mind, however, that obtained this way the actual resistance forces

influence the pile displacements and velocities so that the Resistance Delta curve computed in the above described way can only yield an approximation of the real top force effect. Examples for both Measured and Resistance Delta curves will be given below after a discussion of how resistance forces are functions of displacements and velocities.

3. Relations Between Delta Curves and Soil Resistance

In the previous section a way was illustrated of identifying the soil reaction forces. The soil behavior will be thought of as being dependent on the pile displacement and velocity assuming that the soil motion is negligible during the short time considered. The knowledge of pile top velocity and force makes it possible to predict the velocity of any other point along the pile allowing conclusions on the soil resistance. The Measured Delta curve will be used to determine the magnitudes and locations of soil model parameters.

(i) Shear Resistance at a Point Along the Pile

Shear resistance will be designated herein as all of those resistance forces which are independent of the rate of loading. Thus, shear resistance parameters of soils or of the pile soil interface can be determined in a static test. Although the type of soil failure is at the pile bottom very different from that at the pile skin no differentiation will be attempted. Furthermore, the term shear resistance will be used independent of the nature of these static forces. They might be either due to cohesion or due to internal

friction.

Triaxial tests on sands and clays show basically the same tendency of shear versus displacement behavior. The shear strength can be represented in first approximation by a straight line until a load value - herein called the ultimate shear resistance - is reached. While in clays it is usually not possible to reach higher values of shear stress even for large deflections sands usually show a strength increase after the ultimate strength has been reached. Since this strength increase goes with a much smaller modulus in the beginning of the curve it might not be essential for considerations dealing with relatively small dynamic displacements. However, some special considerations can interpret the results obtained from such an assumption. This will be discussed in Chapter III.

The ultimate shear resistance is reached at a pile deflection value which is usually called "quake" in the pile dynamics literature. Thus, the stiffness of the soil for deflections smaller than the quake is the ultimate shear strength divided by the quake. It can be assumed that the soil has the same stiffness during unloading. See Figure (2.2) for an example.

The value for the quake was found not to be critical for pile driving analysis. Smith (9), for example, recommends a value of 0.1 inches. It was found in analyzing actual records that the displacement reached at the time of maximum velocity is usually in the neighborhood of this value. Choosing that displacement as the value for the quake has the advantage that the quake will

always be exceeded by the pile displacements. This is a necessary condition for obtaining a final set under the hammer blow and for reaching the ultimate capacity. Also, the number of unknowns will be reduced since the knowledge of ultimate shear strength is now sufficient to describe the shear versus displacement behavior completely. Table (2.1) lists the quake values used for some of the piles analyzed. As an upper bound .12 inches had been used. Because of the action of resistance forces the displacements at maximum velocity are usually smaller at the lower parts of the pile than at the top. Thus, the quake will not be constant throughout the depth of the pile.

The force versus time relation of a shear resistance force is easily described when the displacement of the pile at the point where the resistance acts is known. The displacement at the point where the force acts will be zero as long as the stress wave due to the impact did not arrive at this section. At a time, given by the distance from the top divided by the wave speed, the displacement will start to increase and a reaction force will be exerted on the pile. This force will send out two reaction waves in either direction along the pile according to the previously discussed conditions of equilibrium and continuity. The total reaction force will be directed upwards and consequently the stress in the upwards traveling wave will be compressive, that in the downwards moving wave will be tensile. Because of the choice of quake discussed above the quake will be reached at the time when the particle velocity at the considered section becomes a maximum. After this

time no further increase in reaction force can be observed, i.e. the reaction force stays constant until the displacements start to decrease. Then unloading will start.

In order to describe the Resistance Delta curve for a shear resistance at some point, say at a distance x_i below the top, a hypothetical case is considered: The pile is fixed at the top, the bottom is a free end (except if the shear would be acting at the bottom end itself) and the shear force is assumed to be known as a function of time as developed above. For the discussion here this relation can be simplified by assuming that the shear resistance force is zero until a time x_i/c and equal to the ultimate shear resistance thereafter (Figure (2.3a)). This assumed resistance force versus time relation is realistic as long as no unloading occurs.

The stresses in the two generated waves are equivalent to one half the ultimate resistance force. First the upwards moving wave is considered. Its stress is compressive. At a time $2x_i/c$ it will reach the fixed top causing there a reaction force of twice the force in the wave - i.e. a force equal to the ultimate shear resistance. The reflection wave, traveling now downwards, will also have a compressive stress equivalent to one half of the ultimate shear resistance. This reflection wave will be a second time reflected at the pile bottom. Here a free end condition is encountered causing a new reflection wave with tension stresses. At a time $(2x_i + 2L)/c$ this new reflection wave will again reach the top but this time with opposite stresses. The top force effect, therefore,

becomes zero at this time. Figure (2.3b) illustrates the action of this initially upwards moving stress wave.

Turning now the attention to the initially downwards moving stress wave which has a tensile stress, again equivalent to one half of the ultimate shear resistance, it is observed that at a time L/c this wave reaches the free bottom end causing a reflection wave of compressive stress. This wave reaches the top at time 2L/c. The effect at the fixed top will be a reaction force of twice the force in the wave, i.e. a force equal to the ultimate shear resistance. A reflection wave caused at this instant will return not before time 4L/c. No consideration will be given to effects after this time. Figure (2.3c) shows the way the initially downwards moving wave travels along the pile and finally Figure (2.3d) is a plot of the Resistance Delta curve for the shear resistance obtained from superimposing the top force effects of both waves. Summarizing, this Resistance Delta curve reaches a value equal to the ultimate shear resistance at time $2x_i/c$ twice that value at time 2L/c and decreases again to one times the ultimate shear resistance at time $2(x_i + L)/c$. If the shear resistance force would act at the bottom end of the pile then the two waves would act as one wave moving together upwards with a stress equivalent to the ultimate shear resistance. Examples of these Resistance Delta curves will be demonstrated in the next section of this chapter.

(ii) Dynamic Resistance Forces

Dynamic resistance forces are usually assumed to be proportional

to the pile velocity at the location of the resistance force. This can be modeled by a linear viscous damper and, therefore, dynamic resistance forces are also called damping forces. The linear force velocity relation is the feature which distinguishes dynamic from shear resistance forces. Thus, dynamic forces change magnitude while shear resistance forces stay constant after the quake is reached.

In order to construct a Resistance Delta curve for a damper at a distance x_i below the top the force versus time relation must be found. In the case of a linear damper this means that the velocity of the pile section where the damper acts must be known. Waves due to the damping forces, however, will influence this velocity and the computation amounts to a rather difficult bookkeeping of reflection waves. Examples are discussed in Appendix A3. For obtaining an understanding of the main features of a Resistance Delta curve for a damper the assumption will be made that the damping forces are small as compared to the forces applied at the top of the pile. If this is the case then the velocity at the location of the damper is equal to the pile top velocity at a time x_i/c earlier. This is valid until the wave applied by the hammer has been reflected and reaches the damper a second time. Since the reflection was at a free end the velocity in the reflection wave will have the same sign as the applied wave thus increasing the velocity at the damper. Without giving more detail about further changes of the velocity at the damper the Resistance Delta curve for this damper will now be investigated. Again the top force effect due to the damper

will be the result of a superposition of the effects of the two waves generated by the damping force. One of both waves will move upwards to the top so that the damping force can be observed at the top in equal magnitude at a time x_i/c later. The second wave will arrive - after reflection at the bottom end - with a time delay of $(2L - x_i)/c$. Together with this wave, however, the wave which is traveling upwards is arriving at the top. The damping force causing this wave will be increased by the bottom reflected impact wave so that a maximum force effect at the top will result from superposition of both arriving waves. Since in most of the cases of pile driving the impact applied velocity will decrease immediately after its maximum also the effect at the top will decrease after its maximum which is different from the Resistance Delta curve for a shear resistance.

4. Discussion of Computing Delta Curves and Their Meaning

In the preceding sections two different kind of Delta curves were introduced: The Measured and the Resistance Delta curve. Both have in common that they represent resistance forces, acting along the pile and a means of separating their effect on the pile top from the effect which the hammer applied force has on the top. If Resistance Delta curves are found so that their total sum is equal to the Measured Delta curve then the resistance forces are known which were actually acting on the pile when acceleration and force were recorded.

In order to obtain either a Measured or a Resistance

Delta curve two other curves must be found. First, the "free pile solution", i.e. the force on top of a pile whose top input velocity is the prescribed record but has no other external forces along the rest of the pile. Second the force effect on top of the pile must be found whose top has again the prescribed velocity but has resistance forces acting along the pile. In the case of Measured Delta curve this second curve is the force curve measured in the field. In the case of Resistance Delta curve this second curve is determined analytically as explained in the next paragraph.

The first curve which is the free pile solution is obtained either by performing a lumped mass analysis or by using Equation (A3-18). This equation computes the exact solution by accounting for the effects of the applied forces as well as those from reflection waves. Equation (A3-18) can be applied without the use of a digital computer. A disadvantage in using a closed form solution arises in that if it is subtracted from a solution obtained by lumped mass analysis then differences due to inaccuracies in the numerical solution might be introduced which can distort the appearance of the desired Delta curve. For obtaining the second curve - a pile top force due to a resistance force acting on the pile and the measured velocity at the top - a lumped mass analysis has to be employed because the force versus time relation depends on the pile motion. As indicated above in the case of the Measured Delta curve this second solution - where the resistance forces act along the pile and the measured velocity is prescribed on top - is the recorded force itself.

Figure (2.4) shows the "free pile solution" as obtained from

Equation (A3-18). The velocity from which this solution was derived is also plotted after having been multiplied by the proportionality factor EA/c. (A is the cross sectional area of the pile, EA/c relates particle velocity to force in a stress wave).

Three Measured Delta curves are presented in Figures (2.5,6,7). The records were obtained on a special test pile. Figure (2.5) shows the measured force and velocity and the derived Delta curve from records taken when only half of a 50 foot pile had been driven into the ground. The soil offered almost no resistance to driving. The curves in Figure (2.6) are results obtained after the pile had been driven to a depth of 48 feet. A load test performed after this record showed an ultimate strength of only 47 kips. Later, the pile was extended and driven to a depth of 58 feet. At this depth the pile tip hit a hard layer. Figure (2.7) shows results obtained from records taken under these conditions. A load test was again performed and carried up to a load of 180 kips. At this point no higher loads could be applied because of instability in the test set-up.

All three Measured Delta curves in Figures (2.5, 2.6, 2.7) show a steep increase at a time 2L/c after impact due to the returning impact wave which has been changed under the action of resistance forces. For the pile which was only partially driven into the ground it was not possible to obtain higher impact velocities than shown in Figure (2.5) because of the relation between resistance and applied energy in case of Diesel hammers, one of which was used to drive this pile.

However, the fact that the top velocity increases again at a time 2L/c after impact indicates that the resistance forces were sending out waves of smaller magnitude than the applied wave. The Delta curve itself stays zero (small values both positive and negative, due to measurement inaccuracies, were set to zero until the point where the Delta curve starts definitely to increase) until a short time before the steep increase. After the maximum it decreases again with a steep slope. The late onset of positive Delta values indicates no resistances along the upper portion of the pile skin and the rapidly decreasing nature of the curve can be explained with mainly dynamic resistance forces.

The Delta curve in Figure (2.6) shows somewhat different features. Already a short time after impact positive Delta values are observed corresponding to the fact that resistance forces are acting along the upper portion of the pile. The behavior of the curve displays again a sharp decline after the maximum but holds some constant value until time 4L/c. Thus, large dynamic forces and small shear resistance forces are present.

A very different Delta curve is obtained from those records taken after the pile has hit the hard layer shown in Figure (2.7). The resistance encountered by the shorter pile along the skin can again be observed before the steep increase. This time, however, the maximum of the Delta curve is much larger as compared to these skin forces. Also the amount of decrease of Delta after the maximum is relatively small. Another interesting observation can be made on the measured force record in Figure (2.7).. This force shows a

definitive increase after a time 2L/c after impact. Clearly this increase must be due to the reaction waves sent out by the high resistance forces acting at the tip of the pile.

The negative values in the Measured Delta curves occuring after 4L/c and before 6L/c are due to the fact that the resistance forces do not stay constant but decrease in magnitude. Simplified examples in Appendix A3 will clarify this fact.

For obtaining an insight into the meaning of the Resistance Delta curves five different combinations of resistance forces have been used and applied on the pile and the top force computed for the case where the velocity of Figure (2.7) is prescribed on top of the pile. Then the free pile solution obtained from lumped mass analysis was subtracted.

First a shear resistance force having an ultimate of 75 kips was placed at the pile tip. Figure (2.8) shows that the resistance Delta curve for this case obtains a value of 150 kips after a time 2L/c after impact. Subsequent oscillations are due to the finite number of elements in the lumped mass analysis.

Next, a shear resistance of 50 kips was placed at a distance of 0.6L below the top of the pile. Figure (2.9) shows that in this case the Resistance Delta curve first reaches a value equal to this shear force at a time 0.6(2L/c) after impact and a value of twice that much at 2L/c (always after maximum velocity). It is expected that the Delta curve decreases again to 50 kips at (1 + 0.6) 2L/c, however, because of unloading (the applied velocity has decreased considerably) the Delta curve actually decreases to even smaller

values.

Two shear resistance forces of 25 kips ultimate each were placed at the pile at a distance 0.4L and 0.8L below the top. The result is plotted in Figure (2.10). Corresponding to the distances from the top at which these forces act the Delta curve shows a value of 25 kips at 0.4(2L/c) and 50 kips at 0.8(2L/c) after impact. Finally, at 2L/c after impact the Delta curve increases to two times the acting ultimate resistance forces (100 kips) due to the return of the bottom reflected waves. The decrease, thereafter, is again due to both returning tension waves and unloading.

Similar investigations were performed with dynamic resistance forces. Figure (2.11) shows the Resistance Delta curve for a damper at the pile tip. The damping coefficient is 0.2(EA/c). Using Equation (A3-31) the magnitude of the generated damping forces can be calculated using wave considerations and compared with the result from lumped mass analysis. The Delta curve is in this case an image of the applied velocity shifted over a time 2L/c and multiplied by a factor 0.2(EA.c)2.

A damper located at 0.6L below the top having the same coefficient exhibits a Delta curve value greater than zero already at a time 0.6(2L/c). This is shown in Figure (2.12). However, the proportionality between Delta curve and velocity cannot be observed anymore after time 2L/c after impact since the Delta curve becomes here the result of a superposition of two waves: The wave reaching directly the top and the wave initially moving towards the bottom of the pile where it had been reflected. When the latter wave reaches

the damper on the way upwards it itself will influence the damping force. Together with this wave reaching the damper the hammer applied velocity will arrive a second time at the damper after having been reflected at the pile tip. This velocity will superimpose to the velocity applied by the hammer and reaching the damper directly. The damping force at this instant, therefore, will increase, its effect will be carried to the top by the directly upwards moving wave and, in addition, the previously generated damping force will increase the Delta curve a second time due to the arrival and reflection of the initially downwards moving wave. The absolute maximum of the Resistance Delta curve in Figure (2.12) is the result of this superposition.

5. Proposed Prediction Scheme for Computing Soil Resistance

The considerations on stress waves due to resistance forces indicated that from the early portion of the Measured Delta curve conclusions could be drawn on the location and magnitude of resistance forces and that from the variation of this Delta curve a criterion could be derived for separating dynamic from shear resistance forces.

The first step to be undertaken in devising an automated routine for prediction of these reaction forces is to compute the Measured Delta curve which is possible in closed form by using Equation (A3.18). From this an estimate of the total maximum dynamic and total shear resistance force may be calculated using the Phase III scheme of predicting the static bearing capacity which

also gives an estimate on the maximum damping forces. This prediction scheme will be discussed both in Section 6 and in Appendix D.

Next, an assumption has to be made about the distribution of these dynamic resistance forces. Since it is not possible to obtain criteria which would indicate locations of dynamic forces several distributions will be attempted and then a final selection taken. In a first trial the total dynamic resistance is assumed to act only at the bottom end of the pile. Its influence on the top force can be thought of being proportional to the top velocity with a time delay of $2L/c$ as it is demonstrated in Figure (2.11). This gives a means of reducing the Measured Delta curve by the dynamic effect so that a Reduced Delta curve reflects the effects of shear resistance forces only. For ease in predicting the shear resistance forces this Reduced Delta curve can be reduced further to cancel out the effects of the reflection waves arriving from the bottom. In this case a Resistance Delta curve for one half of the total shear resistance force placed at the pile tip is subtracted. The reason for this is that such a Resistance Delta curve which is subtracted approximates the top force effects of all bottom end reflected waves due to shear resistance forces including the immediate reflection effect of the toe shear resistance. It includes, therefore, the quake effect. It is now assumed that the Resistance Delta curves for the various resistance forces to be determined are zero until $2x_i/c$ after impact and equal to the ultimate shear resistances, thereafter, if they are acting at a distance x_i below the top. Then requiring that the sum of the individual Resistance

Delta curves is equal to the Reduced Delta curve leads to the magnitude of the ultimate shear resistances at all locations x_i by successively solving starting with the upmost resistance forces. Thus, the bottom shear resistance will be determined from the Reduced Delta curve at 2L/c after impact. If the predictions and the soil model accurately reflect the real physical behavior then after the shear resistance forces had been computed from the record driving 2L/c after impact then the second time period $2L/c \leq t \leq 4L/c$ (t = 0 at impact) should also be matched. For further details see Appendix A3, Section 5.

In order to complete the prediction the damping coefficient for the bottom damper has to be computed. Since the maximum pile tip velocity can be approximately predicted using both Measured Delta curve and measured top velocity, as shown in Appendix A3, Equation (A3.58) the damping coefficient can be calculated by dividing the maximum total dynamic resistance by the maximum pile tip velocity. Only wave considerations have been used for predicting the complete set of a soil resistance parameter. Simplifying assumptions, however, were used since the effects of resistance forces on pile displacements and velocities can initially only be estimated. Thus, a check and refinement on the predicted forces has to be made. Placing the predicted shear resistance forces and the bottom damper as determined above at corresponding elements of a lumped mass pile model and performing an analysis will yield a new predicted top force and the velocities and displacements along the pile. Subtracting the new predicted top force

from the measured one gives a new difference curve which can again be thought of being a Delta curve. Errors in the prediction of soil resistance forces causing this new Delta curve - which will be referred to as an Error Delta curve - can arise in part from inaccurately estimating the pile tip velocity so that damping coefficient times maximum velocity will not amount to the maximum damping force necessary. Other errors may be introduced due to the neglected portions of the shear resistance Delta curves before the ultimate shear resistance is reached. This error will be larger for longer rise times at impact, i.e. the longer it takes for the displacements to reach the quake. If this time is longer than twice the time in which two consecutive elements reach the quake then the effect of the increasing resistance force on the next lower element will add to the predicted top force. These errors will cause a deviation of the predicted from measured force over the first 2L/c after impact. Deviations in the later portion of the record will be corrected after the first 2L/c match sufficiently well.

Improvements on the new prediction can be obtained first by computing a new damping coefficient using the pile tip velocity determined by the lumped mass analysis and then by computing corrections on the previously predicted shear resistance forces by using the Error Delta curve as a Measured Delta curve. By repeating this process it is usually possible to obtain finally an Error Delta curve which is small over the first 2L/c of the record after impact. (See also Appendix A3 for a computation example). A criterion on the quality of the match can be established by

integrating the Error Delta curve over certain intervals, say from 0 to 2L/c and from 2L/c to 4L/c, and dividing the integrals by the time intervals used. It was found that the requirement of making an average value small is sufficient for obtaining a good match. The only time that rapid changes in the predicted top force can occur is at 2L/c after impact. At this time reflection waves from hammer applied velocity and resistances forces reach the top. Otherwise Resistance Delta curves show a smooth behavior. Special consideration is given to their match at 2L/c (see Appendix A3). Once the absolute value of the average error of the first 2L/c does not anymore improve or once it is small enough the attention has to be directed to the later portion of the record (2L/c to 4L/c). In this portion a difference between measured and predicted force can arise due to a wrong prediction of total dynamic resistance forces. Comparing the Resistance Delta curve obtained for a damper at the pile tip as in Figure (2.11) with that for a shear resistance force, Figure (2.8), it is found that the shear resistance produces a higher top force effect after 2L/c than the damper. Thus, if the Error Delta curve is matched over the first 2L/c but becomes positive after 2L/c, i.e. the predicted top force is smaller than the measured, then the shear resistance force at the tip has to be increased and the dynamic resistance has to be decreased. Of course, for a negative Error Delta curve after 2L/c the opposite has to be done, namely shear resistance has to be replaced by damping. The match over the later portion, therefore, is dependent on the distinguishing features between dynamic and shear resistance

behavior.

Once a best match is obtained for a model with one damper at the pile tip two other approaches are used for distributing the dynamic resistance forces. In these two predictions damping is first distributed along the pile skin so that the first portion of the record (2L/c after impact) is matched by the effects of the dynamic forces only, or if the damping forces are too small, a uniform damping distribution is used together with shear resistance. In a third trial one damper is placed at the location where the maximum skin shear resistance force was determined in the first distribution method. Another damper - if the total dynamic resistance force is larger than the replaced skin shear resistance force - is again placed at the pile tip. In both cases of damping distribution the damping coefficients are determined from the requirement that the sum of the Resistance Delta curves for all dampers equals at 2L/c after impact twice the value of total damping computed from the Phase III method at this time.

Since the maxima of the velocities along the pile during the first L/c after impact, i.e. before the impact wave is reflected at the bottom, are dependent on the magnitude of resistance forces and not on the kind of resistance forces acting (as long as no reflection waves are superimposed it is possible to obtain an estimate on the maximum velocities from Measured Delta curve and measured velocity) the velocities obtained from the best match in the first method can be used for computing the damping coefficients

for the dampers distributed according to the two trial distributions.

Obtaining a match for these distributions must be done under consideration of the variation of the Resistance Delta curves for dampers along the skin. Thus, it is best for ease in computation to set up a influence matrix which contains numbers reflecting the top force effects at a time j of a damper at some location i. A similar matrix can be set up for the influence of shear resistance forces. These two matrices which actually contain the information which Resistance Delta curves provide only for a distinct numbers of points are discussed in Appendix A3.

Once a final Error Delta curve has been obtained for all three damping distributions a final result for estimating shear resistances and damping can be obtained by using a linear combination of all three results. A minimum of the final Error Delta curve can be obtained by performing a least square analysis on the previously obtained smallest Error Delta curves, for the three types of damping distribution.

Again, as in all previous predictions no negative results for the soil resistance parameters can be allowed as an outcome of the least square analysis. Thus, the minimum Error Delta curve might not be permissible and a recalculation needs to be performed in order to make negative values at least zero. Details on the computations and a computation example are given in Appendix A3.

6. Derivation of Simplified Models for Predicting Static Bearing Capacity

In this section a short discussion will be given about existing and newly developed schemes for total static bearing capacity. In Appendix D more detail is presented. The need for a reliable prediction of static bearing capacity was the reason for taking measurements of force and acceleration on top of the pile as outlined in Chapter I. It was hoped that a simple force balance at the time when the top velocity reaches zero would give a good correlation to the static load test result obtained immediately before or after striking the pile. Such a prediction method has advantages if a special purpose computer should be employed for displaying the result during the driving operation. Experience with this Phase I prediction (the predicted static capacity was calculated from force plus total pile mass times deceleration at the time of zero velocity) showed that more consistent results were obtained by using a deceleration value which was averaged over some time. It was found that this new prediction scheme which is referred to as the Phase II model gave good results for full scale piles driven in well drained soils. The predictions were not reliable, however, for short piles and piles driven in highly cohesive soils. One major task in studying pile phenomena was to find out about justifications and limitations of these simple prediction schemes.

For doing so the velocity of the pile top is expressed as a function of both static resistance forces and measured top force. Then computing a velocity difference yields an equation from which the total shear resistance along the pile can be calculated. This

equation proves that the Phase II model was a sound approach for computing static bearing capacity. Since only few changes in the Phase II model are necessary the new computation scheme which can replace Phase II also with respect to simplicity is called Phase II-A. The Phase II-A model also works for short piles since it now accounts for the effects of pile elasticity. Cohesive soils still can lead to generally high predictions since some of the dynamic forces are still acting at and after the time of top zero velocity.

In order to obtain an estimate of dynamic resistance forces encountered during the hammer blow the idea of a Delta function was used. The disadvantage of this method - which separates damping from shear by considering the part of the Delta function when the impact wave returns - is the complexity of computations involved. Therefore, a special purpose computer needs to have storage capacity. In cohesive soils the results from this method might still be high as in the other methods but the magnitude of the predicted damping forces usually indicates the reliability of the static capacity computed. Thus, more information is obtained than from the other models. Appendix D describes derivations and formulations of all of these methods.

CHAPTER III

Results and Correlation

Experimental data were obtained from both full scale and reduced scale piles. For each of these two pile types 24 complete sets of data were available for analysis. A description of the tested piles is given in Table (3.1) and (3.2).

Several results can be obtained from a single data set when applying the methods discussed in Chapter II. These results can be summarized as follows:

(i) Pile top force during driving as a function of time.

(ii) Static bearing capacity.

(iii) Shear resistance distribution along the pile.

(iv) Force in pile and velocity at the pile tip during driving.

In addition, the predicted shear resistance forces can be used for a static load-displacement analysis as discussed in Appendix A2. Such an analysis produces a pile top force versus displacement relation which can be compared with the same curve from the actual field load test. Thus, a further result is

(v) Pile top force during static load test as a function of pile penetration.

Load versus deflection curves obtained in a static load test often show high strength gains with large static pile top deflections which are not reached under a hammer blow. Thus, the prediction of static bearing capacity must be the dynamic displacements of the pile under the blow. A question arises, therefore, as to what the

"expected" bearing capacity will be under a blow. Using an example, this question is discussed in Section 1.

In Section 2 the results (i), (ii), (iii) and (v) all as obtained from wave analysis are presented and illustrated with Figures.

Section 3 is devoted to the discussion of predictions of static bearing capacity from simplified models. The correlation scheme developed in Section 1 using pile elastic considerations is applied. Finally, in Section 4 measured and analytically predicted pile forces and velocities are compared.

1. Proposed Scheme for Correlating Predicted With Measured Pile Bearing Capacity

The considerations in this section are undertaken using data set No. 3 as an example. The description of the corresponding pile is given in Table (3.1). This data set was applied to wave analysis and both damping and shear resistance forces were predicted. The predicted shear resistance forces were then used for a static analysis as described in Appendix A2. The load versus penetration (L.P.) curve resulting from this analysis and the corresponding curve measured in the field static load test are both plotted on the left hand side of Figure (3.3). Both L.P. curves show similar behavior up to a point where the predicted curve suddenly levels off. This is the point where the theoretical load curve reaches the predicted ultimate bearing capacity. The measured L.P. curve, however, shows further increase without an indication that an ultimate bearing

capacity can be reached. If it is assumed that the soil resistance forces are only dependent on the pile displacements, i.e. increases of resistance forces with time are neglected, then the question arises as to what bearing capacity must be compared with the predicted value. This question is now studied in some detail.

In a static load test a load is applied on top of the pile. This load compresses first the pile and then the soil. The elastic deformations of the pile are considerable for all the piles considered in this study. (The pile 531-76 for example compresses 0.57 inch under a uniform load of 100 kip.) Because of this pile elastic deformation the pile tip moves at a much smaller rate than the pile top. In general, the pile tip will be the last point along the pile to reach the quake penetration. If the static soil resistance law of Figure (2.2) were valid then the ultimate capacity were reached at that pile top penetration which produces a pile tip penetration equal to its quake. But this is the case only in theory. In reality, the soil resistance forces increase even after the quake penetration is exceeded now only at a smaller rate. Since the pile penetrations during driving are usually small the assumed elasto-plastic relationship establishes a good approximation for the dynamic case. It can be expected, however, that with higher dynamic penetrations a higher shear resistance is reached. Consequently, the dynamic displacements of the pile have to be considered in more detail. In Figure (3.4) the displacements at the top, the middle and the tip of the pile have been plotted as obtained from the wave analysis. The

pile top reaches a maximum deflection of 0.77 inches while the pile tip only penetrates to a maximum of 0.29 inches into the soil. The expected bearing capacity resisting the motion of the pile, therefore, corresponds to pile deflections of 0.77 inches at the top and 0.29 inches at the tip. In general, the static load test will not reach these two penetration values simultaneously. Thus, an exact correlation between dynamic prediction and static load test is not possible.

In order to find a sensible way of comparing the static load test result with the dynamic prediction assumptions have to be made. The following correlation scheme is proposed:

> Find the maximum dynamic deflection of the pile top under the hammer blow and obtain the corresponding load value from the L.P. curve of the field static load test. Call this load the "bearing capacity at maximum dynamic deflection, R_d".

An explanation why it is reasonable to correlate the dynamically predicted capacity, R_o, with the statically measured capacity, R_d, is given now.

The maximum dynamic deflection, max d_A, is reached when the pile top velocity, $v_A(t)$, reaches zero. Neglecting the influence of dynamic resistance forces allows to assume that

$$\frac{1}{2}R_o \leq F_A(t_m) < R_o \qquad (3.1)$$

where $F_A(t_m)$ is the hammer applied force at the time of maximum

velocity. Equation (3.1) is usually satisfied in practice for the following reasons. If $F_A(t_m)$ were less than $R_o/2$ then no permament set could be obtained under the hammer blow since the waves due to the resistance forces would be larger than applied waves. Thus, a negative velocity would be obtained at some point along the pile before the quake deflection were reached. If $F_A(t_m)$ were greater than R_o then the zero velocity would be reached only after $F_A(t)$ has decreased sufficiently. In such cases the maximum dynamic deflection becomes so large that it is comparable to large deflections in the load test where the load increases only at a small rate. The proposed correlation scheme will, therefore, work even better for such exceptional cases.

However, if as in the usual case, then the inequalities (3.1) will hold. Consequently, the waves generated by R_o (which may be distributed along the pile) will have particles velocities greater than max $v_A = (c/EA)F_A(t_m)$ so that zero velocity is reached at the pile top as soon as the resistance waves reach the top in full magnitude. This is usually not much later than a time 2L/c after t_m. Under these circumstances an approximate value can be calculated for the maximum displacement at the top of the pile, namely

$$\max d_A \approx 1/2(2L/c)\max v_A + q_1 \qquad (3.2)$$

where it is assumed that the applied velocity decreases linearly after maximum velocity and that the quake q_1 was reached at the time of maximum velocity. The inequality (3.2) can be expressed in terms of the applied force $F_A(t)$ by virtue of the proportionality

relation between stresses and velocities in a wave, hence

$$\max d_A = (L/c)(c/EA)F_A(t_m) + q_1 \qquad (3.3)$$

Now using the inequality (3.1) max d_A can be set between bounds

$$\frac{1}{2}\frac{LR_o}{EA} + q_1 \leq \max d_A \leq \frac{LR_o}{EA} + q_1 \qquad (3.4)$$

Generally, in static pile loading the force distribution in the pile is such that the elastic pile deflection is between $\frac{1}{2} LR_o/EA$ (uniform resistance distribution) and LR_o/EA (pile tip resistance only). Adding q_1 to the elastic deflection gives the top displacement necessary to just reach the quake at the pile tip.

The bounds given in the inequalities (3.4) are relatively wide. However, since in most cases the L.P. curve is already flat at max d_A the error introduced in the correlation will not be serious.

In the present example Equation (3.4) yields

$$.57 \leq \max d_A \leq 1.02 \quad \text{(inch)}$$

Using these limits and obtaining the corresponding pile capacity from the measured load test curve at these displacements yields

$$132 \leq R_d \leq 170 \quad \text{(kip)}$$

Using the maximum deflection during driving ($d_A = .77$) gives

$$R_d = 154 \quad \text{(kip)}$$

The best correlation between the dynamic value and the static load test would be to use the elastic deformation computed from the predicted distribution and to add the pile tip quake. The resulting deflection which is marked by an arrow in Figure (3.3)

would yield

$$R_d = 150 \text{ (kip)}$$

2. Results From Wave Analysis

In this section the results from applying wave analysis to all data sets listed in Table (3.1) are discussed and static predictions compared with results of the static load test. Exceptions were data sets No. 1, 2 and 4. The wave analysis could not be applied to these data since the rise time of force and velocity was longer than 2L/c so that reflections waves returned from the pile bottom before the maximum velocity was reached at the pile top. An example record is shown in Figure (3.1). The reason for such records is probably a too early combustion in the hammer which cushioned the blow excessively.

For pile 531-76 (data set No. 3) the same hammer was used, however, a single record was obtained having the usual impact properties. Figure (3.2) is a plot of the top forces both predicted by wave analysis and measured. Also the velocity measured at the pile top (used as input for the analysis) is plotted after being multiplied by EA/c. All three curves differ in the beginning of the record where the proportionality between force and velocity should hold. This difference is due to a relatively slow response of the strain signal conditioning equipment; this amounts to the lag between the two measured curves. Then also a phase shift between input velocity and output force arises from approximating the continuous pile by ten finite elements. These differences, however,

do not present a serious problem since only the portion of the record after maximum velocity is studied where phase shifts have small effects (the curves change at a smaller rate than at impact). Phase shifts of this kind can be observed also in the records discussed below. In some cases where the force transducer was mounted at a considerable distance above the accelerometers the force record might show an earlier rise than the velocity. The effects will be neglected.

Another remark concerning pile 531-76 seems appropriate. This pile was tapered, i.e. its cross sectional area was decreasing over one third of its length. In the present analysis effects of a variable cross section cannot be considered and pile No: 3 was the only pile analyzed with this property. It was assumed that the effects of variable stiffness are small in this case since only a short portion of the pile was affected. In Figure (3.3) results from wave analysis and static load test are graphically summarized. As discussed already in Section 1 the graph at the left hand side represents the two L.P. curves both measured and predicted. The dotted line indicates the maximum dynamic deflection. R_d is found where the dotted line intersects with the measured L.P. curve.

On the right hand side of Figure (3.3) the distribution of predicted shear and predicted maximum damping forces is represented in form of a plot of the forces in the pile. In case of the shear resistance forces these are the predicted forces in the pile when R_o is applied at the pile top. (R_o is the ultimate bearing

capacity predicted). The meaning of the dynamic force distribution is related to the static curve. For plotting this curve the maxima of the damping forces from each element are used. It is assumed that these forces occur at the same time and act statically along the pile, balanced by a pile top force which is equal to their sum. Thus, a curve similar to that for shear resistance forces is obtained. The sum of all maxima of dynamic resistance forces is called max D. This value is listed in Table (3.3) together with other important analysis results to give an indication of the relative magnitude of damping forces as compared to shear.

The shear resistance forces predicted for pile No. 531-76 are acting at the lower pile half distributed rather uniformly. Since this pile was an actual construction pile no force measurements were obtained from locations below grade. However, the blow count (number of blows per unit pile length penetration) gradually increased with depth. Dynamic resistance forces predicted were small and acting concentrated at the pile tip. Agreement between predicted bearing capacity R_o and measured capacity R_d was good. This correlation is discussed in more detail in Section 3.

Figure (3.5) presents the measured and predicted pile top force and the measured velocity of data set No. 5. This data set was obtained on a special test pile (13). The pile was only 33 feet long and equipped with strain gages at both pile top and bottom. The hammer force was larger at impact than the pile resistance, thus, it is not surprising that zero velocity was not

reached within 4L/c. Because of the short length of the pile (one millisecond corresponds to approximately L/2c) the rise time is relatively long and the accuracy of predicting the resistance force locations is, therefore, affected. The match between the predicted and measured pile to force is poor at time 2L/c after maximum velocity and later. Because of the relatively constant behavior of the top velocity it cannot be expected that dynamic resistance force decrease immediately after their maximum. Both shear and dynamic resistance forces, therefore, show a similar behavior and do not provide the necessary force time relation to separate them out and improve the match.

In Figure (3.6) the predictions from wave analysis are compared with the static load test. Agreement is good between R_o and R_d (see dotted line in L.P. curve). A deficiency of the predictions can be found in the distribution of shear resistance forces. Apparently, the wave method failed to predict the proper pile tip resistance force. However, a shift of the predictions over one analysis element is equivalent to a time shift of only 0.2 milliseconds (the time necessary for the wave to travel a tenth of the pile length). The accuracy of both the measurements and the method seems not to be sufficient to distinguish forces acting at such small distances. An explanation is given now.

A relatively arbitrary criterion for choosing the quake was adopted. It is described in Chapter II and in Appendix A3. The quake of a point along the pile was assumed to be equal to the

displacement at maximum velocity. This assumption allowed to compute the shear resistances $S_{o,i}$ from the Measured Delta curve at time $t_m + 2x_i/c$. Suppose, another quake, say a larger one would be assumed. Then the $S_{o,i}$ would have to be obtained from $\Delta(t)$ at another time. Since the total amount of shear resistance acting on the pile is independent of the quake magnitude such another quake would, therefore, merely shift the force predictions to some other point of the pile. It can be understood now that such a shift in the force prediction occured at the pile under discussion. This pile had a relatively slow rise time, thus, the shear resistance for some element was already large before the quake was reached. The force actually acting at the pile tip could, therefore, not be distinguished from the force acting at the element above.

In Figure (3.7) and (3.8) results are presented from data set No. 6. Both data set No. 6 and No. 5 were obtained at the same pile but at different times. Although a strength gain was observed after the waiting period the hammer applied forces were still larger than the resistance force so that in both cases essentially the same match was found.

Results from data set No. 7 are presented in Figures (3.9) and (3.10). The pile (F-50) was the above discussed 33 feet long pile extended by a pile section of 18.5 feet. Strain records were taken at three locations along the pile during the static load tests. The match of the measured with analytically predicted pile top force shows differences a short time after maximu velocity. These dif-

ferences must be due to measuring inaccuracies (the velocity multiplied by EA/c is greater than the force which, if true, means that negative resistance forces act near the top of the pile). Also, in the later part of the record differences in the match can be observed which must be due to an inadequate soil model.

The shear resistance distribution shows more pile tip resistance in the prediction than in the measurements. However, the fact that the pile had basically point bearing properties is brought out in both measurement and prediction.

The results shown in Figure (3.11) and (3.12) for data set No. 8 are again similar to those for set No. 7. The test pile was the same but the time of testing was different. This time the prediction R_o = 230 kip was too high as compared to R_d = 200 kip. Probably, damping forces were predicted too small.

The same test pile, F-50, was extended by a nine foot pile section to give a total pile length of 60.5 feet (F-60). Records were taken again before and after a waiting period. The analysis results for one blow of each data set are shown in Figures (3.13) to (3.16). The match for data set No. 9 is poor for a short time after the maximum velocity. Again, as in the case of Figure (3.9) this must be due to measuring inaccuracies since the proportional velocity is greater than the force.

Data set No. 11 was obtained on an actual construction pile. Measurements were taken only at the pile top. The match shown in Figure (3.17) is fair until time 3L/c after maximum velocity.

After this time the analytically predicted pile top force decreases. It was found that the match could not be improved by replacing damping forces with shear resistance since unloading occured. In studying Resistance Delta curves (Chapter II) it was found that the behavior of both damping and shear forces is similar after the velocity has become zero. Therefore, the match cannot be improved after this time (see also Appendix A3, Section 6).

The prediction of static bearing capacity, R_o, is higher than R_d (Figure 3.18). Comparing both L.P. curves, the predicted and the measured, throughout the examples given, it is observed that the predicted curve shows usually a steeper slope. Two reasons can be responsible for this deficiency. First the static quake is larger than the dynamically predicted and second the soil creeps under the applied load during the relatively long lasting load test. Certainly, the second reason will always yield an effect. Thus, max d_A is smaller than necessary for an accurate correlation and, consequently, R_d is smaller than the ultimate strength to be predicted.

Special problems were encountered in matching the measured pile top force for data set No. 12. The pile was an actual construction pile driven into stiff silt and clay. The pile was tested after a waiting period after driving. The special feature of the record shown in Figure (3.19) is a continuous increase of the pile top force. Also unusual is the behavior of the pile top velocity. After the first local maximum this velocity decreases only slightly and

reaches, thereafter, a second maximum which is higher than the first one. This phenomenon was observed for all blows in this data set but for no other pile. Reasons for such a record can be soft cushion properties or hammer self cushioning by early ignition. In addition, a very high precompression force of 66 kip had to be subtracted. Even after subtracting this force from the record the rise time was relatively long. The late occurance of the first local maximum velocity produces slowly increasing resistance forces which, therefore, have already relatively large effects before the quake is reached. The automated prediction routine, however, requires a short impact and, therefore, failed to produce a good match. (See also discussion of data set No. 5). Figure (3.20) shows the predicted pile top force from the automated routine. A large difference (35 kips) can be observed between measured and predicted top force at time t_8, $(t_m + 2\frac{8}{10}L/c)$ although no resistance force was assigned for the eigth element. However, shear resistance forces of 65 and 73 (kips) were predicted for the ninth and tenth element respectively. (Clearly, the resistance forces produce a top force effect at earlier times than expected due to the slow rise time at impact). To correct the match 35 kips resistance were subtracted from the predicted force for the ninth element and a lumped mass analysis performed. The pile top force obtained from this analysis was now smaller than measured at t_8. This is reasonable since bottom reflected waves effect the pile top force already at time t_8. Adding now 10 kips to the resistance of the eight element

(now 40 kips) produced the match shown in Figure (3.19). Thus, the prediction of bearing capacity was 25 kips lower when obtained "by inspection" rather than from the automated routine. A shortcoming of the match in Figure (3.19) is the very low predicted pile top force for $t > t_m + 2L/c$. The solution obtained by the computer program shows differences of equal magnitude before and after $t_m + 2L/c$. Both predictions, however, show a similar steep decrease in the later part of the record because of an inadequate soil modeling for unloading. The results corresponding to both matches are given in Table (3.3).

Results from data set No. 13 are shown in Figures (3.22) and (3.23). The pile was one of the special test piles described in Chapter I. The soil was a silty clay. A low static capacity of 69 kip was found in the load test immediately after driving. The velocity was increasing at time 2L/c after impact, indicating the low driving resistance. The precompression force subtracted from the force record was 26 kips, a large force compared to the ultimate capacity. The measured and predicted pile top force are both shown in Figure (3.22). This match was obtained by applying more damping forces than resistance forces. Better agreement between the analytical and the measured force could not be obtained because of the relatively constant velocity. Thus, the soil model is, again, not able to describe the soil behavior correctly. The predictions, however, are good as shown in Figure (3.23) and summarized in Table (3.3).

A much better match was obtained for the same pile tested after

a waiting period. Figures (3.24) and (3.25) present the results for this data set No. 14. Here, however, the static capacity prediction was too high. From force measurements taken during the load test along the pile it was found that relatively large resistance forces were acting along the skin of the pile. This fact was clearly recognized by measurements and analysis. An interchange of skin damping forces with skin shear resistance forces would improve the prediction to some degree.

Data set No. 15 and 16 were obtained from the second special test pile at the same site as the pile just discussed. The pile was longer, however, its ultimate bearing capacity was smaller than for the shorter pile. Very similar observations as in No. 13 and 14 can be made on the results of both data sets. The predictions and measurements are plotted in Figures (3.26) to (3.29).

Data set No. 17 was from an actual construction pile without special instrumentation. The soil was gravelly sand. Predictions and measurements were in good agreement as shown in Figures (3.30) and (3.31).

Another construction pile was tested but this time driven into clayey silt (Data Set No. 18). The static resistance of the pile was small although the blow count indicated sufficiently high soil resistance forces. The match between predicted and measured pile top force during driving was almost perfect. However, the prediction of bearing capacity was too high. Thus, the damping forces determined for obtaining the match were actually too low.

Figures (3.32) and (3.33) present the results. It should be mentioned that this pile gave the poorest prediction for static bearing capacity among all piles tested.

Data set No. 19 was obtained at the same pile after it was extended and driven to a depth of 74 feet. This time the maximum bearing capacity determined in a load test after a waiting period was 160 kips. Both Figures (3.34) and (3.35) show matches for the pile top force during driving. Both matches are of the same quality but different at time 2L/c after impact and later. The match in Figure (3.34) which was obtained from the computer routine shows fair agreement throughout the record. The pile top force (shown in Figure (3.35)) predicted by subtracting 10 kips from the predicted toe shear force agrees very well with the measured top force up to time 2L/c but deviates largely thereafter. These results indicate the difficulties in obtaining a match satisfying the matching criteria introduced in Appendix A3. Here, as well as in all other cases where the match was only fair these criteria were not satisfied and the iteration was stopped after the eight cycle in each damping distribution trial. The prediction from the second match agrees better with the load test result (see Table (3.3)). Figure (3.36) shows the static results both predicted automatically and measured. A great portion of shear resistance forces were predicted to act along the skin of the pile. This result is not surprising for a pile driven into cohesive soil.

Another construction pile (data set No. 20) in coarse grained

soil was tested. Figures (3.37) and (3.38) summarize the analysis results. The match of the dynamic forces is good and the prediction of static bearing capacity agrees well with the load test result. The blow count was low until the pile was driven to a depth of 40 feet when driving suddenly became hard. This observation agrees well with the prediction that most of the resistance forces act at the pile tip.

Figures No. (3.39) to (3.46) present the analysis results for the second test pile described in Chapter I. As it was outlined the pile was driven and tested in two steps. First the pile was driven to a depth of 50 feet (Ri-50). This pile was embedded in silty and clayey soil. Later the pile was driven until a stiff soil layer was reached and driving became very hard (Ri-60). The two data sets (No. 21 and 22) for the shorter pile gave results similar to the test piles To-50 and To-60 (Data sets No. 13 through 16). The difference was that the waiting period did not influence the soil properties as much as in the case of the To - piles. Figures (3.39) through (3.42) show the correlation between measurements and predictions. Again as in other cases of piles in cohesive soils relatively high dynamic and skin resistance forces were observed. A remark on the measured force curve in Figure (3.39) is appropriate. This force record did not show negative (i.e. tensile) forces before the precompression force was subtracted. Due to the small resistance forces, however, the top force decreased to very small values at time 2L/c after impact. Thus, after subtracting the precompression force,

S_p = 26 kips, negative values appear in the force curve.

The top force matches for Ri-60 are not very good. A reason for this can be found in the inadequate soil model. Velocity and force measurements were taken at the tip of this pile, examples of which will be presented in Appendix C. Predictions of shear force distribution and bearing capacity are good in this case even though the predicted top force is not good. A discussion of this point is given in Chapter IV. The analysis correctly reflected the strength gain of shear forces along the pile skin during the waiting period. This can be seen by comparing the force distributions along the pile in Figures (3.44) and (3.46).

Attempts were also made for analyzing the reduced scale pile data of Table (3.2). However, similar to the data sets No. 1,2 and 4 of Table (3.1) most of the reduced scale pile data had force rise times longer than 2L/c. Figure (3.47) shows both the measured force and velocity (multiplied by EA/c) and also a predicted top force obtained by assuming soil parameters and checking on the result by performing a lumped mass analysis. Then corrections were made and the process repeated. Data set No. 12 was here used as an example. The maximum velocity occurs only at a time 3L/c. Thus, the wave analysis method is not applicable.

It was tried to obtain data for reduced scale piles such that the maximum velocity occurs at an earlier time. This was done by reducing the cushion between hammer and pile head and resulted in the measured force record shown in Figure (3.48). Due to the very

short rise time the differences in the signal conditioning equipment produced now such large deviations of the necessary proportionality between pile top force and velocity that a meaningful analysis cannot be performed. In Figure (3.48) also a predicted force curve is shown obtained from using the static resistance of the pile as a pile tip resistance force. No effort was made, however, to improve the match.

3. Prediction of Static Bearing Capacity

In the previous section results from wave analysis have been presented by using only one blow as an example. Important results from each of these blows are listed in Table (3.3). However, more than only one blow was usually analyzed. In addition the simplified methods presented in Chapter II and in Appendix D were applied to all data sets for predicting static bearing capacity. The predictions are listed in Table (3.4) for full scale piles and in Table (3.5) for the reduced scale piles. (Reduced scale pile data were only used for analysis by simplified methods).

In most cases a number of blows has been analyzed. Since the correlation scheme - developed in Section 1 - requires comparing the measured bearing capacity at the maximum dynamic displacement of the blow each individual prediction is to be compared with the proper load test value, R_d. However, it was observed that the predictions for different blows are usually quite uniform (except for the results from Phase I). Furthermore, the maximum dynamic displacement usually changes only slightly from blow to blow. It seems, therefore, justified, to compare the averages of the predictions, R_o, with the

R_d values used to correlate the analysis results in Section 2.

The predictions listed in Table (3.4) and (3.5) clearly indicate the improvement of the results by applying any of the methods derived from wave considerations as compared to the rigid pile models (Phase I and II). Best results were obtained using the wave analysis. For application in a field special purpose computer, the Phase IIA method seems as well suited as any of the earlier methods. Also the Phase III method can be applied if some storage capacity can be provided in such a computer. Thus, the two early methods are discarded in further considerations.

A brief statistical investigation of the Phase IIA and the Phase III simplified method together with the results from wave analysis is now presented. Only full scale pile results are considered. In studying the predictions obtained from wave analysis it was found that the differences between measured and predicted static bearing capacity depend mainly on the magnitude of dynamic resistance forces. Dynamic resistance forces, however, depend on the soil properties and not on static bearing capacity. For piles with high damping errors in dynamic predictions can, therefore, result in relatively large differences between measured and predicted static bearing capacity. This is one reason to compare the absolute magnitude of predictions rather than present differences. In addition, a reasonable safety factor can be developed from such a study taking into account the uncertainties in the predictions for piles with low capacity.

Consider Figure (3.49). In this diagram the differences $R_o - R_d$ were plotted for the three methods under investigation. The differences were arranged in the same order as in Table (3.4), however, the results obtained from modifying the solution from the automated routine were omitted. Also, the results from data set No. 12 were omitted because of the unusual records which needed special consideration. Thus, 20 sets of predictions remain for analysis. Figure (3.49) displays an interesting trend namely with a few exceptions the differences are either all high or all low. Thus, these differences must be either due to assumptions inherent in all three methods or due to a lack of information in the records. The largest differences were found in the predictions for pile W-56 (Data set No. 18). This pile was driven into a clayey silt. The match between predicted and measured pile top force during driving was very good (Figure (3.32)). Thus, the soil model adopted seems not to be sufficient to describe the behavior of such a cohesive soil. However, this soil model was the basis in deriving all three methods.

The variety of soil conditions represented by the sample of 20 full scale piles chosen in Figure (3.49) is a fairly representative statistical sample. The computation is done the same way as suggested by Olson and Flaate (16) for the treatment of results from energy formulae. Accordingly, the measured capacity, R_d, is thought of being a function of the predicted capacity, R_o. A best fit straight line

$$R_d = mR_o + b \qquad (3.5)$$

is then determined for each set of predictions by the least square method. The results are shown in Figures (3.50), (3.51), and (3.52) for the Phase IIA, Phase III and the wave analysis, respectively. As a measure of the precision in the predictions also the variances, σ_m^2 and σ_b^2 of m and b are calculated. For illustration the lines

$$R_d = (m \pm \sigma_m)R_o + (b \pm \sigma_b) \qquad (3.6)$$

are plotted together with the best fit lines. Table (3.6) finally lists all parameters calculated together with the correlation coefficient for the three methods under investigation. Also the results of statistical investigations on energy formulae results from 93 piles in sandy soils given in (16) are shown for comparison.

The best predictions can be expected from the wave analysis method. But even the simplified methods, Phase IIA and Phase III, yield a better correlation coefficient than any of the energy formulae. It should be observed that from the 20 sets of data under investigation 9 were taken on piles in cohesive soils while the data in (16) were all from piles in sandy soils.

Compared to the two earlier methods the predictions for reduced scale piles listed in Table (3.5) were considerably improved only by the application of the Phase IIA method. The Phase III method did not yield improvements because - with a few exceptions - no short time impact was measured under the blow. Exceptions were data sets No. 21 through 24 in Table (3.2) where the agreement between R_o and R_u was much better. It is not necessary for

correlating the reduced scale pile predictions to find the value of R_d since the pile elasticity of these piles is small and the slope of the measured L.P. curve was always small at ultimate.

4. Forces and Velocities Along the Pile During Driving

For the two special test piles described in Chapter I dynamic force records were obtained on various locations along the pile. Pile tip velocities were also obtained on piles Ri-50 and Ri-60. In this section examples will be given as to how such measurements compare with the results from analysis.

On the right hand side of Figure (3.53) the discretized pile is shown as applied in the lumped mass analysis. Also, the locations where forces were recorded are indicated. On the left hand side of the same figure the forces are plotted that were recorded at the three different locations below the top. For comparison the force is shown in the spring between element 5 and 6 and the force in the lowest spring. Since the test pile (Ri-50) was 50 feet long one element length is 5 feet. However, the force in the pile was measured at one foot above the pile toe. Thus, the force predicted by the analysis cannot be equal to the measured pile tip force. It can be seen that the predicted curve (10) stays between the measured curves (III) and (IV).

The force measurement taken at a distance of 29 feet above the toe plate (II) agrees well with the spring force between element 5 and 6. The effects of the precompression force and a time lag due to measuring inaccuracies give some deviations.

A similar comparison for measured and predicted forces at the middle and the bottom end of the pile are shown for Ri-60 in Figure (3.54). This time the difficulties arising from different locations in analysis and measurement are avoided by plotting the pile toe resistance force as given by soil model. The agreement of these forces is as good as for the forces at the middle of the pile.

In Figures (3.55) and (3.56), finally, measured and predicted pile tip velocities are plotted. Good agreement is found for both piles Ri-50 and Ri-60.

CHAPTER IV

Discussion of Methods and Results

The studies presented in this paper lead to results on two levels. First, an analysis method for impact driven piles is presented which provides information about both soil response and pile behavior. Second a contribution is made to the development of a dynamic testing method for piles. Both the analysis and the dynamic testing method are based on force and acceleration records taken during a hammer blow.

While the dynamic testing method can be utilized in construction control as a replacement for the static load test the wave analysis method is also able to determine the soil resistance distribution which is needed for pile settlement analysis. However, it is also possible to use the basic approach of wave considerations for other problems associated with pile driving. Such applications will be discussed in Section 1 of this chapter.

Several assumptions were made in developing both analysis and dynamic testing method. Implications and resulting limitations of these approaches are discussed in Sections 2 and 3.

Section 4 is devoted to a summary of observations regarding measurement techniques and related questions of accuracy.

1. Possible Applications of Wave Analysis Method

(i) Summary of Analysis Process

The approach used in this paper for analyzing pile behavior and soil response under a hammer blow can be summarized as follows:

Force and acceleration are measured at the pile top during driving. These two records have been used above to separate the impact stress waves from the waves due to the soil action. The stress waves due to the soil action are then interpreted regarding their locations along the pile and their respective magnitudes. From the soil force versus time behavior, thus determined, conclusions are drawn about the type of resistance force, whether shear or viscous. (The type of resistance force is meant here in the light of a rheological model).

In separating impact from soil action waves the concept of Delta curves proved helpful. An important fact is that a Measured Delta curve can be obtained in closed form from a force and velocity record even without a high speed computer. Measured Delta curves are shown in Figures (2.5,6,7). After some experience it is possible to estimate soil response properties from such Measured Delta curves even without the further use of a complex analysis. Resistance Delta curves were developed to assist in interpreting the Measured Delta curve. As an example consider Figure (2.6). At time 2L/c after impact the Measured Delta curve has a maximum of approximately 300 (kip). Within a short time after the maximum the curve decreases to about one half of the maximum. Thus, approximately half of the total resistance seems to be damping. Also the fact that skin forces act at the pile is represented in the record.

(ii) Pile and Hammer Selection

In developing an automated routine for the prediction of soil

resistance forces a number of equations were derived which can be utilized in applications other than the prediction of soil resistance forces. As an example the selection of a satisfactory pile is illustrated.

Example 1:

Suppose, a pile of known material such as steel or concrete has to be driven by a hammer whose maximum impact velocity, max v_A, is known. Then Equation (A3.43) can be modified to yield

$$\max v_n = 2 \max v_A - c/EA \, S_{n,o} \tag{4.1}$$

where it is assumed that no dynamic resistance forces act on the pile. In the presence of skin shear forces Equation (4.1) is still valid by replacing $S_{n,o}$ by S_o, i.e. the sum of all shear forces acting. Therefore, if it is desired to drive a pile such that it has an ultimate bearing capacity of S_o^* then for the pile tip to exceed the quake and have a permanent set the following condition has to be satisfied

$$2 \max v_A > (c/EA) S_o^* \tag{4.2}$$

which requires that

$$A > (c/2E) S_o^* / \max v_A \tag{4.3}$$

In these considerations damping was not considered. However, for the condition of just reaching a positive velocity this was not necessary because dynamic resistance forces are small for small velocities. If it is intended to require the pile tip to reach a certain velocity, max v_n, then Equation (A3.43) has to be used in its original form together with an estimate for the maximum damping force,

d_n max v_n, (which can be assumed depending on the soil properties). Thus,

$$A = \frac{c}{E} \frac{S_o^* + d_n \max v_n}{2 \max v_A - \max v_n} \qquad (4.4)$$

The reverse approach can be used to find the necessary hammer impact velocity by prescribing the pile cross sectional area and solving for max v_A. Estimates on pile set can be obtained by integrating Equation (A3.43) over time until $v_n(t)$ reaches zero.

(iii) Interpretation of Pile Force Records

In addition to producing a useful set of analysis equations wave considerations also lead to a thorough understanding of pile behavior. In another example it will now be explained why pile driving records (force or velocity) seldom give a clear indication of the time when the impact wave returns from the bottom as was discussed by Tomko (13).

Example 2:

It was observed in Chapter III that damping forces exerted by the soil are acting mainly at the pile tip. For the case of only a damper at the pile tip Equation (A3.41) gives the damping force $D_n(t)$ from the applied velocity $v_{n,a}(t)$. The reflection of the impact wave plus the effect of the damper causes a wave to travel upwards with a particle velocity $v_{up}\ (t - \frac{L - x}{c})$ at time t and at a distance x below the top.

$$v_{up}(t - \frac{L - x}{c}) = v_{n,a}(t) - \frac{cd_n}{EA} \frac{2v_{n,a}(t)}{1 + (cd_n)/EA} \qquad (4.5)$$

or using again the definition (A3.50) Equation (4.4) can be written as

$$v_{up}(t - \frac{L - x}{c}) = v_{n,a}(t)[1 - 2\alpha_n \frac{c}{EA}] \tag{4.6}$$

Suppose, a pulse is applied at the free pile top at a time zero for a pile with free bottom end condition. If the pulse has duration Δt and a particle velocity v_A^* then for no damper at the bottom the pile top velocity is given by

$$v_{top}(t) = \begin{cases} v_A^* & \text{for } 0 \leq t \leq \Delta t \\ 2v_A^* & \text{for } r\frac{2L}{c} \leq t \leq r\frac{2L}{c} + \Delta t \end{cases} \tag{4.7}$$

$r = 1,2,\ldots,$ indicates the time interval considered. Equation (4.7) is plotted in Figure (4.1a).

If a damper is acting at the pile toe then due to the reflection of the upwards traveling wave (whose particle velocity is given by Equation (4.6)) at the pile top

$$v_{top}(t) = \begin{cases} v_A^* & \text{for } 0 \leq t \leq \Delta t \\ 2v_A^*(1 - 2\alpha_n \frac{c}{EA}) & \text{for } 2L/c \leq t \leq 2L/c + \Delta t \\ 2v_A^*(1 - 2\alpha_n \frac{c}{EA})^2 & \text{for } 4L/c \leq t \leq 4L/c + \Delta t \\ 2v_A^*(1 - 2\alpha_n \frac{c}{EA})^r & \text{for } r2L/c \leq t \leq r2L/c + \Delta t \end{cases} \tag{4.8}$$

In Figure (4.1b,c,d) this pile-top velocity is plotted for values of $\frac{c}{EA}\alpha_n = 0.1, 0.5, 0.9$, respectively. It can be observed that $\alpha_n = EA/2c$, i.e. $d_n = EA/c$, gives the solution for an infinitely long pile. No bottom reflection waves reach the top. This damping coefficient, $d_n = EA/c$, can be thought of as a critical value. If the soil would act like a damper having this critical damping coefficient then in absence of all other resistance forces

$$\max D_n = \max v_A(EA/c) \tag{4.9}$$

But because of the proportionality between pile top force and velocity (which holds at time t_m, the time of maximum velocity)

$$\max D_n = F_A(t_m) \tag{4.10}$$

In this context it is interesting to study the damping coefficients obtained from analysis for different soil types. A list of such parameters is given in Table (4.1). The damping coefficients listed in this table are non-dimensionalized by dividing d_n by EA/c. "Critical damping", therefore, corresponds to a value 1.0 in Table (4.1). It can be observed that only two data sets (No. 18 and 19) which were obtained on the same pile are greater than unity. Relatively often, however, values in the neighborhood of 1/2 can be observed.

Of course, damping values non-dimensionalized with respect to pile elastic properties can not be used for comparing the behavior of different types of soils. Table (4.2) lists the natural coefficients d_n. These parameters must be considered with respect to their dimensions. Thus, element surface or the total cross sectional area of the pile toe must be considered when comparing the damping coefficients determined for different piles. A commonly employed method of referring to damping coefficients (10) is in relation with ultimate shear resistance. This procedure was not adopted in developing the predictor method since it was intended to obtain damping and shear parameters independently. However, for further applications of predicted soil parameters this method could

lead to comparable values for different pile and soil types. Further investigations are needed, however, to distinguish more accurately between skin and toe damping at the bottom element.

A shear resistance force acting at the pile tip and having a magnitude equal to $F_A(t_m)$ will also produce a wave such that at time $t_m + 2L/c$ no effect of the impact wave reflected at the pile bottom can be observed. In fact, any combination of resistance forces produces this effect if forces of their respective waves sum to $F_A(t_m)$. These observations can be applied to the interpretation of the three-dimensional force plots shown in Figures (1.1,2,3). (Three or four force measurements were available. The graph was completed by interpolation).

In Figure (1.2) a plot is shown where $F_A(t_m) = 165$ kips and $S_o + \max D = 107$ kips from wave analysis. Thus, there is less force than necessary to cancel out the effects of the reflected impact wave at $t_m + 2L/c$ at the top. Accordingly, a decrease in the pile top force can be observed when the reflection wave arrives at the top. The plot gives also an impression as to how the waves travel through the pile.

Figure (1.3) shows the plot of force measurements taken on a pile with high toe resistance. $F_A(t_m) = 290$ kips and $S_o + \max D = 280$ kips. This means that not much change should be observed in the pile top force at time $t_m + 2L/c$. Indeed, the force record at this time proves this statement. The steep top force increase in the record at a later time is due to the rapid decrease

of impact force immediately after the maximum. Since S_o remains on until zero velocity its effect on the top is to cause an increased force.

Figure (1.1) resulted from measurements on a pile with relatively high skin resistance forces (To-60, data set No. 16). $F_A(t_m)$ = 155 and S_o + max D = 200 (kip) were obtained from measurement and analysis, respectively. This case shows a top force increase already at a short time after time t_m. At time t_m + 2L/c a drop of pile top force can be observed. In this case high dynamic forces were found by wave analysis so that the full effect of the maximum resistance forces does not anymore affect the pile top at the time when the bottom reflection wave returns. However, both hammer and resistance forces were not of very different magnitude so that no wave return can be observed in the force behavior.

Considerations of the force record alone cannot yield any quantitative information. For obtaining accurate results about the magnitude of resistance forces the pile top velocity must also be considered. This point is quite important since previous investigators have restricted their records to either force or acceleration alone, (e.g. Buchnell).

(iv) Prediction of Pile Stresses

Since the force and acceleration records taken at the pile top predict the soil resistance force distribution it must be also possible to compute the stresses in the pile during driving. This

problem is faciliated by the fact that a distinction between dynamic and shear resistance forces is not necessary. Hence, estimates can be obtained from the Measured Delta curve without performing a complete prediction analysis.

Compression stresses reach, in general, extreme values only at the pile top or pile bottom. Along the pile skin only distributed forces act which cause a compression wave above and a tension wave below their respective locations. The effect of a superposition of such compression waves can be observed at the pile top.

A bound on the maximum toe compression stress, $\sigma_n(t)$, can be given by assuming all resistance forces to act at the pile tip. But since the maximum total resistance force is given by the Measured Delta curve, it is possible to estimate the pile tip stress:

$$\sigma_n(t) \leq \frac{1}{2A}\Delta(t_m + 2L/c) \tag{4.11}$$

Tensile stresses which can be critical in driving of concrete piles occur only in the case of small resistance forces and are due to the decrease of the impact velocity. In the absence of resistance forces the stresses, $\sigma_i(t)$, at a point $x = x_i$ is for $0 \leq t \leq (2L + x_i)/c$

$$\sigma_i(t) = E/c[v_A(t - \frac{x_i}{c}) - v_A(t - \frac{2L - x_i}{c})] \tag{4.12}$$

which follows from a superposition of the applied wave (having particle velocity $v_A(t)$ at the pile top at time t) with its own reflection wave. Thus, tension stresses can occur when the particle velocity of the bottom reflection wave is larger than that of the downwards traveling impact wave. The largest tension stress to occur in the pile is, therefore, given by the maximum difference in

pile top velocity during the first 2L/c time interval (after maximum velocity). Compression stresses due to resistance forces below $x = x_i$ reduce this tension stress such that from the Measured Delta curve an estimate on this stress can be given. Thus, for $x_i \neq L$

$$\sigma_i(t) = E/c[v_A(t - x_i/c) - v_A(t - (2L - x_i)/c)] - \frac{1}{A}[\Delta(t_m + \frac{2L}{c})/2 - \Delta(t_m + \frac{2x_i}{c})] \qquad (4.13)$$

Such investigations on the stresses in piles suggest that the hammer and cushion properties have to be selected with respect to the pile strength. In order to prevent tensile stresses in concrete piles cushioning has to be added for obtaining a uniform pile top velocity, $v_A(t)$. Excessive compression stresses in the pile can be prevented by keeping the hammer impact velocity so low that the corresponding stress is one half of the yield stress.

Implications of this kind are known to hammer manufacturers but records and wave considerations as outlined can give valuable information for certain combinations of hammers, piles and soils.

2. Discussion of Soil Force Prediction Analysis.

The wave considerations in Chapter II and in Appendix A3 were limited to a time 4L/c after impact. This time interval may not always be sufficient as when L is small (as for reduced scal piles) in order for the soil response to develop fully within this time period of 4L/c. Since a resistance force distribution along the pile is usually of minor interest for short piles no serious limitation seems to restrict the applicability of the present method

from this point. Clearly, a rigid body, i.e. a pile of zero length, cannot be analyzed regarding resistance force distribution.

A related problem is encountered when the pile is sufficiently long but the impact is too "slow". In such a situation only approximate solutions are found. A match of pile top forces might be obtained by using the lumped mass analysis and assigning soil resistance parameters in a trial and error fashion as indicated above. However, the results thus obtained depend mainly on assumptions regarding the soil stiffness and to a smaller degree on the actual soil properties since these factors can be found from the record due to the numerous reflections occuring during buildup. Two extreme situations may clarify what is meant. A "very slow" impact is the static load test which allows a match between measured and predicted pile top force from the assumption that all resistance forces are concentrated at one point. A corresponding soil stiffness - necessary for the match - can be computed, but the resistance distribution along the pile can not be determined from the top record. The "fastest possible" impact exhibits a step shaped displacement function (the velocity is applied as an impulse) in which case the force distribution can be predicted independent of any knowledge regarding the quake. The latter case is ideal for the present method.

In this context the choice of the quake should be discussed. Frequently, in the analysis quake values are used which are relatively small compared to values commonly recommended. Foehand and Reese

(11) give quake values up to 0.30 inches for certain soil types. Also the investigations in Appendix C showed that the quake might be larger for soft, cohesive soils than the displacement at maximum dynamic deflection. There are several reasons, however, why the adopted method still gives good results.

A first reason is that in all records analyzed a precompression force was acting upon the pile and was imposing displacements such that the soil structure was already compressed before the impact wave arrived and caused the soil to yield.

Second, the sum of the ultimate resistance forces, $S_{i,o}$, is determined directly from the Measured Delta curve, independent of the choice of quake. Wrong assumptions in the quake will, therefore, mainly result in errors in the shear resistance force distribution. This, of course, is true only for small errors in the quake and does not apply to cases where the quake was not reached in the considered time interval. In such cases the ratio of shear to damping forces will be affected at 2L/c after impact in the Measured Delta curve.

In the analysis quakes were used with only small differences between neighboring elements. It can be assumed that also in reality the quakes do not vary substantically with depth. Erroneous assumptions in these quakes will, therefore, produce a shift of all resistance forces along the pile length. The results shown in Figures (3.6 and 8) exhibit such a force shift over one element length.

Other errors in resistance force distribution can arise where large damping and large skin resistance forces are present. In

such cases an incorrect damping distribution will necessarily result in shear resistance forces at locations other than measured in the static load test. (The total amount of resistance forces is dependent on the Measured Delta curve, only). An example to such erroneous results is given in Figure (3.25). Here a large damping force was assigned to a point where actually a relatively large shear force was acting. Note, however, that the character of the shear resistance distribution was still preserved. Errors of this kind occur since no indications as to the damping distribution were found in the records. Because of this lack of information it was decided to use a damping distribution which yields the best match. This approach solves the problem only approximately since even a perfect match does not necessarily give a correct solution.

A remark on the uniqueness of a solution obtained by matching the measured force is appropriate. Certainly, a match with zero differences between predicted and measured forces is not possible, however, within the accuracy of the discussed method it is possible to obtain several solutions with an equivalent match quality. For example it was observed that different damping distributions can lead to almost identical pile top forces. To obtain a solution for the 2n parameter, p_i, which describe either the damping or the shear force behavior at least 2n simultaneous equations have to be satisfied

$$\Delta(t_j) = \sum_{i=1}^{2n} \Delta_i(t_j) \qquad (4.14)$$

$$j = 1,2,\ldots,2n$$

where the t_j are suitably chosen times, e.g.

$$t_j = t_{j-1} + 2\frac{L}{nc} \tag{4.15}$$

$\Delta(t)$ is the Measured Delta and $\Delta_i(t)$ is the Resistance Delta curve associated with p_i.

Of course, the t_j can be chosen arbitrarily over the domain such that actually an infinite number of equations is available. However, the smaller Δt becomes in Equation (4.15) the smaller differences occur between consecutive equations. Thus, if n is too large an ill conditioned set of equations can result which allows several possible solutions. It can be concluded that the information contained in $\Delta(t)$ is not sufficient for obtaining a unique solution.

A further complication is that another soil model could be chosen which would yield another set of $\Delta_i(t)$, accordingly a different set of p_i.

In cases where a good match was obtained with relatively poor predictions of static bearing capacity the use of another, more realistic, soil model would add the information necessary for obtaining a good match together with good predictions. Sandy soils do not present problems of this kind, since the chosen soil model is appropriate.

Several results were obtained with a relatively poor dynamic top force match. (See Figures (3.22,26,39 and 41) for data sets No. 13, 15, 21 and 22, respectively). A better match cannot be obtained when employing the present soil model. Even a quake value different from the one assumed would not improve the situation as

can be seen by inspection from Figures (C.2 and 3). (The theoretical damping forces do not decrease at a sufficiently high rate). By choosing somewhat smaller shear resistance forces than used for the matches in Figures (C.2 and 3) the error in the match of dynamic pile top forces is spread over some time before and after time 2L/c after impact. As a result the prediction of total static bearing capacity is relatively good but errors in the match of dynamic pile top forces are made already before the time when the reflected impact wave returns.

Piles with relatively small resistance forces (the impact force is larger than the sum of all resistance forces) usually show little variation in the pile top velocity. Therefore, Resistance Delta curves do not exhibit the characteristic differences between shear and dynamic resistance which usually allow to distinguish these forces. For predicting the maximum dynamic resistance forces the analysis uses here the observation made in Appendix C on cohesive soils namely a damping force drop independent of the pile velocity. The Phase III simplified method of predicting static bearing capacity uses the same idea for piles with small resistance. Since this Phase III prediction scheme is used as a first guess on the amount of damping forces in the wave analysis a reasonable final result is obtained. In such cases the criteria for a good match cannot be satisfied since the predicted force is always too large after $t_m + 2L/c$. The analysis routine is programmed in such a way that first attempts are made to improve the latter region of the match

by adding more damping and reducing shear resistance forces. If no improvement can be obtained then the matching criteria are relaxed such that the iteration terminates within a few more cycles. This way some more damping is predicted than computed by the Phase III scheme, which means a more conservative result for the static bearing capacity prediction. Certainly, predictions obtained in such a way can only be considered an estimate on the static bearing capacity and further studies on soil models particularly with regard to the damping are necessary to devise a better basis for wave analysis of soils driven into such soft cohesive soils.

Entirely different problems were encountered on piles driven again into cohesive soils but tested after a waiting period long enough to allow the pore water pressure in the soil to dissipate. (Only the first few blows after the waiting period can be expected to reflect a situation different from that encountered immediately after driving). In such cases the wave analysis produced a very good match between predicted and measured dynamic pile top force. Figures (3.24, 28, 32) show such good matches. However, the predictions of ultimate shear resistance were much higher than determined in the static load test. This surprising result can be explained if static and dynamic measurements are obtained and analyzed in a manner similar to those shown in Appendix C. It is suggested that the present soil model does not distinguish sufficiently well between static and dynamic resistance forces, in cohesive soils. In other words, the linear relationship between

pile velocity and damping forces does not hold for all soil types.

While dynamic analysis of piles driven into cohesive soils presents problems regarding a proper soil modeling predictions of static capacity and the static force distribution are reliable for piles in sandy soils. Frequently, it was found that the match was not good in the latter portion of the record. However, as discussed in Appendix C, the soil model is very sensitive to small differences in either the quake value or to the pile displacement accuracy after zero velocity (during unloading). Figure (C.4) shows a case where the measured pile resistance force behaved much smoother than the force determined from using the soil model. Thus, oscillations in the pile top force which are not present in the measured record can be explained from this soil model sensitivity. However, since the unloading portion of the record is not considered for predictions of resistance forces and their distribution no error is introduced in the result.

3. Simplified Prediction Schemes for Dynamic Testing Method

As outlined in Chapter I a dynamic testing method was proposed (12) for predicting pile bearing capacity. In this method the time of testing is delayed for a few days so that soil relaxation after driving cannot affect the result. A detailed discussion of the problem of soil relaxation after driving is given by Yang (18). That dynamic records in fact reflect the change of soil properties during a waiting period is shown in Appendix C. Records obtained this way are then used to predict static bearing capacity from any

of the simplified computation schemes discussed in Appendix D. A special purpose computer is to perform the computation and display the result immediately after the blow.

Differences between predicted and actual static bearing capacity can arise from wrong assumptions about both pile and soil behavior. The investigations in Appendix D clearly show the errors made by assuming the pile to behave like a rigid body in the Phase I and II method. The Phase IIA prediction scheme is a modification of the Phase II method where the pile elasticity has been taken into account. This computation scheme is easily programmed in a special purpose computer. Results seem more reliable than from the best of the energy formulas. Differences between measured and predicted static bearing capacity arise from an uncertainty about the magnitude of damping forces. Since the Phase IIA method uses an average slope approach similar to the Phase II scheme also average damping forces can be included in the static prediction. The choice of the time at which this average is taken insures, however, that the influence of dynamic resistance forces will be small. Numerical difficulties in analyzing digitized records require a modification of the method. The higher accuracy of data directly processed in a special computer can lead to an essential improvement of this method.

A Phase III method was developed using the idea of Delta curves. This method has the advantage of predicting both maximum damping forces and static bearing capacity. Figure (4.2) shows a plot of differences between the measured and predicted static bearing capacity versus

maximum damping forces predicted from the Phase III method. The data set used is the same as for the statistical investigations in Chapter III.In this figure relative differences and relative damping forces were used for showing the trend more clearly. The conclusion can be drawn that a high percentage of predicted damping force induces more uncertainty about the accuracy of the static result. As can be expected cohesive soils are responsible for the largest errors in the method. Thus, the predictions of static capacity of piles in sandy soils can be considered very reliable. The only exception was F-30 which is a relatively short pile.

A disadvantage of the Phase III method is the complexity of the computations involved. However, it is hoped that simplifying assumptions (e.g. as to the time of toe zero velocity) can possibly lead to a computation scheme more suitable for a special purpose computer application. More studies are necessary in this direction.

4. Measurements

Comparisons between predicted and measured pile top force in Chapter III showed frequently differences because of measurement inaccuracies. Most commonly differences in the response of signal conditioning equipment for strain and acceleration lead to time lags. Such differences are serious when short piles are analyzed. (The time lag in Figure (3.48) corresponds to 0.3 L/c). Another error source is the difference in the locations of force and acceleration transducers. Sometimes the time lags arising from signal conditioning and recording location can cancell out.

Acceleration measurements were performed with piezoelectric accelerometers. For measurements at the pile tip an accelerometer was used having a built-in amplifier. This reduces the effects of cable noise. A disadvantage of this accelerometer is the low recordable minimum acceleration (negative accelerations to act away from the base of the transducer). Thus, mounting the instrument upright onto the pile toe plate results in an acceleration cut off at a 250 to 350 g-level. However, a cutoff of a recorded peak value of 100 g's with a duration of 1 millisecond amounts to a velocity error of 1.6 ft/s. Toe accelerations can become very large - positive and negative - depending on the soil resistance forces. Thus, in records where the above mentioned level was reached uncertainty exists as to the actual pile toe acceleration and velocity. Two figures were presented in Chapter III comparing measured with predicted pile tip velocity. Good agreement was obtained in these cases because the accelerations did not exceed the recordable limit.

Another difficulty for comparing acceleration measurements at the pile toe with analysis results from a lumped mass system is the difference in location between recorded and computed results. For short rise times with respect to the pile element length only an average value can be expected from the analysis while the measurement records the extreme toe bottom behavior.

Force records present another problem. Usually it is assumed that no residual forces act on the pile. While this assumption might hold for the first blow after a waiting period errors might be made

for all subsequent blows. Neglecting such residual soil forces will affect the soil force distribution only since at the onset of each new blow a state of equilibrium exists for the pile soil system. It also can be expected that the time lag between successive blows is sufficient to release most of such residual forces by creep. For analysis of piles driven by vibratory hammers this point will require a more detailed study.

CHAPTER V

Conclusions and Recommendations

The methods for pile analysis presented above use measurements, an exact wave theory and a lumped mass analysis in conjunction with an assumption regarding the functional relation between soil forces and soil motion. The analysis allows to compute the location and magnitude of dynamic and static soil resistance forces acting on the pile under a hammer blow. The static soil resistance forces correspond to those forces acting on the pile during a static load test. Another facet of the presented work is the development of a simple prediction scheme for static bearing capacity based on pile elastic theory.

The field measurements of force and acceleration proved to be accurate enough for commonly encountered full scale piles. The information contained in the records was sufficient to predict the magnitude and distribution of the soil resistance forces as long as the soil model was adequate. Distinction of soil force types regarding their velocity or displacement dependency was very successful for piles in sandy soils and yielded relatively good approximations in cohesive soils.

The present method bypasses a major shortcoming of other pile dynamic analyses found in the literature, namely the uncertainty of hammer input and soil parameters. In fact, the results obtained from the automated prediction scheme can be used to give information on soil behavior which is in contrast to the usual procedures of

first obtaining the soil properties by laboratory testing and then performing the pile analysis.

The predictions of static bearing capacity show a correlation better than those obtained from existing methods (13, 17). Improvements can be expected when further soil investigations are performed in a manner as in Appendix C. Thus, different from the usual soil mechanics approach of obtaining soil properties in the laboratory, it is recommended to obtain knowledge about the gross soil response to a certain pile type (the cylindrical piles which were used throughout the experimental work reported herein are very common, however, other pile types might possibly show different behavior due to a pile shape influence. It is possible that an H-pile, for example, will behave very different from a pipe pile). It is hoped that such an effort would lead to an improved soil rheological model which equally well describes both non-cohesive and cohesive soils. (A more realistic model than presently used is discussed in (19)). Then derived from such an improved soil model a classification of the soil type surrounding the pile could complete the prediction of pile static behavior by indicating the soil creep and strength gain behavior.

The computer program was devised for the case of a uniform pile. In order to minimize the input data ten elements were always used and a time increment of one half of the critical time (see Appendix A1). These assumptions might not hold for long and non-uniform piles. For generalizing the present routine a study on

Measured Delta curves for piles with variable stiffnesses and the revision of the lumped mass analysis is recommended.

It was found that damping forces usually act in a large amount at the pile tip while smaller magnitudes of dynamic resistance forces act at the pile skin. In order to simplify the program and to save computing time it can be recommended to decide on the damping distribution a priori and to obtain only on solution.

Another important facet of pile driving is the selection of hammers, piles, and cushions. In Chapter IV hints were given on how to approach such problems, by means of wave considerations. The objective of such investigations would be a closed form method for estimating the necessary properties of piles and pile driving equipment.

Regarding the measurements of pile top force and acceleration the following recommendations can be made:

(i) The transducer cushion (i.e. the cushioning between hammer and force transducer, initially added for obtaining smoother records) has to be reduced if not completely eliminated to obtain a faster impact.

(ii) Another type of signal conditioning equipment for strain has to be used for smaller time lags between force and velocity record.

As discussed in Chapter V care has to be taken in recording pile toe accelerations for piles with low resistance since it is possible that here up to twice the top accelerations

occur and thus, exceed the accelerometer capacity.

The results obtained from the present method were very encouraging. This method seems well suited to be employed in subsurface soil explorations. A related study is reported by Tsai, Schmid (19) where an instrumented penetrometer is used for data collection. However, the present method has the advantage of providing also knowledge about resistance forces acting along the pile skin.

Another important result of the studies presented in this paper was the improvement of an existing simplified prediction scheme for static bearing capacity. A further step to a realistic dynamic pile testing procedure will be to incorporate the Phase IIA scheme in a special purpose computer and to test the method at a sufficient number of piles in the field where common pile materials like timber and concrete should be included. Also, tests on piles of greater length and of variable cross section should be performed. The Phase III method should be modified such that a relatively simple computer can perform the necessary computations. This new computer should yield as an output the predictions of both maximum damping force and the static bearing capacity. With more results from piles tested under different conditions a statistical analysis should then be performed so that an answer about the reliability and precision of the method can be obtained. It would then be possible to recommend with confidence a design load for a certain dynamic prediction of static bearing capacity.

APPENDIX A1

Lumped Mass Analysis

1. Numerical Procedure

The problem is to find the displacements during dynamic loading of all pile elements into which the continuous pile was modeled. Given are either the force acting on the top element or its acceleration, both as a function of time, and various passive force boundary conditions for each element. These passive forces can be regarded as functions of displacement and velocity. In Appendix C a study will be presented on the physical model of resistance used, and its limitations.

The piles encountered during this project were, with only a few exceptions, steel pipes of constant cross section. The program therefore was set up for uniform cross section and steel elastic properties. However, the changes to a more general pile, for example tapered piles or steel piles filled with concrete, could be easily accomplished and examples on how to do it are given in the references, e. g. Ref. (9). The frequency of the top boundary condition is an important factor for the choice of the time increment, Δt. It is important that no extreme values of these functions are missed. If Δt is small enough, errors will be negligible (see Fig. A1-4). It is then possible to approximate the continuous boundary function by a sequence of straight lines. Consequently, it should be sufficiently accurate to express accelerations of pile elements as a sequence of straight lines as well. This leads to velocities and displacements being polynomials of second and third order.

Consider Fig. (A1.1). A continuous pile is replaced by n mass elements and n-1 interconnecting springs. The boundary conditions, either acceleration or force, are supposed to be measured at the middle of the top element. Then it can be justified to assign stiffnesses:

$$k = \frac{EA}{L} n \tag{A1.1}$$

to all the springs and masses:

$$M = \frac{1}{n} AL\rho \tag{A1.2}$$

to all elements.

Some resistance force $r_{i,j}$ acts on the i^{th} element at time $t_j = j.\Delta t$. Displacements, velocities, and accelerations of element i at time $t_j = j.\Delta t$ are $u_{i,j}$, $\dot{u}_{i,j}$ and $\ddot{u}_{i,j}$, respectively. The top element is acted upon by an active force f_j. Velocity and displacement are obtained from the piecewise linear acceleration using:

$$\dot{u}_{i,j} = \dot{u}_{i,j-1} + \frac{1}{2}(\ddot{u}_{i,j-1} + \ddot{u}_{i,j})\Delta t \tag{A1.3}$$

and

$$u_{i,j} = u_{i,j-1} + \dot{u}_{i,j-1}\Delta t + (\ddot{u}_{i,j} + 2\ddot{u}_{i,j-1})\frac{\Delta t}{6} \tag{A1.4}$$

Here a comparison with the method developed by Newmark (14) can be made.

Newmark proposed to use instead of Equation (A1.4) the following equation for computing the displacement

$$u_{i,j} = u_{i,j-1} + \dot{u}_{i,j-1}\Delta t + (\frac{1}{2} - \beta)\ddot{u}_{i,j-1}\Delta t^2 + \beta\ddot{u}_{i,j}\Delta t^2 \tag{A1.4a}$$

Comparing this equation with Equation (A1.4) it can be observed that β is the coefficient obtained by twice integrating a linearly increasing acceleration (e.g. $\ddot{u} = at \rightarrow u = \frac{1}{6}at^3$).

The force in the i-th spring at time t_j is

$$F_{i,j} = k(u_{i+1,j} - u_{i,j}) \tag{A1.5}$$

and applying Newton's Second Law to the i-th element, one obtains at a given time j:

$$M\ddot{x}_{i,j} = k(u_{i+1,j} - u_{i,j}) - k(u_{i,j} - u_{i-1,j}) - r_{i,j}$$

or

$$\ddot{x}_{i,j} = \frac{1}{M}\{k(u_{i+1,j} - 2u_{i,j} + u_{i-1,j}) - r_{i,j}\} \tag{A1.6}$$

Then $u_{i+1,j}$, $u_{i,j}$ and $r_{i,j}$ (a function of $u_{i,j}$ and $\dot{u}_{i,j}$) will be unknown in this equation, therefore, Equation (A1.4) is applied on both $u_{i+1,j}$ and $u_{i,j}$ to obtain:

$$\ddot{u}_{i,j} = \frac{1}{M + \frac{\Delta t}{3}}\{[u_{i+1,j-1}\Delta t + u_{i-1,j} - 2(u_{i,j-1} + \dot{u}_{i,j-1}\Delta t)$$

$$+ \frac{\Delta t^2}{6}(\ddot{u}_{i+1,j} + 2\ddot{u}_{i+1,j-1} - 4\ddot{u}_{i,j-1})]k - r_{i,j}\} \tag{A1.7}$$

Now, the only unknown left is $\ddot{u}_{i+1,j}$ if we determine $r_{i,j}$ by using $\dot{u}_{i,j-1}$ instead of $\dot{u}_{i,j}$ and $\dot{u}_{i,j-1}\Delta t$ instead of $u_{i,j}$. Except for the top and bottom element Equation (A1.7) can be used to compute $\ddot{u}_{i,j}$. For the first prediction $\ddot{u}_{i+1,j}$ is set to zero. For any later iteration step $\ddot{u}_{i+1,j}$ can be used as obtained in the previous

calculation, while $r_{i,j}$ is always computed using the previous results for $u_{i,j}$ and $\dot{u}_{i,j}$. Both $u_{i,j}$ and $u_{i,j}$ are readily obtained using Equations (A1.3) and (A1.4)

For the n-th element, i.e. the pile bottom (A1.7) reduces to:

$$u_{i,j} = \frac{1}{M + \frac{k\Delta^2}{6}} \{[(u_{n-1,j} - (u_{n,j-1} + \dot{u}_{n,j-1}\Delta t + \ddot{u}_{n,j-1}\frac{\Delta t^2}{3})] k - r_{i,j}\} \qquad (A1.8)$$

where r is the only unknown.

At the pile top the force f_j may be prescribed and the acceleration has to be computed, then:

$$\ddot{u}_{i,j} = \frac{1}{M + k\Delta t^2} \{[u_{2,j-1} + \dot{u}_{2,j-1}\Delta t - (u_{1,j-1} + \dot{u}_{1,j-1}\Delta t) + \frac{\Delta t^2}{6} (\ddot{u}_{2,j} + 2\ddot{u}_{2,j-1} - 4\ddot{u}_{1,j-1})K - f_j\} \qquad (A1.9)$$

where the only unknown is $\ddot{x}_{2,j}$ since a passive reaction is not assumed to act on the top element. If the acceleration $\ddot{u}_{1,j}$ is given as a boundary condition then the force has to be calculated from:

$$f_j = M\ddot{u}_{1,j} + K[u_{1,j} - u_{2,j-1} - \dot{u}_{2,j-1}\Delta t - (\ddot{u}_{2,j} + \ddot{u}_{2,j-1})\frac{\Delta t^2}{6}] \qquad (A1.10)$$

where again $\ddot{u}_{2,j}$ can be set to zero for the first step and equal to the previously calculated value for all later iteration steps.

Convergence will be reached when the relative difference between successive results is smaller than a chosen number ε. (The influence of the magnitude ε will be studied in the next section of this Appendix). It is possible to compare displacements, velocities or accelerations. Certainly acceleration will be the

most sensitive variable but it was found that a velocity controlled iteration yields good results. In case of an acceleration input condition on top of the pile, a check has to be performed on the calculated top force. Thus, the convergence criterion which has to be satisfied for all j can be written as

$$\frac{\text{new}(\dot{u}_{i,j}) - \text{old}(\dot{u}_{i,j})}{\text{new}(\dot{u}_{i,j})} < \varepsilon \quad i = 1,2,\ldots n \qquad \text{(A1.11)}$$

where $\dot{u}_{1,j}$ might be replaced by f_j.

2. Analysis Parameter Study

2.1 Number of Elements

The numerical method chosen can at best be expected to give the solution for the pile modeled as an N-degree of freedom system. The question, therefore, is how many elements are necessary to accurately represent the continuous pile. For purposes of comparison, using the same acceleration input, time interval and convergence criterion, a pile without reaction forces was analyzed divided into 5, 10, and 20 elements. The exact solution for the continuous pile is easily obtained for this case (see Appendix A3) and is given together with the lumped mass solution in Figure (A1.2). It should be noted that the actual pile length is not involved in this comparison because it is not a factor in the number of elements needed. As can be seen, while 5 elements represent a poor model, the 10 element system is already a good approximation to the actual solution. 20 elements give noticeable differences only where there are rapid changes of force. It can be deduced that 20 elements

will yield a very accurate solution while 10 elements give good qualitative results.

2.2 Time Increment

Once the number of elements has been determined the choice of a time increment is constrained. The reason for this is the occurence of instability of solution whenever the distance traveled by the stress wave in one time increment is constrained. Investigations into this phenomenon have been undertaken and are discussed by Crandall (17). The suggested limit imposed on Δt is

$$\Delta t \leq \frac{L}{c} \qquad \text{(A1.12,a)}$$

or since

$$c \leq \sqrt{\frac{E}{\rho}}$$

$$t = \sqrt{\frac{M}{K}} \qquad \text{(A1.12,b)}$$

Introducing

$$\phi = \frac{\Delta L}{\Delta t \cdot c} \qquad \text{(A1.13)}$$

as used by Smith (9) then $\phi > 1$ will always yield a stable solution. Figure (A1.3) shows again an exact solution and 3 solutions using $\phi = 1/2$ (unstable), $\phi = 1$ and $\phi = 2$. All 3 solutions were obtained for $n = 20$. The differences between $\phi = 1$ and $\phi = 2$ are very small and can be accounted for by observing that the input condition is not exactly the same when more time increments are placed on the sequence of straight lines. Figure (A1.4) shows what happens to the acceleration input data when used

with different lengths of time increment.

2.3 Convergence Criterion

Various calculations were performed using different ε and also calculations without any iteration. It is seen in Fig. (A1.5) that, whenever enough elements are chosen, say greater than 10, a number $\varepsilon < .1$ will be sufficient and that the iteration starts only to improve the solution after 2L/c. These comparisons, however, might yield quite different results when the solutions is carried forward over a longer time interval.

2.4 Computation Time

In order to draw conclusions about the accuracy and feasibility of the lumped mass analysis method the computation time has to be considered. The calculations listed in Table (A1.1) were performed on a Univac 1108 Computer. The program was written in Fortran V. The computer time in seconds is an approximation because time is listed only in half seconds. However, it can be seen that solutions using less than 3 seconds are not satisfactory. Using 30 elements did not give much improvement while computation time increased considerable (9.5 seconds!) The use of 20 elements together with $\phi = 1$ (Δt = .227 milliseconds in this case) gave a satisfactory result and used only 3 seconds. The result could not be much improved by halving the time increment which resulted in almost doubling the computation time. Note that the only good result for a pure prediction analysis took 2.5 seconds while the result between 2L/c and 4L/c is still quite erroneous as compared to the iterative

computation on line 2 which took only 3 seconds. The method of analysis has the advantage of accuracy and stability within the time domain considered. Only a few rules must be observed in choosing the necessary parameter, i.e. $\phi > 1$, $n > 10$ and $\varepsilon \leq .1$. The application of a predictor-corrector iteration seems justified when considering the increased accuracy in the time region after $2L/c$.

APPENDIX A2

Static Analysis

The resistance parameters obtained from dynamic analysis permits the computation of a load deformation curve to compare to a static load test. The soil parameters describe the shear resistance in the pile soil interface as a function of deformation. Actually, such an analysis should take into account the deformations of underlying soil strata. However, this would make necessary a much better knowledge of static soil behavior than can possibly be obtained from dynamic measurements. The analysis described below will give only results which can be used for correlating dynamic predictions to static measurement. It will, however, provide a valuable tool to obtain an estimate on the pile deformations to be expected. First, the pile is divided into n elements as it was done for the purpose of dynamic analysis in Appendix A1. The static soil resistance acting on the ith element is assumed to be directly dependent on the absolute pile displacement and is modeled again by an elastic plastic spring with stiffness $k_{si} = S_{o,i}/q_i$, where $S_{o,i}$ is the ultimate soil resistance and q_i the quake of the shear resistance at the element.

Under these assumptions the load versus deformation curve of any pile element will be a piecewise linear function. Once all displacements are larger than the quake the ultimate bearing capacity has been reached and no more load increase can be obtained.

Mathematical Formulation

Consider the i-th element in Figure A-1. Using the same notation as in Appendix A1 its equilibrium condition can be written as:

$$k(u_{i-1} - u_i) + k(u_{i+1} - u_i) = k_{si}u_i^* \qquad \text{(A2.1)}$$

where

$$u_i^* = \begin{cases} u_i \text{ for } u_i \leq q_i \\ q_i \text{ for } u_i > q_i \end{cases}$$

Thus, for $u_i \leq q_i$ Equation (A2.1) can be written as

$$-u_{i-1} + (2 + k_s/k)\, u_i - u_{i+1} = 0 \qquad \text{(A2.2a)}$$

and after the displacement has exceeded the quake

$$-u_{i-1} + 2u_i - u_{i+1} = \frac{k_{si}}{k} q_i \qquad \text{(A2.2b)}$$

For the first element on which no reaction forces were assumed to act (Appendix A3) the equilibrium equation becomes

$$u_1 - u_2 = P/k \qquad \text{(A2.3)}$$

where P is the load applied at the top of the pile. At the tip

$$-u_{n-1} + u_n(1 + k_s/k) = 0 \text{ for } u \leq q_n \qquad \text{(A2.4a)}$$

or

$$-u_{n-1} + u_n = (k_s/k)q_n \quad \text{otherwise.} \qquad \text{(A2.4b)}$$

Thus, a system of n equations with n unknowns is obtained which has to be solved for any interval between two consecutive yields of shear resistances. Since shear resistances are acting on n-1 elements this means solving n-1 times.

The procedure followed here uses the same approach as would be followed in a static load test namely first some load P^1 is applied on the top and then the deflections u_i^1 are calculated for all elements. The next step is to determine which of the springs will yield first, this can be done by investigating the ratios u_i^1/q_i. If their maximum happens to be u_j^1/q_j then the first spring to yield will be located at the j-th element. Because of linearity, the displacements for the instant when the j-th ultimate shear is reached can be calculated from proportionality

$$u_{i,j} = u_i^1 \cdot \frac{q_j}{u_j} \tag{A2.5}$$

and the force on top of the pile

$$P_j = P^1 \cdot \frac{q_j}{u_j} \tag{A2.6}$$

This way the first point of the load deflection curve is obtained when plotting P_j versus $u_{i,j}$.

A new system of equations has to be set up now by writing the j-th equation using (A2.2b) instead of (A2.2a). The new system can be solved when using $P^2 = P_j + \Delta P$ where ΔP is an arbitrary load increase and following the same routine as decribed above.

This was n-1 systems of linear equation each having n unknowns and n equations have to be solved. This can be done conveniently by means of iteration always using the previous result as an initial guess.

Results from this analysis were used and are demonstrated in Chapter III for correlating soil resistance predictions with results from actual static load tests.

APPENDIX A3

Wave Propagation in a Pile Under Impact

1. Force and Velocity Relation in a Stress Wave

If $u(x,t)$ is the displacement of a particle in a uniform and elastic rod at dixtance x from some fixed coordinate origin at time t then the governing differential equation - the so-called wave equation - is

$$\frac{\partial^2 u}{\partial t^2} = c^2 \frac{\partial^2 u}{\partial x^2} \tag{A3.1}$$

where $c^2 = E/\rho$.

E and ρ are the Young's Modulus and mass density of the pile material, respectively. The general solution of the equation is

$$u(x,t) = f(x + ct) + g(x - ct) \tag{A3.2}$$

which is easily checked by back substitution. The general solution can be interpreted physically by giving t a fixed value t_1. Then u is a function of x only and can be split into two components: $f(x + ct_1)$ and $g(x - ct_1)$. At a later time t_2

$$f(x + ct_2) = f(x + c(t_2 - t_1) + ct_1) \quad \text{and}$$

$$g(x - ct_2) = g(x - c(t_2 - t_1) - ct_1).$$

If, therefore, a distance $c(t_2 - t_1)$ is subtracted from x then the station is found at which f has the value at time t_2 that it had at x at time t_1; g will have the same value at $x + c(t_2 - t_1)$ at time t_2 which it had at time t_1 at x. In other words, if f and g are considered to be displacement waves then f travels in the negative x-direction and g travels in the positive x-direction, bot having speed c.

Differentiating Equation (A3.2) with respect to time leads to an expression for the velocity v(x,t) of a particle

$$v(x,t) = c\left(\frac{\partial f(\eta)}{\partial \eta} - \frac{\partial g(\mu)}{\partial \mu}\right) \tag{A3.3}$$

where $\eta = x + ct$ and $\mu = x - ct$. Equation (A3.3) can be written as

$$v(x,t) = v_f(x + ct) + v_g(x - ct) \tag{A3.4}$$

thus, v can also be described by two waves v_f and v_g which travel in opposite directions.

Now, suppose that the shape of the functions f and g and, therefore, u(x,t) is known at a certain time t. Then the strain, ε is obtained by differentiating u(x,t) with respect to x

$$\frac{\partial u}{\partial x} = \varepsilon(x,t) = \frac{\partial}{\partial x}\left(f(x + ct) + g(x - ct)\right)$$

or

$$\varepsilon(x,t) = \frac{\partial f(\eta)}{\partial \eta} + \frac{\partial g(\mu)}{\partial \mu} \tag{A3.5}$$

The advantage of using derivatives with respect to η or μ becomes apparent since these derivatives express the behavior of the derivative with respect to both x and t. Using the rod cross sectional area A and taking compressive forces positive, the force F(x,t) in the wave can be calculated

$$F(x,t) = (AE/c)\left(-v_f(x + ct) + v_g(x - ct)\right) \tag{A3.6}$$

Thus, there exists a simple relation between particle velocity and force in a stress wave, the force being proportional to the velocity by a factor AE/c. The force will be compressive when the velocities of particles and wave propagation have the same direction and it

will be a tension force otherwise.

2. Boundary Conditions

So far, only the homogeneous differential equation has been considered and nothing has been said about boundary conditions or external forces. Since the differential equation is linear, superposition is valid, so that a case of complicated boundary conditions can be split into several basic types of easily solvable problems. If the boundary conditions were nonlinear then a result can be obtained by assuming piecewise linear boundary conditions and superimposing their effects. A wave reaching the end of the rod might encounter either prescribed force or displacement conditions. This problem can be split into the case where the wave travels in a rod with homogeneous, i.e. zero force or displacement, boundary conditions plus the case where no wave is present but non zero end forces or displacements. The case where external forces are acting along the rod may also be treated separately and then be superimposed to the homogeneous solution. Prescribed displacements have to be considered at the end of the rod only. Therefore, four basic conditions must be treated

(i) Wave approaching a free end,

(ii) Wave approaching a fixed end,

(iii) Prescribed force acting at a point along the rod,

(iv) Prescribed displacements at the end of the rod.

Case (i) Wave in a Rod with Free End

Consider Fig. (A3.1) where on the left a wave $g(x - ct)$ is

shown approaching the free end (x = L) of the rod. Connected to it on the right is an imaginary rod along which f(x + ct) travels in negative x-direction chosen so

$$f(2L - x + ct) = g(x - ct) \tag{A3.7}$$

Therefore,

$$\frac{\partial f}{\partial x} = - \frac{\partial g}{\partial x}$$

Both waves will arrive at x = L at the same time. From superposition the displacement and strain can be calculated

$$u(L,t) = f(L + ct) + g(L - ct) = 2f(L + ct)$$

$$\varepsilon(L,t) = \frac{f(L + ct)}{x} + \frac{g(L + ct)}{x} = 0$$

Thus the boundary condition of a free end is satisfied. The wave f(x + ct) will now travel in negative x-direction through the rod. It is called a reflection wave. As compared to the initiating wave g(x - ct) it will cause displacements of the same sign but forces of opposite sign. The displacement at the free end will be twice that of the approaching wave.

Case (ii) Wave Approaching a Fixed End

The method of choosing an imaginary rod is used again for the case where the displacement of the end of a rod has to be zero. In this case, however, the wave traveling in the negative x-direction is chosen so that

$$f(2L - x + ct) = -g(x - ct) \tag{A3.8}$$

and, therefore, $\frac{\partial f}{\partial x} = \frac{\partial g}{\partial x}$. As a result of superposition the force at the fixed end will be doubled while the displacements cancel.

The reflection wave will propagate displacements of opposite direction but forces of the same sign as the initiating wave.

Case (iii) Prescribed Force Acting at a Point Along the Rod

If a force is applied at $x = x^*$ along the rod then the continuity condition requires

$$u(x^*_L,t) = u(x^*_R,t) \tag{A3.9}$$

This can also be written in terms of velocity

$$\frac{\partial u(x^*_L,t)}{\partial t} = \frac{\partial u(x^*_R,t)}{\partial t} \tag{A3.10}$$

where x^*_L and x^*_R are on the left and the right side of the loaded cross section, respectively (Figure A3.2).

Also the condition of equilibrium has to be satisfied, i.e.

$$AE\left(\frac{\partial u(x^*_L,t}{\partial x} - \frac{\partial u(x^*_R,t)}{\partial x}\right) = F_A(x^*,t) \tag{A3.11}$$

where $F_A(x^*,t)$ is the applied force at $x = x^*$ and time t. Now recalling Equations (A3.3) and (A3.5), Equations (A3.10) and (A3.11) can be satisfied by choosing

$$\frac{\partial f(\eta)}{\partial \eta}\bigg|_{x=x^*_L} = \frac{\partial g(\mu)}{\partial \mu}\bigg|_{x=x^*_R} = \frac{1}{2}F_A(x^*,t)/EA \tag{A3.12}$$

and

$$\frac{\partial f(\eta)}{\partial \eta}\bigg|_{x=x^*_R} = \frac{\partial g(\mu)}{\partial \mu}\bigg|_{x=x^*_L} = 0 \tag{A3.12}$$

Substituting these two conditions in Equation (A3.10) leads to

$$c[\tfrac{1}{2}F_A(x^*,t)/AE + 0] = c[0 + \tfrac{1}{2}F_A(x^*,t)/AE]$$

thus, satisfying the continuity condition.

Similarly it proves that the equilibrium condition is satisfied. Figure (A3.2) shows that both waves carry a force of one half of

the applied force while the velocities are in both waves the same having the same direction as the applied force and magnitude $\frac{1}{2}F_A(x^*,t)c/EA$.

The case where the force is acting at the end of the rod can be deduced since one of the half-waves is immediately reflected and superimposed to the other one. Therefore, a wave will travel away from the end with particle velocity

$$\frac{\partial u(x,t)}{\partial t} = cF_A(t - (L - x)/c) \qquad \text{(A3.14)}$$

and strain

$$\varepsilon(x,t) = F_A(t - (L - x)/c)/AE \qquad \text{(A3.15)}$$

Case (iv) Prescribed Displacements at the End of the Rod

The case of a displacement condition a point along the rod will not be discussed since this is equivalent to a rod of shorter length with prescribed end displacement. A displacement prescribed at the end of a rod is equivalent to a prescribed velocity: $v_A(L,t)$. From the force velocity proportionality relation this can be considered a force condition where the force has to be chosen as $F_A(L,t) = v_A(L,t)EA/c$. Thus Case (iii) can be applied.

3. Superposition of Waves

In this section certain special cases will be treated where the findings of Section 2 have to be applied. These special cases will be needed in treating problems where external forces act along the pile together with prescribed end conditions.

(i) Free Pile Under Known Velocity at the Top

Suppose a velocity $v_A(t)$ which is zero for $t < 0$ and imposed

on the top of a pile of length, L, and it is desired to know the top force necessary to maintain this velocity when no other forces are acting along the pile.

As long as the wave created by $v_A(t)$ has not yet reached the free end (i.e. for $t < L/c$) a pile particle at a point has velocity

$$v_i(t) = v_A(t - x_i/c).$$

At time $t = L/c$ the wave reaches the free end of the pile and case (i) of Section 2 holds. Thus, a reflection wave having velocities of the same sign but opposite forces will travel back up the pile. The velocity at a station $x - x_i$ becomes for $t \leq \frac{2L + x_i}{c}$

$$v_i(t) = v_A(2L - x_i)/c) + v_A(t - x_i/c) \qquad \text{(A3.16)}$$

A new reflection wave will be generated when this "up"-traveling wave reaches the top since here the velocity is prescribed. Case (ii) of Section 2 describes this situation of a fixed end. This second reflection requires a force; therefore, the proportionality between applied velocity and top forces will not hold any longer. The force at the top of the free pile may be denoted by $F_f(t)$, then for $t<2L/c$

$$F_f(t) = v_A(t)EA/c$$

and for $2L/c \leq t < 4L/c$

$$F_f(t) = [v_A(t) - 2v_A(t - 2L/c)]EA/c \qquad \text{(A3.17)}$$

At a time $t = 3L/c$ the wave will be again reflected at the bottom end (It had been reflected at the top of time $2L/c$.) At time $t = 4L/c$ the wave has to be reflected again at the top but this time it has the opposite stress due to the previous reflection at the free end. In

general for, $\frac{2Lr}{c} \leq t \leq \frac{2L}{c}(r + 1)$

$$F_f(t) = \frac{EA}{c}[v_A(t) + 2\sum_{j=1}^{r} v_A(t - j\frac{2L}{c})(-1)^j] \qquad (A3.18)$$

where $r = 0,1,2,\ldots$, stands for the time interval considered. Equation (A3.18) gives the exact solution for a given top velocity and no reaction forces. This equation can be used as a check on the lumped mass analysis. Comparative results of this kind are shown in Appendix A1. Furthermore, if this solution is subtracted from the measured force then the Measured Delta curve is obtained as defined in Chapter II.

Equation (A3.16) gives an expression for the velocity at some point in the pile for times $t < (2L - x_i)/c$. The equation can be extended for times $\frac{2Lr}{c} \leq t < \frac{2L(r + 1)}{c}$, $r = 0,1,2,\ldots$

$$v_i(t) = \sum_{j=0}^{r}(-1)^j[v_A(t - \{2jL + x_i\}/c) - v_A(t - \{(j + 1)2L - x_i\}/c)] \qquad (A3.19)$$

(ii) External Force Acting on a Pile With Fixed Top and Free Bottom

The force denoted by $R_i(t)$, is assumed to act upwards. If it is acting at $x = x_i$ then the results of Section A3.2 case (iii) apply. Thus, two waves are caused traveling in both directions and having particle velocities (at $x = x_i$ and time t) $v_r(t) = -\frac{c}{2EA} R_i(t)$ and the force in the waves $F_r(t) = \pm 1/2R(t)$, i.e. a compression in the upwards and tension in the downwards traveling wave. The reaction force $F_{top}(t)$ on the fixed top of the pile due to this velocity will be a compression force of twice the magnitude of the

force in the wave (Case (ii) Section 2). The upwards traveling wave will arrive at the top at a time x_i/c after it was applied, hence

$$F_{top}(t) = R_i(t - x_i/c) \qquad \text{(A3.20)}$$

which is valid for a time as long as it takes the initially downwards traveling wave to reach the top after reflection at the bottom. This reflection at the free bottom end causes the initially downwards traveling wave to change the sign in force (Case (i) Section 2) and therefore, is also a compression wave after reflection. Reaching the top at a time $(2L - x_i)/c$ after it was generated by the resistance force this wave also will produce twice the force at the top which it was propagating. The next wave to arrive at the top will be the initially upwards traveling wave, its sign will be converted so that a tension wave arrives.

This way the reaction at the fixed pile top due to $R_i(t)$ can be calculated for $0 \leq t < 4L/c$

$$F_{top}(t) = R_i(t - \frac{x_i}{c}) + R_i(t - \frac{2L - x_i}{c}) - R_i(t - \frac{2L + x_i}{c}) - R_i(t - \frac{4L - x_i}{c}) \qquad \text{(A3.21)}$$

For later times it can be observed that all the waves which arrived at a time t_1 at the top have in the mean time changed their sign twice thus arriving again with the same sign at a time $t_1 + 4L/c$. This result can be expected since a pile of length L has a lowest natural frequency of $c/4L$, its meaning is that in absence of external forces a harmonic behavior can be observed. Therefore, for times

$r\ 4L/c \leq t < (r + 1)\ 4L/c$

$$F_{top}(t) = \sum_{j=0}^{r} [R_i(t - \frac{x_i}{c} - j\frac{4L}{c}) + R_i(t - \frac{2L - x_i}{c} - j\frac{4L}{c}) + R_i(t - \frac{2L + x_i}{c} - j\frac{4L}{c}) - R_i(t + \frac{x_i}{c} - (j + 1)\frac{4L}{c})] \quad \text{(A3.22)}$$

and r = 0,1,2,..n indicates the time interval considered.

Somewhat more complicated is the problem to obtain the particle velocities at a point $x = x_h$ when the load, $R_i(t)$ is acting at $x = x_i$. The problem can be split in two parts first considering the wave which is initially moving upwards and then second the wave which initially moves downwards. Both of these waves have a particle velocity $-c/2EA\ R_i(t)$. In order to facilitate the derivation it is further assumed that $x_h > x_i$. Then the velocity $v_{h,up}(t)$ at $x = x_h$ due to the upwards traveling wave obtains its first contribution after a time $(x_h + x_i)/c$, i.e. the time necessary for the wave to reach the top and upon reflection the station $x = x_h$. The wave will again be reflected at the bottom end with no sign change in velocities and reach $x = x_h$ a second time with the same sign in velocities. Thus, when observing the wave's action at $x = x_h$ for a time $t < 4L/c$ then

$$v_{h,up}(t) = \frac{c}{EA}[R_i(t - \frac{x_h + x_i}{c}) + R_i(t - \frac{2L + x_i - x_h}{c}) - R_i(t - \frac{2L + x_h + x_i}{c}) - R_i(t - \frac{4L + x_i - x_h}{c})] \quad \text{(A3.23)}$$

Similarly one can find how the initially downwards traveling wave influences the velocity at $x = x_h$

$$v_{h,down}(t) = \frac{c}{2EA}[-R_i(t - \frac{x_h - x_i}{c}) - R_i(t - \frac{2L - x_i - x_h}{c}) + R_i(t - \frac{2L + x_h - x_i}{c}) + R_i(t - \frac{4L - x_i - x_h}{c})] \quad (A3.24)$$

Observing that the waves arrive with the same sign of force and velocity after every 4L/c then superimposing the results from Equation (A3.23) and (A3.24) the velocity $v_h(t)$ due to $R_i(t)$ becomes for $r\frac{4L}{c} \leq t \leq (r+1)\frac{4L}{c}$

$$\begin{aligned} v_h(t) = \frac{c}{2EA}\sum_{j=0}^{r}\{&R_i(t - \frac{x_h + x_i}{c}) + R_i(t - \frac{2L + x_i - x_h}{c} - j\frac{4L}{c}) \\ &- R_i(t - \frac{2L + x_h + x_i}{c} - j\frac{4L}{c}) - R_i(t - \frac{x_i - x_h}{c} \\ &\qquad - (j+1)\frac{4L}{c}) \\ &- R_i(t - \frac{x_h - x_i}{c} - j\frac{4L}{c}) - R_i(t - \frac{2L - x_i - x_j}{c} - j\frac{4L}{c}) \\ &+ R_i(t - \frac{2L + x_h - x_i}{c} j\frac{4L}{c}) + R_i(t - \frac{-x_i - x_h}{c} \\ &\qquad -(j+1)\frac{4L}{c})\} \end{aligned} \quad (A3.25)$$

where again r = 0,1,2,..., indicates the time interval considered.

(iii) Free Pile With Known Force at the Top

In this case a force $F_A(t)$ is prescribed at the top and no forces act along the pile. It is desired to obtain an expression for the velocity at the pile top $v_{top}(t)$, due to this force. The reflections of waves at both ends of the pile have force but no displacement

restrictions. Thus, if the applied wave applies compressive strains then all the reflection waves will have tensile velocities. Thus, reflections will always add to the top velocity on every wave arrival at the top. From proportionality and due to the discussed reflections the result can be readily obtained.

$$v_{top}(t) = \frac{c}{EA}(F_A(t) + 2F_A(t - 2L/c) + 2F_A(t - 4L/c) + \ldots) \quad (A3.26)$$

or using the notation as above Equation (A3.26) can be rewritten to yield for $r\frac{2L}{c} \leq t \leq (r + 1)\frac{2L}{c}$

$$v_{top}(t) = \frac{c}{EA}(F_A(t) + 2\sum_{j=1}^{r} F_A(t - j\frac{2L}{c})) \quad (A3.27)$$

(iv) External Force Acting on a Pile with Free Top and Bottom

The external force may again be denoted by $R_i(t)$ and act at $x = x_i$. The reflections will again be of such a nature that the waves arriving at the top always add to the top velocity $v_{top}(t)$ if $R_i(t)$ does not change sign. Hence for $0 \leq t < 2L/c$

$$v_{top}(t) = \frac{-c}{EA}[R_i(t - \frac{x_i}{c}) + R_i(t - \frac{2L - x_i}{c})] \quad (A3.28)$$

and for $r\ 2L/c \leq t \leq (r + 1)2L/c$

$$v_{top}(t) = \frac{-c}{EA}\sum_{j=0}^{r}\{R_i(t - \frac{x_i}{c} - j\frac{2L}{c}) + R_i(t - \frac{2L - x_i}{c} - j\frac{2L}{c})\} \quad (A3.29)$$

4. Soil Resistance Forces

This section will derive the relation between the velocity on top of the pile and the magnitude of reaction forces which are assumed to depend on the pile displacements and pile velocity. A discussion

of this soil model is given in Appendix C. For ease in computation the resistance forces are assumed to act at a finite number of stations at uniform spacing so that their application in a lumped mass analysis is possible. The model splits the soil resistance force $R_i(t)$, forces acting at time t and $x = x_i$ to two components: a static component called the shear resistance $S_i(t)$ dependent upon the pile displacements and a dynamic component $D_i(t)$ referred to as the dynamic or damping resistance which is dependent on the velocity at $x = x_i$.

(i) Shear Resistance Forces

The shear resistance force acting at $x = x_i$ and time t whose force displacement relation is illustrated in Figure (2.2) can be expressed as

$$S_i(t) = \begin{cases} k_i u_i(t) & \text{for } u_i(t) < q_i \quad \text{(a)} \\ S_{i,o} & \text{for } u_i(t) > q_i,\ v_i(t) > 0 \quad \text{(b)} \\ S_{i,o} - k_i(\max u_i - u_i) & \text{for } u_i(t) < \max u_i \quad \text{(c)} \end{cases} \tag{A3.30}$$

where k_i is the soil stiffness, $S_{i,o}$ is the ultimate shear resistance, $u_i(t)$, $v_i(t)$ are pile displacement and velocity, respectively and $\max u_i$ is the maximum displacement before or at time t. As a theoretical example how a shear versus time relation can be developed it is now assumed that only one shear force is acting, that it is caused by a velocity $v_A(t)$ which is applied at the pile top and that at the pile bottom is a free end. This example will demonstrate the main features of wave propagation effect of a shear force. Subsequent quantitative results, however, will be much easier

obtained by a lumped mass analysis. The shear versus displacement relation requires the individual treatment of the three different laws described in Equations (A3.30 a, b, c).

Suppose the wave caused by the hammer blow is described by a pile top velocity $v_A(t)$. Then at a time x_i/c the wave will arrive at $x = x_i$. Thus, $v_i(t)$, $u_i(t)$ the velocity and displacement of the pile are zero at $x = x_i$ before x_i/c. When the wave arrives the shear resistance force $S_i(t)$ will tend to resist the motion of the pile and reduce the applied velocity by sending out waves in both directions along the pile. This reduction in velocity is proportional to the acting shear resistance force $S_i(t)$ which in turn is proportional to the actual displacement. Thus, if x_i is far enough from the ends of the pile so that no reflection wave will arrive within the time interval now considered then the actual velocity $v_i(t)$ at $x = x_i$ is given by

$$v_i(t) = v_A(t - x_i/c) - c/2EA\ S_i(t) \qquad \text{(A3.31)}$$

For the actual displacement $u_i(t)$ being smaller than the quake q_i the shear resistance is given by Equation (A3.30a).

$$S_i(t) = k_i u_i(t)$$

but $v_i(t) = \dfrac{du_i(t)}{dt}$ so that Equation (A3.31) can be written as

$$\frac{du_i}{dt} + k_i \frac{c}{2EA} u_i(t) = v_A\left(t - \frac{x_i}{c}\right) \qquad \text{(A3.32)}$$

By introducing an integration variable s and initial condition $u_i(t - x_{i/c}) = 0$ and by defining $\tau = t - x_i/c$ then the solution of Equation (A3.32) yields the actual displacement $x = x_i$

$$u_i(\tau) = \int_0^{\tau} v_A(s)\exp\{(-\frac{ck_i}{2EA}(s - \tau)\}ds \qquad (A3.33)$$

Defining t_{i1} as the time when $u_i(t)$ becomes equal to q_i then Equation (A3.33) is valid for $x_i/c \leq t \leq t_{i1}$. At time t_{i1} the shear force reaches its ultimate value. Therefore, from Equation (A3.31)

$$v_i(t) = v_A(t - x_i/c) - c/2EA\ S_{i,o} \qquad (A3.34)$$

and

$$u_i(t) = q_i + \int_{t_{i1}}^{t_{i,o}} v_A(t - \frac{x_i}{c})dt - \frac{c}{2EA} S_{i,o}(t - t_{i1}) \qquad (A3.25)$$

This equation is valid until a time $t_{i,o}$ when the maximum displacement is reached. This happens when $v_i(t)$ becomes zero, thus, from Equation (A3.34)

$$v_A(t_{i,o} - x_i/c) = c/2EA\ S_{i,o} \qquad (A3.36)$$

These equations assume no reflection waves have reached $x = x_i$.

In most of the cases the velocity $v_A(t)$ stays greater than one half of the proportional resistance forces for a time until the first reflection wave returns from the bottom end. Also the initial portion of the reflection wave which carries the effects of $S_i(t) < S_{i,o}$ has usually passed the station $x = x_i$ before $t_{i,o}$ is reached. Then the above condtions (A3.36) becomes

$$v_A(t_{i,o} - x_i/c) + v_A(t_{i,o} - \frac{2L - x_i}{c}) = \frac{c}{EA} S_{i,o} \qquad (A3.37)$$

Here the first term on the left hand side is due to the directly arriving wave caused by the impact wave, the second is also due to the impact wave but after reflection at the bottom and the term on the right hand side is due to the effects of both the ultimate shear

resistance at time $t_{i,o}$ plus the shear acting at a time $2(L - x_i)/c$ earlier.

After $t = t_{i,o}$ unloading will start i.e. the shear resistance force will decrease by virtue of Equation (A3.30c). Unloading effects will be investigated in the later section using a simple example. Their effect at the top of the pile will, in general, be observed at a later time and are, therefore, not considered in detail here.

Examples for shear resistance forces and their effects on the pile top will be given below and in Chapter II.

(ii) Dynamic Resistance Force Acting at the Pile

The dynamic resistance law is assumed to follow the law of a linear viscous damper. If the damping constant at a point $x = x_i$ is denoted by d_i and the actual velocity by $v_i(t)$ then the dynamic resistance force $D_i(t)$, defined to be a concentrated force, is

$$D_i(t) = d_i v_i(t) \qquad \text{(A3.38)}$$

The actual velocity at $x = x_i$ is determined by the particle velocities of the two waves in the pile v_f and v_g (Equation (A3.4)) traveling in negative and positive x-direction, respectively. Further, the effect of the damper itself has to be superimposed. The particle velocity at $x = x_i$ due to the dynamic resistance is again determined from Equation (A3.12). Thus, if the velocities of the waves arriving at $x = x_i$ at time t add up to $v_{i,a}(t)$ then the actual velocity is

$$v_i(t) = v_{i,a}(t) - \tfrac{1}{2}D_i(t)\, c/EA$$

and after inserting Equation (A3.38) this becomes

$$v_i(t) = v_{i,a}(t)/(1 + d_i c/EA)$$

Therefore the damping force can be calculated from

$$D_i(t) = d_i(v_{i,a}(t)/(1 + d_i c/EA) \qquad \text{(A3.39)}$$

This dynamic resistance force sends out waves in either direction having particle velocity $-\frac{1}{2}D_i(t)c/EA$. While for times $x_i/c < t < \frac{2L - x_i}{c}$ or $x_i/c < t < 3x_i/c$ after one of the waves resulting from $D_i(t)$ or the impact wave reach again $x = x_i$ after having been reflected at top or bottom end of the pile. If the damper is located at the bottom end of the pile then simpler superpositions occur. In this case the initiating wave, $v_{n,a}(t)$, will be reflected at the same time when the damper reacts, thus

$$v_n(t) = 2v_{n,a}(t) - D_n(t)\frac{c}{EA} \qquad \text{(A3.40)}$$

and the damping force exerted by a damper located at the bottom end having damping coefficient d_n is determined by

$$D_n(t) = \frac{2v_{n,a}(t)}{1 + cd_n/EA}\, d_n \qquad \text{(A3.41)}$$

If the only wave arriving is that due to the impact then

$$D_n(t) = \frac{2v_A(t - L/c)}{1 + cd_n/EA}\, d_n \qquad \text{(A3.42)}$$

(iii) Dynamic and Shear Resistance Force Together

An important result can be obtained for the specific case where a shear resistance force $S_n(t)$ and a damper having coefficient d_n resist together the motion at the pile bottom. For clarity no other resistance forces are assumed to act along the pile.

Considering only a time after the bottom displacement has become greater than the quake and only before a time 3L/c, i.e. before the impact wave arrives a second time at the bottom, then the only one wave arriving is due to the impact. Thus, because of immediate reflection alone

$$v_{n,a}(t) = 2v_A(t - L/c).$$

Due to the shear a reaction wave will be sent upwards having particle velocity

$$v_s(t) = - \frac{c}{EA} S_{n,o}$$

and due to the damper

$$v_d(t) = - \frac{c}{EA} D_n(t)$$

But

$$D_n(t) = d_n v_n(t)$$

where $v_n(t)$ is the actual pile toe velocity given by superposition of all waves. Thus,

$$v_n(t) = 2v_A(t - L/c) - c/EA(S_{n,o} + d_n v_n(t))$$

which leads to

$$v_n(t) = \frac{2v_A(t) - c/EA\ S_{n,o}}{1 + cd_n/EA} \qquad \text{(A3.43)}$$

and the damping force $D_n(t)$, therefore, becomes

$$D_n(t) = d_n \frac{2v_A(t) - c/EA\ S_{n,o}}{1 + cd_n/EA} \qquad \text{(A3.44)}$$

5. Resistance Delta Curves

In ChapterII Delta curves were introduced as a means of studying the effects of the actual resistance forces at the pile top by

means of the Measured Delta curves here referred to as $\Delta(t)$. The effect of resistance forces acting at $x = x_i$ due to the chosen soil model were investigated by means of Resistance Delta curves, called $\Delta_i(t)$.

All Delta curves are defined to be the effects of the acting resistance forces (depending on pile displacements and velocities) at a fixed pile top when the pile tip is a free end.

In the previous section the resistance forces had been derived for specific cases as a function of time, depending on the impact velocity $v_A(t)$. In the following paragraphs examples will be given using either a theoretical resistance versus time relation or based on a simplified top input velocity $v_A(t)$. Since a resistance Delta curve, $\Delta_i(t)$, for a force $R_i(t)$ acting at $x = x_i$ is the force on the fixed top of a pile under action of $R_i(t)$ only, the Delta curve is expressed by Equation (A3.22) as derived in Section A3.3. Thus

$$F_{top}(t) = \Delta_i(t) = \sum_{j=0}^{r} \{R_i(t - \frac{x_i}{c} - j\frac{4L}{c}) + R_i(t - \frac{2L - x_i}{c} - j\frac{4L}{c}) - R_i(t - \frac{2L + x_i}{c} - j\frac{4L}{c}) - R_i(t - \frac{4L - x_i}{c} - j\frac{4L}{c})\} \tag{A3.45}$$

for $r4L/c \leq t \leq (r + 1)4L/c$ where r, therefore, indicates the time interval considered.

Suppose a shear resistance force acting at $x = x_i$ is given by

$$S_i(t) = H(t - \frac{x_i}{c})S_{i,o} \tag{A3.46}$$

This shear resistance force has zero magnitude until $t = x_i/c$ and is constant thereafter, as described by the unit step function $H(t - x_i/c)$. Using Equation (A3.45)

$$\Delta_i(t) = S_{i,o} \sum_{j=0}^{r} \{H(t - \frac{2x_i}{c} - j\frac{4L}{c}) + H(t - \frac{2L}{c} - j\frac{4L}{c}) - H(t - \frac{2L - 2x_i}{c} - j\frac{4L}{c}) - H(t - \frac{4L}{c} - j\frac{4L}{c})\} \qquad (A3.47)$$

Both shear resistance force and the corresponding Delta curve are plotted in Figure (A3.3 a,b) for two cases of shear resistance namely $x_i = L/2$ and $x_i = L$, respectively. In comparing Figures (A3.3 a,b) with Figures (2. 8,9) it can be observed that the simplified resistance law as expressed by Equation (A3.46) gives a good approximation of the actual circumstances. In order to study the effect which unloading has on a shear resistance Delta curve a second example will now be given for a shear resistance acting at $x = x_i$ given by

$$S_i(t) = S_{i,o}[H(t - x_i/c) - \tfrac{1}{2}H(t - \tfrac{2L}{c})] \qquad (A3.48)$$

This means that at time 2L/c the resistance force is assumed to decrease to half its ultimate value. Figure (A3.4a) shows the shear versus time relation for $x_i = L/2$ and $x = L$. The resistance Δ-curves obtained from applying Equation (A3.45) are shown in Figure (A3.4b) . The terms resulting from applying Equation (A3.45) are individually shown before they are added. Worth noting in this figure is the fact that negative resistance Delta values are obtained for $4L/c < t < 6L/c$ and it can be concluded that negative values

in the Measured Delta curve, as for example in Figures (2.5,6,7), will arise from decreasing resistance forces, either shear or dynamic. Somewhat more complicated is obtaining a dynamic resistance force as a function of time even if an idealized velocity input is used.

In order to compute $D_i(t)$ the velocity of the pile particles at $x = x_i$ has to be found. This velocity multiplied by the damping coefficient d_i yields the damping resistance force. If the sum of the particle velocities of the two waves arriving from either direction at $x = x_i$ at time t is denoted by $v_{i,a}(t)$ then the actual velocity of the particles at the damper, $v_i(t)$, can be computed by use of Equation (A3.39).

$$v_i(t) = \frac{d_i}{1 + \frac{d_i c}{EA}} v_{i,a}(t) = \alpha_i v_{i,a}(t) \qquad \text{(A3.49)}$$

Thus,

$$\alpha_i = \frac{d_i}{1 + d_i c/EA} \qquad \text{(A3.50)}$$

It should be noted that the waves arriving from either direction at $x = x_i$ can be the result of a superposition of various other waves. A general derivation of $D_i(t)$ becomes very involved and amounts to a complicated bookkeeping of all the waves traveling through the pile. Therefore, two special cases will be presented as an illustration of the main features of dynamic resistance forces. A damper at $x = L/2$ and a damper at $x = L$ will be chosen as examples and the computation limited to times $t < 4L/c$.

In order to find out the magnitude of the velocities of the arriving waves applied velocity and velocities due to the damping force will be considered separately. If a velocity $v_A(t)$ is applied at the top of the pile at times t then due to this velocity alone the velocity at x = L/2 for times $t \leq 4L/c$ can be computed from Equation (A3.19) which leads to

$$v_{i,A}(t) = v_A(t - L/2c) + v_A(t - 3L/2c) - v_A(t - 5L/2c) - v_A(t - 7L/2c) \quad \text{(A3.51)}$$

If a damping force $D_i(t)$ is acting at x = L/2 at time t then two waves are generated traveling upwards and downwards away from the location of the damper both having the same particle velocity $-cD_i(t)/2EA$. Due to the initially upwards traveling wave the pile at x = L/2 is subjected to the velocity

$$v_{i,up} = \frac{c}{2EA}[D_i(t - L/c) + D_i(t - 2L/c) - D_i(t - 3L/c)] \quad \text{(A3.52)}$$

The three terms on the right hand side are due to reflection waves arriving. The first coming from the top after the first reflection, the second arriving from the bottom after the second reflection and the third is again due to a wave arriving after a reflection at the top, this time having been reflected a third time.

The effects of the initially downwards moving wave on the velocity at the damper location can be expressed as

$$v_{i,down} = \frac{c}{2EA}[-D_i(t - L/c) + D_i(t - 2L/c) - D_i(t - 3L/c)] \quad \text{(A3.53)}$$

Summing up all the effects of applied and resistance waves yields, after simplification, a velocity of the arriving waves for $t \leq 4L/c$

$$v_{i,a}(t) = v_A(t - L/2c) + v_A(t - 3L/2c) - v_A(t - 5L/2c) - v_A(t - 7L/2c) + c/EA\ D_i(t - 2L/c) \qquad (A3.54)$$

But $D_i(t - 2L/c) = \alpha_i v_{i,a}(t - 2L/c)$

$$= \alpha_i[v_A(t - 5L/2c) + v_A(t - 7L/2c)]$$

and therefore

$$v_{i,a}(t) = v_A(t - L/2c) + v_A(t - 3L/2c) - v_A(t - 5L/2c)(1 - \alpha_i c/EA) - v_A(t - 7L/2c)(1 - \alpha_i c/EA) \qquad (A3.55)$$

which leads to $D_i(t)$ by multiplication with α_i.

Figure (A3.5a) shows the graph of $D_i(t)$ for an assumed constant velocity of magnitude $v_A(t)/c = 1$ and a damping coefficient $d_i = EA/c$, so that $\alpha_i = EA/2c$. Figure (A3.5b) shows $\Delta_i(t)$ due to this damping force obtained from applying Equation (A3.45) by graphically superimposing the applicable terms as it was shown in Figure (A3.4).

If a damper is located at the pile bottom then only waves arriving from one direction have to be considered. This leads to simpler computations. The arriving wave velocity for times $t \leq 4L/c$ is then given by

$$v_{n,a} = 2[v_A(t - L/c) - v_A(t - 3L/c) + c/EA\ D_i(t - 2L/c)]$$

or

$$v_{n,a} = 2[v_A(t - L/c) - v_A(t - 3L/c)(1 - \alpha_i c/EA)] \qquad (A3.56)$$

and therefore the resistance Delta curve for $t \leq 4L/c$

$$\Delta_n(t) = 2\alpha_n[v_A(t - 2L/c)] \qquad \text{(A3.57)}$$

since $D_n(t) = \alpha_n \cdot v_{n,a}(t)$.

Both $D_n(t)$ and $\Delta_n(t)$ are shown in Figure (A3.5c,d), respectively. Applied velocity and damper coefficients were chosen the same way as in the previous example. This resistance Delta curve seems identical to that for a shear resistance at the tip of the pile. Of course, this is a result of the choice of a constant velocity at the pile top. It was found in analyzing actual records where the velocity showed only a small decrease after the maximum that it is, in fact, difficult if not impossible to distinguish between shear and dynamic resistance forces. Further detailed discussion of this important point is presented in Chapter IV.

6. Prediction of Soil Resistance Forces Acting Along the Pile Under a Hammer Blow

Using the concept of Measured and Resistance Delta curves a prediction scheme will be developed for the magnitude of forces which act along the pile under a hammer blow. Their effects at the pile top are displayed in the Measured Delta curve which is derived from acceleration and force measured at the pile top.

The actual resistance forces are distributed along the pile. For ease in computation it will be assumed that they act as concentrated forces on n equally spaced locations along the pile. The number of unknowns is slightly reduced by assuming that the pile top element has no resistance forces acting, an assumption

which is sensible because part of the pile is mostly above grade and the upmost soil is usually not in contact with the pile due to transverse pile vibrations. Thus, the magnitudes of (n - 1) quakes, q_i, (n - 1) ultimate shear resistance $S_{i,o}$, and (n - 1) damping coefficients, d_i, have to be computed.

As outlined in Chapter II the i-th quake will be assumed to be reached when the velocity at the point $x = x_i$ reaches a maximum velocity. If no resistance forces were acting then this displacement would be the same as the displacement at the top at time t_m, the time when the top velocity has a maximum. Only the bottom end would obtain twice the displacement due to the reflection of the arriving wave. The effect of the resistance forces can be estimated by considering the Measured Delta curve. In Section 5 it was found that a shear resistance force produced a pile top force effect of twice its ultimate shear resistance value at time $t_m + 2L/c$. A damper at the pile toe also yields a top force effect of twice its maximum resistance force at this same time. The Measured Delta curve is equal to the sum of all Resistance Delta curves if the parameters are correct. Thus, $\Delta(t)$ shows at a time $2L/c$ after impact twice the magnitude of the sum of all resistance forces if all the damping force is assumed to act concentrated at the bottom end. The effect of all ultimate shear resistance forces and the effect of the toe damping force on the toe velocity is proportional to their respective wave particle velocities or magnitudes of resistance forces. Thus, the maximum velocity at the pile bottom

at time $L/c + t_m$ is

$$\max v_n = 2 \max v_A - \frac{c}{EA}\frac{1}{2}\Delta(t_m + 2L/c) \qquad \text{(A3.58)}$$

where $v_A(t)$ is the top measured velocity and $\Delta(t)$ is the magnitude of the Measured Delta curve at time t.

A good estimate on the bottom end displacement can be obtained by assuming that the ratio of pile top and pile tip displacement is linearly proportional to their respective velocity ratio thus

$$q_n = u_n(t + L/c) = u_A(t_m)\frac{\max v_n}{\max v_A} \qquad \text{(A3.59)}$$

$u_A(t)$ being the pile top and $u_n(t)$ the pile tip displacement. The quakes for locations other than pile top or pile tip are linearly interpolated so that

$$q_i = v_A(t_m) - [u_A(t_m) - u_n(t_m + L/c)]\frac{x_i}{L} \qquad \text{(A3.60)}$$

Quakes resulting from this calculation which are larger than .12 (inch) are set equal to this value the quake, therefore, cannot exceed commonly recommended values for sand (9). A lower bound is not introduced because it is desired to keep the quakes small enough so that the ultimate resistance can be reached at all elements. The prediction scheme for quakes is based on the following considerations:

Examples of Measured Delta curves are shown in Chapter II, Figures (2.5), (2.6) and (2.7). All three curves, although obtained from very differently behaving piles have their maximum value at a time 2L/c after maximum velocity at the top. If skin damping forces are considered small then this means that the maximum shear and damping forces were all reached before or at a time L/c

after maximum velocity at the top. Then, the toe shear resistance force must have reached its ultimate shear resistance force at the same time. This time, however, is the time of maximum velocity at the pile tip. Consequently, the quake of the tip shear resistance force is reached at the time of maximum tip velocity a result which is extended to all points along the pile. In Chapter III and IV this point will be further discussed.

Although several simplifications have been made in the above described computation quakes will in general result which lead to the ultimate shear esistance at the i-th element at or before a time $t_m + x_i/c$. Therefore, in the absence of dynamic resistance forces the value of the Measured Delta curve at time $t_m + 2x_i/c$ will be a result of a superposition of the top force effects of the first i ultimate shear resistances plus some small influence of the already increasing shear resistances of lower elements due to the part of the before maximum velocity. Calling this influence ε_i and defining $t_i = t_m + 2x_i/c$ then

$$\Delta(t_i) = \sum_{j=1}^{i} S_{o,j} + \varepsilon_i \qquad \text{(A3.61)}$$

and for $t_{i-1} = t_m - 2x_{i-1}/c$

$$\Delta(t_{i-1}) = \sum_{j=1}^{i-1} S_{o,j} + \varepsilon_{i-1} \qquad \text{(A3.62)}$$

Subtracting Equation (A3.62) from Equation (A3.61) leads to

$$S_{o,i} = \Delta(t_i) - \Delta(t_{i-1}) + \varepsilon_i - \varepsilon_{i-1} \qquad \text{(A3.63)}$$

If it is then assumed that the difference $\varepsilon_{i+1} - \varepsilon_i$ is small the i-th ultimate shear resistance has been found. Figure (A3.6) serves to clarify this point by use of a theoretical example. Several theoretical Resistance Delta curves (a_i) are shown - corresponding to shear resistance forces - whose sum corresponds to the Measured Delta curve (b). At times t_i an influence ε_i from the next lower shear resistance force can be observed. The $S_{o,i}$ were assumed to be equal in this example so that $\varepsilon_i = \varepsilon_{i+1}$ for $i < n-1$.

This computation can be performed the same way for all elements except for the bottom where the effect of all the bottom reflected waves requires a top reaction force of twice the total resistance. Thus, an approximation for the n-th shear resistance force can be computed from

$$S_{o,n} = 1/2[\Delta(t_m) - \Delta(t_{n-1})] \qquad \text{(A3.64)}$$

This computation scheme will not apply when damping forces have to be considered and when t_m is reached so late that $\Delta(t_{n-1})$ contains already effects of the return of reflection waves from the bottom. In that case an improvement of the above described method for predicting ultimate shear resistance forces can be obtained if the damping effects and the effects due to reflection waves are subtracted from the Measured Delta curve. For doing so the magnitude of damping forces must be known. An estimate of the maximum damping force max D can be obtained from the simplified Phase III prediction

method as described in Chapter II, Section 5 and in Appendix D. If it is assumed that all this damping is concentrated at the pile bottom (actually damping will be distributed but a large percentage is in most cases found to be concentrated at the bottom) then its effect at the top will be proportional to the top velocity shifted over a time of 2L/c as shown by the Resistance Delta curve in Figure (2.11). (This is actually only true for no other resistance forces acting, but since the shear resistance forces are constant except for a small portion before the quake is reached this gives still a good approximation).

The doubling effect due to the return of reflection waves from shear resistance can be assumed to be proportional to the Resistance Delta curve for a shear force at the pile bottom. Such a Resistance Delta curve, however, can be thought of being a curve proportional to the pile top displacement until t_m and constant, thereafter, with a time lag of 2L/c.

The resulting Reduced Delta curve is then

$$\Delta_{red}(t) = \Delta(t) - 2 \max D \frac{v_A(t - \frac{2L}{c})}{\max v_A} - S_o \frac{u_A^*(t - \frac{2L}{c})}{q_1} \qquad \text{(A3.65)}$$

where

$$u_A^*(t) = \begin{cases} u_A(t) & \text{for } t < t_m \\ q_1 & \text{for } t > t_m \end{cases}$$

and S_o is the sum of all ultimate shear resistance forces.

Using the Reduced Delta curves the equation for the prediction of ultimate shear resistance forces becomes (see Equation (A3.63))

for $i = 1,2,\ldots,n$

$$S_{o,i} = \Delta(t_i) - \Delta(t_{i-1}) \qquad \text{(A3.66)}$$

It is now left to compute the damping coefficient for the bottom damper. From Equation (A3.58) it is possible to predict the maximum velocity at the pile tip using both measured velocity and Measured Delta curve. Therefore,

$$d_n = \max D/(2 \max v_A - (c/2EA)\Delta(t_m + 2Lx_c)) \qquad \text{(A3.67)}$$

All necessary parameters for performing a lumped mass analysis have now been approximately determined and the top force and all displacements can be calculated using the measured velocity and the predicted soil resistance forces as an input. To improve the values an analysis should be done.

The difference between measured and the pile top force computed in the lumped mass analysis using the predicted soil parameter can be considered again a Delta curve. It will be referred to as an Error Delta curve, $\Delta_e(t)$, and provide a means of computing corrections on the first predictions. These errors can be due to a pile tip velocity different from the prediction, also the assumptions used in reducing the Measured Delta curve can account for errors. Other errors, however, will also be introduced from assuming that i-th shear resistance force had the same top force effect at time t_{i-1} that $S_{i+1}(t)$ had at t_i (i.e. $\varepsilon_i = \varepsilon_{i+1}$).

The Error Delta curve can be considered a Measured Delta curve which must be the sum of Resistance Delta curves. This time the

computation becomes somewhat simplified since for every element both a velocity and displacement versus time relation are available which can be considered an approximation, whose quality depends on the relative magnitude of the Error Delta curve. Using, again, the concept of Resistance Delta curves it is now possible to set up matrices whose coefficients are influence numbers reflecting the top force effect of a resistance force at time $t_j = 2x_j/c$ at the i-th element. Thus, for the shear resistance forces a matrix C is defined with elements

$$c_{j,i} = u_i^*(t - x_i/c)/q_i + u_i^*(t - \frac{2L - x_i}{c})/q_i \qquad \text{(A3.68)}$$

where

$$u_i^*(t) = \begin{cases} u_i(t) & \text{for } u_i(t) < q_i \\ q_i & \text{for } u_i(t) \geq q_i \end{cases}$$

As an example of the meaning of $c_{j,i}$

$$\Delta_i(t_j) = S_{o,i}c_{j,i} \qquad \text{(A3.69)}$$

In the same way for damping forces a matrix E is set up having elements

$$e_{j,i} = (v_i(t - x_i/c) + v_i(t - \frac{2L - x_i}{c}))/ \max v_i \qquad \text{(A3.70)}$$

So that

$$\Delta_i(t_j) = \max D_i e_{j,i} \qquad \text{(A3.71)}$$

This matrix is used later on for distributed damping resistances.

It will be understood that max D_i is the maximum damping force occuring on the first arrival of the impact wave. It is expected that a higher, second maximum is obtained (of about 2 max D_i as can

be seen in Figure (2.12)) after the impact wave is reflected at the pile bottom. This maximum damping force max D_i is known to occur at a time $t_m + x_i/c$ and therefore, its top force effect will be seen on top at time $t_m + 2x_i/c = t_i$. Thus, $e_{j,i}$ will be a convenient tool for computing damping resistance forces when D_i is not zero along the pile skin. By use of $c_{j,i}$ and $e_{j,i}$ it is now easy to reduce the Error Delta curve by the effect of reflection waves at $2L/c$ and by the difference ΔD between necessary damping (max D) and damping found in the previous analysis (max D^a), thus, if ΔD = max D - max D^a

$$\Delta_{e,red}(t_j) = \Delta_e(t) - e_{j,n}\Delta D \qquad \text{(A3.72)}$$

The corrections on the shear resistance forces, $\Delta S_{o,i}$, can now be computed using the same approach as in the initial shear force prediction

$$\Delta S_{o,i} = \Delta_{e,red}(t_i) - \Delta_{e,red}(t_{i-1}) \qquad \text{(A3.73)}$$

The corrected damping coefficient can be computed from Equation (A3.67) where the expression in the denominator on the left hand side is replaced by max v_n as obtained in the lumped mass analysis.

In order to further improve the predictions another lumped mass analysis can be performed and further corrections obtained and this process has to be continued until the Error Delta is small enough. The number of necessary iteration cycles depends on how well the soil model describes the actual soil behavior. For good agreement between the assumed and actual soil action four iteration steps

usually suffice. In many cases, however, the Delta curve portion of the record for 2L/c after impact cannot be reduced to small values. In such cases the computation is terminated after the 8th attempt.

When requiring the Error Delta curve to become smaller than a certain bound it is important to realize the different sensitivity of an Error Delta curve at different times to a change in prediction. As in any other Delta curve an error ΔS_i at $x = x_i$ will result in a Delta curve approximately given by

$$\Delta_e(t) = \Delta S_i \text{ for } t_i < t < t_n$$

and

$$\Delta_e(t) = 2\Delta S_i \text{ for } t_n < t < t_{i,o} + x_i/c$$

thus, the portion of the record for $t_m < t < t_n$ is less sensitive to errors than the later portion of the record. The following criteria, therefore, have been established for a sufficiently small Error Delta curve accounting for the different sensitivities in the record (a further discussion of these criteria is given in the example in the next section).

$$|E_1| = \left| \frac{1}{t_{n-1} - t_2} \int_{t}^{t_{n-1}} \Delta_e(t)dt \right| < CR_1 = 0.02 \max F_A \qquad \text{(A3.74a)}$$

$$|E_2| = \left| \frac{1}{t_n - t_{n-1}} \int_{t_{n-1}}^{t_n} \Delta_e(t)dt \right| < CR_2 = 0.05 \max F_A \qquad \text{(A3.74b)}$$

$$|E_3| = \left| \frac{1}{t_f - t_n} \int_{t_n}^{t_f} \Delta_e(t)dt \right| < CR_3 = 0.10 \max F_A \qquad \text{(A3.74c)}$$

where max F_A is the maximum measured force

and

$$t_f \leq \begin{cases} 4L/c & \text{for no unloading} \\ t_{n,o} + L/c & \text{otherwise} \end{cases} \qquad \text{(A3.75)}$$

with $t_{n,o}$ being the time of zero velocity at the pile tip. This way it is not required that the predicted and measured top forces match after unloading effects become apparent at the top. It was found in applying the above described error criteria that the $|E_i|$-numbers can be efficiently used to control the computation process: As long as $|E_1|$ is too large the shear resistance forces $S_{i,o}$ along the pile skin have to be corrected, when $|E_1|$ is sufficiently small but $|E_2|$ is not less than CR_2 than either toe damping or toe shear have to be adjusted by an amount equal to one half of $|E_2|$, and when $|E_1|$ and $|E_2|$ are small then a check on $|E_3|$ allows to decide whether or not the total maximum amount of damping used was correct. This is due to the fact that a Resistance Delta curve for damping decreases with a higher rate after $t_m + 2L/c$ than a Resistance Delta curve for shear forces. Therefore, damping has to be added and shear resistance subtracted at the same time if the predicted force is greater than the measured force for $t > t_m + 2L/c$, i.e. for $E_3 < 0$. For $E_3 > 0$ the opposite has to be done.

Thus, an improved total damping value will result from

$$\max D_{imp} = \max D - E_3/2 \qquad \text{(A3.76)}$$

where it is assumed that the shear resistance forces are staying constant while the damping forces decrease immediately to zero after $t_m + 2L/c$. This scheme - although being quite crude - usually leads to a satisfactory match over the third portion that is t from t_n to t_f as long as the soil model allows a good match in that region.

Once, the inequalities (A3.74a,b,c) have been satisfied the prediction for all damping at the tip is accomplished.

The assumption of all damping concentrated at the pile tip might yield a good match, however, it is possible and probable that damping forces act also at the pile skin. For finding out how the damper locations influence the predicted top force two more methods of damping distribution will be tried. One of these methods is to place damping forces uniformly along the skin i.e. for $i = 2,3,\ldots,n-1$. Thus, (n-2) damping forces are chosen to replace the bottom damper. Calculating with the damping maxima, $\max D_i$, occuring before the impact wave reaches the bottom and assuming that the $\max D_i$ are one half of the maximum damping effect felt at the top at time 2L/c (see example in Figure (2.12)) leads to

$$\max D_i = \frac{\max D_{imp}}{2(n-2)} \qquad \text{(A3.77)}$$

However, it has to be checked whether these damping forces would not result in top force effects larger than specified by the Measured Delta curve. Using the E-Matrix this can be checked

$$\sum_{i=2}^{n-1} \max D_i e_{j,i} < \Delta(t_j) \qquad \text{(A3.78)}$$

If for some time $t = t_j$ this inequality does not hold than max D_j has to be reduced

$$\max D_j \leq \Delta(t_j) - \sum_{i=2}^{j-1} \max D_i e_{j,i} - \sum_{i=j+1}^{n-1} \max D_i e_{j,i}$$

$$j = 2,3,\ldots,n-1 \qquad \text{(A3.79)}$$

Also it has to be checked whether the maximum total damping force on the return of the reflection wave would exceed the necessary total damping force as determined in the first prediction. Again using the E-Matrix this check requires

$$\sum_{i=2}^{n-1} \max D_i e_{n,i} = \max D_{imp} \qquad \text{(A3.80)}$$

which can be accomplished by adding a max D_n if the left hand side is smaller than the right hand side or to subtract from all max D_i $i = 2,3,\ldots,n-1$ if the opposite holds. If for $j = 2,3,\ldots,n-1$ turns out to be negative then neighboring damping forces have to be reduced until the maximum possible damping forces are found. The corresponding damping coefficients can be found from the previously predicted velocities (which had been used also for computing the $e_{i,j}$). Errors resulting from this assumption must be small since a good match had been determined previously and the maximum velocities for $t < t_m + 2L/c$ will be the same for $\Delta_e(t)$ being small no matter how the match was accomplished. (The particle velocities in the waves due to either resistance forces have to be the same).

The computations for obtaining the ultimate shear resistances $S_{o,i}$ can be obtained in a similar manner as described above for one damper at the bottom only that the Reduced Delta curve has to be computed by accounting for all damping forces, thus

$$\Delta_{red}(t_j) = \Delta(t_j) - \sum_{i=2}^{n} e_{j,i} \max D_i - S_o c_{j,n} \qquad (A3.81)$$

The variation of the damping forces and the effects of the reflection wave on damping usually introduces more errors in the prediction than in the case of only one damper at the bottom, therefore, if damping is large more computations have to be performed until the final distribution produces a small enough Error Delta curve, if this is possible. Otherwise the computation is terminated after the 8th iteration.

A third way of distributing damping forces is to place only one damper at the skin, at the point where the maximum skin resistance force in the upper half of the pile had been determined in the first prediction. If max $S_{o,i}$ > max D_{imp} $\frac{1}{2}$ then max D_i = max $D_{imp}/2$ and if max $S_{o,i}$ < max $D_{imp}/2$ then max D_i = max $S_{o,i}$ and toe damping has to be added. Essentially this computation is the same as when damping forces are distributed uniformly.

Once the final Error Delta curves have been found (these three curves usually differ at and after $t_m + 2L/c$ for all three damping distributions) a linear combination of their $S_{o,i}$ and d_i is used to find a final selection by minimizing the resulting Error Delta curve. If p^j_i stands for the i-th resistance force (either $S_{o,i}$

or d_i) obtained in the j-th damping distribution method and a superscript f is used for the final result, then

$$p_i^f = a_1 p_i^1 + a_2 p_i^2 + a_3 p_i^3 \tag{A3.82}$$

where

$$a_1 + a_2 + a_3 = 1 \tag{A3.83}$$

and

$$\Delta_e{}^f(t) = a_1 \Delta_e{}^1(t) + a_2 \Delta_e{}^2(t) + a_3 \Delta_e{}^3(t) \tag{A3.84}$$

For $\Delta_e{}^f(t)$ to become a minimum the coefficients a_1, a_2, a_3 can be determined using

$$\frac{\partial}{\partial a_i} \int_0^{4L/c} (\Delta_e{}^f(t)^2 w(t) dt = 0 \tag{A3.85}$$

where w(t) is a weighting function. Since the errors in the initial portion of the match are due to measuring inaccuracies these effects can be removed from the computation by setting

$$w(t) = 0 \text{ for } 0 \leq t \leq t_2 \tag{A3.86a}$$

Also the portion of the record where unloading effects the match will be disregarded (See Chapter III for examples), thus

$$w(t) = 0 \text{ for } t > t_f \tag{A3.86b}$$

where t_f is as defined in Equation (A3.75). In order to place more emphasis on the improvement of the first 2L/c of the match the rest of the weighting function may be defined as

$$w(t) = \begin{cases} 1 & \text{for } t_2 < t < t_n \\ 1 - \left(\frac{t - t_n}{t_f - t_n}\right)^2 & \text{for } t_n < t < t_f \end{cases} \tag{A3.86c}$$

However, not too much improvement can be expected from choosing a proper weighting function since it is possible that an application of the least square method results in some $S_{o,i}$ or d_i negative. Since negative values are not allowable the a_1, a_2, and a_3 coefficients have to be adjusted under observing their relative magnitudes. As an example suppose that $a_3 < 0$ and that for some j the ratio $\frac{a_3 p_j^3}{a_1 p_j^1 + a_2 p_j^2} < 0$ and smaller than any other ratio $i \neq j$, $i = 2,3,\ldots n$, then the new constants a_1^n, a_2^n, a_3^n can be determined from

$$a_3^n = \frac{1}{p_j^3}(a_1^n p_j^1 + a_2^n p_j^2)$$

$$a_1^n + a_2^n + a_3^n = 1 \qquad \text{(A3.87)}$$

and

$$a_1/a_2 = a_1^n/a_2^n$$

Using a_1^n, a_2^n, a_3^n in Equation (A3.82) leads to the final result if not a second coefficient was negative in which case the process has to be repeated.

7. Computation Example

As a computation example the record obtained from pile F-60, Blow No. 26-A is used. The record, i.e. force and velocity, is shown in Figure (B.1). After subtracting the precompression force, S_p, (for explanation see Appendix B) in this case S_p = 40.6 (kip), the force curve as shown in Figure (2.1) was obtained.

The pile length below the accelerometer was 59 feet. The pile was of 12-inch diameter pipe with 1/4-inch wall thickness

having a cross sectional area of A = 9.82 (inch)

The wave speed for such a steel pipe pile had been experimentally determined by placing one accelerometer on either end of a 50 foot pile and applying a hammer blow on one end. The wave speed thus determined was c = 17,000 (ft/s) and with ρ = .285/386 ($lb/s^2/in^4$)

$E = c^2\rho = 30.8 \times 10^6$ [psi]

This dynamic modulus is used in all the analyses. The proportionality factor EA/c becomes 17.8 (kip/ft/s), which means that a particle velocity of 1 ft/s corresponds to a 17.8 kip force in the pile.

The maximum pile top velocity encountered in the example problem was 9.1 ft/s which corresponds to a maximum pile tip force of 169 (kip). (The yield load of the pile is 320 kip).

The Measured Delta curve is shown in Figure (A3.7a) and was obtained by subtracting the free pile solution - Equation (A3.18) - from the measured force record.

It can be observed that $\Delta(t)$ has non zero values before time t_m which are mainly due to recording inaccuracies. These values are set to zero until a time 1.2 L/c after which $\Delta(t)$ starts definitely to increase. In some of the records effects of high frequency vibrations are observed which are undesired in the analysis since they represent only local effects and could lead to misinterpretations. For cancelling out such effects a new, smooth $\Delta(t)$ was obtained by time averaging the original one.

The result is shown as curve b in Figure (A3.7b)

Integrating the top velocity until time t_m leads to a displacement of 0.107 (inch). Estimating the maximum toe velocity using Equation (A3.58) with the maximum top velocity being 9.1 [ft/s] and $\Delta(t_m + 2L/c) = 422$ kips leads to

$$\max v_{n(toe)} = 2 \times 9.1 - \frac{422}{2 \times 17.8} = 6.5 \text{ [ft.s]}$$

So that an estimate for the toe displacement at maximum toe velocity can be given using Equation (A3.59)

$$u_n(t_m + L/c) = 0.107 \frac{6.5}{9.1} = .075 \text{ (inch)}$$

Linear interpolation leads to the quakes shown in Table (2.1). The Phase III prediction for total static resistance is 146 kips and the estimated maximum damping force 65 kips. Reducing the Measured Delta curve by the damping effect leads to curve c in Figure (A3.7). This curve is then reduced further in order to remove the effect of initially downward traveling waves from shear resistance forces. The resulting curve (d) is a Delta curve due to the effect of the upwards traveling waves from shear resistance forces only. (An infinitely long pile would show the same top force effect due to shear forces).

This curve can be used to determine the individual ultimate resistance forces by applying Equation (A3.66). In Figure (A3.7) the t_i ($t_i = t_m + 2x_i/c$) are marked with dashed lines. Accordingly the $S_{o,i}$ were determined as the differences between the indicated $\Delta_{red}(t_i)$ - values. The last two shear resistances $S_{o,n-1}$ and $S_{o,n}$ are averaged since the accuracy of distinguishing these two

forces is small due to the large increase of top forces at $t = t_{n-1}$. Using the maximum toe velocity as calculated above leads to the damping coefficient

$$d_n = 65/6.3 = 10.3 \text{ [kips/ft/s]}$$

All soil parameters predicted so far are listed in Column 2 of Table (A3.2). As a check on the quality of this prediction a lumped mass analysis is performed. The measured pile top velocity and the predicted soil parameters are used and the corresponding pile top force is computed. If the soil model would be correct and if the soil parameters were predicted precisely then this computed pile top force would be equal to the measured force (in absence of measurement inaccuracies). In general, however, differences between measured and computed pile top force occur. Subtracting the predicted from the measured curve leads to an Error Delta curve. For the present example curve (a) in Figure (A3.8) shows this difference curve.

A remark on this graph is appropriate. For clarity the force scale was chosen five times larger than in the graphs for the Measured and Reduced Delta curves in Figure (A3.7). Considering the first portion of the Error Delta curves (i.e. for $t_m < t < t_m + 2L/c$) it can be noticed that local peaks and valleys of this curve are preserved and the differences of the Error Delta curves occur only in an averaged manner. Clearly, this is due to the constant behavior of shear resistance forces. The later portion of the graph ($t_m + 2L/c < t$) shows this behavior for Error Delta curves a and b

only. But it must be recalled that the amount of damping had been changed for obtaining curve c and curve d. These changes influence only the behavior of this later portion. The high frequency oscillations in the Error Delta curves are due to small time lags from Measurement inaccuraries causing a shift between the predicted and the measured force, also the accuracy of reading the original measured force record is responsible as can be seen Figure (2.1) where the relative smoothness of the velocity compared to that of the measured force becomes apparent.

It is not possible to influence the high frequency behavior of the Error Delta curves by applying low frequency resistance forces and a check on the absolute values of $\Delta_e(t)$ could lead to unnecessary computations without convergence. Thus, an average is used. Also, when using the Error Delta curve for computing corrections on the $S_{o,i}$ and d_i only a smoothened $\Delta_e(t)$ is used as in the case of the Measured Delta curve.

The maximum damping force obtained by using $d_n = 10.3$ in the analysis was 70 kips. Using the Error Delta curve for calculating the $\Delta S_{o,i}$, correcting the damping coefficient and performing another lumped mass analysis leads to the Error Delta curve (b) in Figure (A3.8). The damping coefficient is corrected to produce the assumed damping force of 65 kips (i.e. $d_n = 10.3(\frac{65}{70})$). The criteria CR_i of the Inequalities (A3.74) are shown in this figure. Here, it also can be observed that over the first and second region the average Error Delta curve stays within the bounds. Thus,

$$|E_1| = CR_1$$

$$|E_2| = CR_2$$

however

$$|E_3| < CR_3$$

and

$$E_3 = 26 \text{ (kips)} > 0$$

E_3 is the average delta value between $t = 2L/c + t_m$ and $t = t_f$. Since the sign of E_3 is positive, it means that not enough shear resistance force was applied. Thus, 13 (kips) total damping will be subtracted and 13 (kips) shear resistance added both at the pile tip.

The Error Delta curve resulting from the redistribution is shown in curve c, Figure (A3.8). Error Delta curve c satisfies the conditions in region one and region two but not in region three since $E_2 < 0$ and $E_3 < 0$ this will be corrected by subtracting shear resistance. However, since E_2 was also less than zero no damping is added this time. After another lumped mass analysis is performed Error Delta curve d is obtained which satisfied all three criteria. The final result is given in column 3 of Table (A3.2). As an example for the C and E matrix the displacements and velocities were used from this final match of the first distribution. The resulting matrices are shown in Table (A3.1). Ten elements are used in the lumped mass analysis together with $\phi = 2$ (see Appendix A1), therefore, $x_i/c = 2\Delta t$. Thus, the influence numbers represent relative displacements or velocities which are taken at time

differences of two time increments. (Δt = .178 milliseconds). It can be observed in the E-matrix that max v_i was not reached exactly at $t_m + x_i/c$ but at $t_m + x_i/c + \Delta t$ a time for which there is no matrix element. Thus, $e_{i,j} = 1.0$ was not obtained. A serious defect is not introduced since the E-matrix recognizes this fact. Note, that at j = 7 the influence of the returning wave can be observed in both C and E - Matrix. The C and E matrix are always recalculated when a lumped mass analysis is performed.

The second damping distribution leads to max D_i 55/8 = 6.9 (kips) maximum damping force for the second through ninth element. The Measured Delta curve, however, indicates that the predicted force would become too large in the beginning of the record. Therefore, these damping forces have to be reduced. The result are the parameters listed in Column 4 of Table (A3.2).

It can be observed that some damping was used at the pile tip element in order not to exceed allowable top force effects before time $t_m + 2L/c$. The $S_{o,i}$ had been obtained after reducing the Measured Delta curve by means of the E and C - matrix. Figure (A3.9) shows the successively improved Error Delta curve obtained until finally the error criteria were satisfied. The final result is given in Column 5 of Table (A3.1).

In the third distribution a max D_3 = 6.4 (kips) was used corresponding to $S_{o,3}$ which was the maximum shear resistance force at the pile skin in the upper pile half for the first distribution. Corresponding for the pile toe a damper was necessary for max D_n =

57 (kip) (the total damping determined in the second method was 69.8 (kip), therefore, max D_n = 69.8 - 2 x 6.4 = 57.0).

Since the difference between the third and the first method is small for a small damping force at the skin a sufficiently small Error Delta curve (see Figure (A3.10) was obtained already from the prediction. Soil resistance parameters obtained from this distribution are given in Table (A3.2), Column 6.

In Figure (A3.11) the predicted top forces are shown for all three predictions together with the measured force.

Now, the least square procedure can be performed. This leads to

a_1 = 1.48

a_2 = 0.09

a_3 = -0.57

The negative a_3 produces a negative damping parameter, d_3 = -0.3 which is discarded since its effect is small. The final result is tabulated in Column 7 of Table (A3.1). Thus, S_o = 157.4 (kip) and max D = 52 (kip).

This S_o is the shear resistance acting under impact. But the hammer compression force S_p, had been subtracted from the total record. This static force has to be added to S_o in order to obtain R_o, the total static bearing capacity. As for the distribution it is sensible to add to all $S_{o,i}$ a contribution of this static force proportional to the dynamically predicted value. The total static bearing capacity then becomes R_o = 157.4 + 40.6

= 198.0 (kip). The final distribution and the load test curve predicted from this result are presented in Chapter III.

APPENDIX B

Study on Characteristics of Force and Acceleration Records

As a basis for the studies on pile dynamics presented in this work two quantities must be available as continuous functions over time, namely force and acceleration measured at the top of the pile. Transducers, signal conditioning and recording devices have been described in References (3, 20). Several observations were made which need to be explained. In records taken on a pile driven by a Diesel hammer an increase in force was noticed some time before the impact. This force can be explained with pressure building up in the combustion chamber of the hammer. It seemed surprising, therefore, that no acceleration was recorded before the impact. Thus, the proportionality between force and velocity derived from wave theory appeared to be questionable. This and further details observed in acceleration and force records are discussed in Section 1. Another phenomen on which had to be investigated was the existence of an oscillation appearing in both velocity and force. Since this frequency was not the pile natural frequency several possible models of pile-soil and hammer-pile were studied. The results of these studies are presented in Section 2 of this appendix.

1. Observations on Force and Acceleration in Diesel Hammer Records

Because of the proportionality between force and velocity in a stress wave it is advantageous to deal with pile velocities rather than with acceleration. From findings about velocities conclusions can be drawn regarding the measured acceleration.

Consider Figure (B-1) showing the measured force and the velocity which was multiplied by the proportionality constant EA/c. The time scale chosen is in L/c units. The time when impact occurs is easily identified from the steep increase in both force and velocity. In this particular record the force starts to build up at a time of the order 10 L/c before impact while the velocity stays zero through the first 9 L/c.

In order to explain this lack of proportionality it is now assumed that the pile is fixed at the bottom end and the force is for the first 9 L/c approximated by a piecewise linear function as indicated in Figure (B-2a). This piecewise linear function can be approximated again by superimposing two linear functions $F_{A,1}(t)$ and $F_{A,2}(t)$. For the time until the first reflection wave reaches the top again after having been reflected at the bottom, force and velocity must be proportional. Thus, for $t \leq 2L/c$ the velocity is $c/EA\ F_{A,1}(t)$. When the first wave returns from the fixed bottom end its particle velocities will have changed sign. This leads to a decrease in top velocity. At a time 4 L/c two reflection waves will reach the top with different signs of velocities. Thus, the pile top velocity can be written as

$$v_{top}(t) = \frac{c}{EA}\left(F_A(t) - 2F_A\left(t - \frac{2L}{c}\right) + 2F_A\left(t - \frac{4L}{c}\right) - \ldots + \ldots\right) \tag{B.1}$$

Using this equation it is seen that for a linearly increasing top force the velocity at the top will oscillate between zero and the value proportional to the force at time 2L/c. Figure (B-2b) shows

the velocity derived from superimposing the solutions for the two linear force functions. This superposition can only produce a slope in the velocity which is less than or equal to the maximum proportional slope in the force record. A simple calculation can then lead to the maximum acceleration. Suppose max f is the maximum slope encountered in the record before impact then the maximum slope of the velocity, max a, is given by

$$\max a < \max f \frac{c}{EA} \tag{B.2}$$

But max f can be expressed by a force difference ΔF over a time L/c then

$$\max a = \frac{\Delta F}{L/c} \frac{c}{EA} \tag{B.3}$$

and with $c^2 = E/\rho$ and $AL\rho g = W$ the weight of the pile

$$\max a = \frac{\Delta F}{W} g \tag{B.4}$$

In the example of Figure (B.2) $\Delta F = 5.7$ kips and $W = 2.0$ (kip) so that max a = 2.9 g's. The acceleration is read from a record in which a 1 inch amplitude corresponds to 375 g's (see Figure B.3). It is, therefore, not surprising that small magnitude accelerations like the 2.9 g's obtained in the example computation were not recognized in the record.

The results of these considerations can be expressed as follows: The acceleration will reach a noticeable non off zero value in the record only when the time derivative of the force becomes large enough. Second, the velocity of the pile will have obtained some value greater than zero which will be dependent mainly on the

stiffness of the soil, if this stiffness would be infinite then the above derived relations would hold. Third, the proportionality between velocity and force was lost because of the long time over which the force built up. It can be argued that this precompression force is applied in a "static" way and, therefore, should be separated from the dynamic portion of the record if dynamic analysis is to be used. The dynamic record might then be defined from that point at which an acceleration greater than zero can be observed. In most of the records this is the time when a proportionality between force and velocity can be observed. For comparison Figure (2.1) shows force and proportional velocity after the precompression force had been subtracted. The record was the same as analyzed above.

The study of the forces recorded before the actual impact occurs leads to another interesting observation. Frequently in pile dynamics it is necessary to predict the hammer impact velocity max v_h. In the case of a gravity hammer this can be done when the dropheight, h, of the hammer is known. Then

$$\max v_h = \sqrt{2hg} \tag{B.5}$$

For Diesel hammers, however, a free fall cannot occur under the action of the fuel compression force. In this case the velocity has to be computed by subtracting the velocity due to these forces, thus,

$$\max v_h = \sqrt{2hg} - \frac{1}{M_h} \int_{t=0}^{t=t_a} F_{top}^{a}(t)\, dt \tag{B.6}$$

where M_h is the ram mass and t_a is the time where the "dynamic record" starts. In the example of Figure (B.2) the evaluation of the

integral in Equation (B.6) leads to a difference velocity (the second term on the right handside in Equation (B.2) of 2.7 ft/s (M_h = 3.51 g kips/g) which is substantial compared to the velocity encountered at impact (max v_h = 9.6 ft/s). Although the energy which the hammer supplied does not change due to the compression another kind of energy will be utilized having smaller velocities but being spread over time. This fact might prove essential when applying the wave equation method proposed by Smith (9) where one of the input parameters used is the impact velocity.

A remark on the accuracy of the velocity seems appropriate. The usual recording sensitivity for acceleration is between 300 and 400 g's for one inch amplitude in the record. Records are read with an accuracy of about 1/150 inch. A shift of the assumed zero acceleration line with this amount can produce over the length of the record (usually about 20 milliseconds) a considerable velocity. This effect will be even amplified when considering displacements. Using the average of two acceleration records taken on opposite sides of the pile should lead to an improvement in accuracy but velocities and displacements can still not be reliable after some time of integration. It was noticed in applying the Phase I simplified theory (see Chapter II, Section 5) that sometimes no zero velocity was reached, which can be explained from the facts under consideration. The Phase II-A method (see Appendix D) will introduce a major improvement because only differences in velocity are considered over a relatively short time and the time of zero

velocity is no longer an important parameter.

Another inaccuracy can be observed in Figure(2.1)before maximum velocity occurs. The force should be exactly equal to the velocity times EA/c. However, it is noticed that there is a time lag between force and velocity the reason of which is a different response time in the signal condition equipment. This time lag causes often large Delta curve values in the beginning of the record which must be discarded in an analysis.

Another interesting observation can be made on records obtained under a single acting Diesel hammer. Such a hammer consists basically of two parts: a cylinder whose top is open and a piston, i.e. the hammer, which falls freely in the beginning and by falling compresses the air in the combustion chamber. When the piston reaches the cylinder bottom fuel is injected so that metal to metal impact between hammer and anvil occurs together with the combustion. Impact plus combustion force will move the pile head. In the first instant both hammer and pile head will move together with the velocity of the impacting hammer. The hammer cylinder originally resting at the pile top cannot follow this rapid movement, thus it will start to fall under gravity. When assuming that most of the deflection of the pile head is due to penetration into the ground and only a smaller portion is due to elastic deflection of pile and soil, then the hammer cylinder will reach the pile only after the pile has established its final position. The hammer cylinder then will impact upon the pile top and a force and acceleration due to

this (smaller) impact can be observed in these records. Figure (B.3) shows a record in its original scale. In both force and acceleration the second impact can be observed after a time ΔT. It is now interesting to compute the distance u_f which the hammer cylinder was falling freely disregarding any friction in the leads or other losses from the time Δt between the impact of the piston and that of the cylinder

$$u_f = \frac{1}{2} g(\Delta T)^2 \qquad (B.7)$$

and, therefore, in the example of Figure (B.3)

$$u_f = \frac{1}{2} 386(.054)^2 = .562 \text{ [inch]}$$

During the driving operation an average set of .06 inch under one hammer blow was measured. It seems that in cases where the set of the pile is large enough and where a single acting hammer is used more accurate information about the pile set can be obtained from this observation.

2. Studies of Vibration Frequences Occuring on the Pile Head During Driving

Figure (2.1) shows typical force and velocity curves having the above mentioned oscillations about an essentially linear behavior. If the lowest pile natural frequency would be responsible only pile length and material properties would be necessary to predict these frequencies but this is not the case. Vibrations might also occur due to the interaction of soil stiffness with pile mass, a system which is represented in Figure (B.4b). Another explanation for this phenomenon developed herein is that the cushion hammer system

supported by the pile exerts forces upon the pile head which are due to its natural frequencies. The model for such a system is shown in Figure (B.4c). In the following the frequencies expected for the discussed models will be investigated and compared to those observed in the record.

The lowest natural frequency of a pile of length L is

$$f_1 = \frac{c}{4L} \tag{B.8}$$

where c is the wave speed.

Assuming the soil stiffness k_s to be approximately

$$k_s = \frac{R_u}{q} \tag{B.9}$$

where thequake q can be chosen as .12 inches and R_u as the ultimate bearing capacity of the pile; then for the system of Figure (B.4b) a frequency of

$$f_2 = \frac{1}{2\pi}\sqrt{\frac{R_u}{AL\rho g}} \tag{B.10}$$

would be obtained if A, L, ρ or pile cross sectional area, length, and mass density. In the examples given below in Table (B.2) steel piles will be considered having a cross sectional area A = 9.82 (inch). For these cases

$$f_2 = 49.4\sqrt{\frac{R_u}{L}}$$

if L is inserted in feet and S_{ult} in kip. The system shown in Figure (B.4c) has two degrees of freedom. If the upper cushion stiffness is k and the lower one k.s and if the upper and lower elements have masses rm and m, respectively then the two natural

frequencies can be computed from

$$f_{3,4} = \frac{1}{2\pi}\left[\frac{k}{m}\left\{\frac{1 + r(1 + s)}{2r} \pm \left(\frac{(1 + r(1 + s)^2}{4r^2} - \frac{s}{r}\right)^{\frac{1}{2}}\right\}\right]^{\frac{1}{2}} \qquad (B.11)$$

The cushion stiffnesses for the transducer cushion (ks) were obtained experimentally. This transducer cushion was built using alternated layers of 3/4-inch plywood and 1/4-inch neoprene sheets. 3 or 5 plywood and 4 or 6 neoprene sheets were used. The pile cushions stiffnesses (k) were obtained from Reference (10). In both cases statically obtained load versus deflection curves were used and stiffnesses were obtained at the different load levels observed in the force record. All the parameters necessary for computing $f_{3,4}$ are listed in Table (B.1). The correlation of frequencies calculated from all three methods with the observed are listed in Table (B.2).

As an example consider again Figure (2.1) representing Pile F-60, Blow No. 26-A. The average frequency observed in force and velocity record is 409 (cps), (Figure 2.1). The length of the steel pile was 60.5 feet and hence $f_1 = \frac{17{,}000}{4 \times 60.5} = 70$ (cps) from Equation (B.8). The ultimate resistance obtained in the CRP test was 242 kips which leads to a $f_2 = 99$ (cps) using Equation (B.10),. The transducer cushion consisted of 3 sheets of plywood and 4 sheets of neoprene. The average force acting on the pile top during the blow was 150 kips as can be observed in Figure (B.3). From Table (B.1) this gives a transducer cushion stiffness of 7,250 kips/inch. The driving hammer was a Linkbelt 440 which has a cushion stiffness

of 9.300 kips/inch under the given circumstances. Thus k = 9.300 (kips/inch) and s = 7,250/9.300 = 0.78. Also from Table (B.1) $m = \frac{1.10}{g}\frac{kips}{g}$ and $r = \frac{4.71}{1.10} = 4.28$. Inserting these values in Equation (B.11) leads to a lower frequency f_3 = 89 and a higher frequency f_4 = 398 (cps). As in all the other cases presented in Table (B.2) f_4 is the only frequency of a magnitude comparable to the measured one (409 cps in the discussed example). It seems that the only reasonable explanation for the occurence of frequencies higher than 100 cps for the listed cases is that the two degree of freedom system described above vibrates in its second mode, thus, exerting forces and velocities upon the pile head reflecting this higher frequency.

APPENDIX C

Soil Model Studies

The investigations presented in this Appendix give an insight into the relations between the pile motion and the soil resistance response. This soil response is approximated in Chapter II by a simple model, which is also employed by other investigators in the pile dynamics literature (9, 10). Results in Chapter III show that this model does not always describe the soil resistance force, $R_i(t)$, accurately for all times t.

The soil model is shown in Figure (2.2). It consists of a spring and a dashpot in parallel, thus

$$R_i(t) = S_i(t) + D_i(t) \tag{C.1}$$

$S_i(t)$ and $D_i(t)$ are the shear and dynamic resistance, respectively. The index "i" indicates the location where the resistance force acts.

The spring in the soil model is thought to have elasto-plastic properties such that

$$S_i(t) = k_i u_i^*(t) \tag{C.2}$$

where k_i is the soil stiffness at $x = x_i$ and

$$u_i^*(t) = \begin{cases} u_i(t) & \text{for } u_i(t) \leq q_i \\ \max u_i + q_i - u_i(t) & \text{for } u_i(t) \geq \max u_i \end{cases} \tag{C.3}$$

$u_i(t)$ being the displacement of the pile at $x = x_i$ and time t; q_i is the quake and $\max u_i$ is the maximum displacement reached at or before time t.

It is further assumed that

$$S_i(t) \geq -k_i q_i \tag{C.4}$$

and that

$$S_n(t) \geq 0 \tag{C.5}$$

i.e. no tension shear forces are allowed to act at the pile tip, $x = x_n$. This is a reasonable assumption for the soil forces acting against the pile toe plate. The quantity $k_i q_i$ is the ultimate shear resistance force and is denoted by $S_{i,o}$. A typical force versus displacement relation resulting from the definitions in Equations (C.2) through (C.5) is shown in Figure (2.2).

The dynamic or damping resistance force, $D_i(t)$, is linearly proportional to the pile velocity, $v_i(t)$, at $x = x_i$, thus

$$D_i(t) = d_i v_i(t) \tag{C.6}$$

where d_i is a damping coefficient. Again, it is assumed that only compressive resistance forces act at the pile toe. Figure (2.2) shows the damping velocity relation graphically.

To investigate the validity of the above soil model measurements were taken during driving at the pile bottom end. Both force and acceleration records are available. Also the pile tip force was measured as a function of pile penetration during a static load test. The force was always recorded at some distance above the pile toe plate to which the accelerometer was connected. From these measurements the soil resistance force, $R_n^M(t)$, acting against the pile toe plate during driving can be approximated by

$$R^M_n(t) = F(t) - Ma(t) \qquad (C.7)$$

where F(t) is the measured force, a(t) is the measured acceleration and M is the mass of the pile below the point of force measurement.

Five representative records are selected for investigation. One set of measurements - obtained from a reduced scale pile - is typical for the soil response in coarse grained soils (see Table 1.3 for the soil profile). Two records are from full scale pile Ri-50 (see Chapters I and III) where the soil surrounding the pile tip was highly cohesive. The records were obtained immediately after driving and also after a waiting period of three days. In a similar manner records were taken on full scale pile Ri-60. This pile had a high point resistance due to a sandy gravel layer at the bottom of the pile. Table (1.2) gives the soil profile for both piles Ri-50 and Ri-60.

1. Reduced Scale Pile in Sand

The discussion is illustrated in Figure (C.1). At the top of this Figure a plot is shown of both velocity, $v_n(t)$, and displacement, $u_n(t)$, as obtained by integrating the measured toe acceleration. The measured resistance force, $R^M_n(t)$, computed from Equation (C.7) is plotted at the bottom of Figure (C.1). For further discussions the index n is omitted.

The first remarkable observation is that $R^M(t)$ has its maximum at the same time as the velocity v(t). Thus, dynamic forces seem to be present. After its maximum the measured resistance force

decreases monotonically. This is in agreement with the decreasing velocity and corresponds after zero velocity to the pile rebound.

The soil model under discussion requires three parameters to describe the behavior of R(t) in terms of u(t) and v(t). These parameters (q,d and S_o) give the theoretical resistance curve such that it agrees with the measured curve at three points. Using the same approach as in Chapter II for finding the quake, i.e. assigning the displacement at maximum velocity to be quake, leads in the example of Figure (C.1) to

$$q = 0.08 \text{ (inch)}$$

With this choice only two parameters are left to be determined. Selecting the time of both maximum velocity and zero velocity t_o, for obtaining agreement between measured and theoretical resistance force then

$$R^M(t_m) = S_n(t_m) + D_n(t_m)$$

and

$$R^M(t_o) = S(t_o) + D(t_o)$$

However,

$$S(t_m) = S(t_o) = S_o$$

and

$$D(t_o) = 0$$

so that

$$S_o = R^M{}_n(t_o)$$

and

$$D(t_m) = R^M(t_m) - S_o$$

Thus,

$$d = \frac{R^M(t_m) - S_o}{v(t_m)}$$

In the example of Figure (C.1) the soil parameters become

$$S_o = 6.75 \text{ (kip)}$$

$$\max D = 10.0 - 6.75 = 3.25 \text{ (kip)}$$

$$d = 3.25/8.3 = 0.39 \text{ (kip·sec/ft)}$$

Using now Equation (C.1) through (C.6) the theoretical resistance curve can be plotted. In Figure (C.1) both R(t) and S(t) are plotted and can be compared with the measured curve. Since no negative damping forces are allowed for the bottom end of a pile R(t) = S(t) when the velocity v(t) is negative. The resistance curves R(t) and $R^M(t)$ agree quite well before and at zero velocity. After this time the theoretical curve decreases at a slower rate than measured. Certainly, a smaller quake could match this portion of the record better, however, such a change would also affect the quality of the match before maximum velocity. Furthermore, the resistance force is very sensitive to changes in either the quake or the displacement during unloading. An error of 0.01 inches in the displacement at the end of the record would amount to a difference of the theoretical resistance force of 12.5% of the predicted ultimate shear resistance. The displacement curve is not very accurate for later times, therefore, not much accuracy can be expected in predicting the quake from the unloading behavior.

To summarize the results obtained from this record: A maximum damping force was found of approximately one half of the ultimate

shear resistance. The match between theoretical and measured resistance force is good before zero velocity. The ultimate shear resistance force S_o = 6.75 (kip) compares well with the point resistance under the static load test which is plotted in Figure (D.6a). (7.3 kips at ultimate and 6.6 kips at maximum dynamic displacement). Also soil stiffness and quake are in good agreement.

2. Full Scale Pile in Cohesive Soil

Two records taken on a pile in a cohesive soil are shown in Figures (C.2) and (C.3). The records were obtained before and after a waiting period, respectively. The following characteristics are common to both records.

At time zero a force, S_p, can be observed which must be due to the hammer precompression. For further considerations S_p is thought to be a static force independent of velocity and displacement and is, therefore, disregarded. (S_p = 3 kips in Figure (C.2)). The resistance forces show a steep rise together with the corresponding velocity. After the maximum the resistance force rapidly decreases to a magnitude not much greater than S_p. Thereafter, an almost steady strength increase can be observed. This strength increase corresponds to the monotonically increasing displacement while oscillations in the force show some relation to the velocity record.

The velocity shown in Figure (C.2) reaches no zero within the time period considered but a small value at the end of the record. Thus, defining for this case t_o to be the time of minimum velocity the match shown in Figure (C.2) is obtained. The soil parameters,

thus determined, are:

$q = .12$ (inch)

$S_o = 15$ (kip)

$d = 1.24$ (kip/fts)

This match is very poor immediately after the time of maximum velocity. Several reasons can be responsible.

(i) The proportionality between damping force and velocity holds only until time t_m, the time of maximum velocity. Immediately after this time damping forces become very small.

(ii) High pore water pressures are building up during the time of the initial load application and are released slowly, thereafter.

(iii) A strength increase can be observed throughout the resistance force record. Since the velocity is positive and decreasing this strength gain must be due to the displacement gain.

Comparing Figure (C.3) with Figure (C.2) it is observed that higher resistance forces were acting at the pile toe although the displacements were smaller. Thus, a strength gain due to the waiting period can be observed. A match was performed using the same procedure as described before. The soil parameter thus determined are

$q = .096$ (inch)

$S_o = 24$ (kip)

$d = 2.5$ (kip/ft·s)

$R_o = S_o + S_p = 29$ (kip)

As in Figure (C.2) the predicted soil forces in Figure (C.3) are to large after maximum velocity and agree quite well thereafter.

In Figure (C.6b) are shown the two pile tip force versus pile

tip penetration curves obtained from static load test and corresponding to the two records just discussed.

At ultimate the point resistance is 14 and 18 (kip) for the cases in Figure (C.2) and (C.3), respectively. This compares to 18 and 24 (kip) from the dynamic measurements. Thus, both dynamic resistances are high at about 25 to 30%.

3. Full Scale Pile with High Point Resistance

Two cases where the soil consisted of a very hard grave' and sand layer are shown in Figure (C.4) and (C.5). The resistance force shown in Figure (C.4) can be represented with a fair degree of accuracy by the proposed soil model. A small difference occurs at the second local maximum of the $R^M(t)$ curve. A sensible explanation is a further strength gain due to still increasing displacements. Differences in the unloading portion are again due to the high sensitivity of the soil model to small errors in quake and displacements. This was outlined in Section 1.

A time lag between velocity and force (a measurement inaccuracy discussed in Appendix B and Chapter III) imposes problems on the match in the first portion of the record. In Figure (C.4) this difficulty leads to determine the quake at the time of maximum force.

A different way of match was used in Figure (C.5) namely by assuming that the quake is greater than maximum displacement and then matching the maximum resistance values. The special feature of this record are the small displacements (Note the change in scale), and the smooth resistance force curve. Except for a time lag due to

measurement difficulties the resistance force essentially follows the behavior of the displacement curve. The fact that this proportional relation holds throughout the record indicates that only little or no yielding occurred. Thus, the hammer did not supply enough energy to overcome the soil resistance forces. Small damping forces can be observed at the time of maximum velocity.

The static load tests corresponding to the records of Figure (C.4) and (C.5) had to be terminated before the ultimate load was reached. However, the soil stiffnesses from static and dynamic measurements can be compared. This is shown in Figure (C.6c) Apparently the soil offered a stiffer resistance during the dynamic load application than during the static test. Such a loading rate dependent behavior can be expected. Interesting to note is that the soil lost stiffness during the waiting period; an effect which is reflected in both dynamic and static measurements.

4. Summary

The following conclusions can be drawn from the records presented in Figures (C.1) through (C.5).

The present soil model describes fairly well the force versus displacement and velocity relation for granular soils. The unloading portion, however, is difficult to match although the model might still hold.

Cohesive soils present characteristic resistance force patterns which cannot be described by a simple spring - dashpot model. Further studies on how to model such soils must be conducted, including

other independent variables like pore water pressure or soil dynamic effects. The prediction of static capacity from dynamic records can give good results for piles driven into granular soils. In the cohesive soils as in Figures (C.2) and (C.3) it is seen that the shear resistance forces vary throughout the records and no indication is given of the static resistance. A more realistic soil model could improve this situation. In Chapter IV further discussion of this problem is given with respect to the results which can be expected by employing the present soil model in a wave analysis. It should be noted that an average value of the measured soil resistance curve immediately after the maximum leads to a reasonable answer. One important observation is made when studying the dynamic and static load versus penetration curves plotted in Figures (C.6b and c). For cohesive soils a strength increase is observed during the waiting period. The soil stiffness decreased, however, for the granular material. These effects were measured both dynamically and statically, thus, justifying the proposed method of taking dynamic measurements always after a waiting in order to obtain meaningful predictions on the static pile behavior.

APPENDIX D

Simplified Methods For Predicting Static Bearing Capacity

In Chapter I efforts were discussed on how to develop a simple method for predicting static bearing capacity. Such a method utilizing in a special purpose computer would display in the field the prediction within a short time after the hammer blow. Thus, decisions could be taken during driving. In the following two previously developed methods (13) are briefly reviewed. The earlier methods were based on a rigid pile model. Using wave considerations, i.e. employing an elastic pile model, two new computations schemes are derived. Results from all methods are given in Chapter III.

1. Rigid Body Models

Suppose, a rigid body of mass M is acted upon by a force F(t), and a resistance force R(t). If the acceleration of this mass is denoted by a(t) then the static bearing capacity, R_o, is given by

$$R_o = F(t_o) - M\, a(t_o) \qquad (D.1)$$

where t_o is the time of zero velocity. The derivation of Equation (D.1) is given in Chapter I. The sign convention is shown in Figure (D.1). Equation (D.1) is referred to as the Phase I prediction scheme.

The results obtained from the Phase I prediction scheme were promising when compared with the maximum bearing capacity determined in the static load test. However, the results differed substantially from blow to blow and it was found that small changes in t_o, the time

of zero velocity, often amount to large differences in the predictions. Figure (D.2) illustrates this sensitivity of R_o to changes in t_o. In this Figure are plotted the measured acceleration and the velocity and displacement obtained by integration. Also the measured force and the resistance, R(t), are shown where

$$R(t) = F(t) - M\, a(t) \tag{D.2}$$

The point of zero velocity is indicated by a dotted line in the force diagram. If this point of zero velocity were shifted even only a small time increment (due to measurement inaccuracies such a shift is always introduced) then predictions ranging from 150 to 200 kips could be obtained.

This defect of the Phase I prediction method lead to an averaging method referred to as the Phase II prediction scheme. Consider the velocity graph in Figure (D.2). A straight line marks the trend of the descending velocity curve. Using the slope of this line instead of $a(t_o)$ in Equation (D.1) the new prediction scheme becomes

$$R_o = F(t_o) - \frac{M}{\Delta T}\int_{t_1}^{t_1 + \Delta T} a(t)dt \tag{D.3}$$

where t_1 was chosen as the time of maximum velocity and the average was taken until the time of zero velocity ($t_1 + \Delta T = t_o$). As a result of the averaging procedure the variations in the predictions from blow to blow were relatively small. Another method was proposed where the force F(t) is also time averaged, however, results were little affected because of the relatively smooth force records.

2. Elastic Pile Models

The above methods used a rigid body as a pile model. To explain and clarify limitations on these methods the traveling wave solution of the linear, one-dimensional wave equation is utilized.

(i) Phase IIA

In Appendix A3 relations were developed by which the pile top velocity $v_{top}(t)$, can be expressed as a function of external forces. In particular, if a force, $F_A(t)$, is acting at the pile top then Equation (A3.27) can be used to compute $v_{top}(t)$. Similarly, Equation (A3.29) expresses the pile top velocity as a function of a resistance force $R_i(t)$ acting at $x = x_i$ and time t at the pile in upward direct direction. If it is assumed that n resistance forces act along the pile together with the force applied at the pile top then the resulting pile top velocity can be calculated by superimposing the solutions from Equations (A3.27,29). Thus, with r indicating the time interval considered, i.e. $r\frac{2L}{c} \leq t \leq (r + 1)\ 2L/c$

$$v_{top}(t) = \frac{c}{EA}\Big[F_A(t) + 2\sum_{j=1}^{r} F_A(t - j\tfrac{2L}{c}) - \sum_{k=1}^{n}\sum_{j=0}^{r}\{R_k(t - \frac{x_k}{c} - j\tfrac{2L}{c}) + R_k(t - \frac{2L - x_k}{c} - j\tfrac{2L}{c})\}\Big] \qquad (D.4)$$

It is assumed now that the resistance forces, $R_i(t)$, are only due to shear. Effects of dynamic resistance forces will be included later. Therefore,

$$R_i(t) = S_i(t) \qquad (D.5)$$

and using the simplified expression for a shear force as given in

A3.5, Equation (A3.46), then

$$R_i(t) = S_{i,o}\, H(t - \frac{x_i}{c}) \tag{D.6}$$

which means that the quake is assumed to be zero. Inserting Equation (D.6) into (D.4) yields

$$v_{top}(t) = \frac{c}{EA}[F_A(t) + 2\sum_{j=1}^{r} F_A(t - j\frac{2L}{c}) - \sum_{k=1}^{n}\sum_{j=0}^{r} \{S_{k,o}H(t - \frac{2x_k}{c} - j\frac{2L}{c}) + S_{k,o}\, H(t - \frac{2L}{c} - j\frac{2L}{c})\}] \tag{D.7}$$

Now, two different times, t_1 and t_2, are chosen so that

$$t_2 = t_1 + 2L/c \tag{D.8}$$

therefore, if $r\frac{2L}{c} \leq t_1 \leq (r + 1)2L/c$ then $(r + 1) \leq t_2 \leq (r + 2)\frac{2L}{c}$. The difference between the velocities at both times, Δv_{top}, is

$$\begin{aligned}\Delta v_{top} = v_{top}(t_2) - v_{top}(t_1) = c/EA[&F_A(t_1 + 2L/c) - F_A(t_1) \\ &- 2\sum_{j=1}^{r} F_A(t_1 - j\frac{2L}{c}) + 2\sum_{j=1}^{r+1} F_A(t_1 + 2L/c - j\frac{2L}{c}) \\ &- \sum_{k=1}^{n}[-\sum_{j=0}^{r} S_{k,o}\, H(t_1 - 2x_k/c - j\frac{2L}{c}) + H(t_1 - j\frac{2L}{c}) \\ &+ \sum_{j=0}^{v} S_{k,o}\{H(t_1 - 2x_k/c - (j - 1)\, 2L/c) + H(t_1 - j\frac{2L}{c})\}]\end{aligned} \tag{D.9}$$

This expression can be simplified to yield

$$\Delta v_{top} = c/EA[F_A(t_1 + 2L/c) + F_A(t\ ) - \sum_{k=1}^{n}[S_{k,o}\{H(t_1 - 2x_k/c + 2L/c) + H(t_1)\}]] \tag{D.10}$$

The arguments of the step function terms on the left hand side of Equation (D.10) are non negative so that

$$\Delta v_{top} = c/EA[F_A(t_2) + F_A(t_1) - 2\sum_{k=1}^{n} S_{k,o}] \qquad (D.11)$$

which can be written as

$$\frac{\Delta v_{top}}{2L/c}\frac{L}{c}\frac{EA}{c} = \frac{F_A(t_2) + F_A(t_1)}{2} - \sum_{k=1}^{n} S_{k,o} \qquad (D.12)$$

However, $c^2 = E/\rho$ and $AL\rho = M$, M being the mass of the pile. In addition $2L/c = \Delta T$, i.e. the time between t_1 and t_2, thus, with

$$\sum_{k=1}^{r} S_{k,o} = R_o$$

$$R_o = 1/2(F_A(t_1) + F_A(t_2)) - \frac{M}{\Delta T}\int_{t_1}^{t_2} a(t)dt \qquad (D.13)$$

Equation (D.13) establishes a simple method for computing the static bearing capacity, R_o, if the force and the acceleration at the pile top are known. Because of the similarity between Equations (D.13) and (D.3) this method is referred to as the Phase IIA prediction scheme.

Two differences can be observed between Equations (D.13) and (D.3). First, the force term has to be calculated as an average of the forces where the acceleration average starts and ends. The second difference is the need of restricting ΔT to exactly 2L/c.

In order to under the actual meaning of the results obtained by applying Equation (D.1) Equation (D.7) has to be differentiated with respect to time and the result, the acceleration of the pile head, substituted into Equation (D.1).

$$a(t) = \frac{c}{EA}\left[\frac{d\,F_{top}(t)}{dt} + 2\sum_{j=1}^{r}\frac{d\,F_A(t - j\frac{2L}{c})}{dt} - \sum_{k=1}^{n}\sum_{j=0}^{r}\{S_{k,o}(\delta(t - 2\frac{x_k - jL}{c}) + \delta(t - 2\frac{(j+1)L}{c})\}\right] \qquad (D.14)$$

where $\delta(t - a)$ stands for the Dirac δ-function which is zero for $t \neq a$.

Inserting (D.14) into (D.2) and avoiding times t_o such that

$$t_o = \begin{cases} 2\frac{x_e - jL}{c} \\ 2\frac{(j+1)L}{c} \end{cases} \quad \text{for } j = 0,1,\ldots,r \text{ and } t = 1,2,\ldots,n$$

yields at $t = t_o$

$$R_o = F(t_o) - M\frac{c}{EA}\left[\frac{dF_A(t_o)}{dt} + 2\sum_{j=1}^{r}\frac{dF_A(t_o - j\frac{2L}{c})}{dt}\right] \qquad (D.15)$$

The second term consists of the slopes of the force record taken at time intervals of $2L/c$. These slopes of the force record change rapidly over short times due to vibrations in the hammer cushion system (see Appendix B). Therefore, it is not surprising that the results from the Phase I method changed largely whenever the time t_o was changed by small amounts.

In deriving the Phase IIA prediction scheme dynamic resistance forces were not considered. Such forces can be thought of being linearly proportional to the pile velocity. Thus, Equation (D.13) is only applicable at all time pairs t_1 and t_2 if either the dynamic resistance forces are identically zero because of special soil properties or the pile is not moving. Practically, there exists no case of pile driving without velocity dependent forces and the pile motion ceases only after the pile has rebounded and also shear forces reached zero. However, due to the negative particle velocities of waves caused by resistance forces the velocities along the pile are usually small - positive or negative - when the pile top velocity has reached zero. For this reason a good approximation to the

prediction of static resistance forces can be found if t_1 is chosen to be the time of zero velocity at the pile top and t_2 at a time 2L/c later.

In analyzing field measurements it was frequently found that zero velocity was not reached even for long times after impact. This non negative velocity can be explained due to measuring inaccuracies as explained in Appendix B. In such cases a prediction can be obtained by taking t_1 as the minimum velocity encountered. Since only the difference velocity between t_1 and t_2 affects the result no major error is introduced into the computation.

(ii) Phase III

The studies on wave propagation in Chapter II and in Appendix A3 showed that the Measured Delta curve reflects the effects of soil resistance forces at the pile top. Figures (2.5,6,7) show three such Measured Delta curves. Also Resistance Delta curves were investigated which display an approximate pile top force effect of a certain resistance force acting at some point along the pile.

It is now intended to show how the concept of Delta curves can be used to obtain a simple computation scheme for predicting static bearing capacity. In such a simplified analysis it is not possible to find where the resistance forces act. Therefore, the portion of the Measured Delta curve with $t \leq t_m + 2L/c$ (t_m being the time of maximum velocity at the pile top) is of minor interest. However, important information regarding the total amount of static and dynamic resistance forces can be obtained from the Measured

Delta curve for $t_m + 2L/c \leq t \leq t_m + 4L/c$.

A first assumption in the derivation of the Phase III prediction scheme is to neglect any influence of skin damping forces. That this assumption is at least a good approximation is proven by the results in Chapter III. Next it will be shown how the Measured Delta curve can be modified such that the effect of skin shear forces can be converted to an equivalent effect of pile tip forces. This then will reduce the problem to a pile with only pile toe resistance forces.

Consider Figure (D.3a) which shows a theoretical Delta curve for a shear force $S_{n,o}$ acting at the pile tip. (Such a theoretical shear force is discussed in A3.5). A shear force having the same magnitude acting at $x = x_i$ produces a Resistance Delta curve as shown in Figure (D.3b). The difference between these two Delta curves is the earlier pile top effect of the upwards traveling wave generated by the skin force. A modified Delta curve can be obtained by delaying the earlier effects by a time $2(L - x_i)/c$. Figure (D.3c) illustrates this procedure. Analytically, the Modified Delta curve can be obtained from the Measured Delta curve, $\Delta(t)$, and the pile top velocity, $v_A(t)$, using

$$\Delta_{mod}(t) = \Delta(t) + \Delta(t - 2L/c) - 1/2 \frac{v_A(t - 4L/c)}{\max v_A} \Delta(t_m + 2L/c) \tag{D.16}$$

which is valid for $t_m + 2L/c \leq t \leq t_m + 4L/c$, and only if skin forces are of the step shaped type as in Figure (D.3). The third term in this equation is necessary for not delaying effects of the already

returning waves after reflection at the bottom end. (This is a similar approach as used in the derivation of $\Delta_{red}(t)$ in A3.6). In further derivations of the Phase III method the subscript "mod" is dropped and it is understood that $\Delta(t)$ means the modified Delta curve.

If all resistance forces act at the bottom end of the pile then their effect can be felt at the pile top at a time L/c later. Thus, the Measured Delta curve is given by

$$\Delta(t) = 2[D_n(t - L/c) + S_n(t - L/c)] \qquad (D.17)$$

where the notation of Appendix A3 is used. The velocity of the pile tip that results from the velocity $v_A(t)$, imposed on the pile top and from both shear and damping forces acting at the tip is given by

$$v_n(t) = \frac{2v_A(t - L/c) - (c/EA)S_{n,o}}{1 + cd_n/EA} \qquad (D.18)$$

where $S_{n,d}$ is as defined earlier the ultimate shear resistance at the pile top. (This is Equation (A3.43) derived in A3.5). Equation (D.18) is valid for $L/c \leq t \leq t_{n,o}$, i.e. after the quake is reached until the pile tip velocity becomes zero and unloading starts. The time $t_{n,o}$, i.e. the time of zero velocity at the pile tip can be determined from Equation (D.18)

$$v_n(t_{n,o}) = 0 = 2v_A(t_{n,o} - L/c) - (c/EA)S_{n,o} \qquad (D.19)$$

However, $S_{n,o}$ can be expressed in terms of the Measured Delta curve by using Equation (D.17) and by observing that at time $t_{n,o}$ damping is zero and $S_n(t_{n,o}) = S_{n,o}$. Thus,

$$2v_A(t_{n,o} - L/c) - (c/2EA)\Delta(t_{n,o} + L/c) = 0 \qquad (D.20)$$

or rewritten

$$\Delta(t_{n,o} + L/c) = 4\frac{EA}{c} v_A(t - L/c) \qquad (D.21)$$

Equation (D.21) shows how to find the time of zero velocity at the pile tip from pile top velocity and Measured Delta curve. A comment is appropriate. Suppose that the pile had a fixed bottom end (this is the condition which yields the largest possible pile resistance forces assuming that there are no forces acting at the pile which could produce a negative pile permanent set). At a fixed end reflection waves are generated such that no movement occurs. This constraint requires a reaction force, $R_f(t)$, of twice the magnitude of the forces in the wave. Therefore,

$$R_f(t) = 2\frac{EA}{c} v_A(t - L/c) \qquad (D.22)$$

if it is assumed that the only wave arriving is due to the hammer impact. The Measured Delta curve resulting from a fixed end is then

$$\Delta(t) = 4\frac{EA}{c} v_A(t - 2L/c) \qquad (D.23)$$

Hence, whenever the Measured Delta curve exhibits a value four times larger than the force proportional velocity at a time 2L/c earlier then no motion of the pile tip will occur at a time L/c earlier.

In the usual case of pile driving a motion of pile will always occur before the fixed end condition, Equation (D.23), is satisfied. Such a motion is necessary to activate the resistance forces. Once, however, the resistance forces have reached a value large enough or

once the applied velocity, $v_A(t - 2L/c)$, became small enough then Equation (D.21) will be satisfied. (An exception is the case where the hammer applied forces are so large that the motion will not cease before time $t_m - 3L/c$; this case will be discussed later).

Once the time of zero velocity at the pile tip has been determined the ultimate shear resistance force can be found using Equation (D.17)

$$S_{n,o} = \frac{1}{2}\Delta(t_{n,o} + L/c) \qquad (D.24)$$

Also, the maximum damping, max D, force which acts at the pile tip at the time of maximum tip velocity can be found. Since the effect of the maximum pile tip velocity is felt at time $t_m + 2L/c$ at the pile top one obtains again from Equation (D.17)

$$\max D = \Delta(t_m + 2L/c)/2 - S_{n,o} \qquad (D.25)$$

To illustrate the prediction scheme as developed so far a computation example is given. The acceleration and force record used is the same as in the computation example in A3.7. In Figure (D.4) both Measured and Modified Delta curve are shown together with the force proportional to velocity and the curve obtained by multiplying the velocity by 4c/EA and shifting it over 2L/c. The point where both curves intersect is at a time 3.91 L/c and at a Delta curve value of 292 kips. This intersection represents the solution to Equation (D.21). The maximum Delta is 422 kips, thus

$S_{n,o}$ = 146 (kip) (from Equation D.24)

max D = 65 (kip) (from Equation D.25)

The precompression force, S_p = 41 kips, had to be subtracted in this

method as well as in the wave analysis (see Appendix A3) so that the prediction of static capacity becomes:

$R_o = 146 + 41 = 187$ (kip).

For the same record analyzed by wave analysis the results were:

$R_o = 198$ and max D = 52 (kip).

Special consideration was necessary for cases with low driving resistance in the Phase IIA derivation. In such cases no zero velocity was encountered at the pile top throughout the analyzed record. A similar difficulty can arise in the Phase III method. Suppose, that $t_{n,o} \geq 3L/c + t_m$ then the fixed end condition (D.23) is not satisfied within the considered time interval ($t \leq 4L/c + t_m$). An approximate prediction scheme for such cases is to neglect presumably small dynamic force effects at the pile top at time $3L/c + t_m$ (the maximum damping effect is displayed in the Measured Delta curve at time $2L/c + t_m$). This assumption is derived from studies at piles with low shear resistance and relatively high damping as discussed in Appendix C. In order to avoid using a local extreme value for predicting the ultimate shear resistance an average Delta is taken over some time before and after $t_m + 3L/c$. Thus,

$$S_{o,n} \approx \frac{c}{2L} \int_{t_m+2.5L/c}^{t_m+3.5L/c} \Delta(t)\, dt \qquad (D.26)$$

An example to this computation scheme is given in Figure (D.5). It can be observed that $(4EA/c)v_A(t - 2L/c)$ is always greater than $\Delta(t)$, within the time interval $t_m + 2L/c \leq t \leq t_m + 4L/c$. The predictions taken from Figure (D.5) are:

max D = 72 and $S_{n,o}$ = 46 (kip).

The Phase III method is used as an initial estimate on the magnitudes of shear and damping forces in the wave analysis, discussed in Chapter II. Table (D.1) gives the results from both Phase III and analysis for the cases discussed in Chapter III. It can be seen that the Phase III method gives good results in most cases.

APPENDIX E

Computer Program

In the following a brief description is given of the computer program used for predicting the soil resistance forces from measurements of both pile top force and acceleration. The program is demonstrated using block diagrams and short descriptions. Only the main features of the program are discussed. Emphasis is placed on a description of both input and output.

The program consists of two parts. The first part is an ALGOL 60 routine employed for reading the dynamic data and the pile parameters. All necessary arrays are declared in this program, thus, dynamic allocation is possible.

The second part of the program consists of several FORTRAN V subroutines. A subroutine MAIN controls the actual computation process.

1. ALGOL Program PREDIC

One force record and two acceleration curves (see MAIN) are needed as dynamic input. The continuous records are digitized by placing points on the traces such that linear interpolation between these points closely resembles the original record. Both the time and the function values are then determined in units of 0.02 (inch).

Frequently, the portion of the record before impact (the acceleration is still zero while the force is already increasing as shown in Appendix B) is long. It would be unreasonable to include this portion of the record in the dynamic analysis. Therefore, an

input parameter SUB is included which is the time at which to start the dynamic computations. Also, the maximum time is limited by an input value MAXT.

The following input is necessary:

N1,N2,M	The number of values of the first acceleration, second acceleration and force trace, respectively.
S1,S2,S3,S4	Four string variables describing pile, blow, soil, and transducers, respectively.
SUB,MAXT	Time at which to start and terminate computations, respectively.
UA1,UA2	Calibration constants for first acceleration (A1) and second acceleration trace (A2), respectively.
UF,UT	Calibration constants for force values and length to time conversion, respectively.
MASS	Mass of pile
AE,LE	Cross sectional area and length of pile, respectively.
TF(J)	Force time vector in units (J = 1,2,...,M).
FO(J)	Vector of force values in units (J = 1,2,...,M).
T1(J)	Accel.-1 time vector in units (J = 1,2,...,N1).
A1(J)	Vector of accel.-1 values in u's (J= 1,2,..,N1).
T2(J)	Accel.-2 time vector in units (J = 1,2,...,N2).
A2(J)	Vector of accel.-2 values in u's (J= 1,2,..,N2). (If N2 = 0 then no values for T2(J)and A2(J) have to be given).

Procedure:

From MASS and LE together with $\phi = 2$ and N = 10 (N being the number of elements to be used in the lumped mass analysis) the time increment DET is computed (see Appendix A1). From the total time interval (MAXT - SUB) one obtains NT, the number of time increments necessary. PREDIC now calls MAIN.

2. FORTRAN Subroutines

MAIN controls the computation process. The following subroutines are called:

ANALYS	For lumped mass analysis (see Appendix A1).
DISTRI	For computing shear resistance distributions.
LEASTS	For performing a Least Suare Analysis.
PILEPL	For plotting results.
RESIST	For finding soil resistances (Eqs (A3.30,38)).
SMOOTH	For smoothing a given function.
STATIC	For finding a theoretical load versus penetration curve see Appendix A2).

In the following these subroutines and MAIN are discussed in more detail.

(a) ANALYS (see Appendix A1)

Problem: For given pile top acceleration (velocity, displacement), pile properties and resistance force parameters find the pile top force and displacements along the pile.

Input:

A(1,J)	Pile top acceleration (J = 1,2,...,NT)
V(1,J)	Pile top velocity (J = 1,2,...,NT)
D(1,J)	Pile top displacement (J = 1,2,...,NT)
K	Element stiffness
MA	Element mass
N	Number of pile elements
NT	Number of time increments

Procedure: see Block Diagram

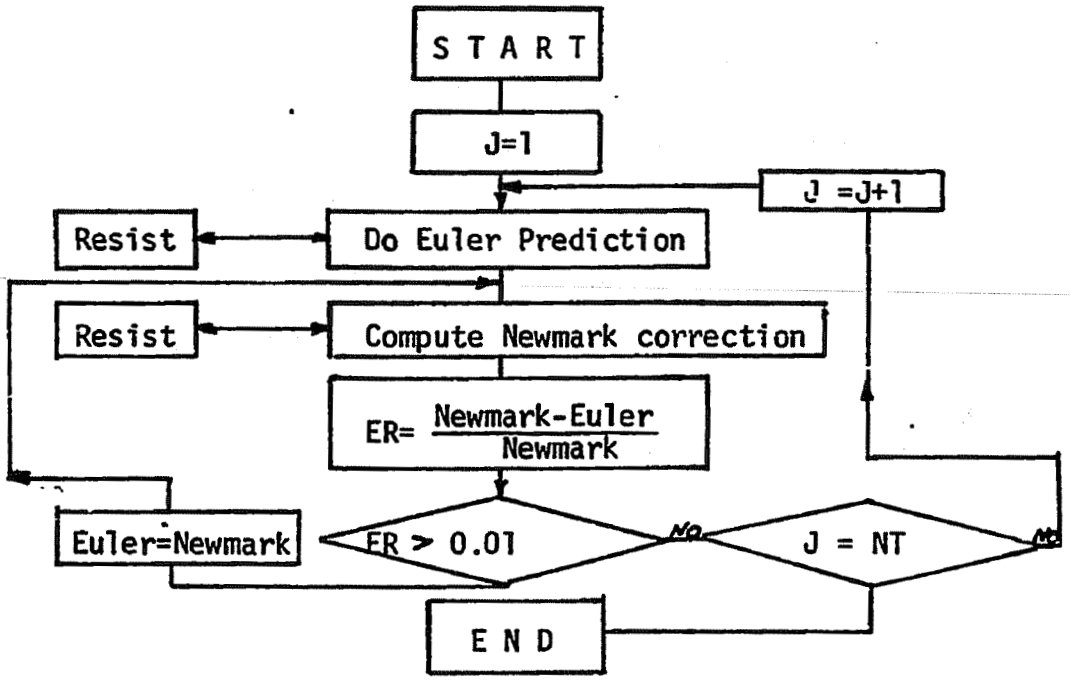

(b) DISTRI (see A3.6)

Problem: Compute corrections on predicted shear resistance forces and damping coefficients for given Error Delta curve and displacements and velocities from corresponding analysis.

Input:

DN(J)	Error Delta curve
RE(I)	Previous ultimate shear resistance forces
CO(I)	Previous damping coefficients
ITIME(I)	Time value at which full effect of ultimate shear resistance RE(I) can be felt at pile top.
V(I,J)	Velocity of i-th element at time J*DET
D(I,J)	Displacement of i-th element at time J*DET
DAMP(I)	Damping force to effect pile top at time ITIME(I).
DET	Time increment.
N,NT	As introduced in PREDIC

J = 1,2,...,NT I = 1,2,...,N

Procedure:

Compute C- and E-Matrix. Compute differences ΔD between proposed and actually obtained damping forces. Reduce Error Delta curve by ΔD effects. Reduce Error Delta curve by the effects of returning reflection waves due to shear forces. Compute corrections on ultimate shear resistance forces and find new damping coefficients.

(c) LEASTS

Problem: Compute coefficients A1, A2, A3 such that

$$A1 + A2 + A3 = 1$$

and

$$\int \{ \Delta(t) \}^2 dt \text{ becomes a minimum}$$

where

$$\Delta(t_j) = A1*DN1(J)+A2*DN2(J)+A3*DN3(J)$$

Input:

DN1(J)	Error Delta curve for first damping distribution
DN2(J)	Error Delta curve for 2nd damping distribution
DN3(J)	Error Delta curve for third damping distribution
DET	As in PREDIC
NT	As in PREDIC
	J = 1,2,...,NT

Procedure:

Generate a weighting function w(t).

Set up Normal Equations.

Solve Normal Equations.

Output: A1, A2, A3.

(d) PILEPL

Problem: Plot measured and predicted pile top force as a function of time.

Input:

FTOP(J)	Measured pile top force

	F(1,J)	Predicted pile top force
	NT	As introduced in PREDIC
		J = 1,2,...,NT

(e) RESIST (see Equations (A3.30,38)

Problem: Compute shear and damping resistance force for element INOW at time JNOW*DET.

Input:	INOW	Element number
	JNOW	Time increment number
	RE(INOW)	Ultimate shear resistance of element INOW
	QO(INOW)	Quake of element INOW
	CO(INOW)	Damping coefficient of element INOW
	V(INOW,J)	Velocity at element INOW
	D(INOW,J)	Displacement at element INOW
		J = 1,2,...,JNOW

Procedure:

Solve Equation (A3.30).

Solve Equation (A3.38).

Output:	RESI	Shear resistance at element INOW and time JNOW*DET
	DI	Damping resistance at element INOW and time JNOW*DET.

(f) SMOOTH

Problem: Time average a given curve to obtain a smooth curve.

Input:	ROUGH(J)	Original function.

	ISTART	First value of ROUGH to be included in smoothing.
	ISTOP	Last value of ROUGH to be included in smoothing.
	ITVAL	Time interval DET*ITVAL is to be used as interval over which to integrate for smoothing. Odd integer.
	CUT	Option: CUT = 1 means no change of function before ISTART. CUT = 2 means set all function values to zero before ISTART.

Procedure:

Integrate ROUGH over time interval ITVAL*DET and divide result by ITVAL*DET. This yields the new function value at the middle of the time interval. The new function is called SMOOTH.

Output: SMOOTH(J) New smooth function between ISTART and ISTOP.

Either SMOOTH(J) = 0
Or SMOOTH(J) = ROUGH(J) } for J < ISTART

and SMOOTH(J) = ROUGH(J) for J > ISTOP

(g) STATIC (see Appendix A2)

Problem: For given static soil resistance parameters and pile stiffness compute static load versus deflection curve.

Input:	RE(I)	Shear resistance force at i-th element
	QO(I)	Quake at i-th element
	K	Stiffness of pile element
	N	As introduced in PREDIC.
		I = 1,2,...,N

Procedure: see Block Diagram

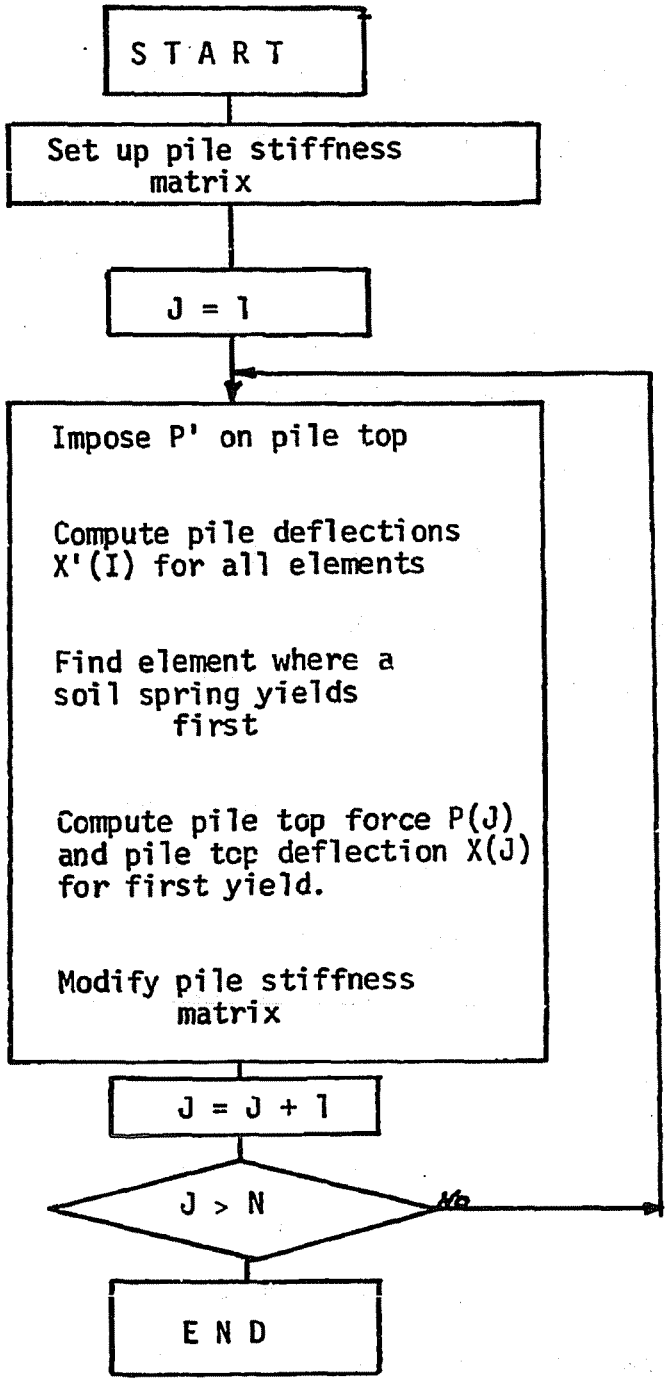

(h) MAIN (see Appendix A3)

Problem: For given pile properties and both measured force and acceleration find shear and damping resistance distribution for a best match of predicted with measured top force. Also, predict static load versus deflection curve. Plot and print pile top forces both measured and predicted. Print predicted pile displacements, velocities and forces below pile top.

Input:

A1(J)	Acceleration 1	} measured at opposite sites of pile
A2(J)	Acceleration 2	
FTOP(J)	Measured pile top force	
DET	Time increment	
N	Number of pile elements	
NT	Number of time increments	
LE	Length of pile	
AE	Pile cross sectional area	
MASS	Pile Mass	

Procedure: see Block Diagram

"Prepare" stands for the following manipulations:
Use E =30.8 (psi) and compute pile element stiffnesses K. Compute element mass MA. Average both acceleration curves. Integrate acceleration twice. Subtract precompression force from force record.

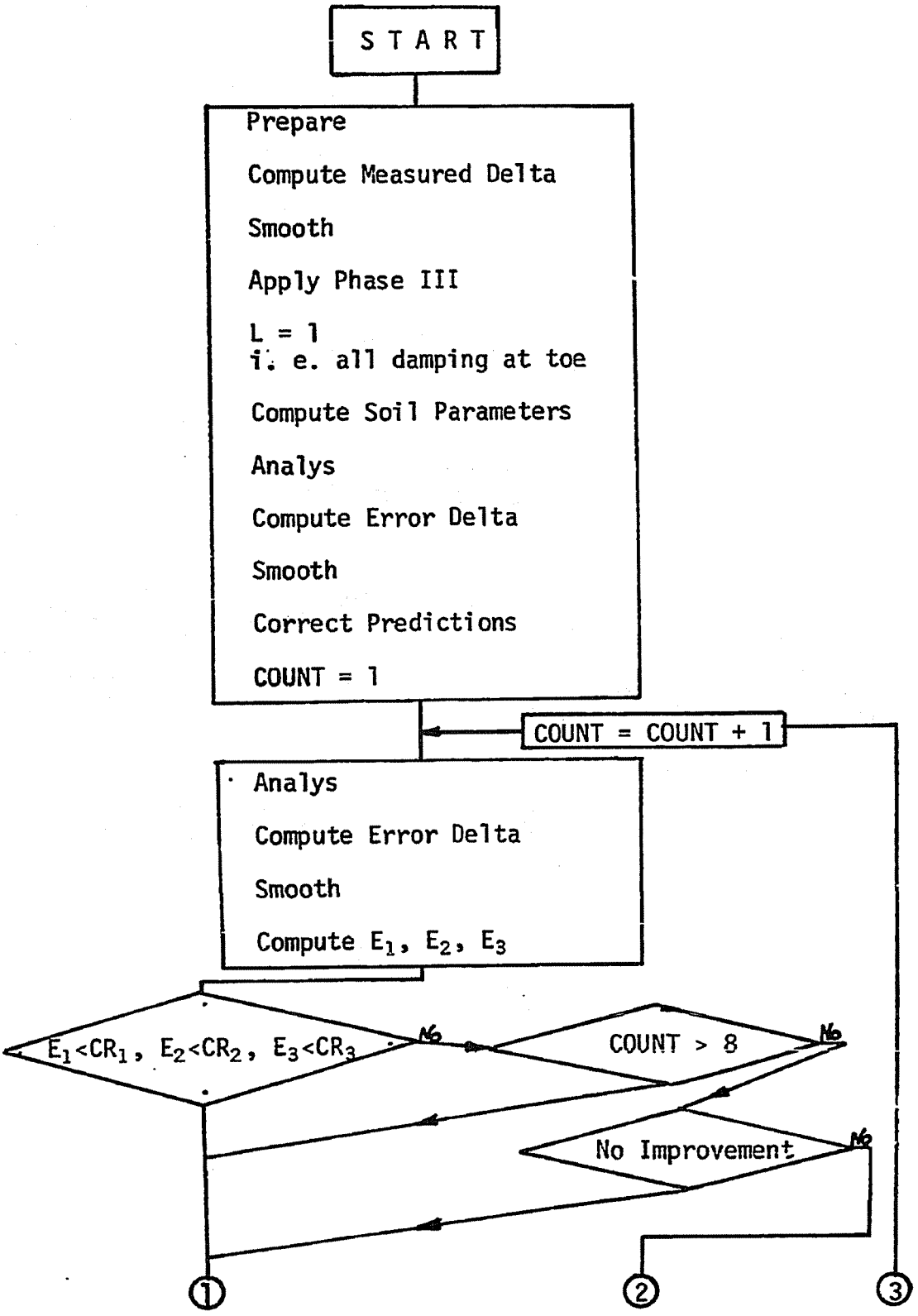
START
Prepare
Compute Measured Delta
Smooth
Apply Phase III
L = 1
i. e. all damping at toe
Compute Soil Parameters
Analys
Compute Error Delta
Smooth
Correct Predictions
COUNT = 1
COUNT = COUNT + 1
Analys
Compute Error Delta
Smooth
Compute E1, E2, E3
E1<CR1, E2<CR2, E3<CR3
No
COUNT > 8
No
No Improvement
No
1
2
3

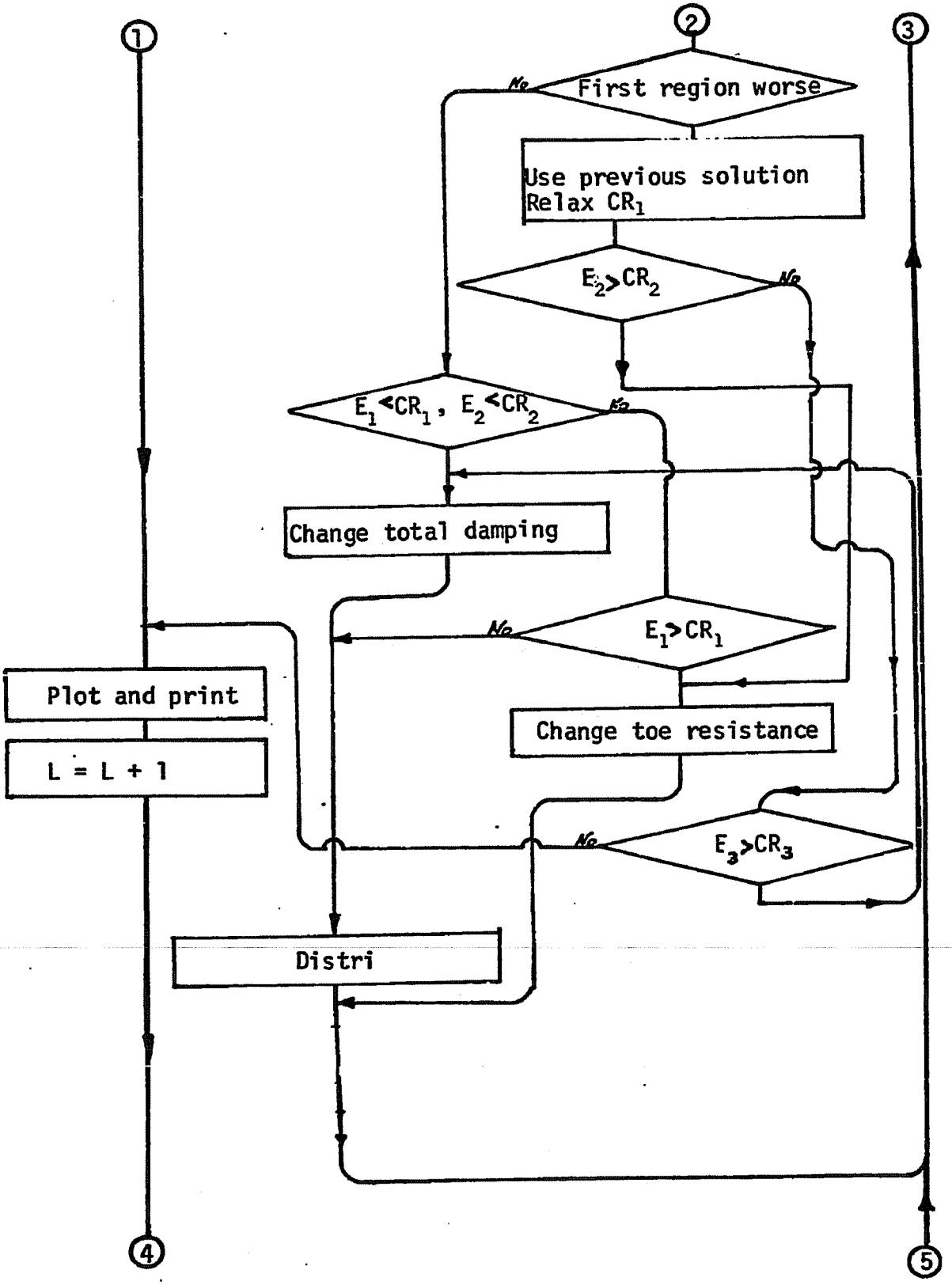
1
2
3
First region worse
No
Use previous solution
Relax CR1
E2>CR2
No
E1<CR1, E2<CR2
No
Change total damping
E1>CR1
No
Plot and print
L = L + 1
Change toe resistance
E3>CR3
No
Distri
4
5

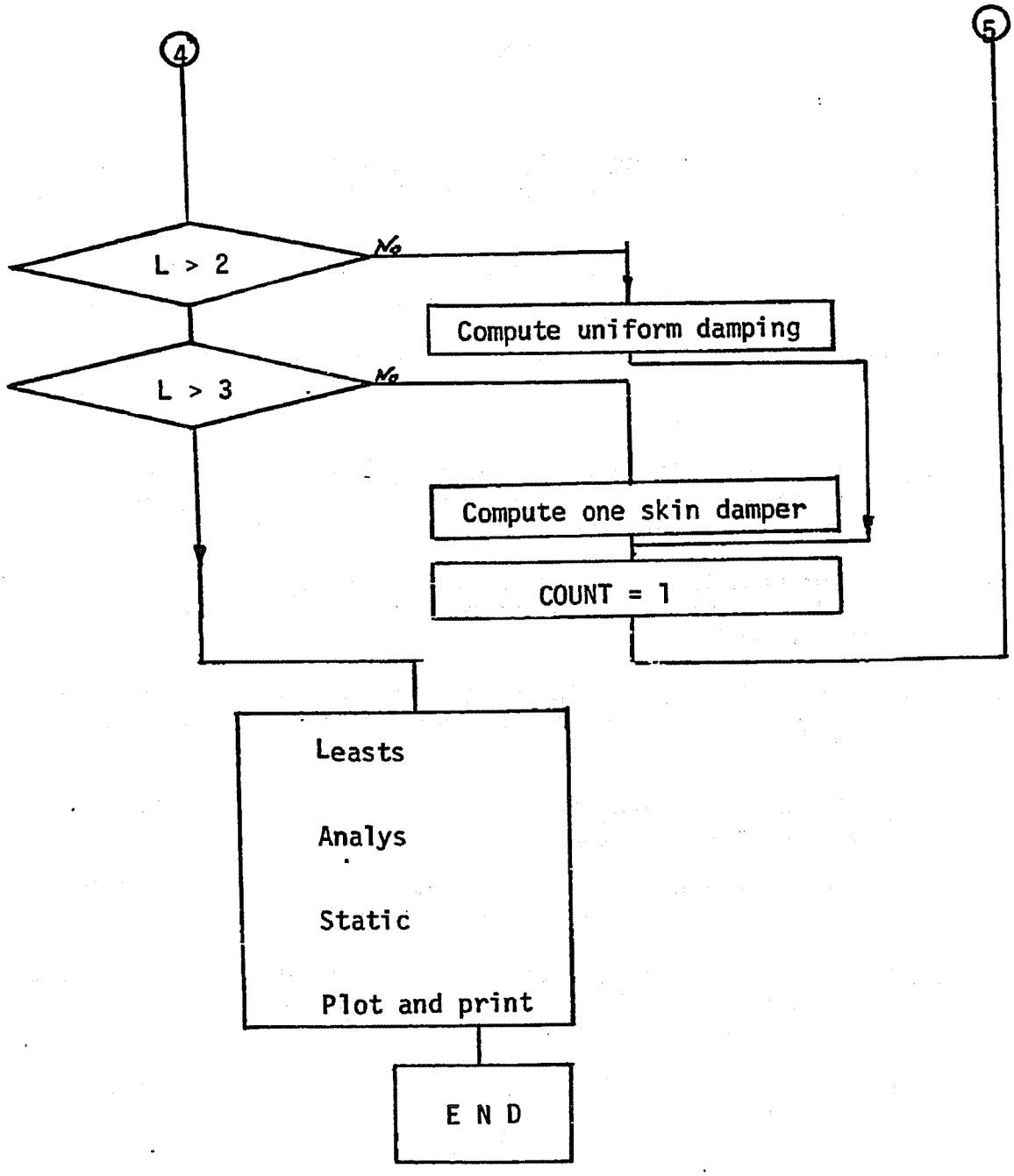
4
5
L > 2
No
Compute uniform damping
L > 3
No
Compute one skin damper
COUNT = 1
Leasts
Analys
Static
Plot and print
E N D

References

1. Mattes,N.S. and Poulos,H.G.(1968),"Analysis of the Settlement of a Single Compressible Pile",Civil Engng Res. Rep. No. R94, University of Sidney.

2. Poulos,H.G. and Mattes,N.S.(1969),"The Behavior of Axially Loaded End-Bearing Piles",Geotechnique 19, No.2, 285-300.

3. LaPay,W.S.,"Dynamic Pile Behavior - Literature Survey and Response Studies", Master's Thesis, Case Institute of Technology, 1965.

4. Coyle,H.M. and Sulaiman,I.H.,"Bearing Capacity of Foundation Piles -- State of the Art", paper presented to the Highway Research Board Annual Meeting, January, 1970, Washington, D.C.

5. "A Performance Investigation of Pile Driving Hammers and Piles", Michigan State Highway Commission, Lansing, Michigan, March, 1965.

6. Isaacs,D.V.,"Reinforced Concrete Pile Formulas", Transactions of the Institution of Engineers, Australia,XII, 1931,pp 305-323.

7. Fox,E.N.,"Stress Phenomena Occurring in Pile Driving", Engineering, 134 (Sept. 2, 1932), 263-265.

8. Timoshenko,S.and Goodier,J.M.,"Theory of Elasticity", McGraw-Hill, Second Edition, 1951, p. 438.

9. Smith, E. A. L.,"Pile Driving Analysis by the Wave Equation", Journal of Soil Mechanics and Foundations, American Society of Civil Engineers, 86, August, 1960, pp. 35-61.

10. Samson, C. H., Hirsch,T. L. and Lowery, L.L.,"Computer Study of the Dynamic Behavior of Piling," Journal of the Structural Division, Proceedings, ASCE, Paper No. 3608, ST4, August, 1963.

11. Forehand, P. W. and Reese, J. L.,"Prediction of Pile Capacity by the Wave Equation", Journal of the Soil Mechanics and Foundation Division, ASCE, 90, (March 1964), pp. 1-25.

12. Goble, G.G., Scanlan, R.H., Tomko, J. J., "Dynamic Studies on the Bearing Capacity of Piles", paper presented to the Highway Research Board Annual Meeting, Jan. 1967, Washington D.C.

References (cont'd)

13. Tomko, J. J., "Dynamic Studies on Predicting the Static Bearing Capacity of Piles", Ph. D. Dissertation, Case Western Reserve University, 1968.

14. Newmark, N. M., " A Method of Computation for Structural Dynamics" Proceedings,ASCE,85, EM3, 1959, p. 67.

15. Donnell, L. H., "Longitudinal Wave Transmission and Impact", Transactions, ASME, Applied Mechanics Division, APM-52-14, 1930.

16. Olson, R.E. and Flaate, R.S., "Pile Driving Formulas for Friction Piles in Sand," Journal of the Soil Mechanics and Foundation Division, ASCE, Vol. 93, No. SM6, November, 1967, pp 279-296.

17. Crandall, S. H., "Engineering Analysis", McGraw-Hill, 1956, p.396.

18. Yang, N.C., "Relaxation of Piles in Sand and Inorganic Silt", Journal of the Soil Mechanics and Foundation Division, Proc. ASCE, SM2, March, 1970.

19. Tsai, K. W. and Schmid, W. E., "Penetrometer Method for Determining Soil Parameters", Proceedings of the Seventh International Conference on Soil Mechanics and Foundation Engineering, Mexico, 1969, Vol. I, pp 443-448.

20. Goble, G. G. and Rausche, F., "Pile Load Test by Impact Driving", paper presented to the Highway Research Board Annual Meeting, January, 1970, Washington D. C.

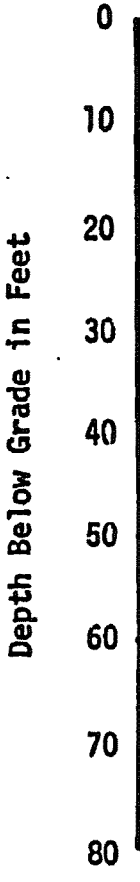

Description	Surface Elevation at 610 Feet						
	Sample No.	Physical Characteristics in %					
		Agg.	C.S.	F.S.	Silt	Clay	W.C.
Brown Silt Gray Silt	2	0	0	0	78	22	24
Gray Silt Gray Clayey Silt	4	0	1	1	64	34	28
Gray Silt Gray Silt	8	0	0	0	73	27	25
Gray Clayey Silt Gray Gravelly Silt Gray Sandy Silt	11	13	5	6	39	37	18
Gray Sandy Silt Gray Silt and Clay	15	0	6	11	41	42	17
Gray Silt and Clay Gray Gravelly Clay	18	15	5	9	35	36	16
Gray Gravelly Clay Cray Silt and Clay	20	0	4	11	29	56	18
Gray Sandy Silt Gray Clayey Silt	22	0	4	6	42	48	18

TABLE 1.1: SOIL CHARACTERISTICS AT TEST SITE IN TOLEDO

Surface Elevation at 951.1 Feet

Depth Below Grade in Feet	Description	Sample No.	Physical Characteristics in %					
			Agg.	C.S.	F.S.	SILT	CLAY	W.C.
0	Brown Clayey Silt Slightly Organic	3	0	1	8	49	42	30
10	Gray Silt and Clay	6	0	3	13	40	44	27
20	Gray Silt and Clay	9	0	2	1	44	53	25
30	Gray Silt and Clay	11	0	1	0	45	54	30
40	Gray Silt	13	0	1	1	71	27	31
50	Gray Silty Clay	15	0	0	1	24	75	28
60	Gray Silty Sandy Gravel	17	15	49	9	2	7	13
70	Bottom of Boring at 70 Feet Below Grade							
80								

TABLE 1.2: SOIL CHARACTERISTICS AT TEST SITE IN RITTMAN OHIO

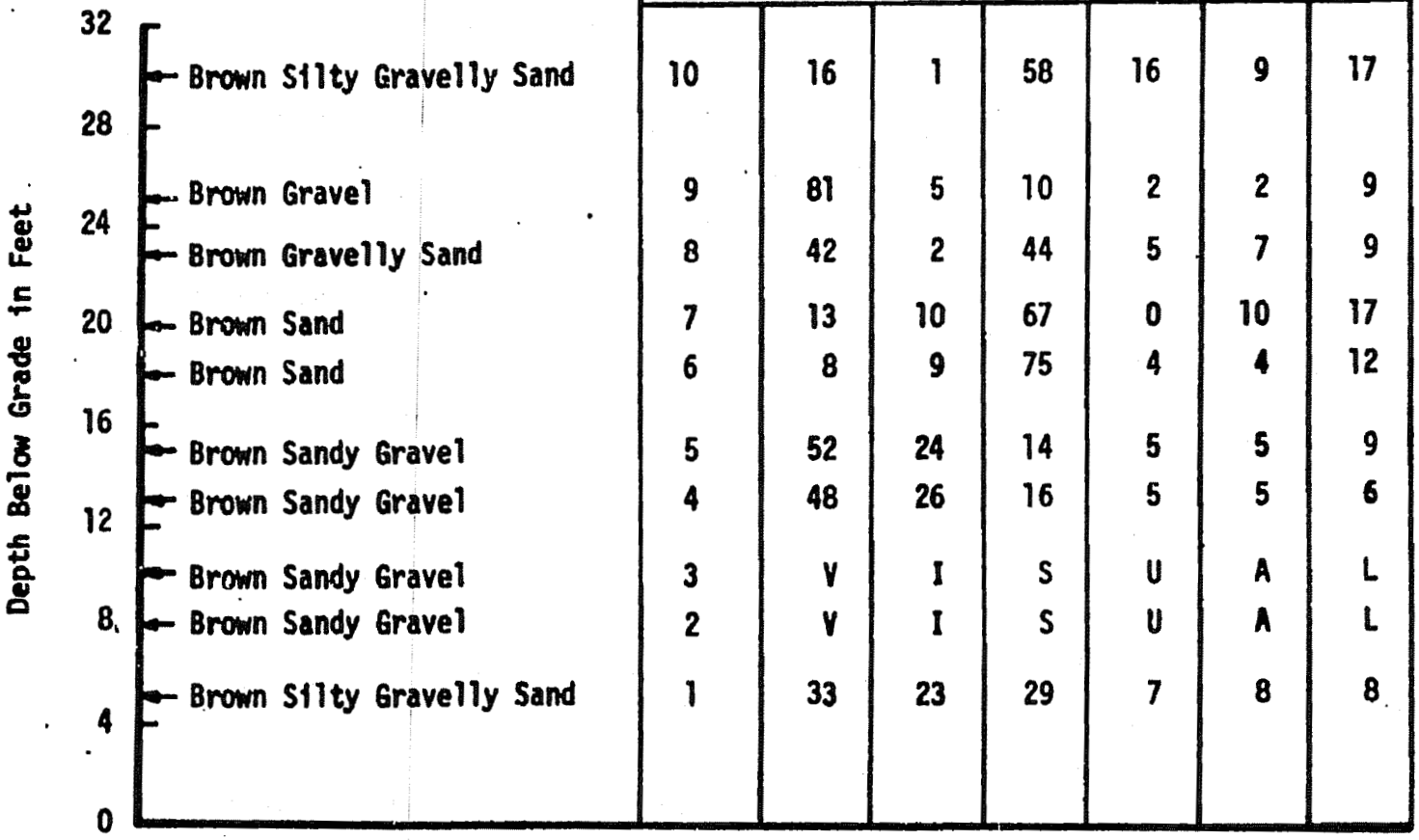

Sample No.	Physical Characteristics in %					
	Agg.	C.S.	F.S.	Silt	Clay	W.C.
10	16	1	58	16	9	17
9	81	5	10	2	2	9
8	42	2	44	5	7	9
7	13	10	67	0	10	17
6	8	9	75	4	4	12
5	52	24	14	5	5	9
4	48	26	16	5	5	6
3	V	I	S	U	A	L
2	V	I	S	U	A	L
1	33	23	29	7	8	8

TABLE 1.3: SOIL CHARACTERISTICS AT TEST SITE FOR REDUCED SCALE PILES

Pile No.	Pile Name	q_1	q_5	q_{10}
3	531-76	.12	.12	.09
5	F-30	.07	.06	.05
6	F-30A	.09	.07	.05
7	F-50	.10	.08	.07
8	F-50A	.10	.07	.05
9	F-60	.12	.09	.07
10	F-60A	.11	.09	.07
11	Cincinnati	.11	.09	.06
12	272 Toledo	.12	.09	.07
13	To-50	.08	.07	.06
14	To-50A	.11	.09	.07
15	To-60	.07	.06	.05
16	To-60A	.10	.08	.06
17	Logan	.12	.12	.10
18	W-56	.12	.10	.07
19	W-76	.12	.10	.07
20	Chillicothe	.10	.08	.06
21	Ri-50	.06	.06	.05
22	Ri-50A	.12	.12	.10
23	Ri-60	.11	.10	.09
24	Ri-60A	.11	.10	.08

Not listed values can be obtained by interpolation

TABLE 2.1: TABULATION OF QUAKES USED IN PREDICTION ANALYSES

DATA SET NO.	PILE NAME	DATE DRIVEN	DATE LOAD TESTED	DATE OF DYN. MEAS.	SOIL	LENGTH L	AREA A IN^2	HAMMER	REMARKS
1	C-1	12-28-66	12-30-66	1-3-67	G.Sa.	58	5.81	D-12	Fluted and taperd
2	531-70	4-12-67	5-12-67	4-13-67		70	5.81		
3	531-76	4-13-67	4-17-67	4-18-67		82	5.81		
4	531-83	4-18-67	4-18-67	4-18-67		82	5.81		
5	F-30	6-21-67	6-21-67	6-21-67	Si& Sa	32.5	9.82	L.B.	Specl. Test (13)
6	F-30A	6-21-67	6-28-67	6-28-67		32.5	9.82		
7	F-50	6-28-67	6-28-67	6-28-67		50.5	9.82		
8	F-50A	6-28-67	7-5-67	7-6-67		50.5	9.82		
9	F-60	7-7-67	7-7-67	7-7-67		59.5	9.82		
10	F-60A	7-7-67	7-20-67	7-20-67		59.5	9.82		
11	Cincinnati	12-22-67	1-4-68	1-4-68	G.Sa.	69	6.66	D-12	
12	272 Toledo	4-10-68	4-17-68	5-18-68	Si.&C	54	6.66	L.B.	
13	To-50	9-6-68	9-6-68	9-6-68	see Table (1.1)	49	9.82	D-12 L.B.	Specl. Test Ch. I
14	To-50A	9-6-68	9-9-68	9-10 68		49	9.82		
15	To-60	9-11-68	9-11-68	9-11-68		59	9.82		
16	To-60A	9-11-68	9-18-68	9-18-68		59	9.82		
17	Logan	11-25-68	11-5-68	11-5-68	G.Sa	57	6.66		
18	W-56	6-11-69	6-18-69	6-18-69	Si.&C	55	6.66		
19	W-76	6-19-69	6-24-69	6-24-69		75	6.66		
20	Chillicothe	9-18-69	9-25-69	9-25-69	G.&S	40.5	6.66		
21	Ri-50	1-6-70	1-6-70	1-6-70	see Table (1.2)	49	9.31		Specl. Test Ch. I
22	Ri-50	1-6-70	1-6-70	1-6-70		49	9.31		
23	Ri-60	1-9-70	1-9-70	1-9-70		61.5	9.31		
24	Ri-60A	1-9-70	1-20-70	1-20-70		57	9.31		

All piles were of 12-inch diameter pipe.

G.Sa. Gravelly Sand
Si & Sa Silt and Sand
Si & C Silt and Clay
G & S Gravel and Sand

D-12 Delmag
L.B. Linkbelt 440

TABLE 3.1: DESCRIPTION OF FULL SCALE TEST PILES

DATA SET NO.	PILE NAME	DATE DRIVEN	DATE LOAD TESTED	DATE OF DYN. MEAS.	SOIL	LENGTH L FT	REMARKS
1	2-R-10	7-27-67	7-27-67	7-27-67	see Table (1.3)	10.8	
2	2-R-10A	7-27-67	8-1-67	8-1-67		15.8	
3	2-R-15	8-1-67	8-1-67	8-1-67		15.8	
4	2-R-15A	8-1-67	8-4-67	8-4-67		20.8	
5	2-R-20	8-4-67	8-4-67	8-4-67		20.8	
6	2-R-20A	8-4-67	8-9-67	8-9-67		23.8	
7	3-R-10	8-18-67	8-18-67	8-18-67		10.8	
8	3-R-10A	8-18-67	8-22-67	8-22-67		15.8	
9	3-R-15	8-22-67	8-22-67	8-22-67		15.8	
10	3-R-15A	8-22-67	8-28-67	8-28-67		20.8	
11	3-R-20	8-30-67	8-30-67	8-30-67		20.8	
12	3-R-20A	8-30-67	9-5-67	9-5-67		23.8	
13	1-T-15/20	11-25-67	11-25-67	11-25-67	Silt and Clay	22.4	3 additional Accel at force records tip
14	1-T-15/20A	11-25-67	12-2-67	12-2-67		22.4	
15	2-T-15/20	12-28-67	12-28-67	12-28-67		22.4	
16	2-T-15/20A	12-28-67	1-13-68	1-13-68		22.4	
17	3-T-15	6-11-68	6-11-68	6-11-68		22.4	
18	3-T-15/20A	6-11-68	6-17-68	6-17-68		22.4	
19	4-T-15/20	6-29-68	6-29-68	6-29-68		22.4	
20	4-T-15/20A	6-29-69	7-3-68	7-3-68		22.4	
21	6-T-15	7-31-69	7-31-69	7-31-69		20.1	
22	6-T-15A	7-31-69	8-7-69	8-7-69		20.1	
23	6-T-20	8-7-69	8-7-69	8-7-69		20.1	
24	6-T-20A	8-7-69	8-15-69	8-15-69		20.1	

Cross Sectional Area = 1.7 in^2 for all listed piles.

TABLE 3.2: DESCRIPTION OF REDUCED SCALE TEST PILES

DATA SET NO.	PILE NAME	LOAD TEST RESULT AT max d_A R_d	LOAD TEST RESULT AT ULTIMATE[1] R_o	PRECOMPRESSION FORCE S_p	PREDICTED SHEAR FORCES S_o	PREDICTED STATIC RESISTANCE R_o	TOTAL MAX. DAMPING FORCES max D
3	531-76	151	198	18	141	159	15
5	F-30	97	103	33	55	88	39
6	F-30	107	114	30	106	;36	24
7	F-50	172	224	29	138	167	41
8	F-50	200	238	52	178	230	52
9	F-60	176	204	29	171	200	25
10	F-60	174	242	40	158	198	52
11	Cincinnati	137	190	39	122	161	17
12	272 Toledo	183	221	66	138	229	22
12[2]	272 Toledo	183	221	66	138	204	22
13	To-50	60	69	26	36	62	57
14	To-50	93	94	33	86	119	88
15	To-60	32	43	29	26	55	69
16	To-60	75	86	25	94	119	106
17	Logan	165	220	13	167	180	54
18	W-56	90	92	20	123	143	125
19	W-76	125	160	22	139	161	141
19[2]	W-76	125	160	22	129	151	127
20	Chillicothe	152	207	18	133	151	18
21	Ri-50	40	46	23	22	45	88
22	Ri-50	64	64	15	70	85	105
23	Ri-60	176	-[3]	22	167	189	92
24	Ri-60	174	-[3]	9	185	194	48

[1]Ultimate may be defined here as the maximum value obtained in the load test
[2]Obtained by Inspection
[3]Load test incomplete

ALL RESULTS IN KIPS

TABLE 3.3: SUMMARY OF RESULTS FROM WAVE ANALYSIS

DATA SET NO.	PILE NAME	R_d	R_u	PHASE I	PHASE II	PHASE IIA	PHASE III	WAVE ANALYSIS
1	C-1	180	192	174^{1}	138^{1}	173^{3}	170^{3}	*
2	531-70	122	190	201^{3}	197^{3}	141^{3}	173^{3}	*
3	531-76	151	198	170^{4}	157^{4}	115^{4}	137^{4}	159^{1}
4	531-83	110	200	211^{3}	187^{3}	143^{3}	154^{3}	*
5	F-30	97	107	125^{5}	113^{5}	110^{5}	98^{5}	91^{2}
6	F-30A	107	112	162^{4}	152^{4}	164^{5}	172^{5}	136^{1}
7	F-50	172	224	281^{3}	197^{3}	177^{3}	175^{3}	163^{3}
8	F-50A	200	238	294^{4}	258^{4}	205^{4}	236^{4}	233^{2}
9	F-60	176	204	288^{4}	251^{4}	207^{4}	233^{4}	210^{2}
10	F-60A	174	242	355^{3}	226^{3}	188^{3}	195^{3}	180^{2}
11	Cincinnati	137	190	250^{3}	185^{3}	138^{3}	175^{3}	166^{3}
12	272	183	221	315^{7}	275^{7}	267^{7}	231^{7}	204^{1}
13	To-50	60	69	69^{3}	63^{3}	77^{5}	60^{5}	69^{2}
14	To-50	93	94	121^{6}	129^{6}	105^{6}	115^{2}	119^{1}
15	To-60	32	43	89^{4}	81^{4}	77^{4}	62^{4}	56^{2}
16	To-60A	75	86	141^{3}	137^{3}	113^{3}	121^{3}	122^{2}
17	Logan	165	220	275^{4}	223^{4}	180^{4}	177^{4}	173^{2}
18	W-56	90	92	207^{4}	227^{4}	161^{4}	184^{4}	151^{4}
19	W-76	125	160	276^{5}	264^{5}	167^{5}	143^{1}	151^{1}
20	Chillicothe	152	207	316^{3}	200^{3}	180^{3}	173^{3}	163^{2}
21	Ri-50	40	46	-	-	64^{3}	70^{3}	45^{1}
22	Ri-50A	64	64	-	-	120^{3}	110^{3}	84^{3}
23	Ri-60	176	-	264^{3}	251^{3}	140^{3}	172^{3}	184^{2}
24	Ri-60A	174	-	179^{2}	184^{2}	162^{3}	187^{3}	187^{2}

Numerals on predictions indicate the number of blows analyzed.

TABLE 3.4: SUMMARY OF RESULTS FOR PREDICTING STATIC BEARING CAPACITY ON FULL SCALE PILES

PILE NO.	PILE NAME	R_u	PHASE I	PHASE II	PHASE IIA	PHASE III
1	2-R-10	12.1	19.6[2]	19.2[2]	12.9[3]	19.3[3]
2	2-R-10A	12.1	23.5[2]	17.4[2]	15.5[3]	23.4[3]
3	2-R-15	13.0	26.2[3]	17.1[3]	20.7[3]	30.2[3]
4	2-R-15A	16.3	31.8[3]	26.4[3]	21.0[3]	34.2[3]
5	2-R-20	18.1	33.5[4]	37.1[4]	22.2[4]	38.4[4]
6	2-R-20A	20.2	39.4[4]	44.8[4]	32.6[4]	41.7[4]
7	3-R-10	10.8	15.0[3]	16.3[3]	13.0[3]	22.2[3]
8	3-R-10A	11.5	26.9[3]	16.5[3]	12.7[3]	21.8[3]
9	3-R-15	11.0	20.2[3]	14.8[3]	8.5[3]	27.8[3]
10	3-R-15A	15.3	31.8[3]	23.4[3]	13.8[3]	32.5[3]
11	3-R-20	16.0	24.0[3]	20.4[3]	9.5[3]	35.1[3]
12	3-R-20A	17.7	34.8[6]	34.9[6]	20.5[6]	35.2[6]
13	1-T-15/20	15.8	23.0[1]	16.1[1]	12.1[1]	9.6[1]
14	1-T-15/20A	17.4	26.4[3]	23.5[3]	16.1[3]	22.5[3]
15	2-T-15/20	15.0	17.9[1]	14.3[1]	8.7[1]	15.5[1]
16	2-T-15/20A	22.0	20.6[1]	20.5[1]	13.1[1]	24.7[1]
17	3-T-15/20	14.0	16.7[3]	12.8[3]	13.1[3]	14.6[3]
18	3-T-15/20A	15.1	22.2[3]	16.4[3]	15.4[3]	18.1[3]
19	4-T-15/20	12.4	13.1[5]	10.3[5]	12.3[5]	13.6[5]
20	4-T-15/20A	13.8	15.4[4]	11.9[4]	13.0[4]	18.0[4]
21	6-T-15	12.6	25.2[2]	14.3[2]	9.8[2]	12.7[2]
22	6-T-15A	14.5	18.3[3]	15.4[3]	10.8[3]	15.5[3]
23	6-T-20	12.8	24.5[3]	11.7[3]	12.7[3]	16.6[3]
24	6-T-20A	15.2	14.3[2]	13.2[2]	8.0[2]	17.3[2]

Numerals on predictions indicate the number of blows analyzed.

TABLE 3.5 SUMMARY OF RESULTS FOR PREDICTING STATIC BEARING CAPACITY ON REDUCED SCALE PILES

METHOD	SLOPE $m \pm \sigma_m$	Intercept (kips) $b \pm \sigma_b$	CORRELATION COEFFICIENT r
Phase IIA	0.998 ±0.146	-19 ±22	.83
Phase III	0.867 ±0.108	-7 ±17	.87
Analysis	0.949 ±0.067	-11 ±10	.94
Enging. News	.33	+74	.29
Gow	.32	+74	.36
Hiley	.92	+14	.72
Pacific Coast	1.04	+14	.76
Jambu	.87	+20	.81
Danish	.77	-4	.81
Gates	1.81	-96	.81

TABLE 3.6: STATISTICAL PARAMETERS FOR SIMPLIFIED METHODS AND ENERGY FORMULAS (16)

	ELEMENT NUMBER										
DATA SET NO.	1	2	3	4	5	6	7	8	9	10	EA/c
3	0	0	0	0	.017	0	0	0	.173	.148	10.5
5	0	0	0	0	.025	0	0	0	.160	.158	17.8
6	0	0	0	0	.104	0	0	0	.129	.317	17.8
7	0	0	0	0	0	0	0	0	.158	.150	17.8
8	0	0	0	.009	.081	.046	.049	.055	.055	.090	17.8
9	0	0	0	0	.003	0	.001	.024	.028	.140	17.8
10	0	0	0	0	.001	.005	.003	0	.560	.394	17.8
11	0	0	0	0	.134	0	0	0	0	.041	12.1
12	0	0	0	0	0	0	0	0	0	.254	12.1
13	0	0	0	.032	0	0	0	.114	.234	.122	17.8
14	0	0	0	.435	0	0	0	0	.112	.412	17.8
15	0	0	.157	.012	0	0	.001	.008	0	.554	17.8
16	0	0	.312	0	0	0	0	0	.431	.424	17.8
17	0	0	.009	0	0	.012	0	.020	.025	.455	12.1
18	0	0	0	.021	.445	.032	.040	.047	.042	1.312	12.1
19	0	.072	.053	0	.308	0	.042	0	0	2.370	12.1
20	0	0	.110	0	0	0	0	0	0	.260	12.1
21	0	0	0	.100	0	0	0	0	.263	.292	16.9
22	0	0	.039	0	0	0	0	0	.246	.309	16.9
23	0	0	0	.087	0	.013	0	0	.017	.338	16.9
24	0	0	0	.110	.016	.017	.018	.019	.020	.117	16.9

TABLE 4.1: DIMENSIONLESS DAMPING COEFFICIENT $d_n/(EA/c)$ AS DETERMINED BY WAVE ANALYSIS

DATA SET NO.	ELEMENT NUMBER 1	2	3	4	5	6	7	8	9	10	Element length ft	Enclosed cross sectional area in^2
3	0	0	0	0	.18	0	0	0	1.82	1.55	8.20	28 (at tip)
5	0	0	0	0	.45	0	0	0	2.86	2.80	3.25	128
6	0	0	0	0	1.85	0	0	0	2.29	5.65	3.25	128
7	0	0	0	0	0	0	0	0	2.80	2.68	5.05	128
8	0	0	0	.16	1.44	.82	.88	.98	.99	1.60	5.05	128
9	0	0	0	0	.06	0	.02	.43	.49	2.50	5.95	128
10	0	0	0	0	.03	.09	.05	0	.10	6.97	5.95	128
11	0	0	0	0	1.62	0	0	0	0	.50	6.90	113
12	0	0	0	0	0	0	0	0	3.17	3.17	5.40	113
13	0	0	0	.56	0	0	0	2.03	4.17	2.17	4.90	128
14	0	0	0	7.75	0	0	0	0	2.00	7.35	4.90	128
15	0	0	2.81	.20	0	0	.02	.14	0	9.89	5.90	128
16	0	0	5.55	0	0	0	0	0	7.67	7.54	5.90	128
17	0	0	.06	0	0	.14	0	.24	.30	5.50	5.70	113
18	0	0	0	.25	5.37	.39	.48	.57	.51	15.84	5.50	113
19	0	.87	.64	0	3.70	0	.50	0	0	28.6	7.50	113
20	0	0	1.33	0	0	0	0	0	0	3.15	4.05	113
21	0	0	0	1.67	0	0	0	0	4.44	4.93	4.90	113
22	0	0	.65	0	0	0	0	0	3.90	5.22	4.90	113
23	0	0	0	1.47	0	.23	0	0	.29	5.70	6.15	113
24	0	0	0	1.85	.28	.29	.30	.32	.34	1.97	5.70	113

TABLE 4.2: NATURAL DAMPING COEFFICIENTS d_n[kips/ft/sec] AS DETERMINED BY WAVE ANALYSIS

No. of Computation	No. of Elements (L in Ft)	$\phi = \frac{\Delta L}{\Delta t \cdot c}$ (Δt in Ms)	Convergence Crit. ε	Time Consumption in Seconds	Plotted in Figure
1	5(15.6)	1(.908)	.01	1/2	-
2	5(15.6)	2(.454)	.01	1	-
3	5(15.6)	4(.227)	.01	2	A1.2
4	10(7.8)	2(2.77)	.01	2	A1.2
5	10(7.8)	2(.227)	No Iteration	1	-
6	20(3.9)	$\frac{1}{2}$(.454)	.01	2 (unstable)	A1.3
7	20(3.9)	1(.227)	.01	3	A1.2, A1.3
8	20(3.9)	2(.113)	No Interation	$2\frac{1}{2}$	A1.5
9	20(3.9)	2(.113)	.01	$5\frac{1}{2}$	A1.3, A1.5
10	20(3.9)	2(.113)	.1	5	A1.5
11	30(2.6)	2(.076)	.1	$9\frac{1}{2}$	-

TABLE A1.1: COMPARISON OF VARIOUS LUMPED MASS ANALYSES USING THE SAME INPUT BUT DIFFERENT PARAMETERS

C-Matrix: Influence of i-th Shear Resistance on $\Delta(t_j)$

j \	1	2	3	4	5	6	7	8	9	10
1	0	0	0	0	0	0	0	0	0	0
2	0	1.00	.67	.15	.01	0	0	0	0	0
3	0	1.00	1.00	.69	.16	.02	0	0	0	0
4	0	1.00	1.00	1.00	.71	.17	.02	0	0	0
5	0	1.00	1.00	1.00	1.00	.74	.18	.03	0	0
6	0	1.00	1.00	1.00	1.00	1.00	.77	.19	.03	.01
7	0	1.01	1.01	1.01	1.02	1.02	1.02	.80	.20	.05
8	0	1.13	1.14	1.09	1.16	1.17	1.18	1.19	.85	.39
9	0	1.66	1.67	1.51	1.71	1.74	1.76	1.77	1.55	1.54
10	0	2.00	2.00	2.00	2.00	2.00	2.00	2.00	2.00	2.00

E - Matrix: Influence of i-th Damping Force on $\Delta(t_j)$

1	0	0	0	0	0	0	0	0	0	0
2	0	.87	.96	.39	.05	.01	0	0	0	0
3	0	.61	.87	.96	.38	.05	.01	0	0	0
4	0	.65	.61	.87	.95	.37	.05	.01	0	0
5	0	.64	.66	.62	.88	.95	.38	.07	.01	0
6	0	.44	.65	.66	.61	.88	.95	.40	.08	.02
7	0	.36	.44	.63	.65	.61	.90	1.01	.46	.14
8	0	.71	.62	.55	.88	.86	.84	1.19	1.24	.81
9	0	1.18	.121	1.02	1.19	1.39	1.38	1.38	1.74	1.91
10	0	1.04	1.14	1.24	1.08	1.16	1.34	1.29	1.47	1.75

TABLE A3.1: C-and E-MATRIX

Column No. 1	2	3	4	5	6	7
Soil Parameter Element No.	First Damping Distribution Initial	Final	Second Damping Distribution Initial	Final	Third Damping Distribution Initial & Final	From Column 3,5,6 Final Distribution
1	0	0	0	0	0	0
2	0	0	0	0	0	0
3	12.0	6.4	6.4	4.0	4.4	0
4	4.8	0	0	0	0	0
5	18.2	0	0	0	0	0
$S_{o,i}$ 6	15.7	34.1	34.0	24.7	32.9	34.0
7	19.1	1.1	0	17.4	5.4	0
8	17.5	0	0	14.6	0	1.6
9	38.7	56.4	4.92	55.7	54.9	57.2
10	38.3	56.4	57.3	50.9	54.9	57.3
1	0	0	0	0	0	0
2	0	0	0	0	0	0
3	0	0	.36	.36	.71	0
4	0	0	.53	0	0	0
d_i 5	0	0	.36	.36	.0	.03
6	0	0	.99	1.00	0	.08
7	0	0	.55	.55	0	.05
8	0	0	0	0	0	0
9	0	0	1.18	1.13	0	.10
10	10.0	7.71	1.14	.99	8.00	7.00

TABLE A3.2: SOIL PARAMETERS PREDICTED (F-60, BLOW NO. 26-A)

CUSHION STIFFNESSES k in kips/inch

Applied Force kips	Transducer 3-4	Transducer 5-6	Oak 15/15/5 (Delmag D-12)	Phenol 11"ϕ/2.5" Link Belt 440
100	4,600	3,500	1600	8,600
150	7,250	5,500	2400	9,300
200	10,000	8,000	3300	11,600

WEIGHTS of RAM and ANVIL in kips

	Ram and Anvil	Capblock and Adaptor
Delmag D-12	3.50	1.20
Link Belt 440	4.71	1.10

TABLE B.1 : CUSHION STIFFNESSES AND HAMMER WEIGHTS

PILE	BLOW NO.	LENGTH FT.	P_{ult} KIPS	AVG. KIPS	HAMMER	$f_1 = \frac{c}{4L}$ 1/s	$f_2 = 49.4\sqrt{\frac{P}{L}}$ 1/s	f_3 1/s Equ. 3	f_4 1/s Equ. 3	MEAS. 1/s	ERROR %
F-30	13	33	104	100	Link Belt 440	129	88	75	360	400	10
	14		104	100			88	75	360	400	10
	15		104	110			88	78	367	409	10.3
	16		104	110			88	78	367	402	8.7
	1-A		114	120			92	81	375	409	8.3
	5-A		114	110			92	78	367	409	10.3
	6-A		114	110			92	78	367	409	10.3
	7-A		114	110			92	78	367	409	10.3
F-50	18	51.5	224	140	Link Belt 440	83	103	86	390	418	6.7
	19		224	140			103	86	390	422	7.6
	20		224	140			103	86	390	422	7.6
	10-A		238	190			106	99	443	425	-4.1
	13-A		238	20			106	102	454	418	-8.0
	14-A		238	190			106	99	443	427	-3.7
	15-A		238	140			106	86	390	427	8.7
F-60	17	60.5	204	180	Link Belt 440	70	91	97	431	435	.9
	18		204	140			91	86	390	427	9.5
	19		204	150			91	89	390	418	4.8
	22-A		242	140			99	86	390	414	5.8
	26-A		242	150			99	89	393	409	2.7
	27-A		242	130			99	83	382	418	6.2

TABLE B.2 : MEASURED AND CALCULATED FREQUENCIES ON TOP OF PILE

TABLE (B.2) continued

PILE	BLOW NO.	LENGTH FT.	P_{ult}	AVG. KIPS	HAMMER	$f_1 = \frac{c}{4L}$ 1/s	$f_2 = 49.4\sqrt{\frac{P}{L}}$ 1/s	f_3 1/s Equ. 3	f_4 1/s Equ. 3	MEAS. 1/s	ERROR %
TO-50	III-2	50	69	140	Delmag D-12	85	58	68	272	313	13.1
	III-3		69	110			58	50	239	292	18.1
	IV-2		69	110			58	60	239	298	19.2
	3-A		95	180			68	77	314	303	-3.6
	I-4A		95	200			68	82	333	313	-6.4
TO-60	IV-9	60	43	120	D-12	71	42	62	250	274	8.8
	II-5-A		86	100			59	57	228	285	20.0
	III-1-A**		86	90			59	51	198	244	18.9
TO-50-c*	I-9-A**	50	130	230	D-12	60	23	88	338	324	8.0

* Concrete filled pile here c = 12,000 ft/s was used.

** Transducer cushion with 5 plywood and 6 rubber sheets.

DATA SET NO.	MAXIMUM DAMPING FROM PHASE III kips	MAXIMUM DAMPING FROM ANALYSIS kips
3	14	15
5	44	50
6	25	23
7	40	41
8	60	52
9	42	25
10	65	57
11	13	17
13	44	57
14	57	88
15	68	70
16	98	106
17	55	54
18	102	125
19	65	58
20	59	61
21	80	87
22	67	106
23	96	93
24	44	48

TABLE D.1: COMPARISON OF MAXIMUM DAMPING FORCE AS PREDICTED FROM PHASE III AND FROM WAVE ANALYSIS

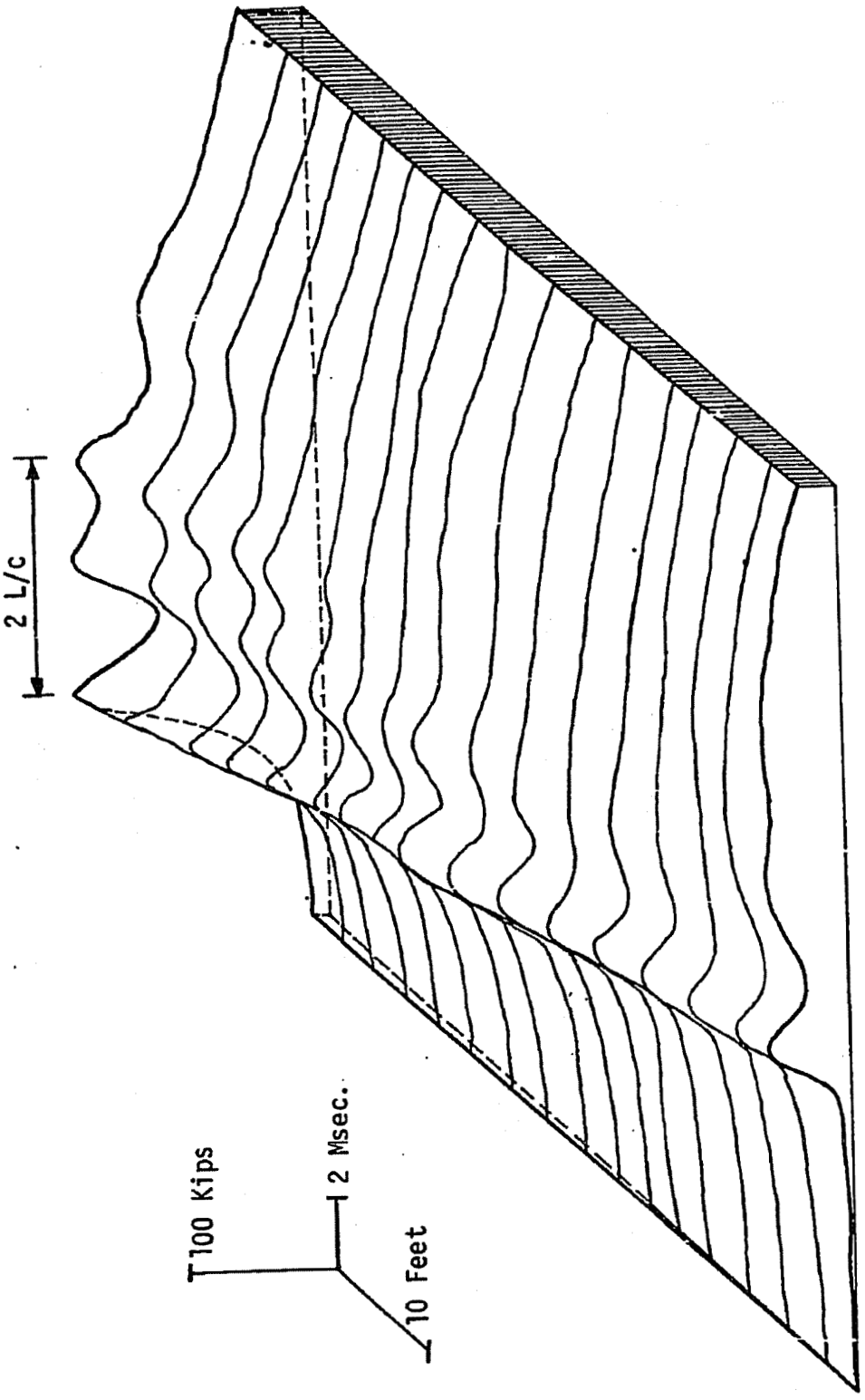

FIGURE 1.1: FORCES IN PILE UNDER A HAMMER BLOW (To-60 BLOW No. 4-A)

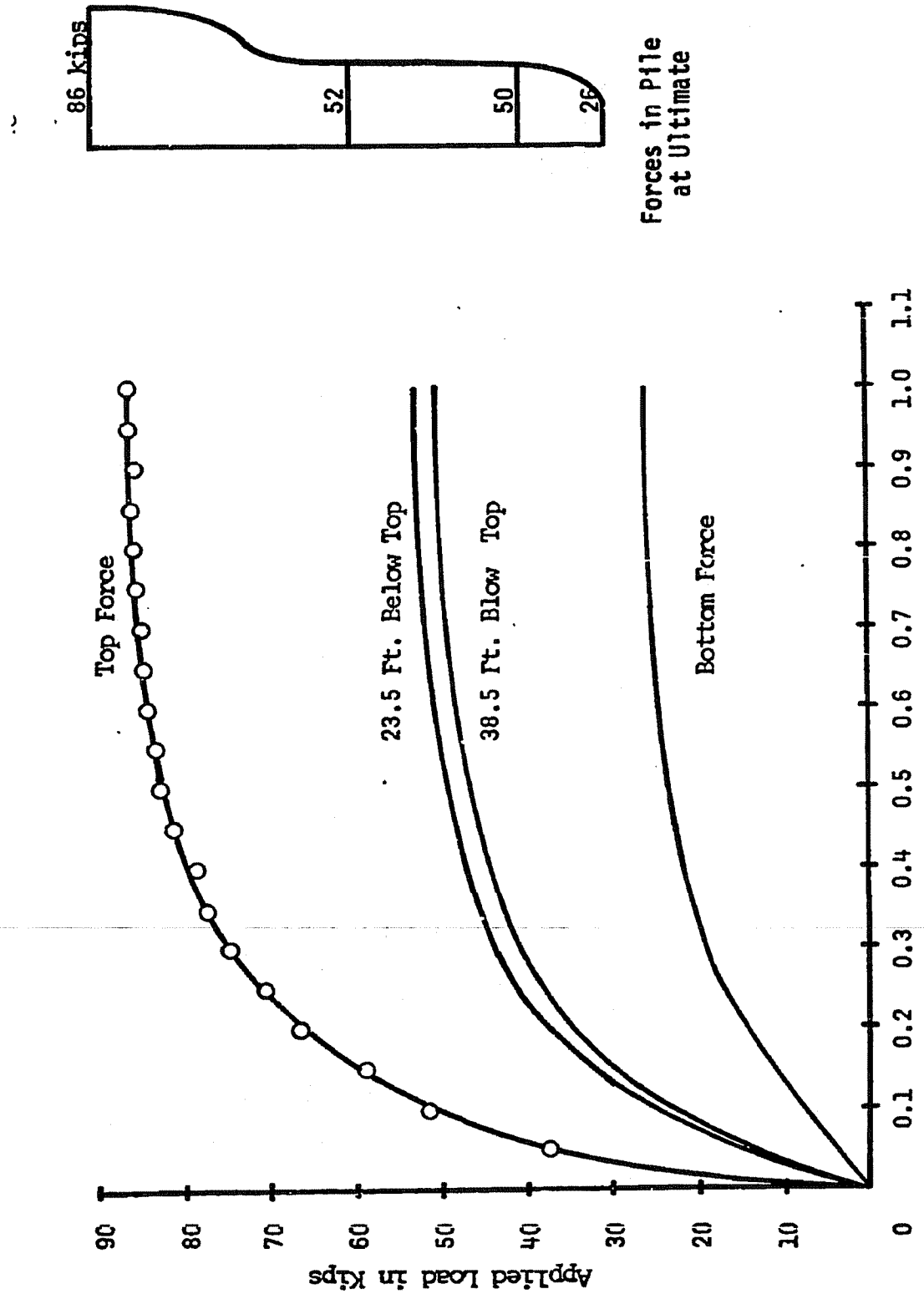

FIGURE 1.2: STATIC LOAD TEST RESULTS FOR FULL SCALE PILE To-60

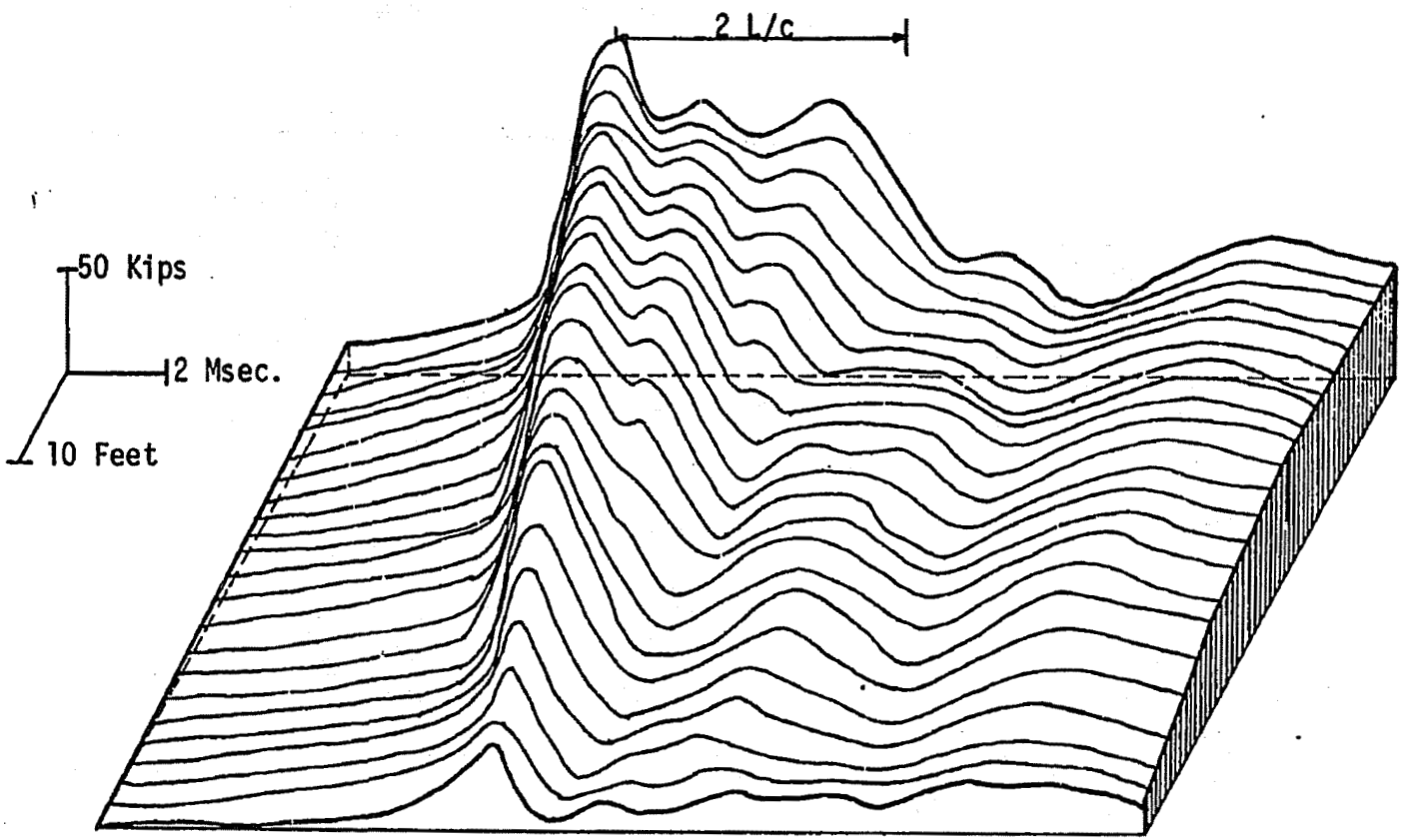

FIGURE 1.3: FORCES IN PILE UNDER A HAMMER BLOW (Ri-50 BLOW No. 8-A)

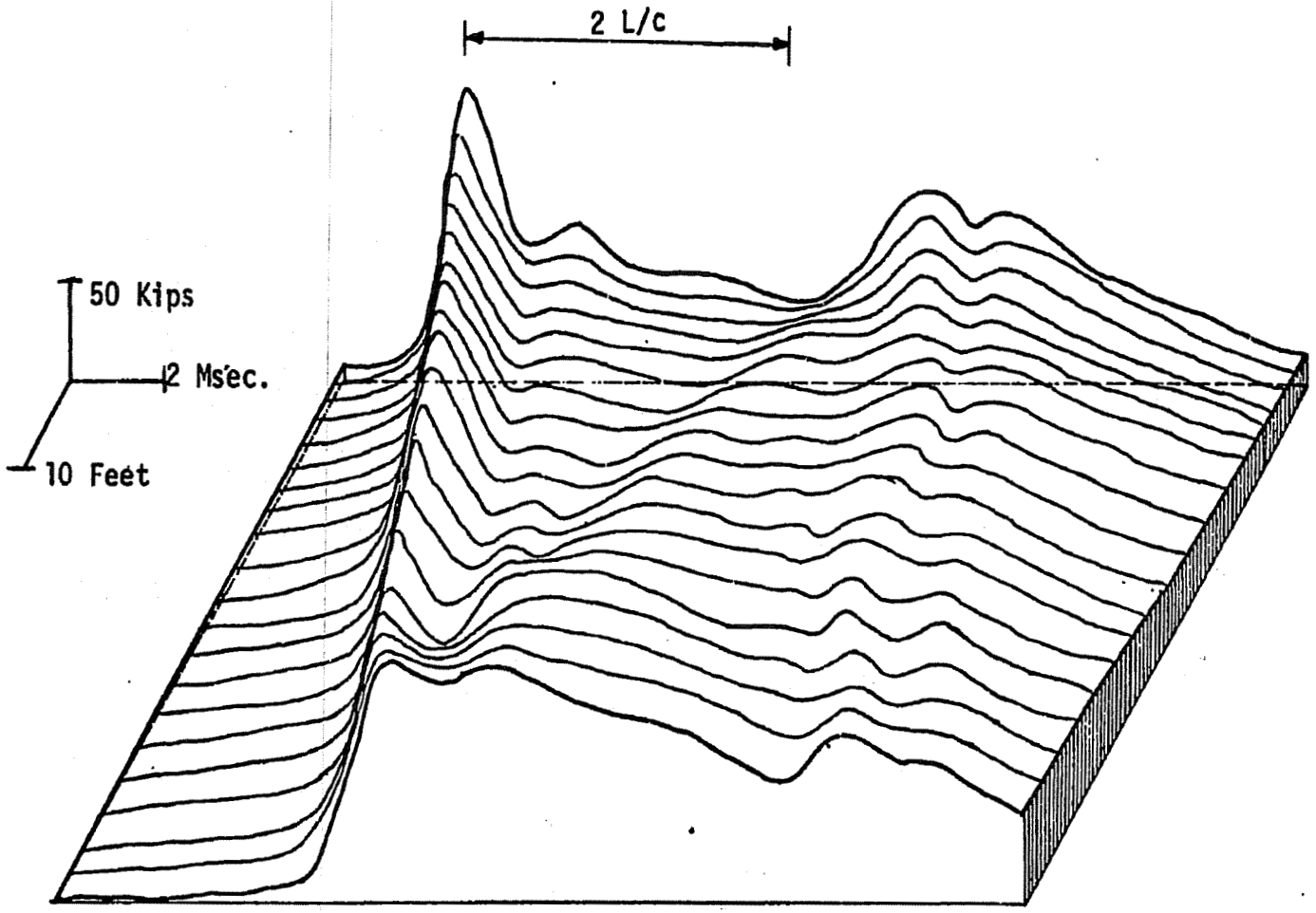

FIGURE 1.4 : FORCES IN PILE UNDER A HAMMER BLOW (Ri-60 BLOW No. 22)

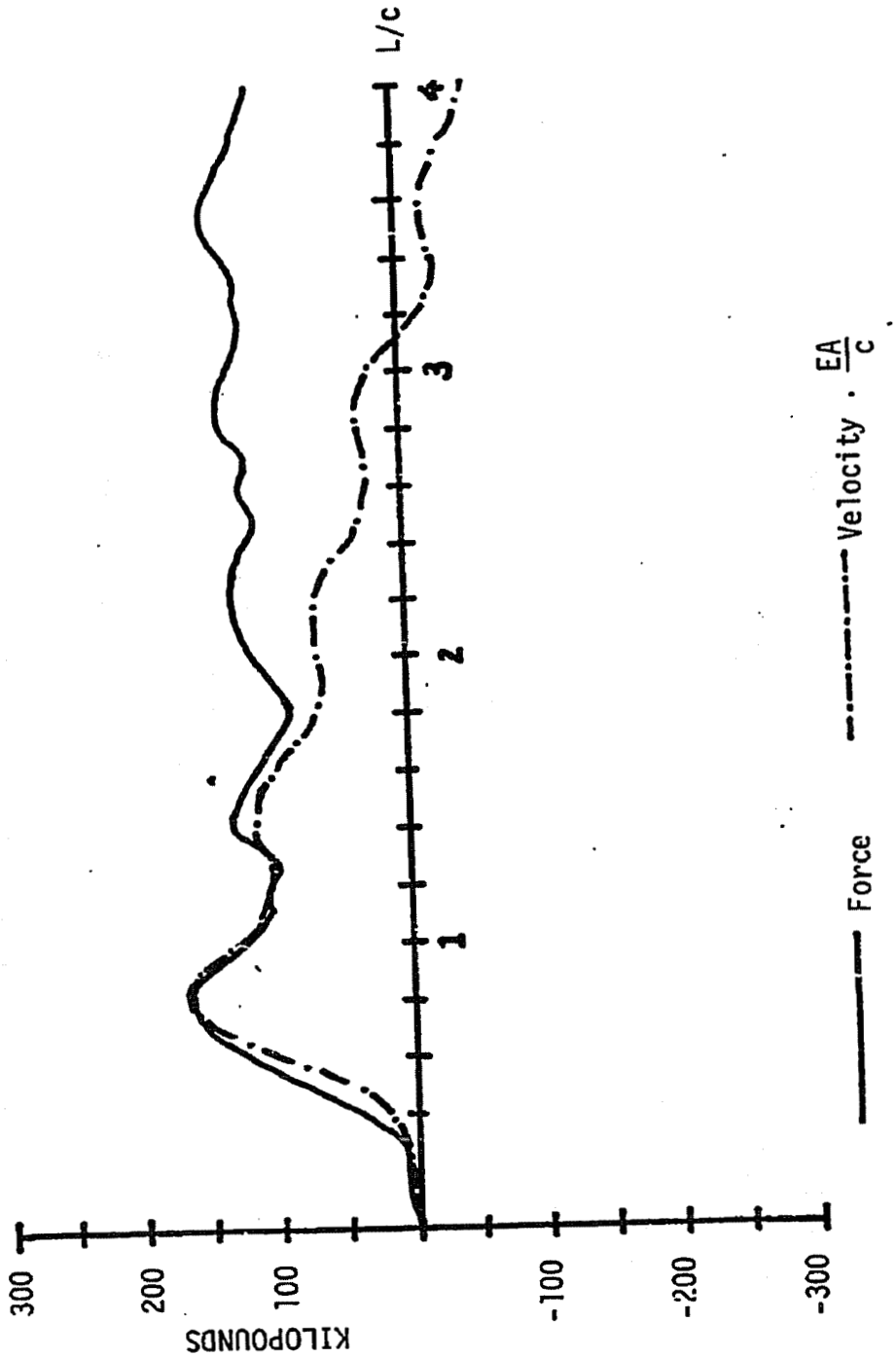

FIGURE 2.1: TYPICAL FORCE AND VELOCITY RECORD (FULL SCALE PILE F-60A, BLOW NO. 26-A)

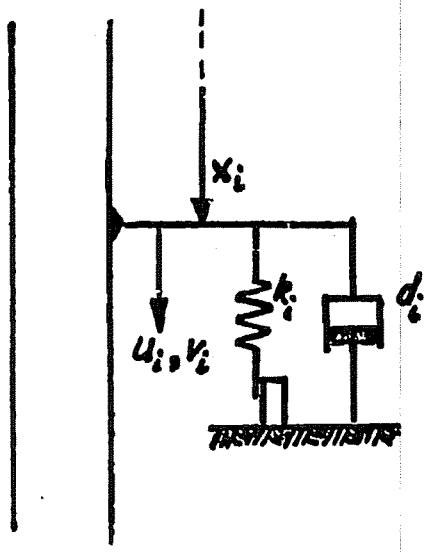

a. Soil Rheological Model

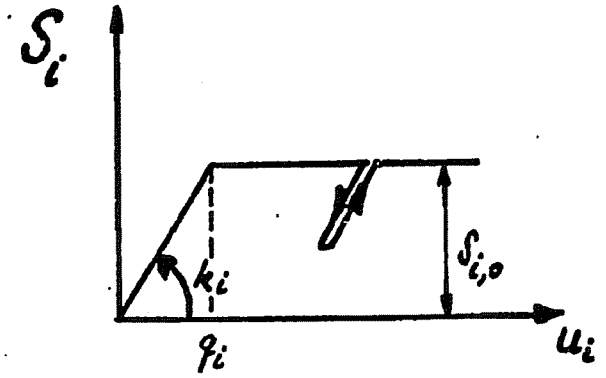

b. Shear Force versus Pile Displacement

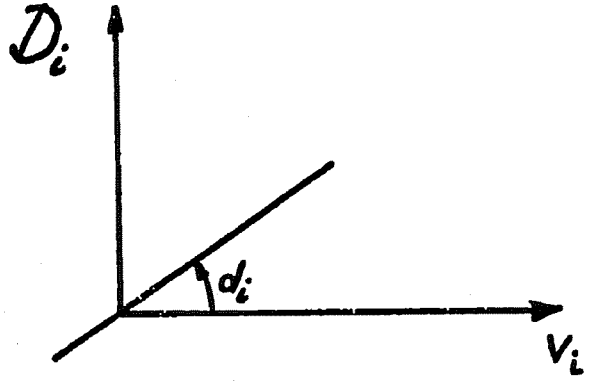

c. Damping Force Versus Velocity

FIGURE 2.2: SOIL RESISTANCE LAW

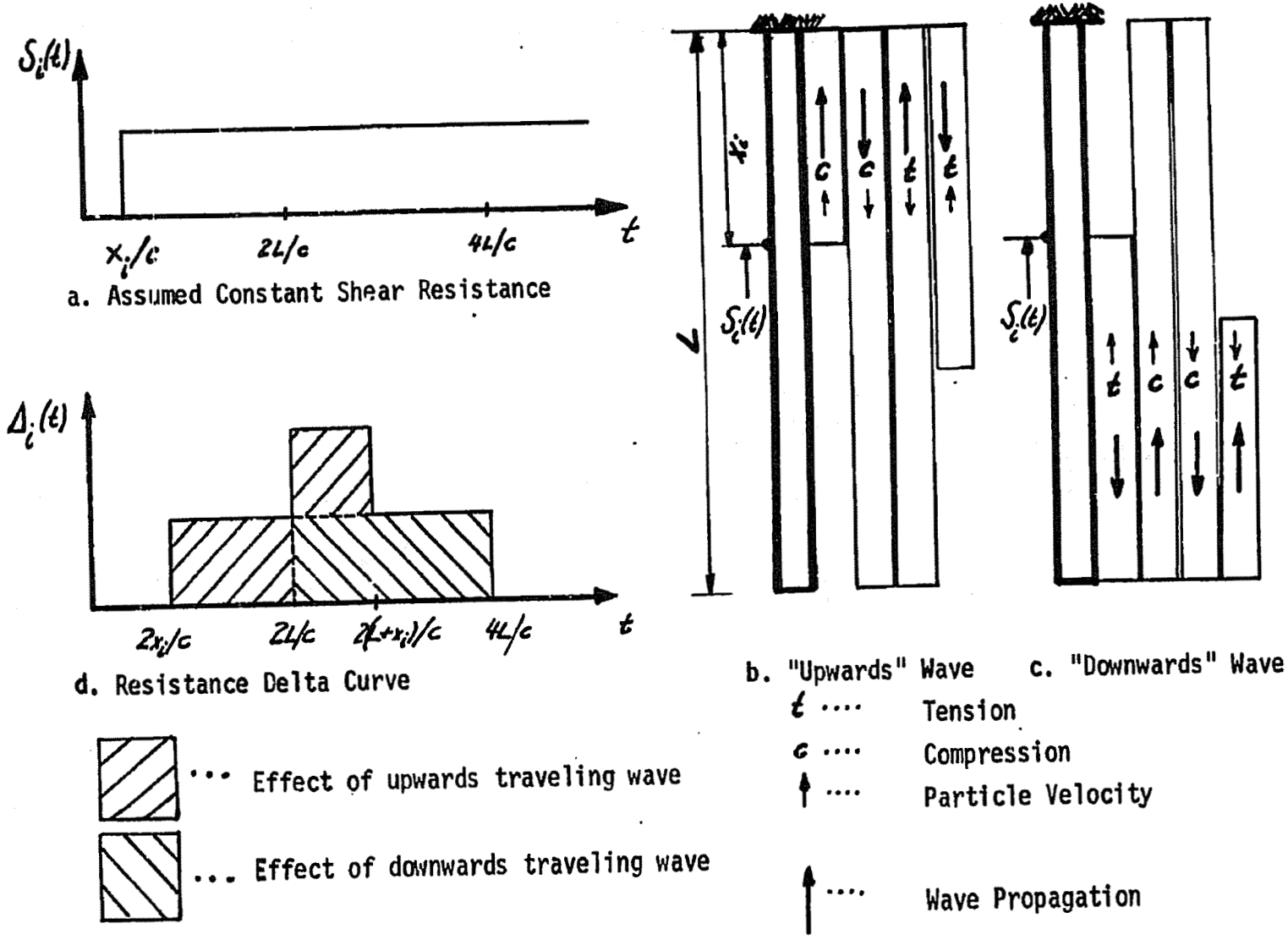

FIGURE 2.3: DEVELOPMENT OF RESISTANCE DELTA CURVE FOR CONSTANT SHEAR FORCE

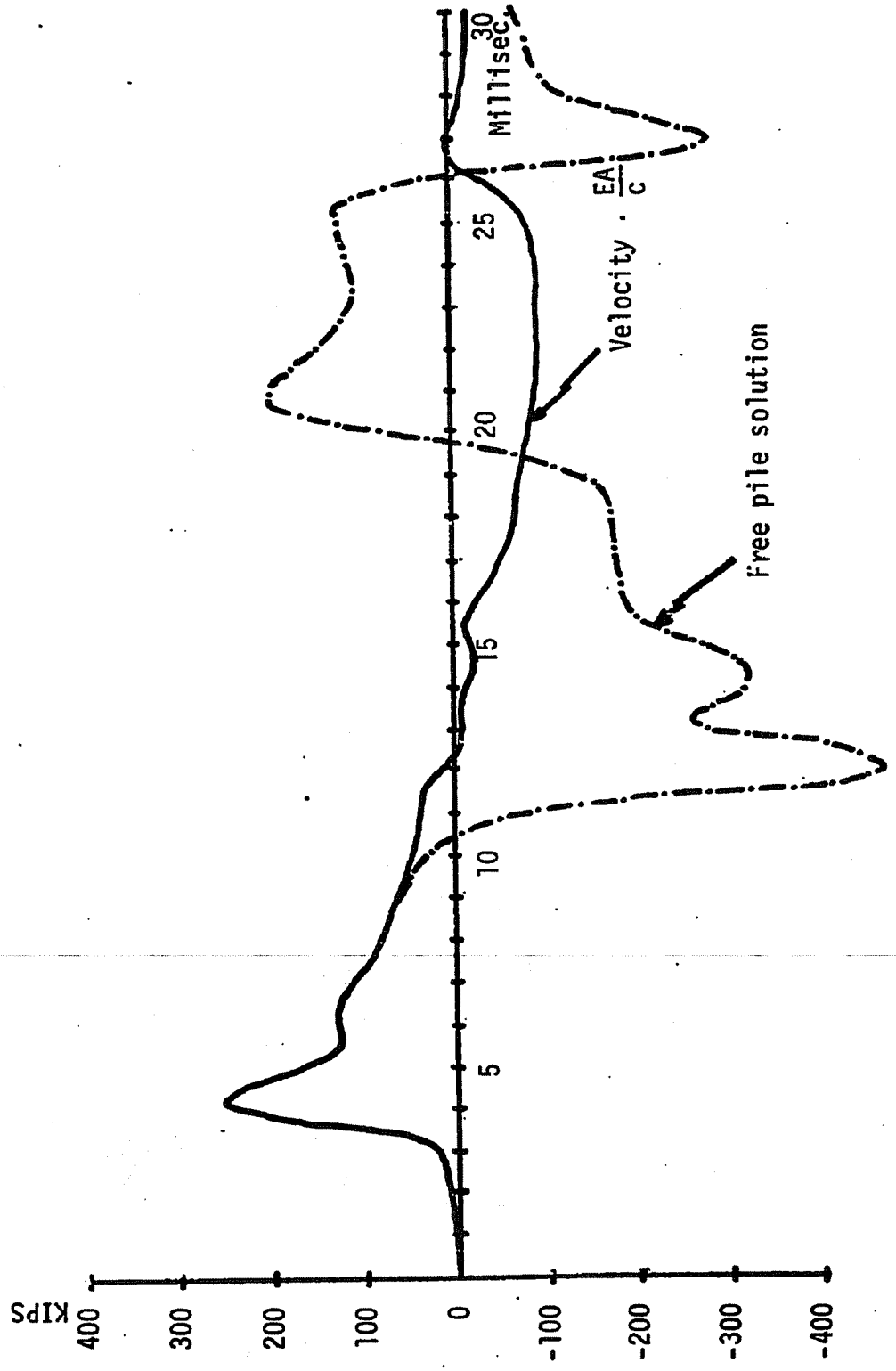

FIGURE 2.4: VELOCITY MULTIPLIED BY EA/c AND FREE PILE SOLUTION (RI-60 BLOW NO. 18)

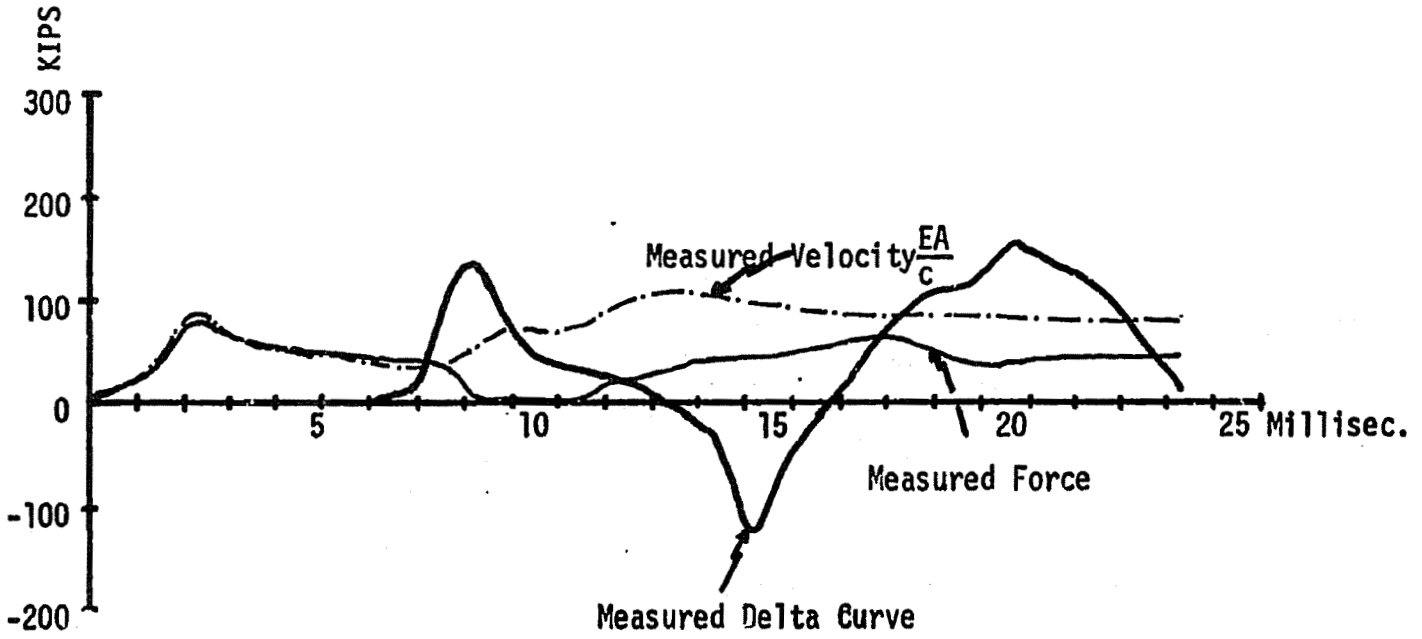

FIGURE 2.5: MEASURED FORCE AND VELOCITY AND DERIVED MEASURED DELTA CURVE (RI-50, HALF DRIVEN)

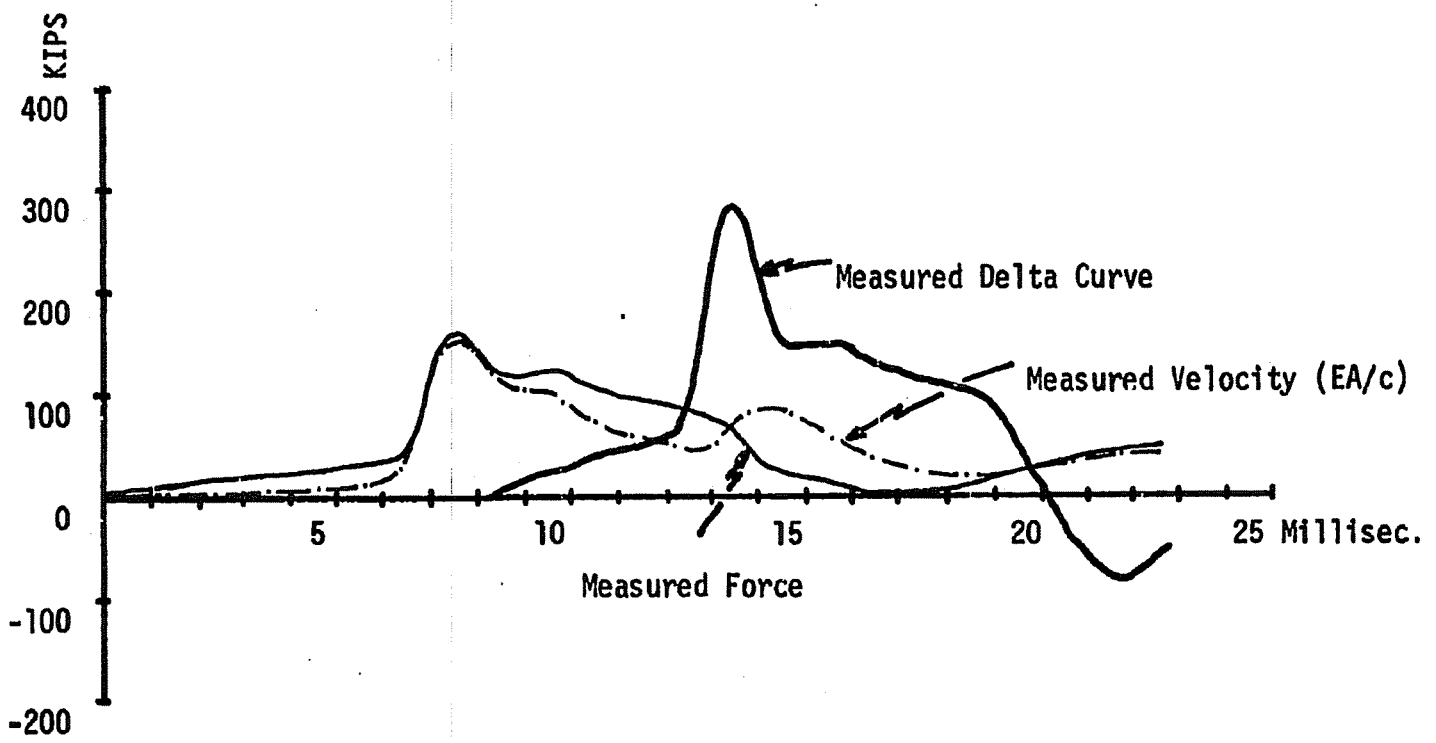

FIGURE 2.6: MEASURED FORCE AND VELOCITY AND DERIVED MEASURED DELTA CURVE (RI-50, BLOW NO. 20)

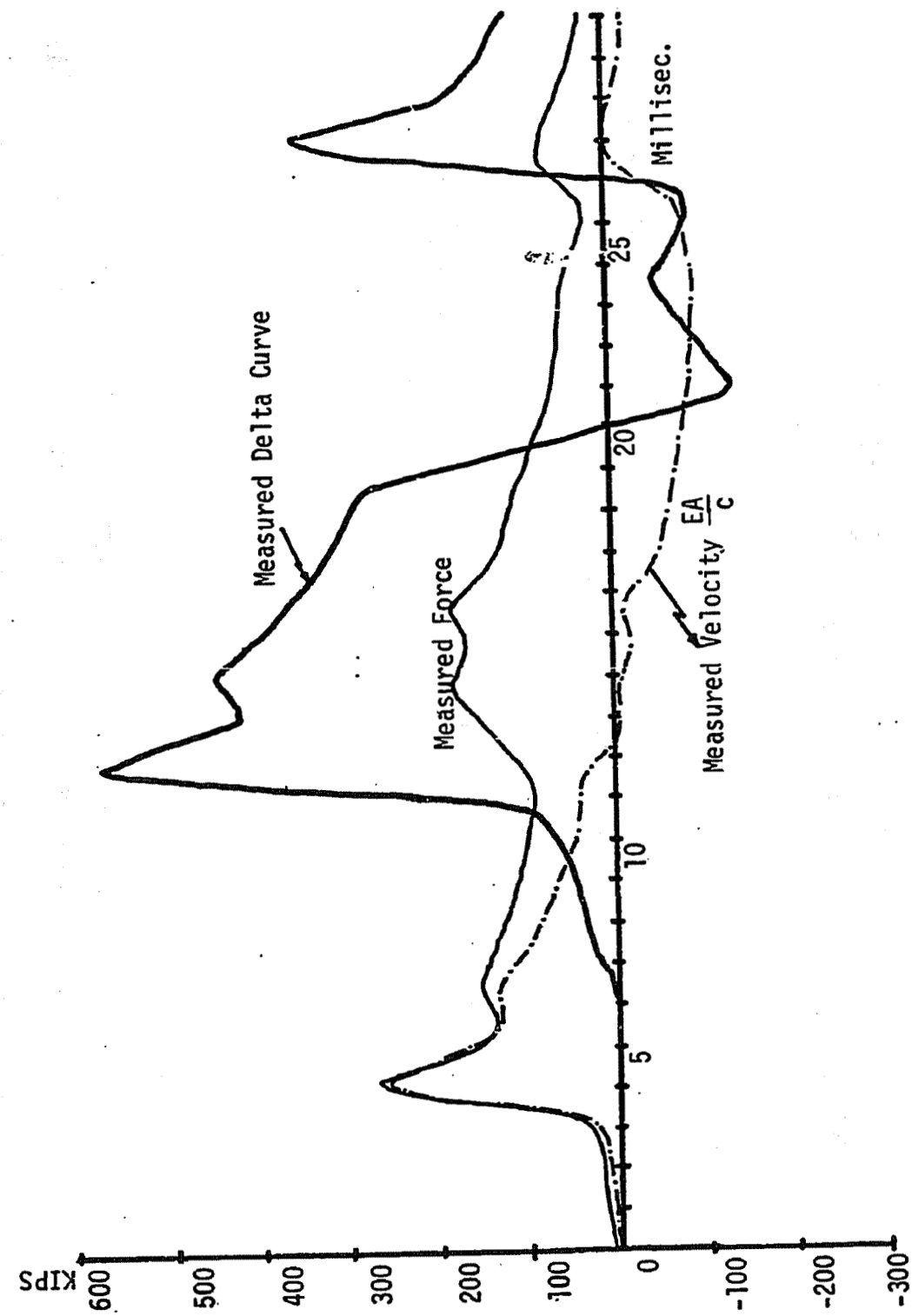

FIGURE 2.7: MEASURED FORCE AND VELOCITY AND MEASURED DELTA CURVE (Ri-60,#18)

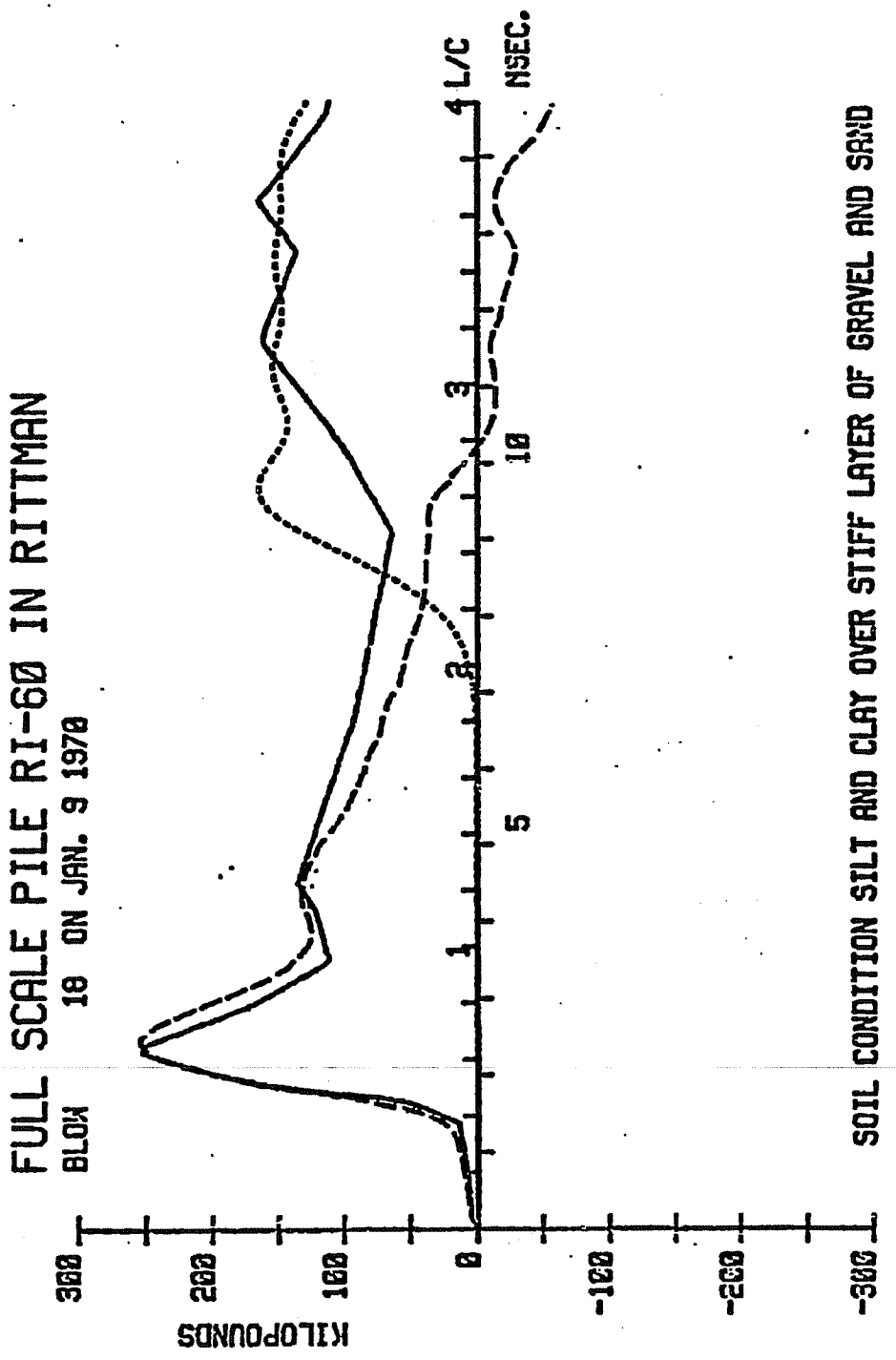

FIGURE 2.8: MEASURED FORCE AND VELOCITY AND RESISTANCE DELTA CURVE FOR SHEAR RESISTANCE FORCE OF 75 KIPS AT PILE BOTTOM END

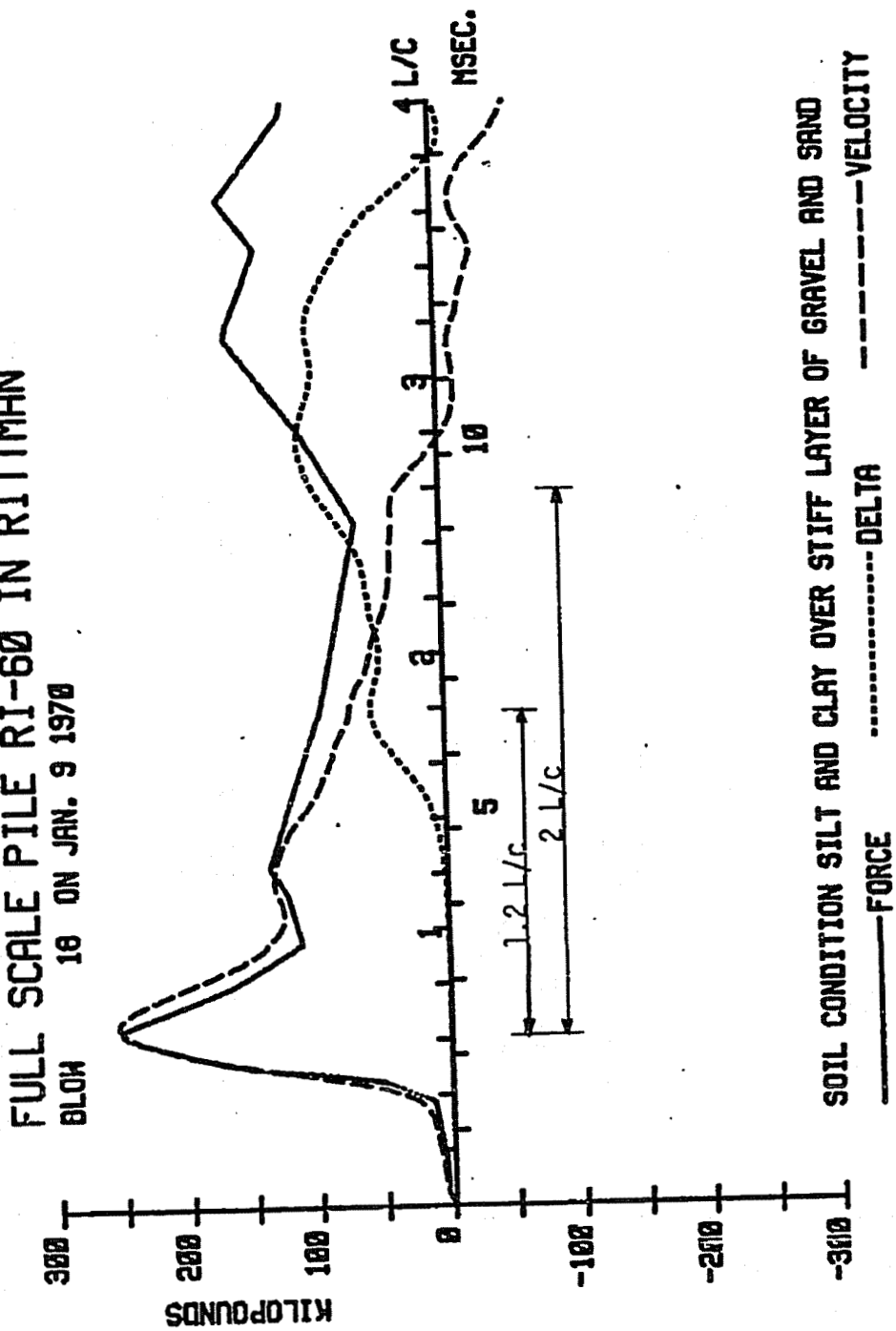

FIGURE 2.9: MEASURED FORCE AND VELOCITY AND RESISTANCE DELTA CURVE FOR SHEAR RESISTANCE FORCE OF 50 KIPS AT 0.6L

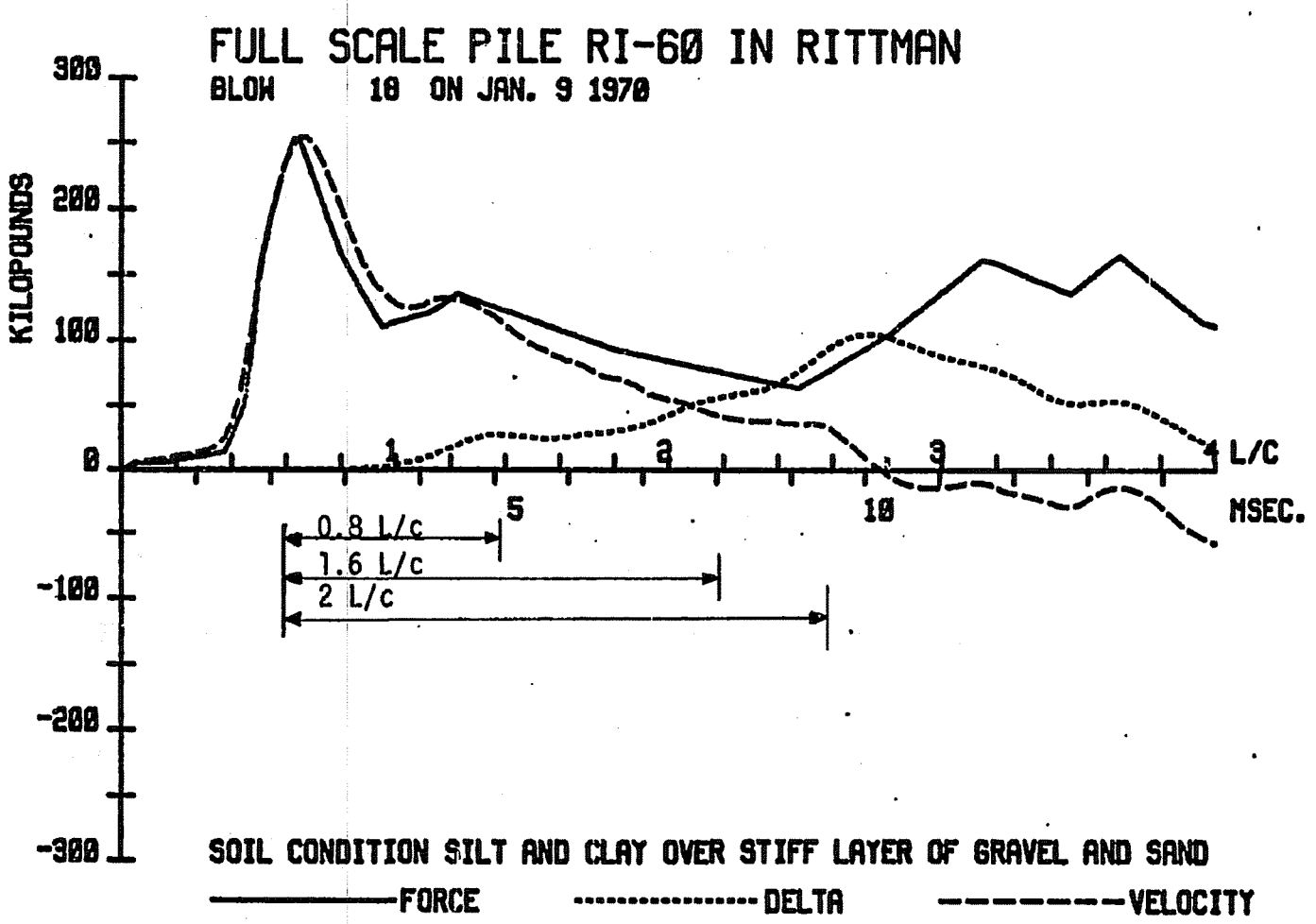

FIGURE 2.10: MEASURED FORCE AND VELOCITY AND RESISTANCE DELTA CURVE FOR A SHEAR RESISTANCE FORCE OF 25 KIPS AT BOTH 0.4L AND 0.8L

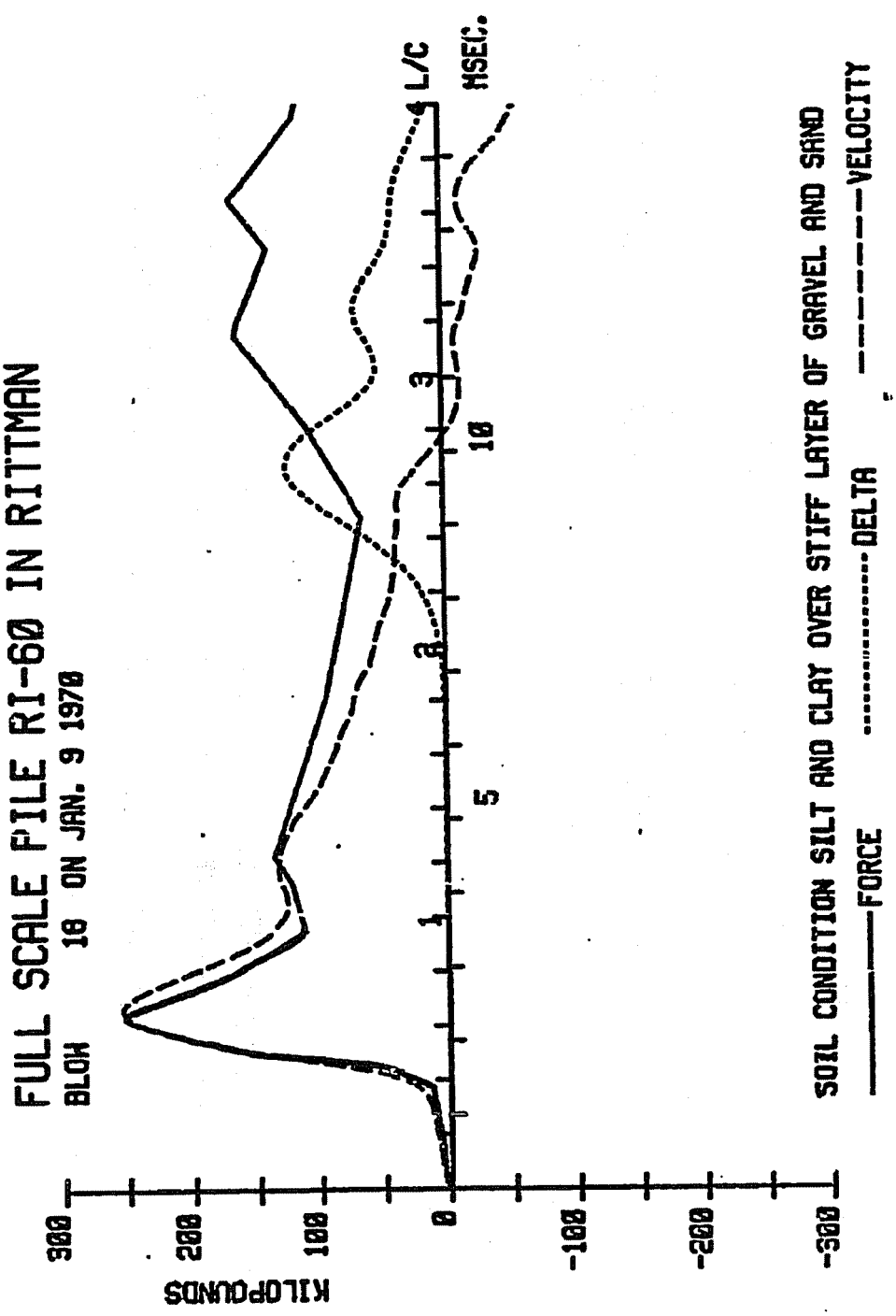

FIGURE 2.11: MEASURED FORCE AND VELOCITY AND RESISTANCE DELTA CURVE FOR A DAMPER AT THE PILE TIP (d_n = EA/c)

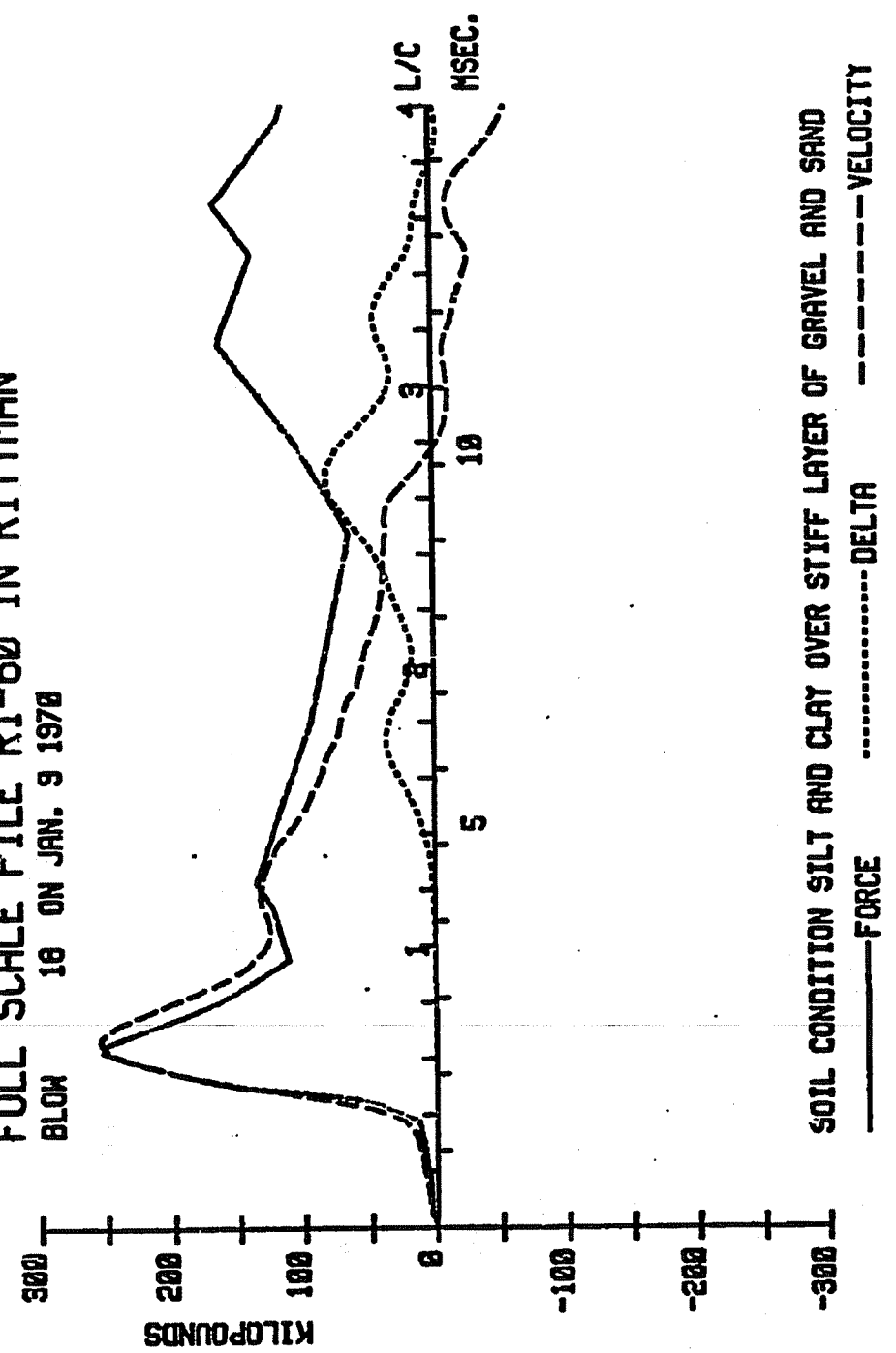

FIGURE 2.12: MEASURED FORCE AND VELOCITY AND RESISTANCE DELTA CURVE FOR DAMPER AT 0.6L (d_i = EA/c)

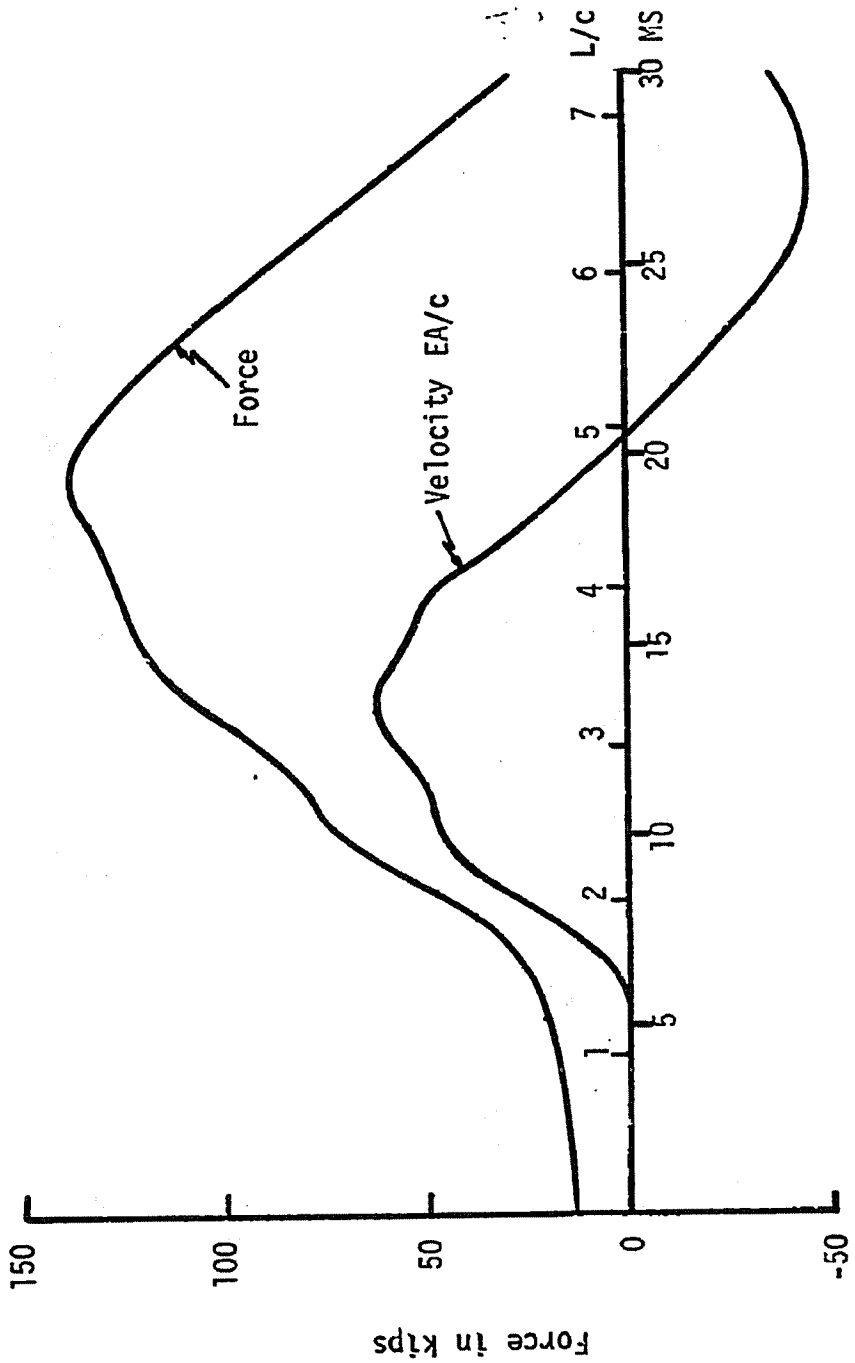

FIGURE 3.1: MEASURED TOP FORCE AND VELOCITY OF PILE 531-70 BLOW NO. 13-A

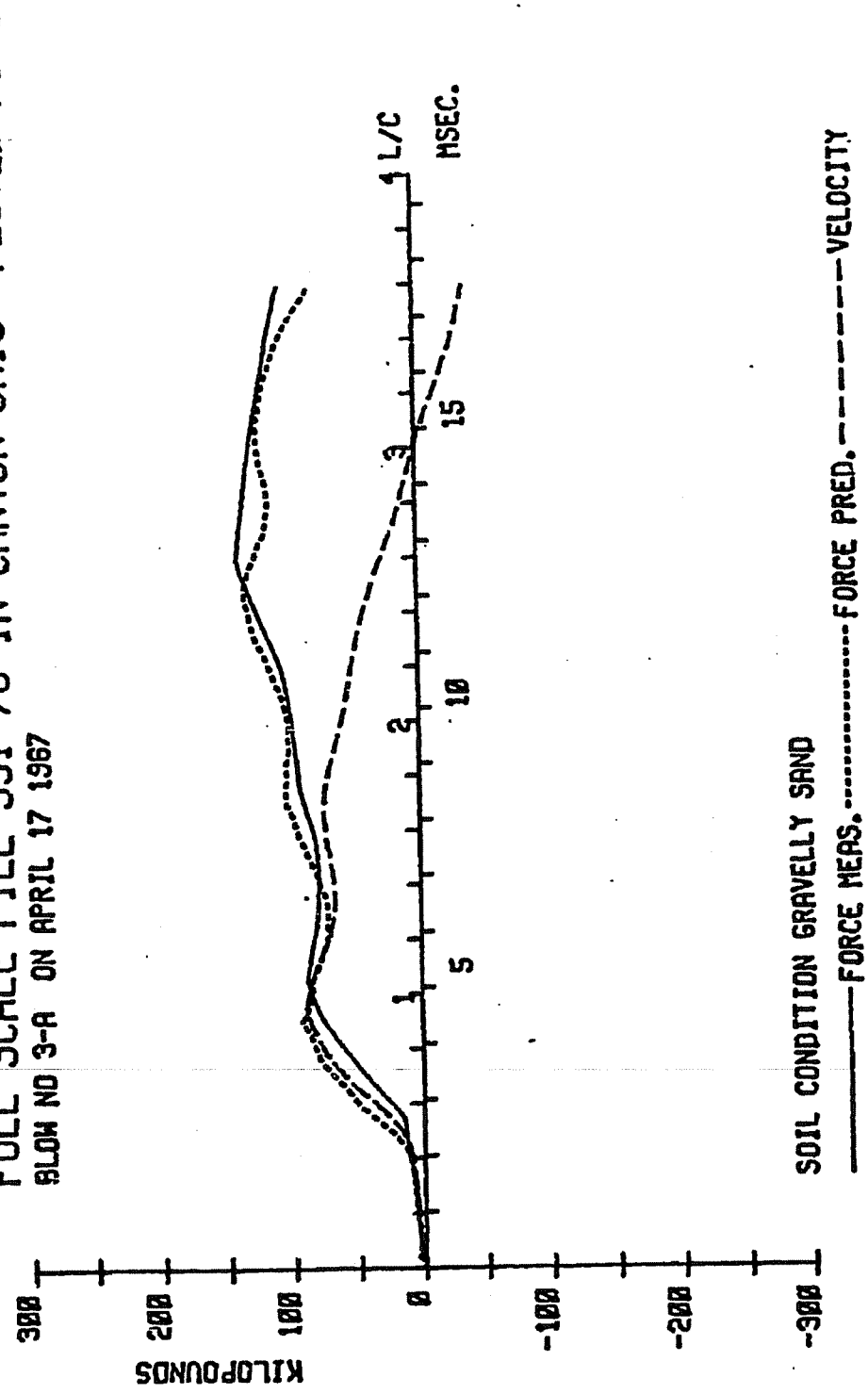

FIGURE 3.2: COMPARISON OF PREDICTED WITH MEASURED PILE TOP FORCE FOR DATA SET NO. 3

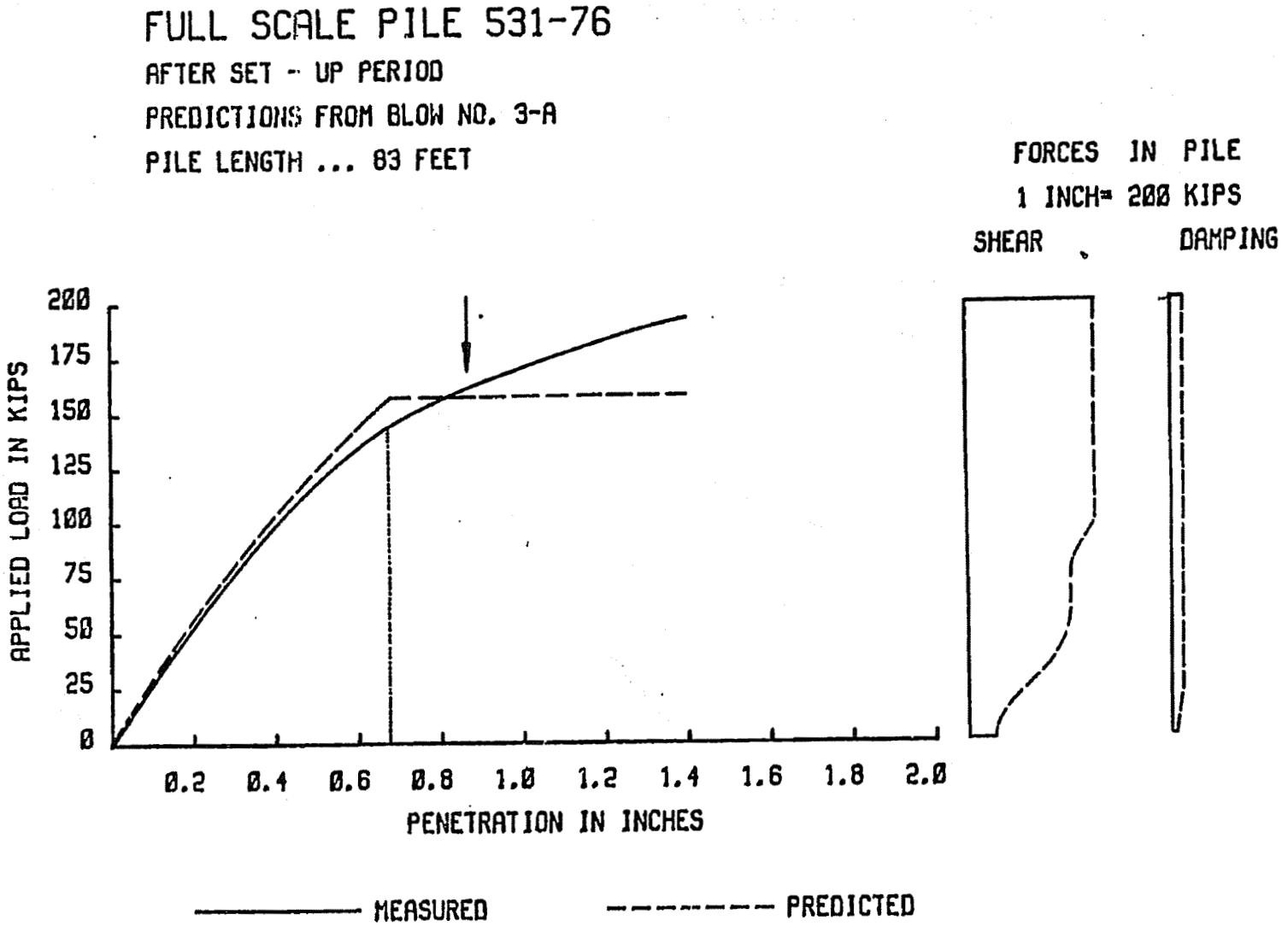

FIGURE 3.3: COMPARISON OF PREDICTED STATIC RESULTS WITH LOAD TEST AND PREDICTED FORCES IN PILE

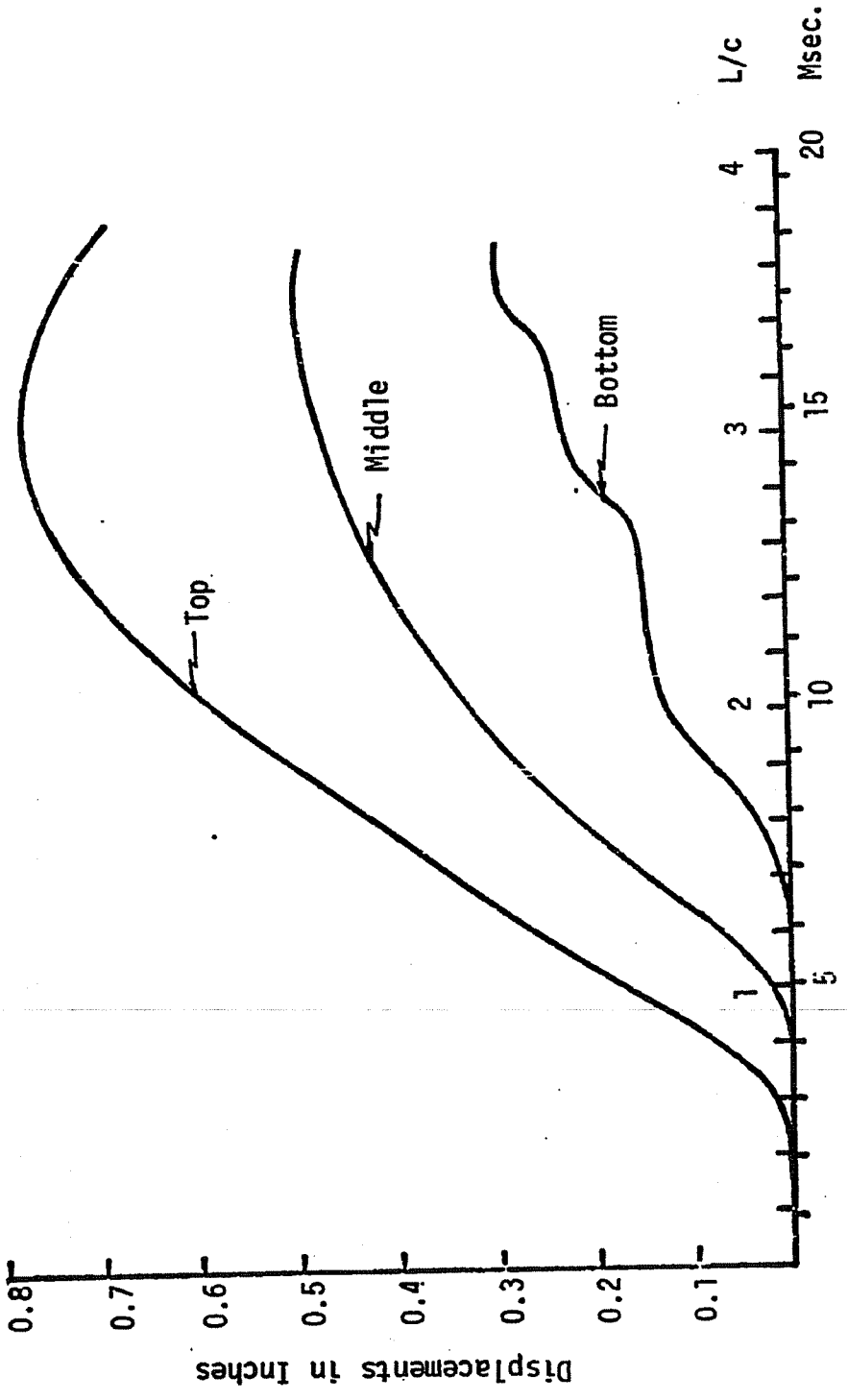

FIGURE 3.4: DISPLACEMENT AT TOP, MIDDLE, AND BOTTOM AS OBTAINED FROM DYNAMIC ANALYSIS (Pile 531-76, BLOW NO. 3-A)

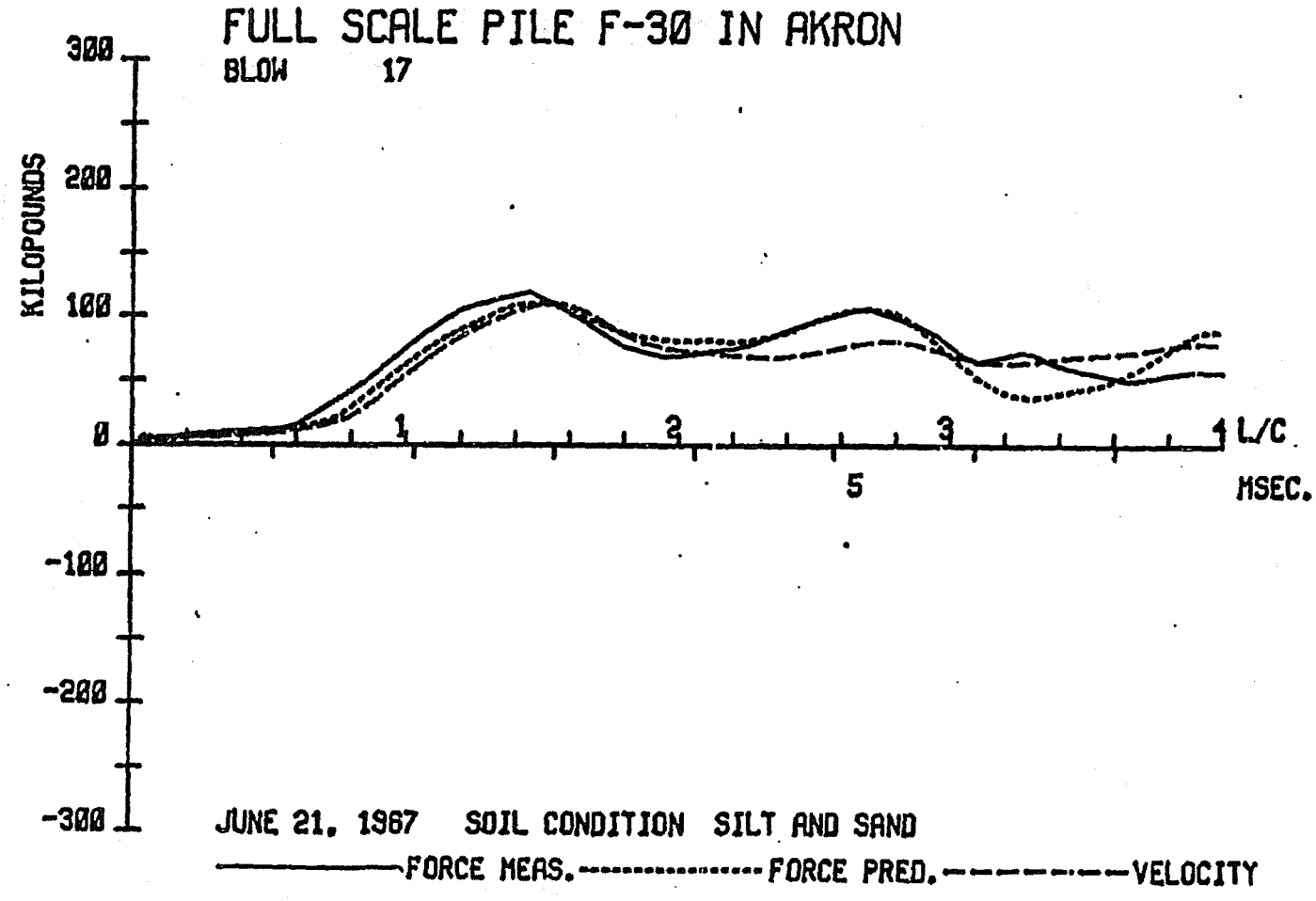

FIGURE 3.5: COMPARISON OF PREDICTED WITH MEASURED PILE TOP FORCE FOR DATA SET NO. 5

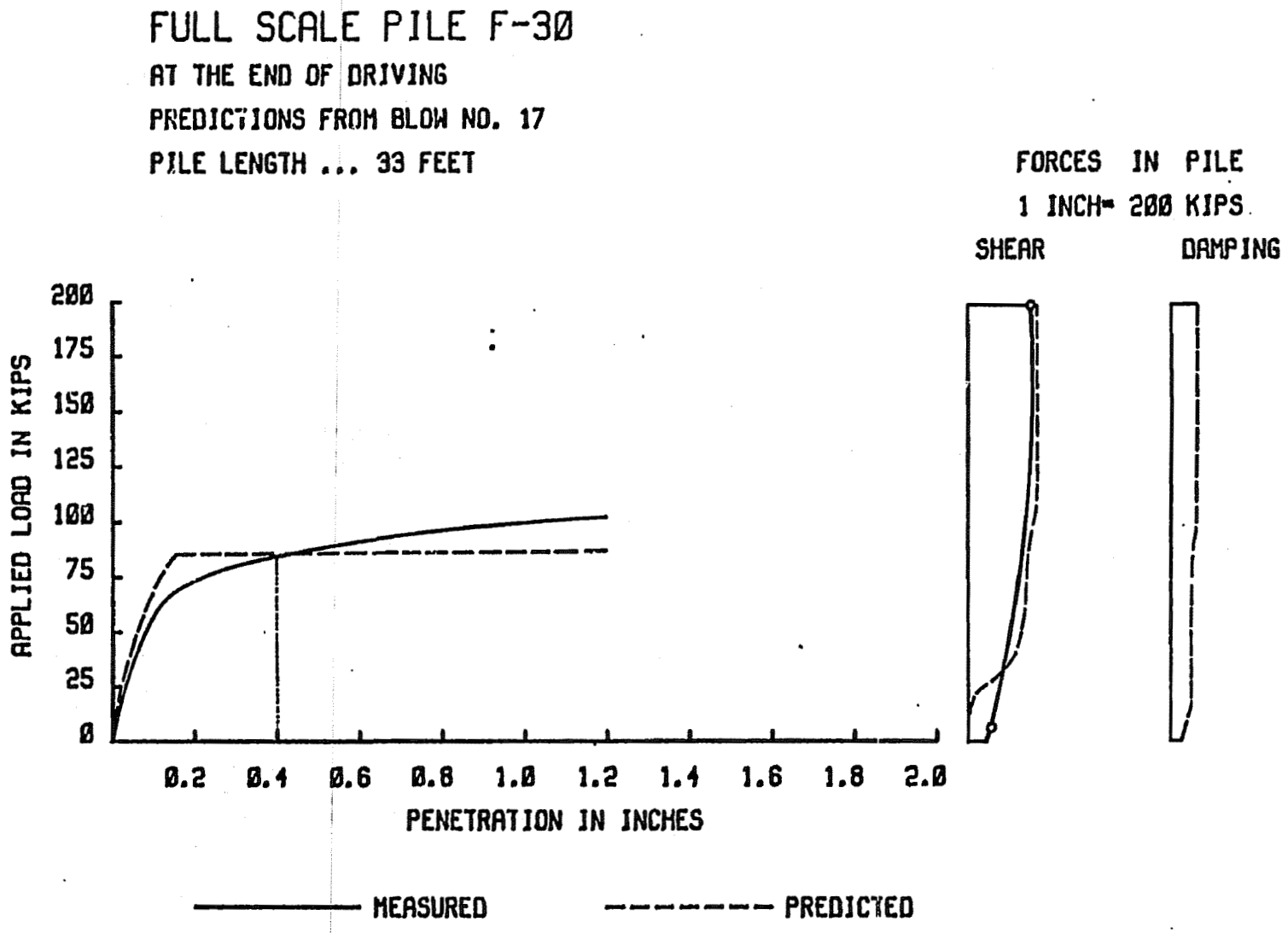

FIGURE 3.6: COMPARISON OF PREDICTED STATIC RESULTS WITH FIELD LOAD TEST AND FORCES IN PILE

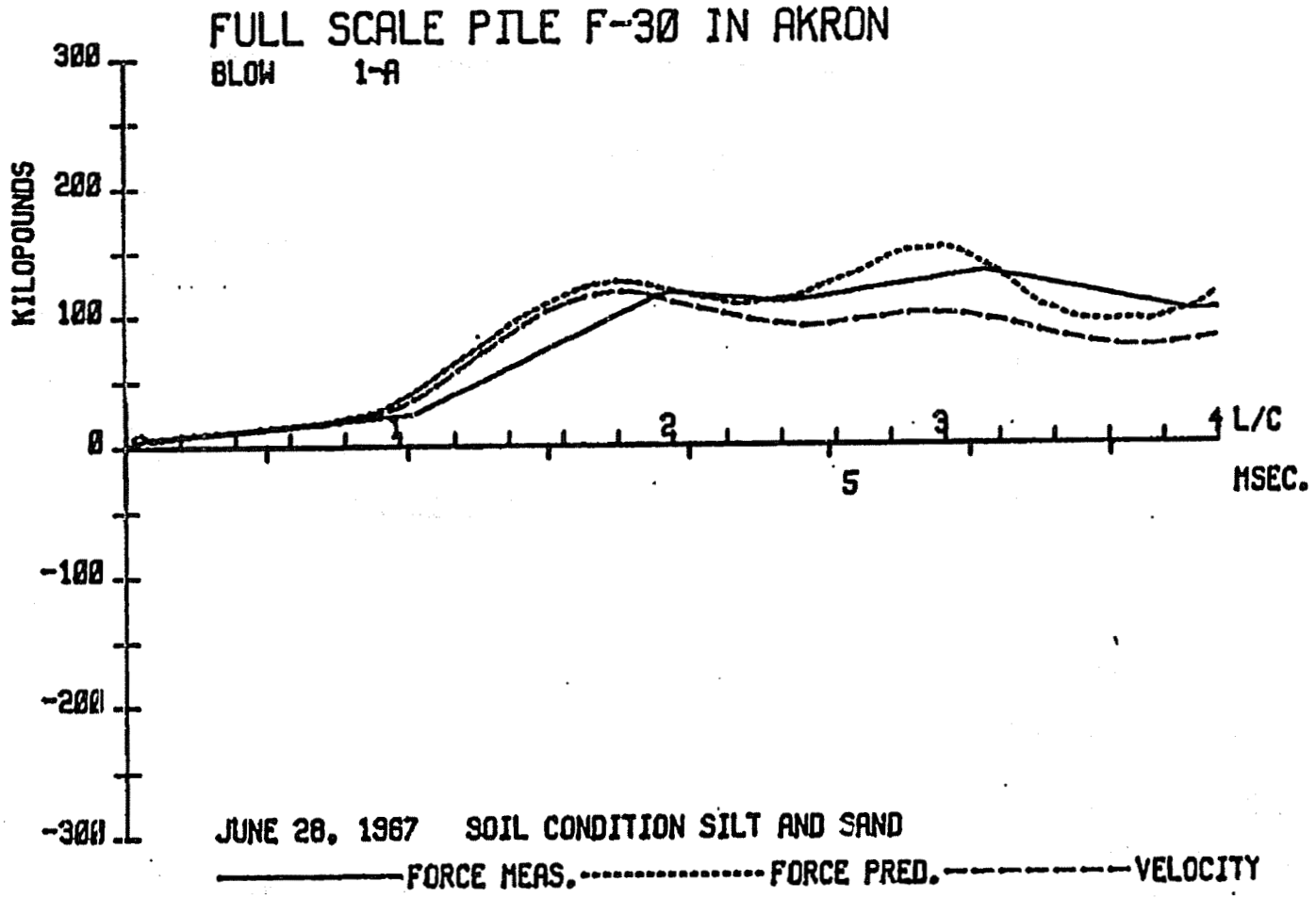

FIGURE 3.7: COMPARISON OF PREDICTED WITH MEASURED PILE TOP FORCE FOR DATA NO. 6

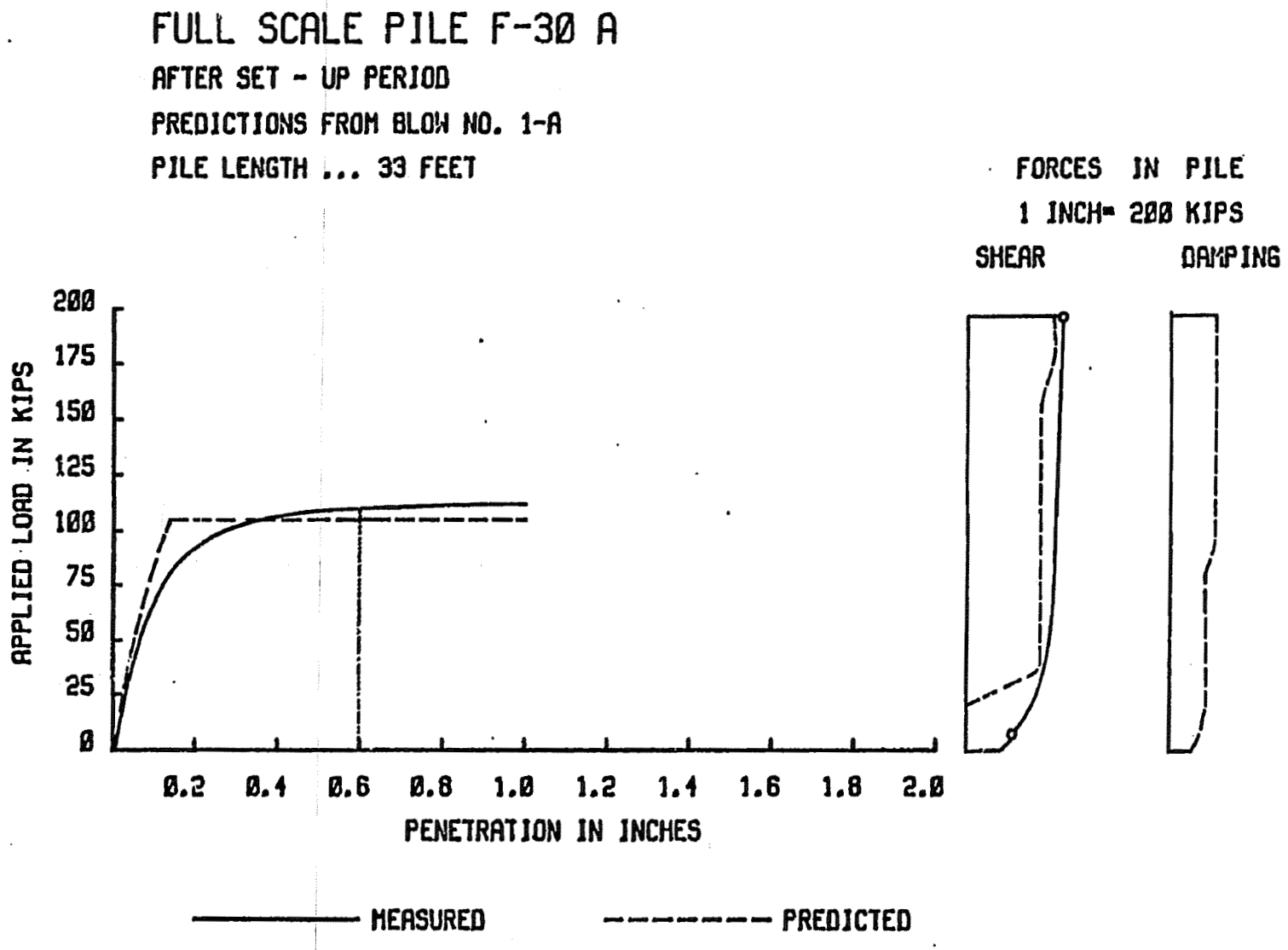

FIGURE 3.8: COMPARISON OF PREDICTED STATIC RESULTS WITH FIELD LOAD TEST AND PREDICTED FORCES IN PILE

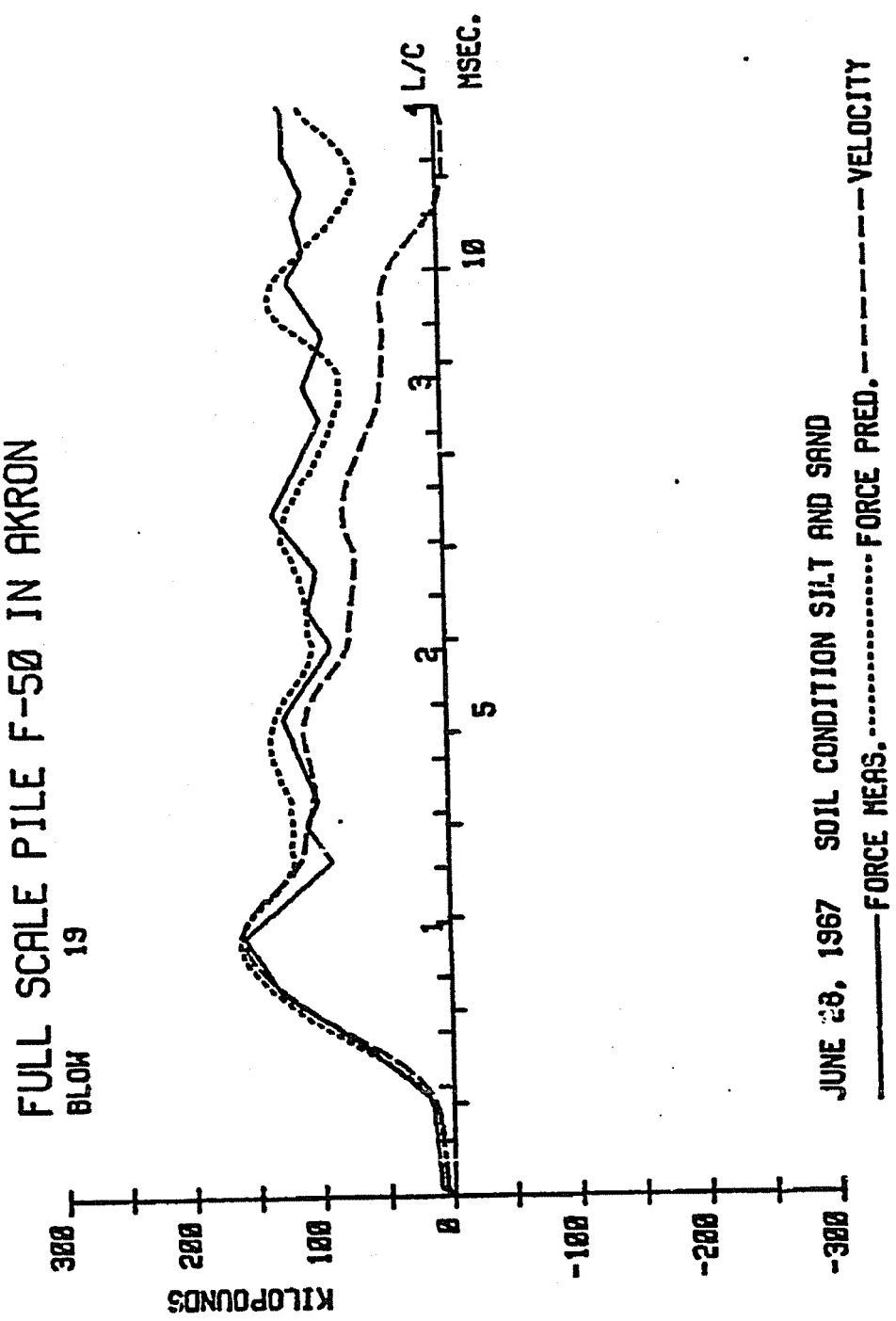

FIGURE 3.9: COMPARISON OF PREDICTED WITH MEASURED PILE TOP FORCE FOR DATA SET NO. 7

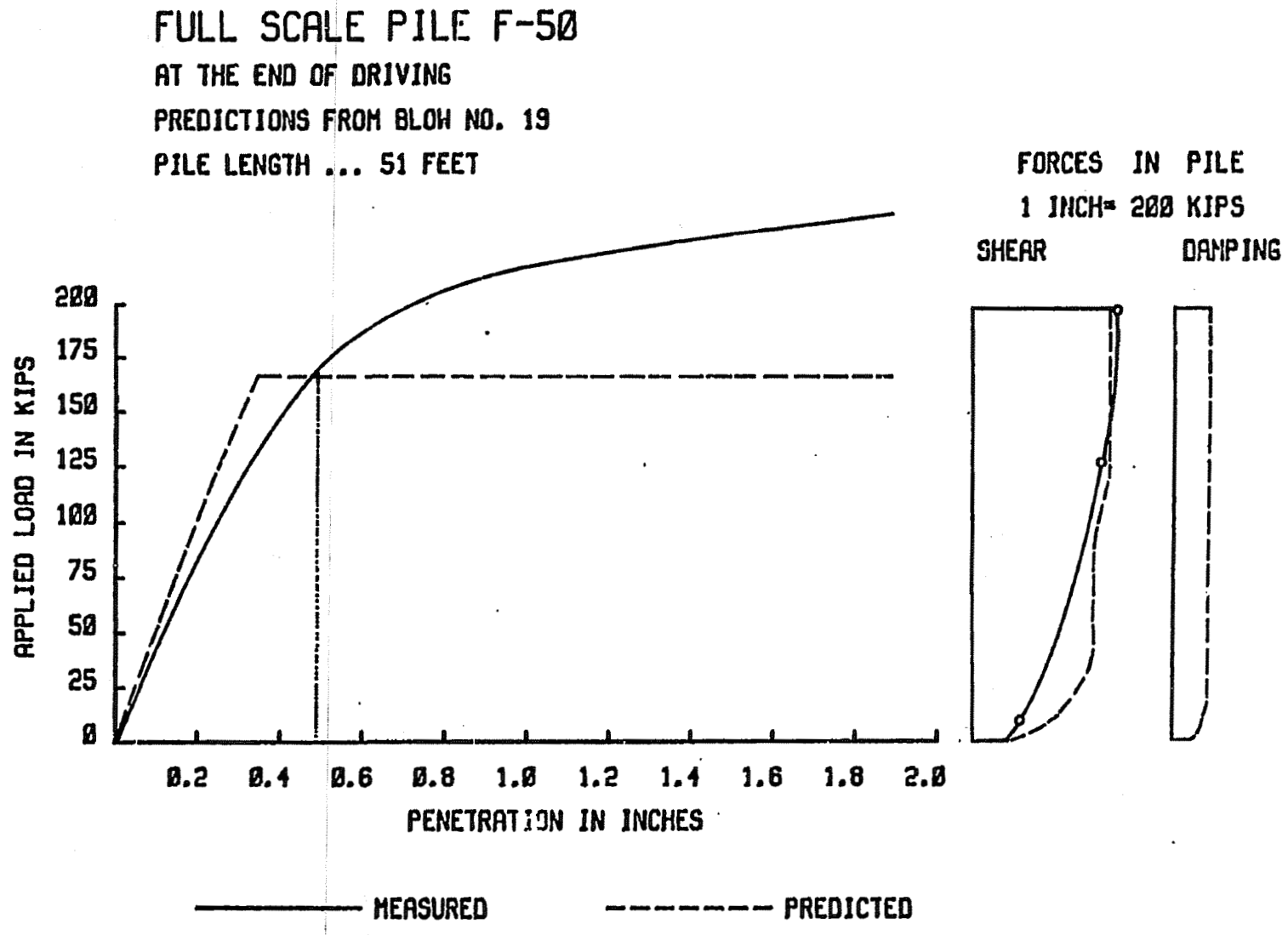

FIGURE 3.10: COMPARISON OF PREDICTED STATIC RESULTS WITH FIELD LOAD TEST AND PREDICTED FORCES IN PILE

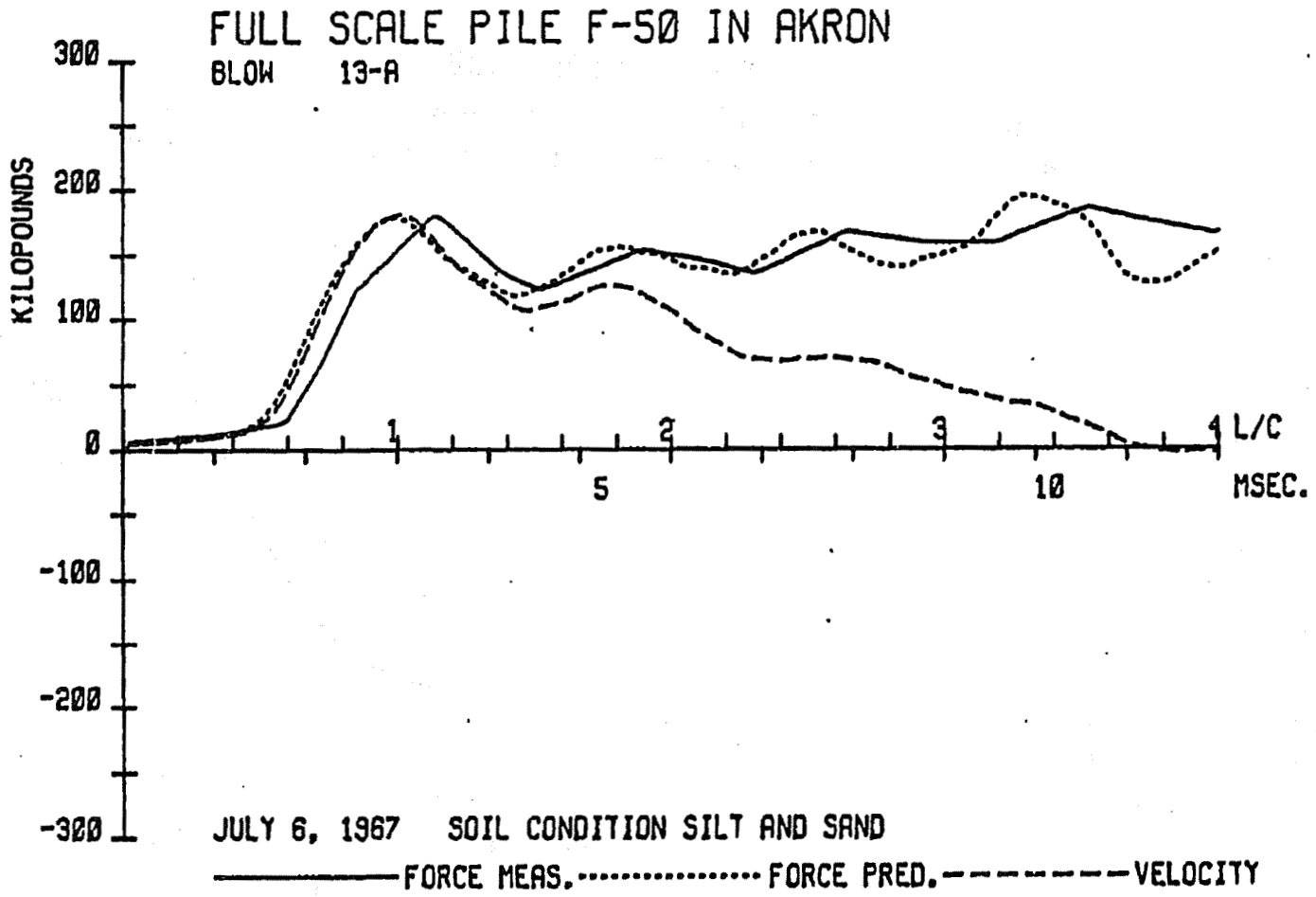

FIGURE 3.11: COMPARISON OF PREDICTED WITH MEASURED PILE TOP FORCE FOR DATA SET NO. 8

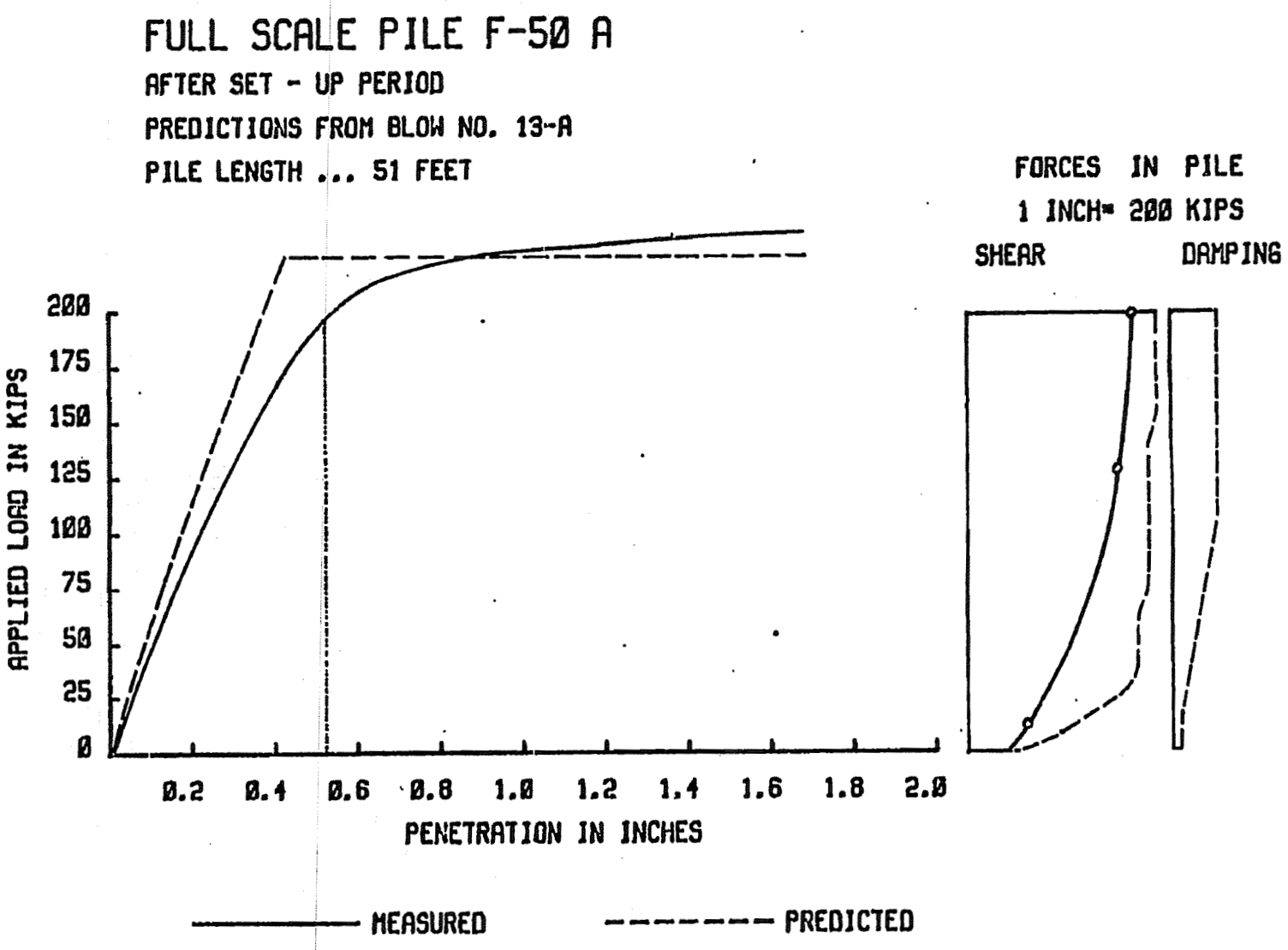

FIGURE 3.12: COMPARISON OF PREDICTED STATIC RESULT WITH FIELD LOAD TEST AND PREDICTED FORCES IN PILE

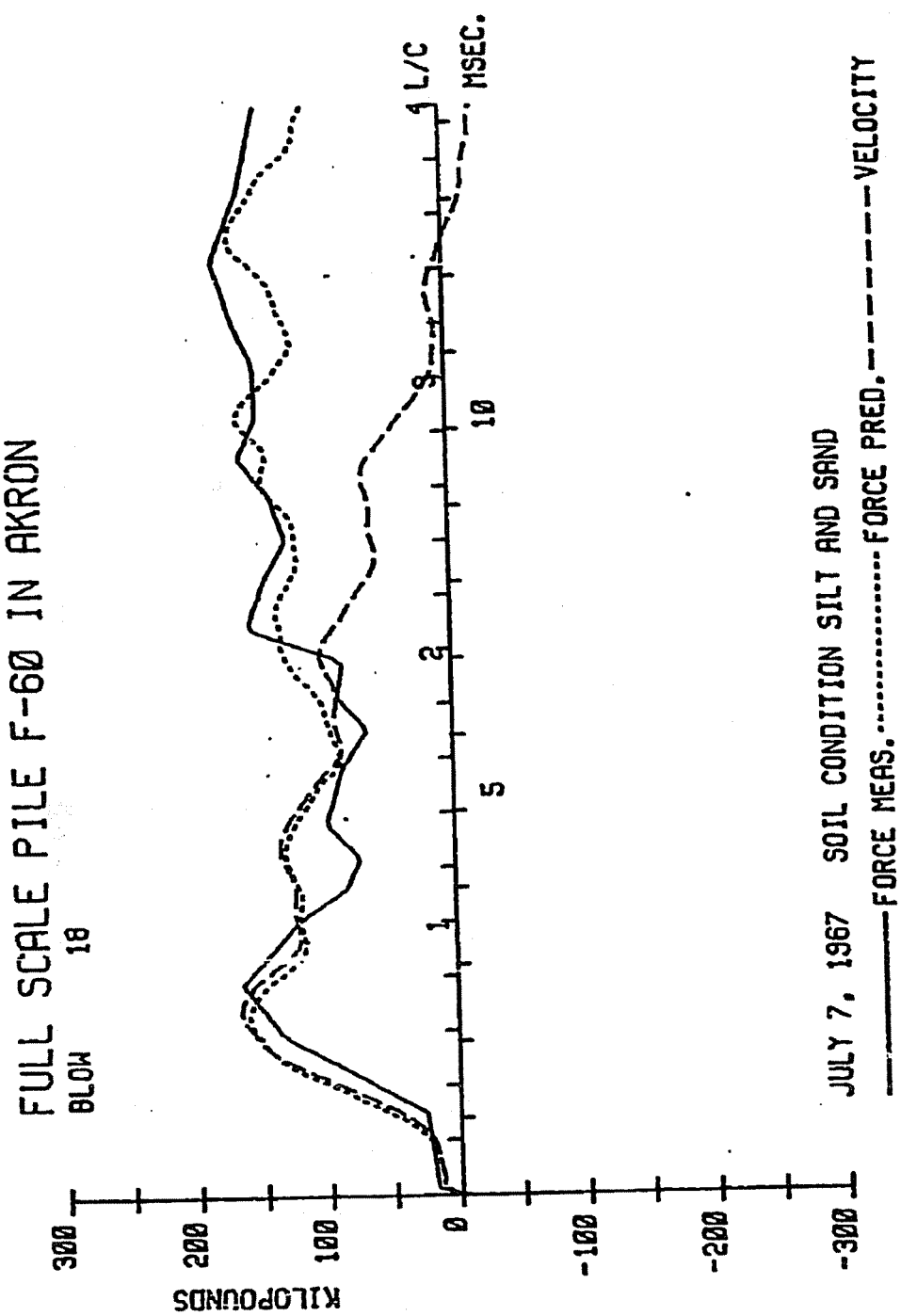

FIGURE 3.13: COMPARISON OF PREDICTED WITH MEASURED PILE TOP FORCE FOR DATA SET NO. 9

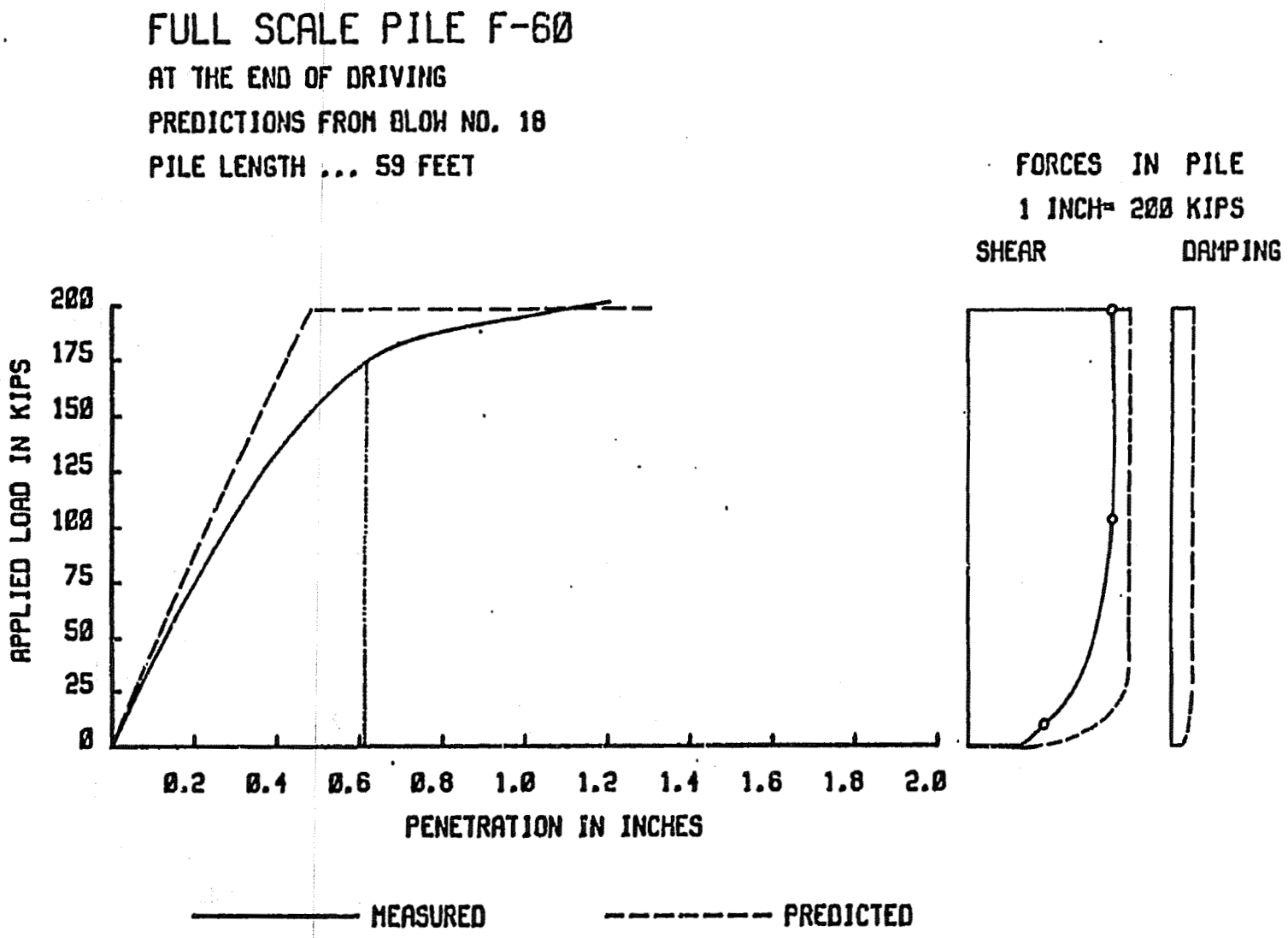

FIGURE 3.14: COMPARISON OF PREDICTED STATIC RESULT WITH FIELD LOAD TEST AND FORCES IN PILE

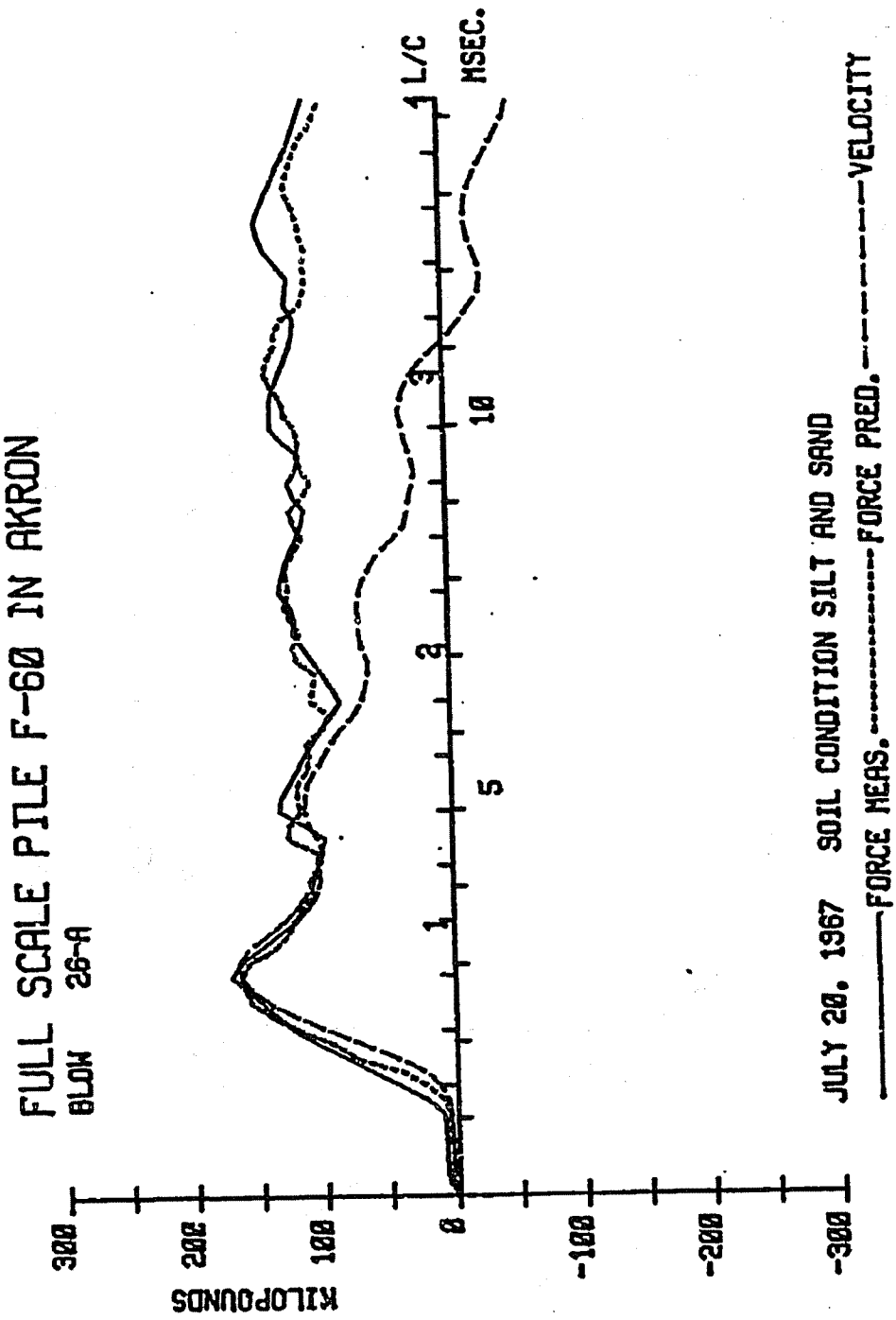

FIGURE 3.15: COMPARISON OF PREDICTED WITH MEASURED PILE TOP FORCE FOR DATA SET NO. 10

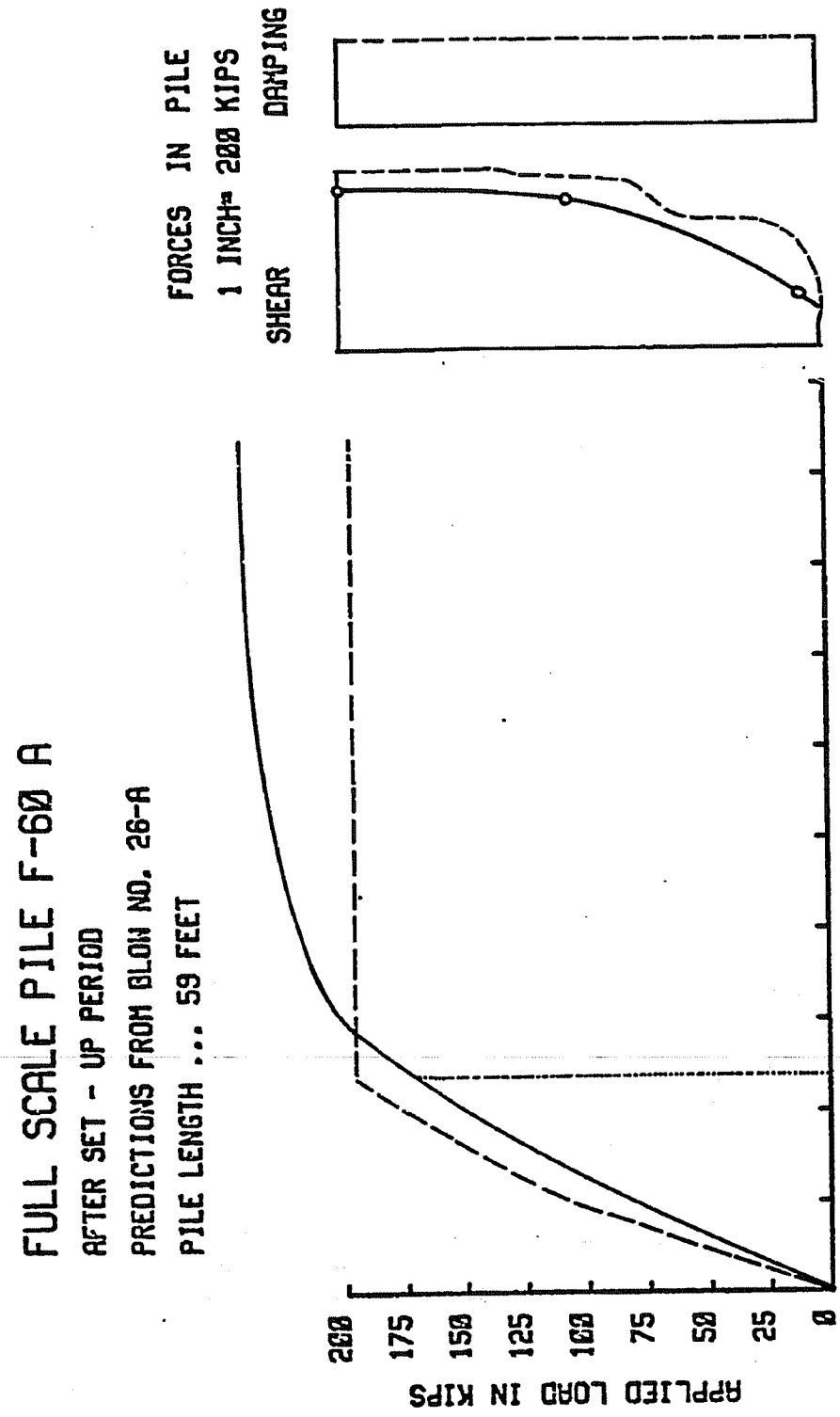

FIGURE 3.16: COMPARISON OF PREDICTED STATIC RESULT WITH FIELD LOAD TEST AND FORCES IN PILE

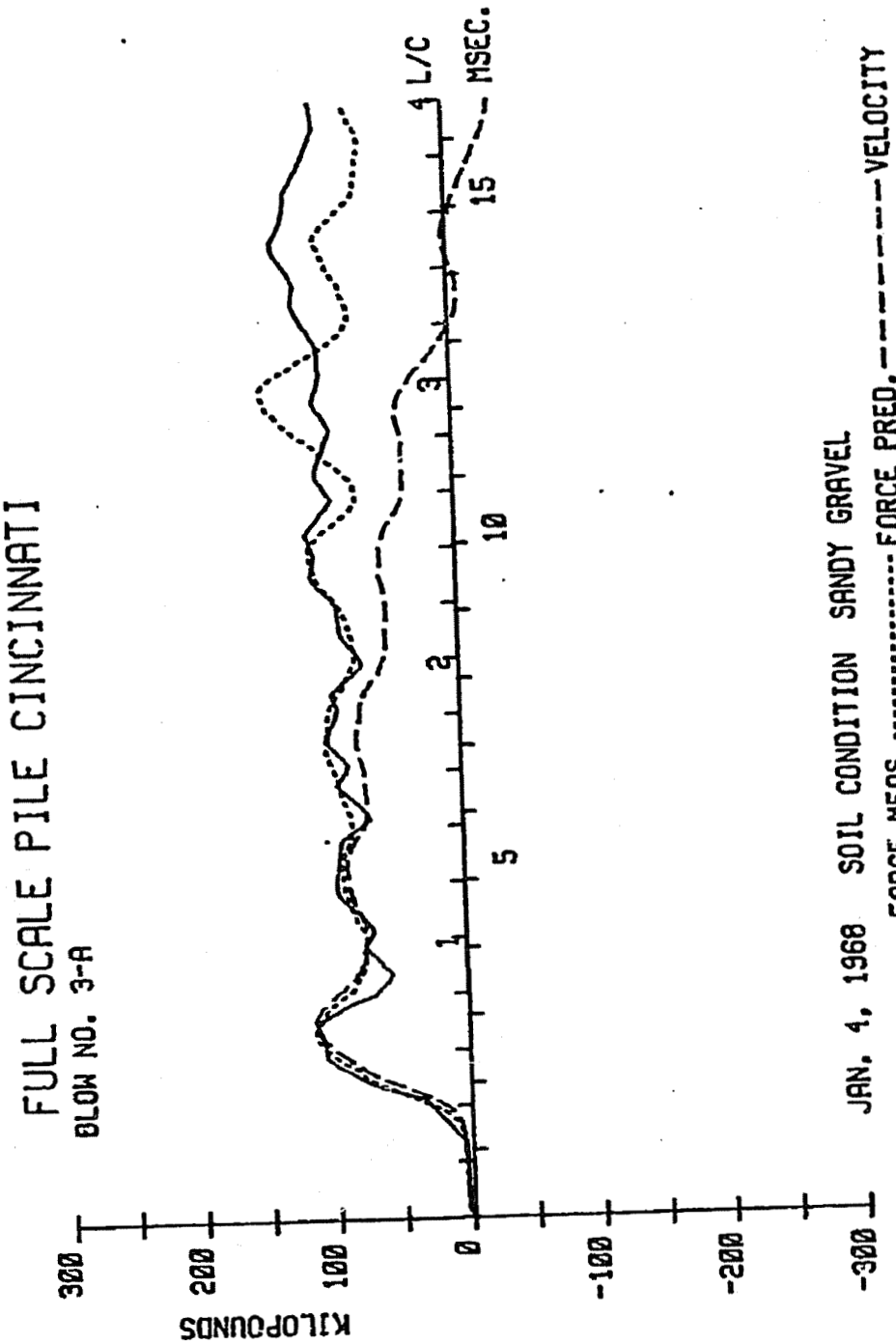

FIGURE 3.17: COMPARISON OF PREDICTED WITH MEASURED PILE TOP FORCE FOR DATA SET NO. 11

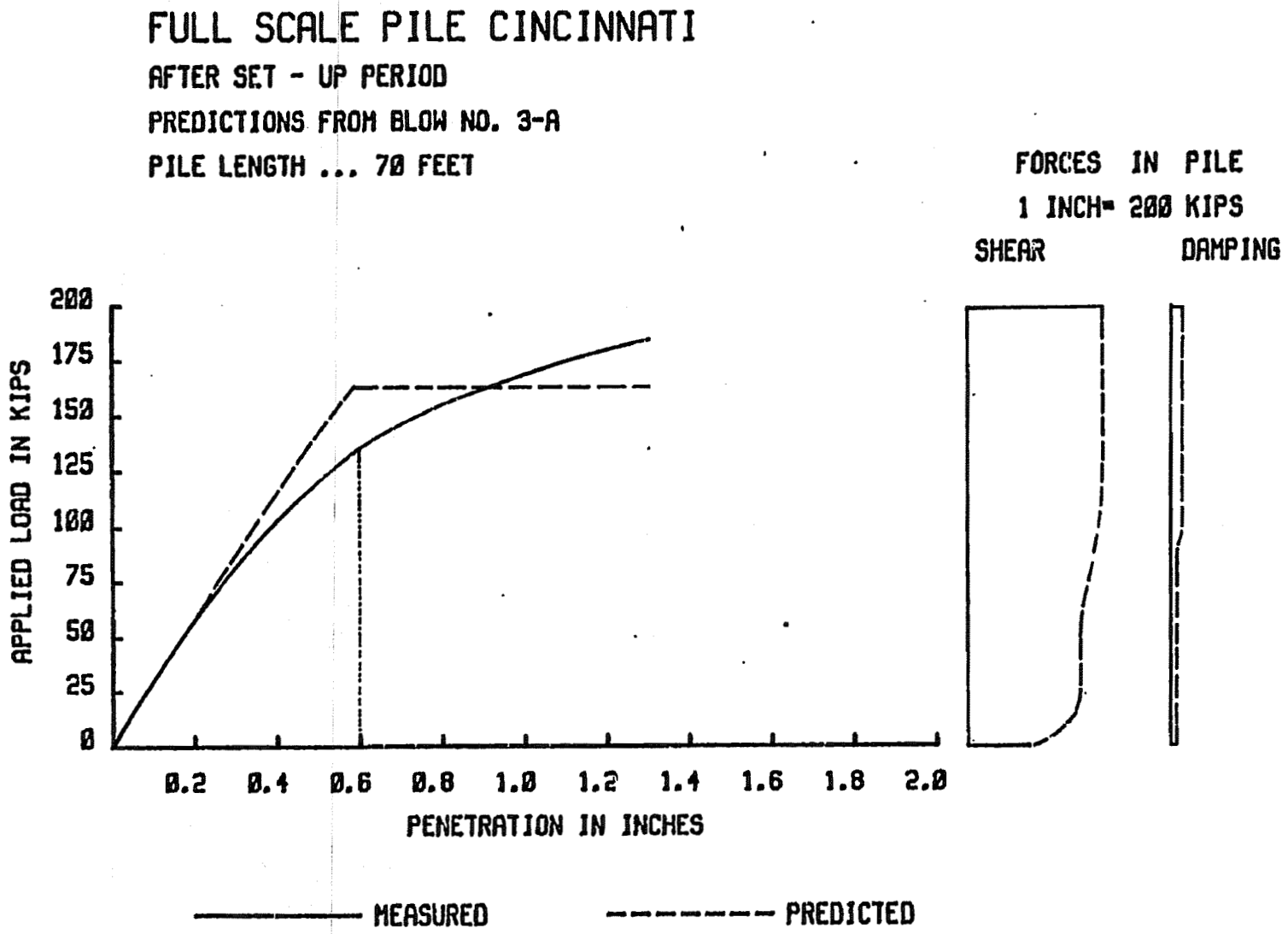

FIGURE 3.18: COMPARISON OF PREDICTED STATIC RESULTS WITH FIELD LOAD TEST AND FORCES IN PILE

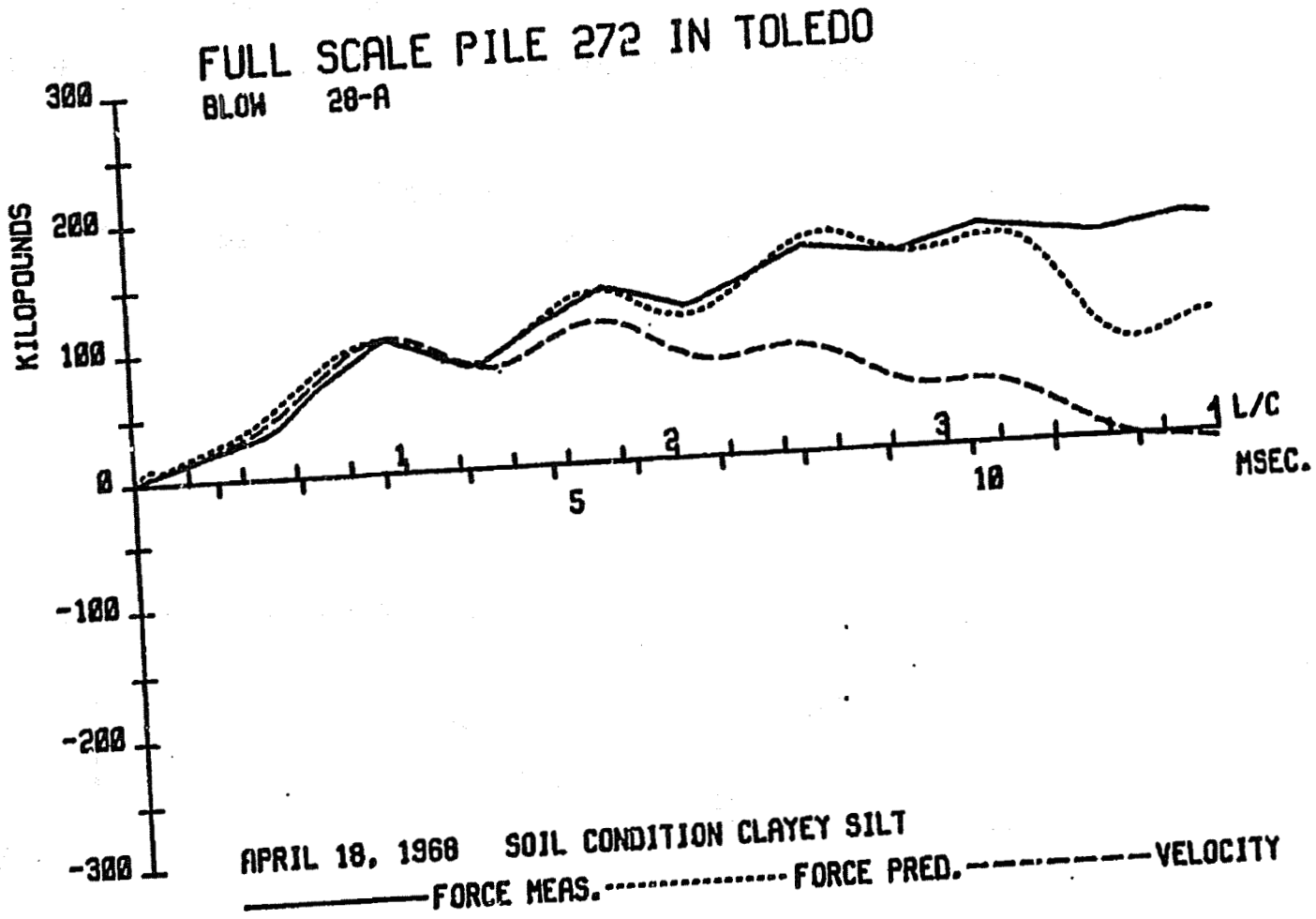

FIGURE 3.19: COMPARISON OF PREDICTED WITH MEASURED PILE TOP FORCE FOR DATA SET NO. 12

PREDICTION OBTAINED BY INSPECTION

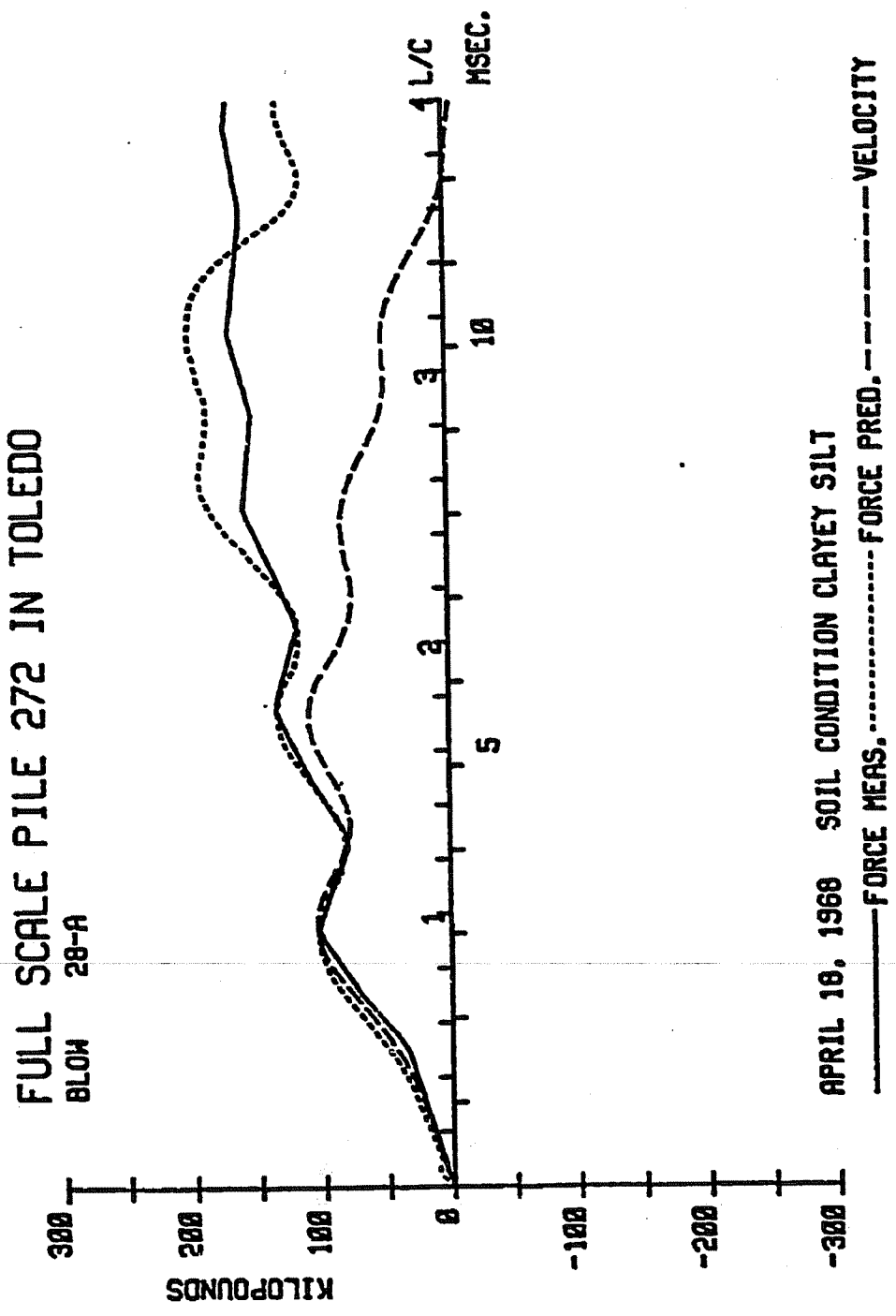

FIGURE 3.20: COMPARISON OF PREDICTED WITH MEASURED PILE TOP FORCE FOR DATA SET NO. 12 PREDICTION FROM AUTOMATED ROUTINE

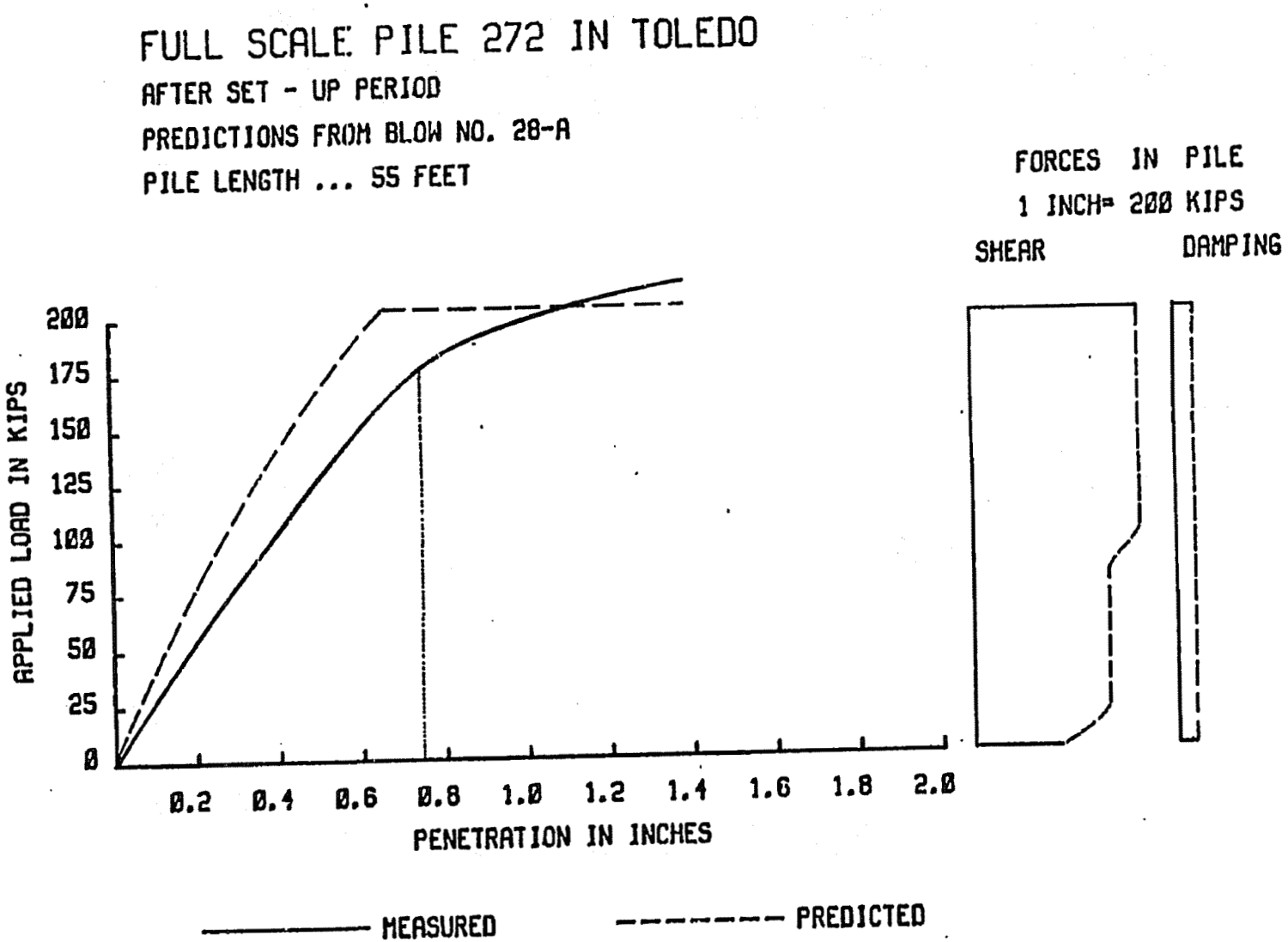

FIGURE 3.21: COMPARISON OF PREDICTED STATIC RESULTS WITH FIELD LOAD TEST AND FORCES IN PILE PREDICTION OBTAINED BY INSPECTION

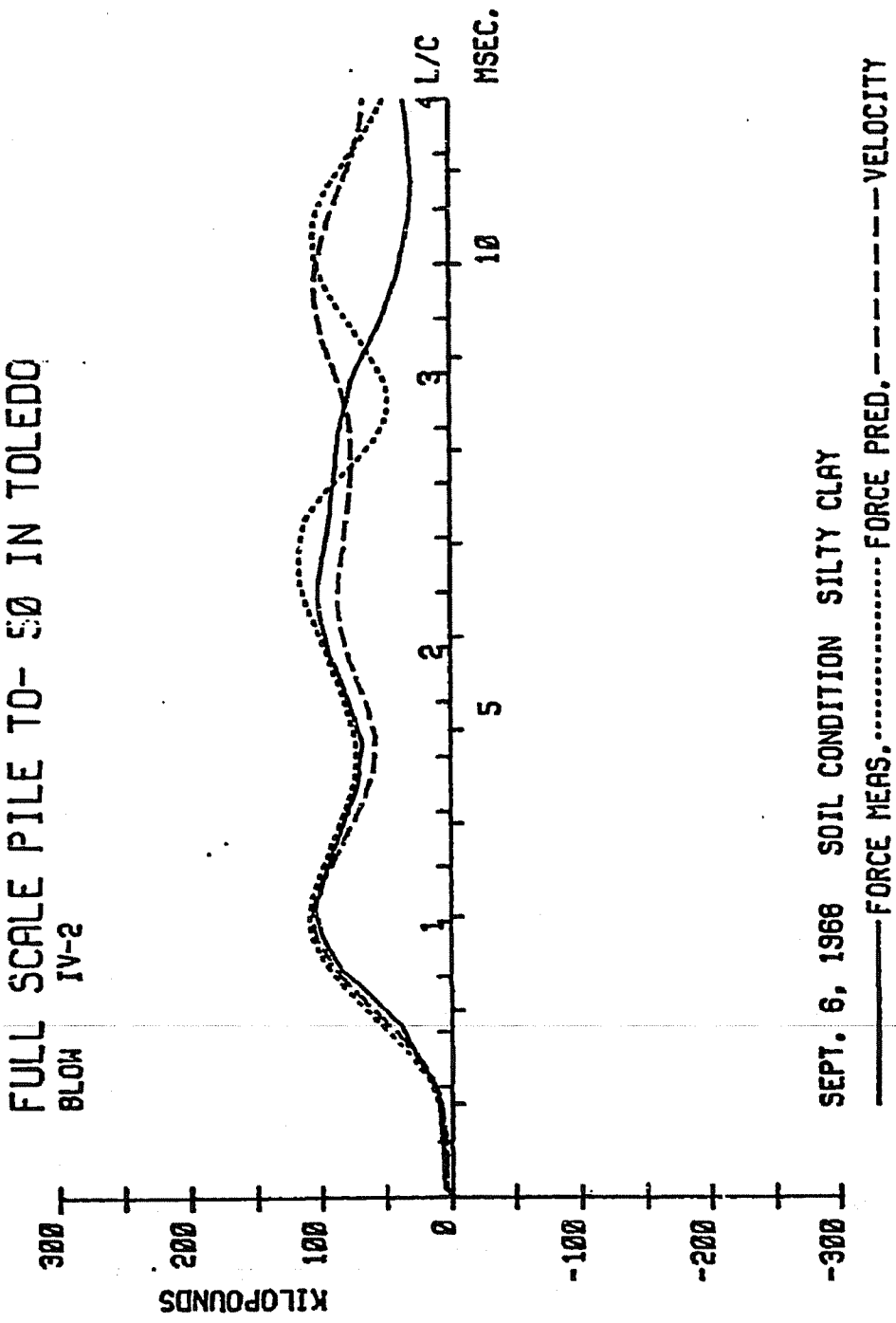

FIGURE 3.22: COMPARISON OF PREDICTED WITH MEASURED PILE TOP FORCE FOR DATA SET NO. 13

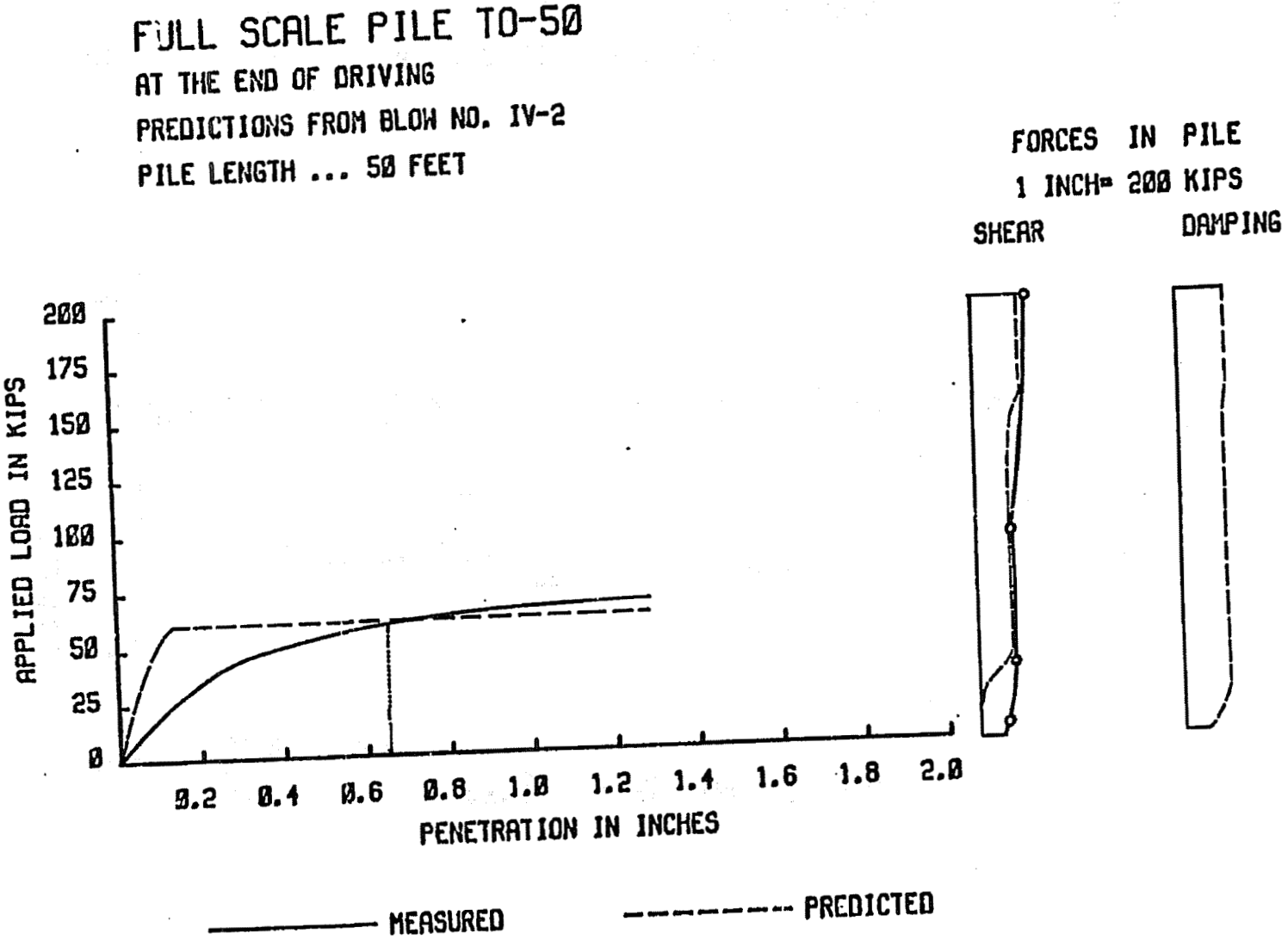

FIGURE 3.23: COMPARISON OF PREDICTED STATIC RESULTS WITH FIELD LOAD TEST AND FORCES IN PILE

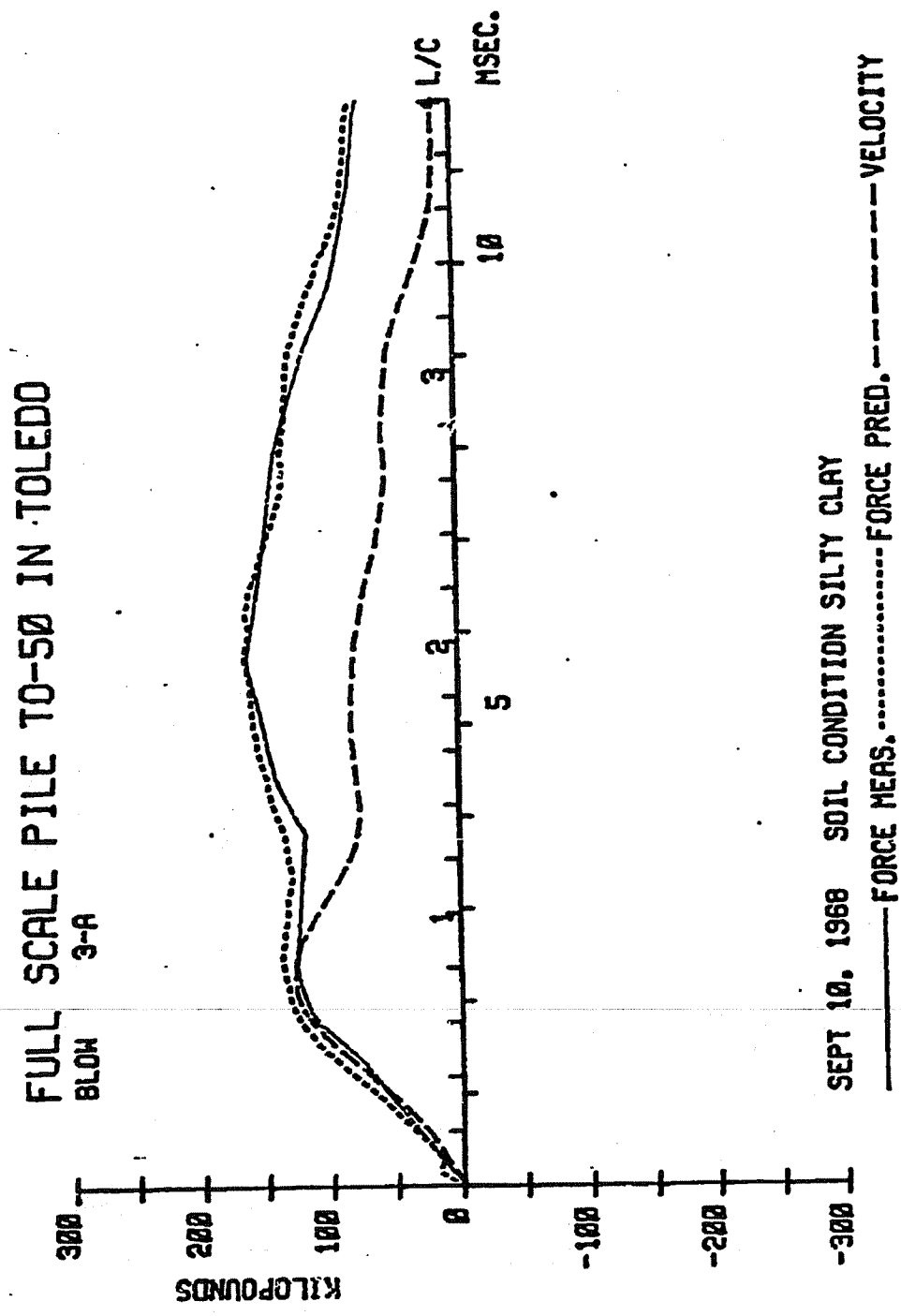

FIGURE 3.24: COMPARISON OF PREDICTED WITH MEASURED PILE TOP FORCE FOR PILE NO. 14

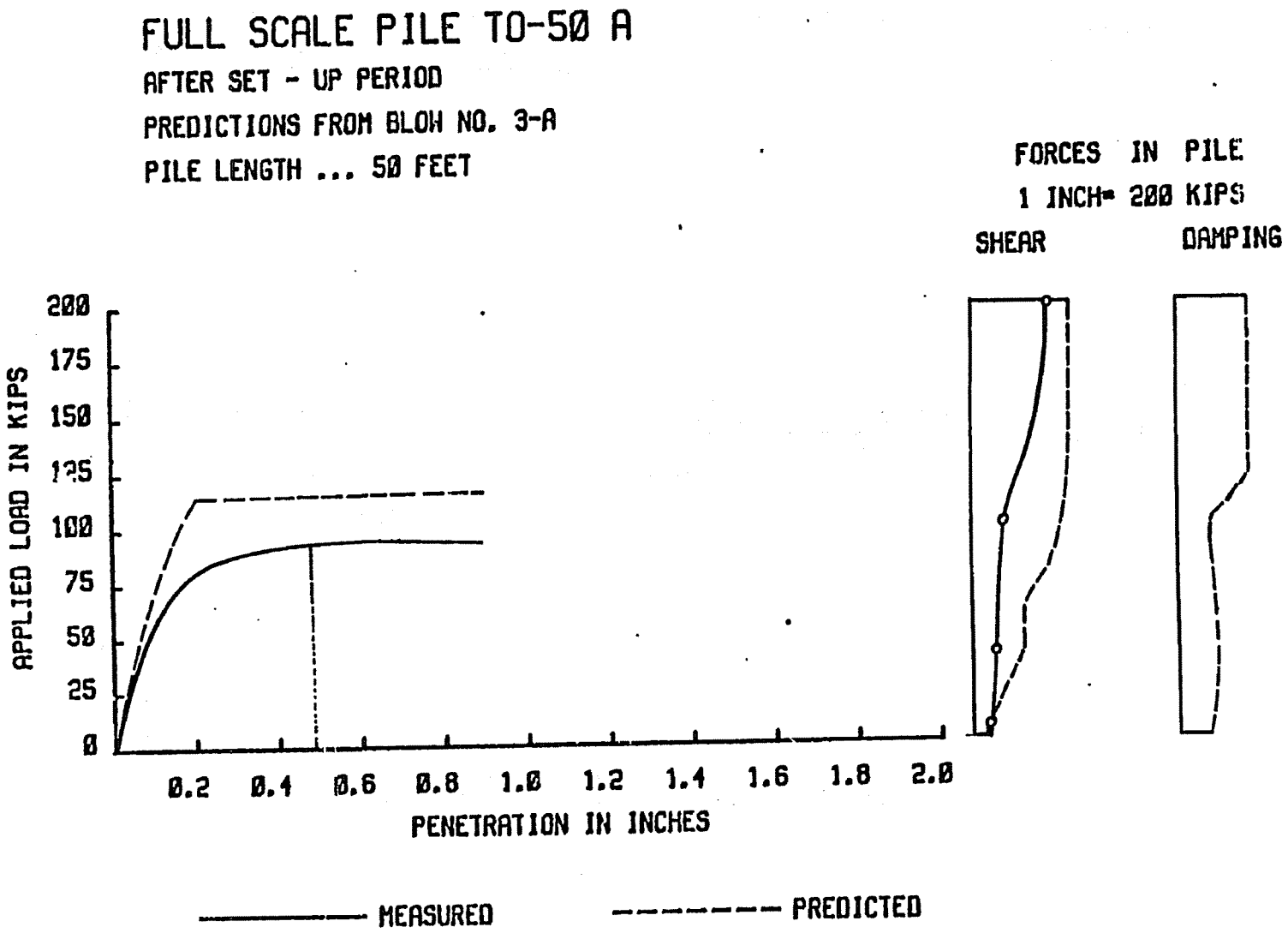

FIGURE 3.25: COMPARISON OF PREDICTED STATIC RESULTS WITH FIELD LOAD TEST AND FORCES IN PILE

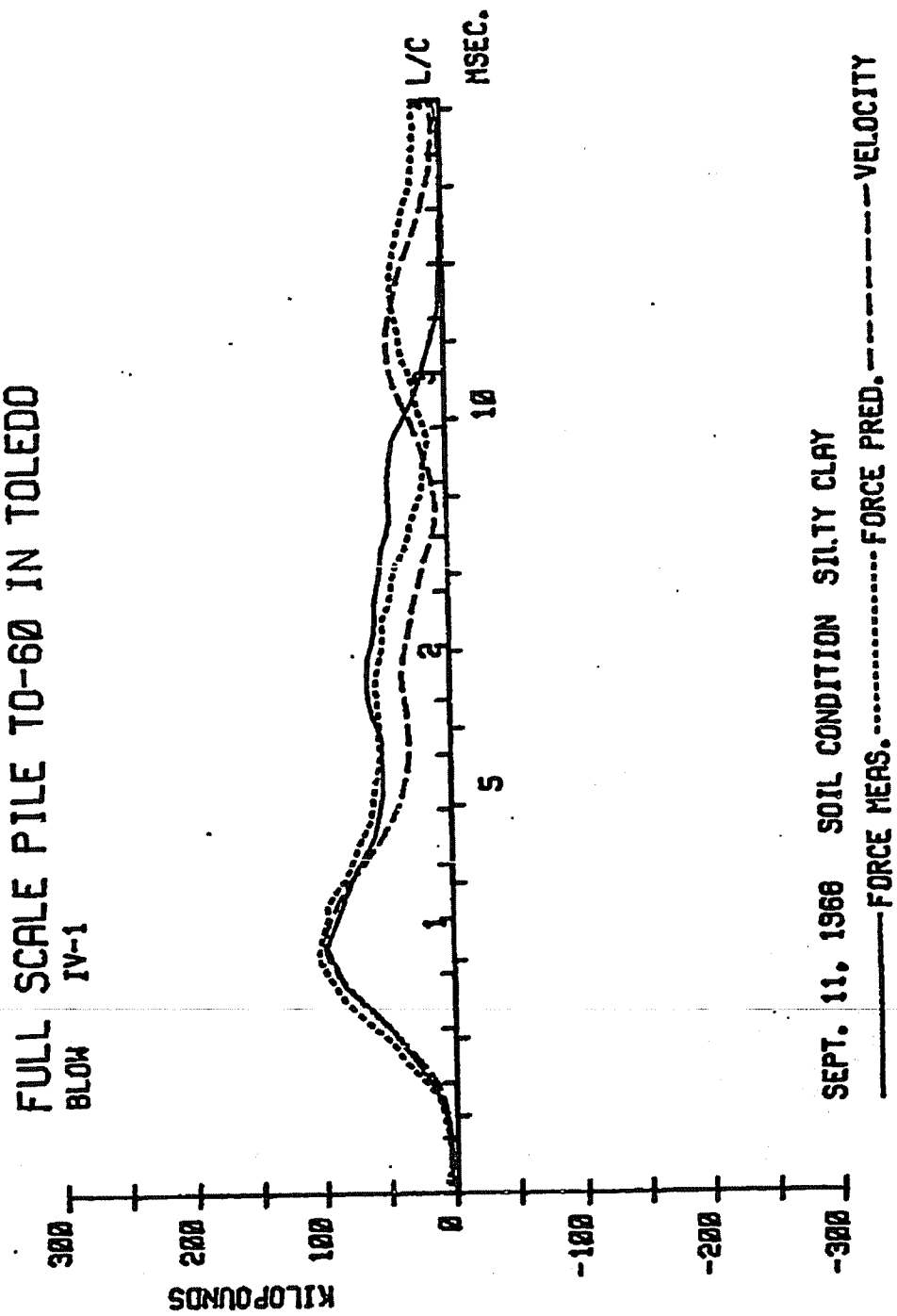

FIGURE 3.26: COMPARISON OF PREDICTED WITH MEASURED PILE TOP FORCE FOR DATA SET NO. 15

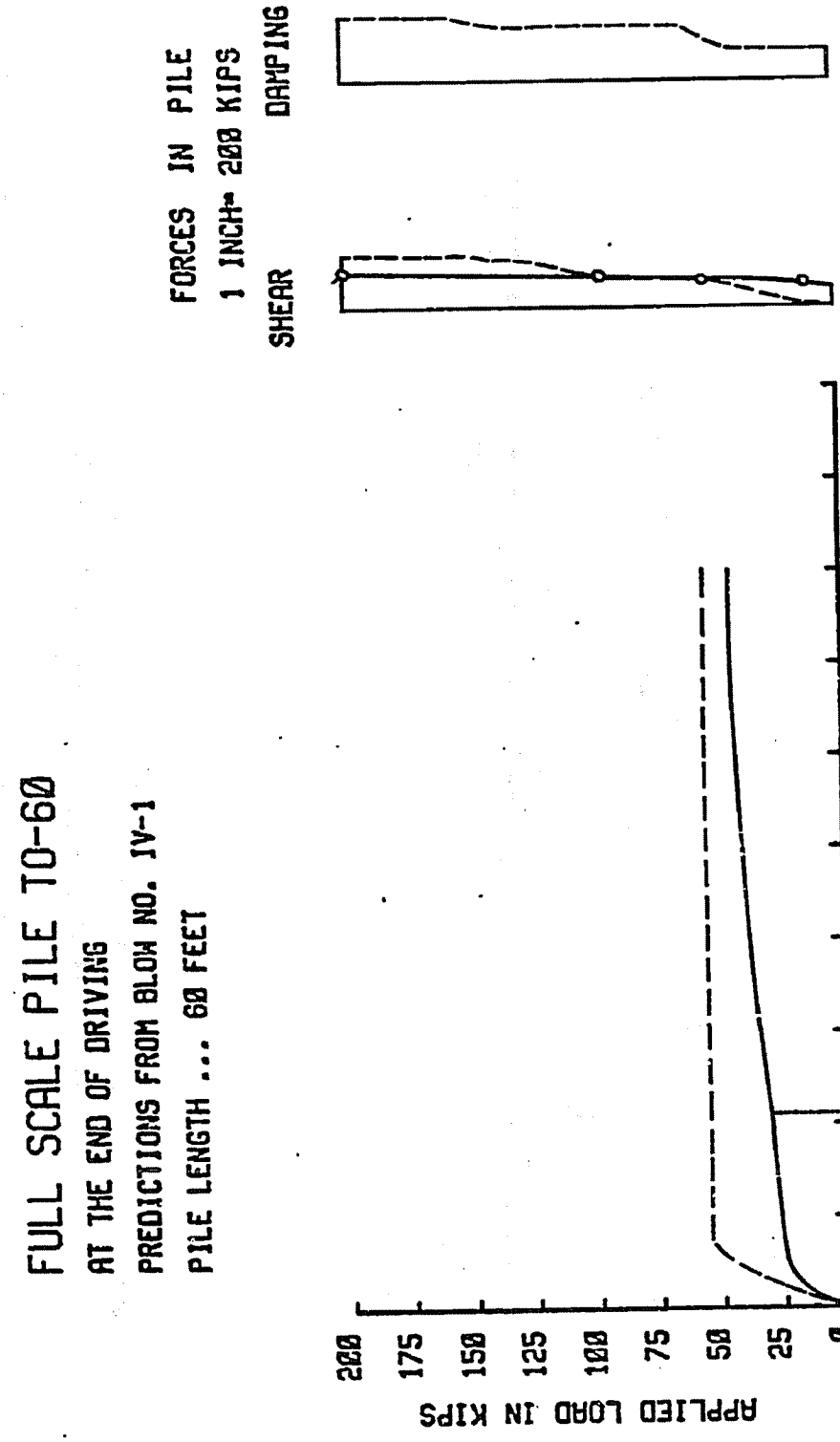

FIGURE 3.27: COMPARISON OF PREDICTED STATIC RESULT WITH FIELD LOAD TEST AND FORCES IN PILE

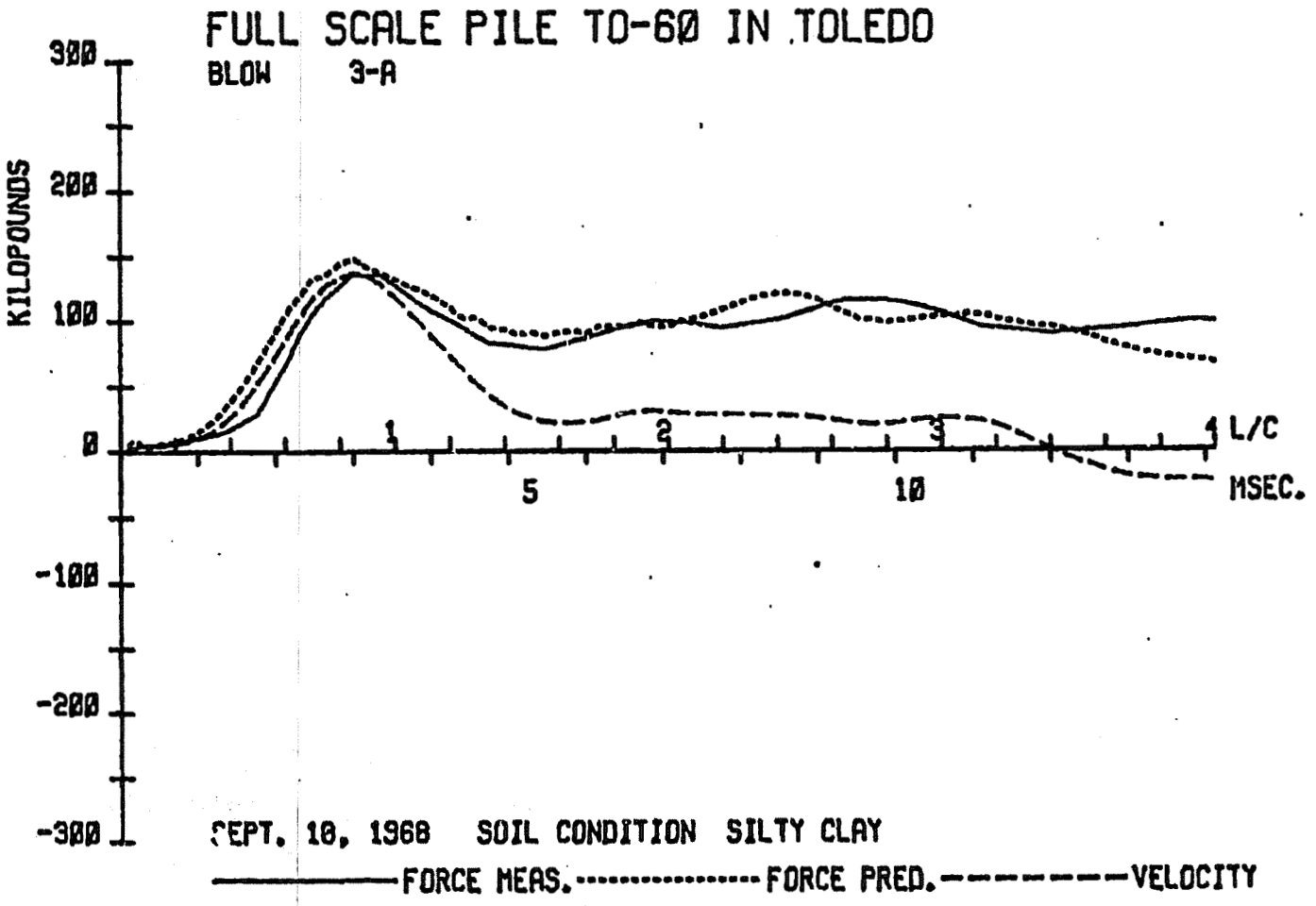

FIGURE 3.28: COMPARISON OF PREDICTED WITH MEASURED PILE TOP FORCE FOR DATA SET NO. 16

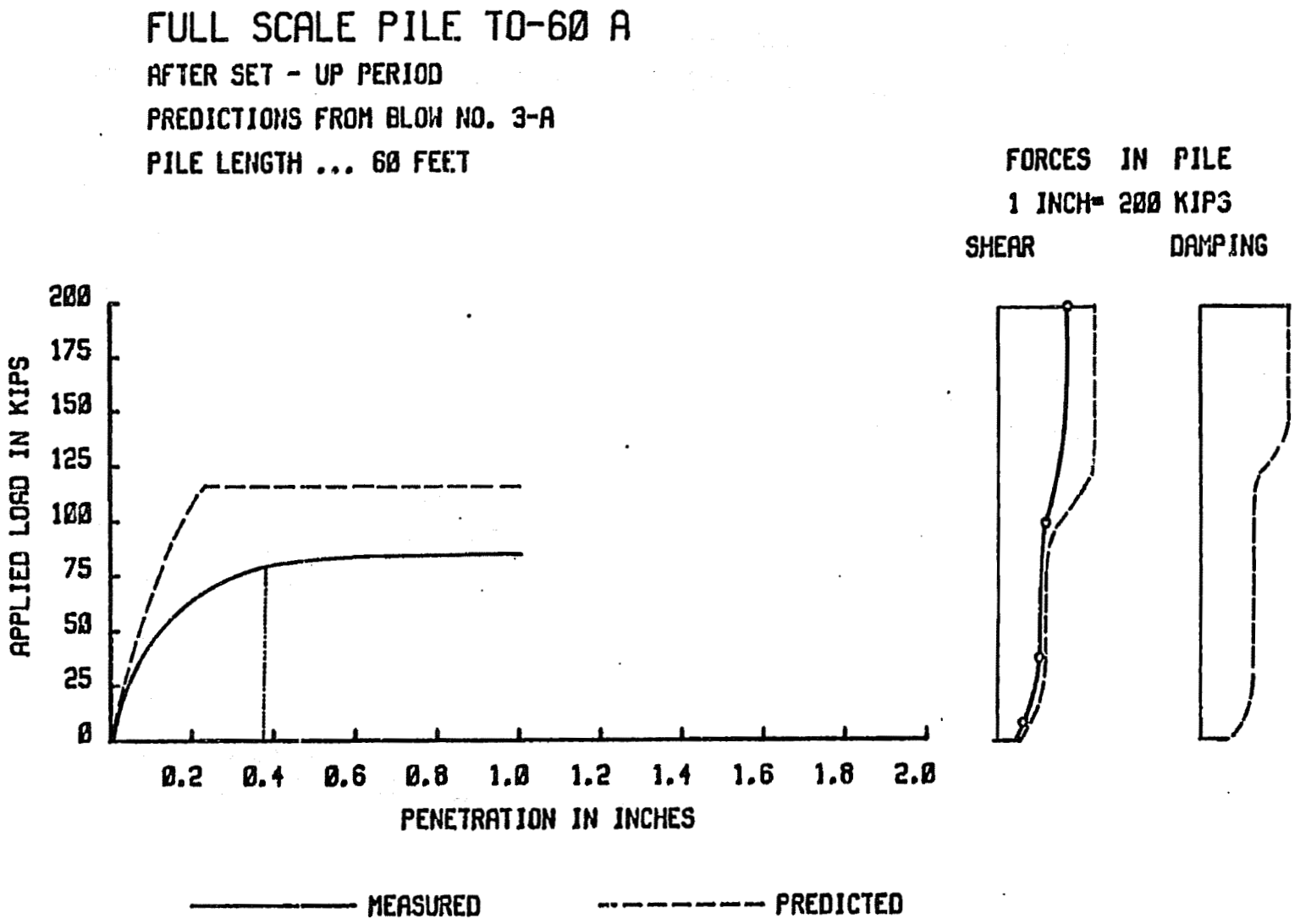

FIGURE 3.29: COMPARISON OF PREDICTED STATIC RESULTS WITH FIELD LOAD TEST AND FORCES IN PILE

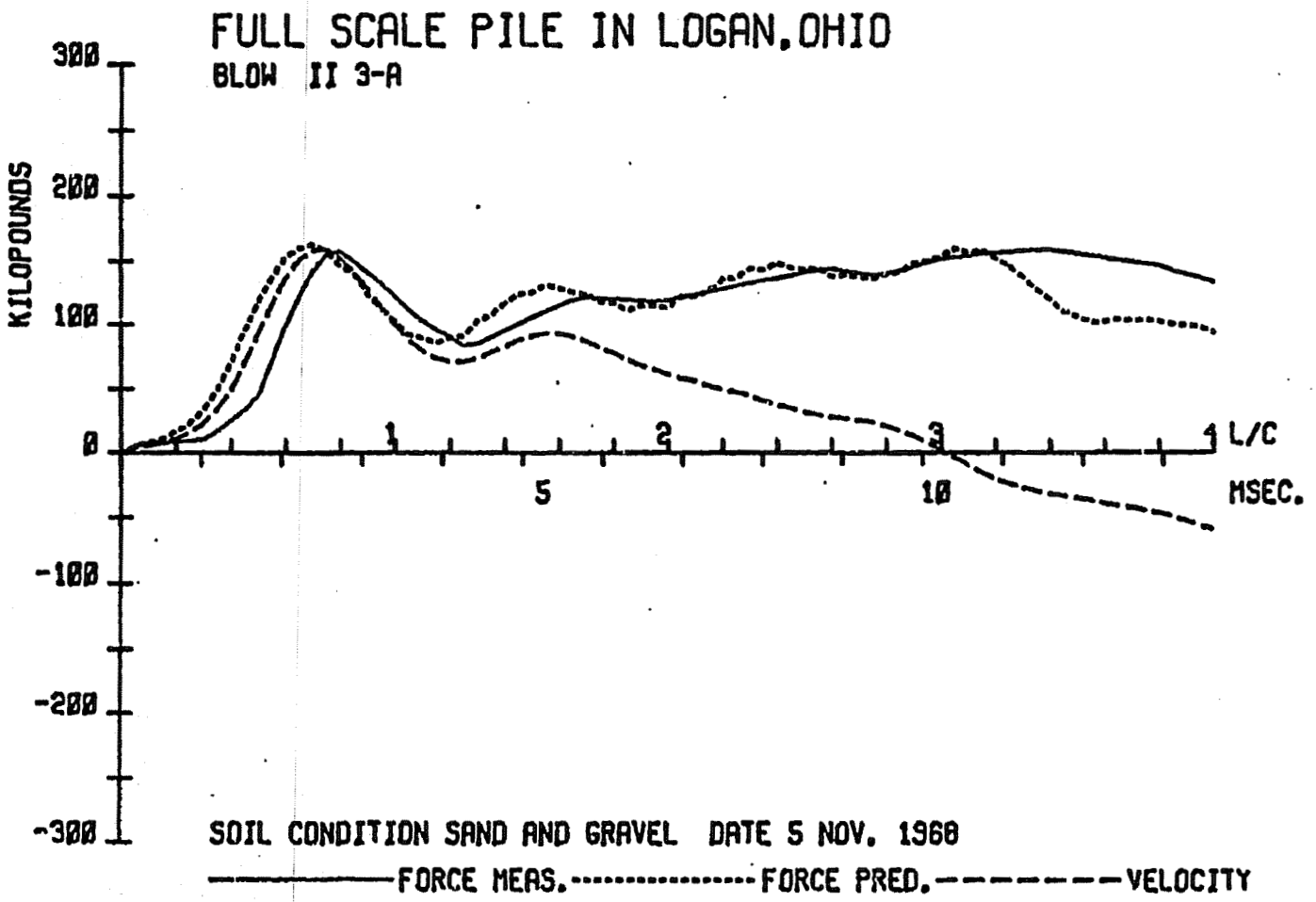

FIGURE 3.30: COMPARISON OF PREDICTED WITH MEASURED PILE TOP FORCE FOR DATA SET NO. 17

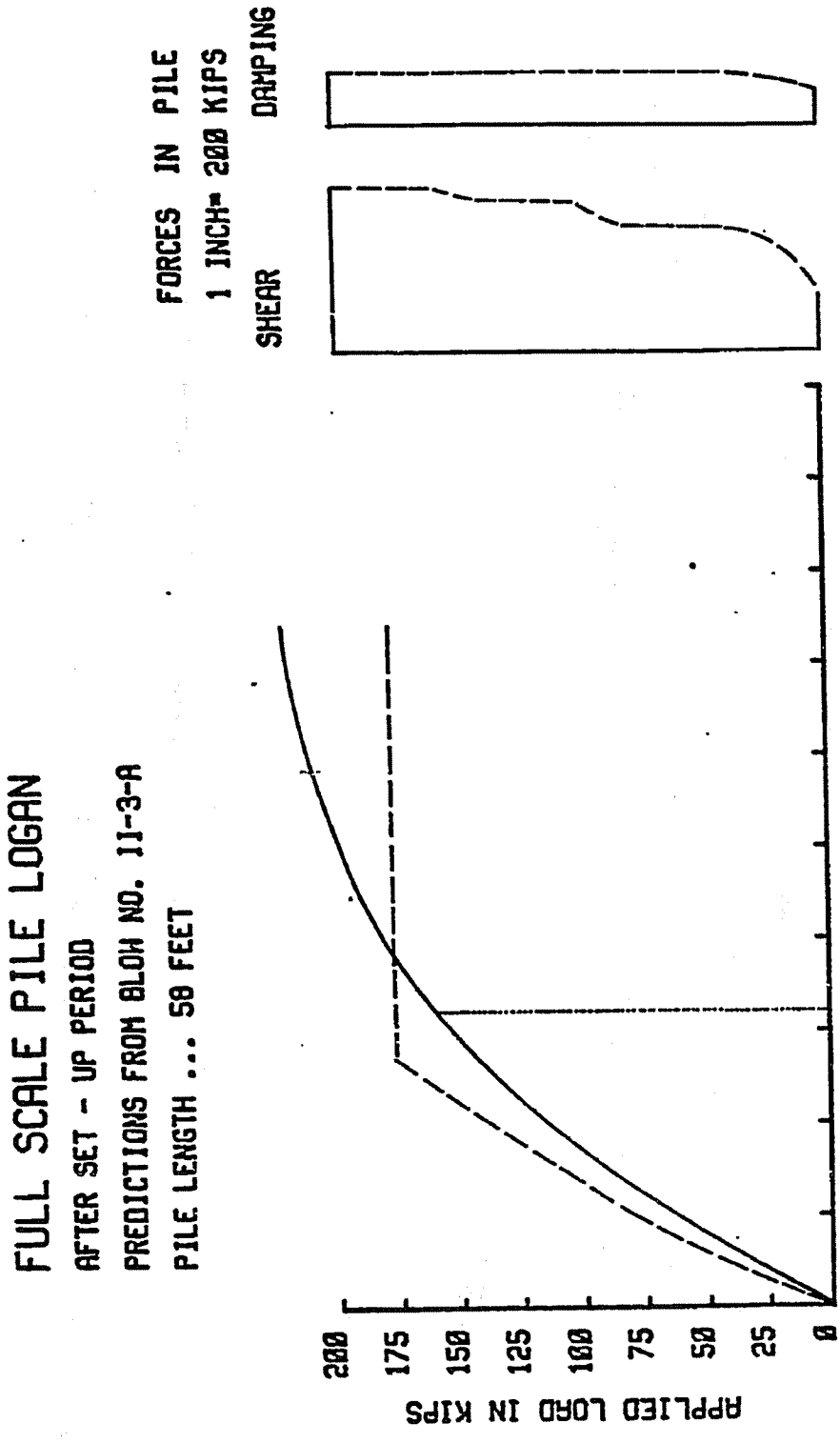

FIGURE 3.31: COMPARISON OF PREDICTED STATIC RESULTS WITH FIELD LOAD TEST AND FORCES IN PILE

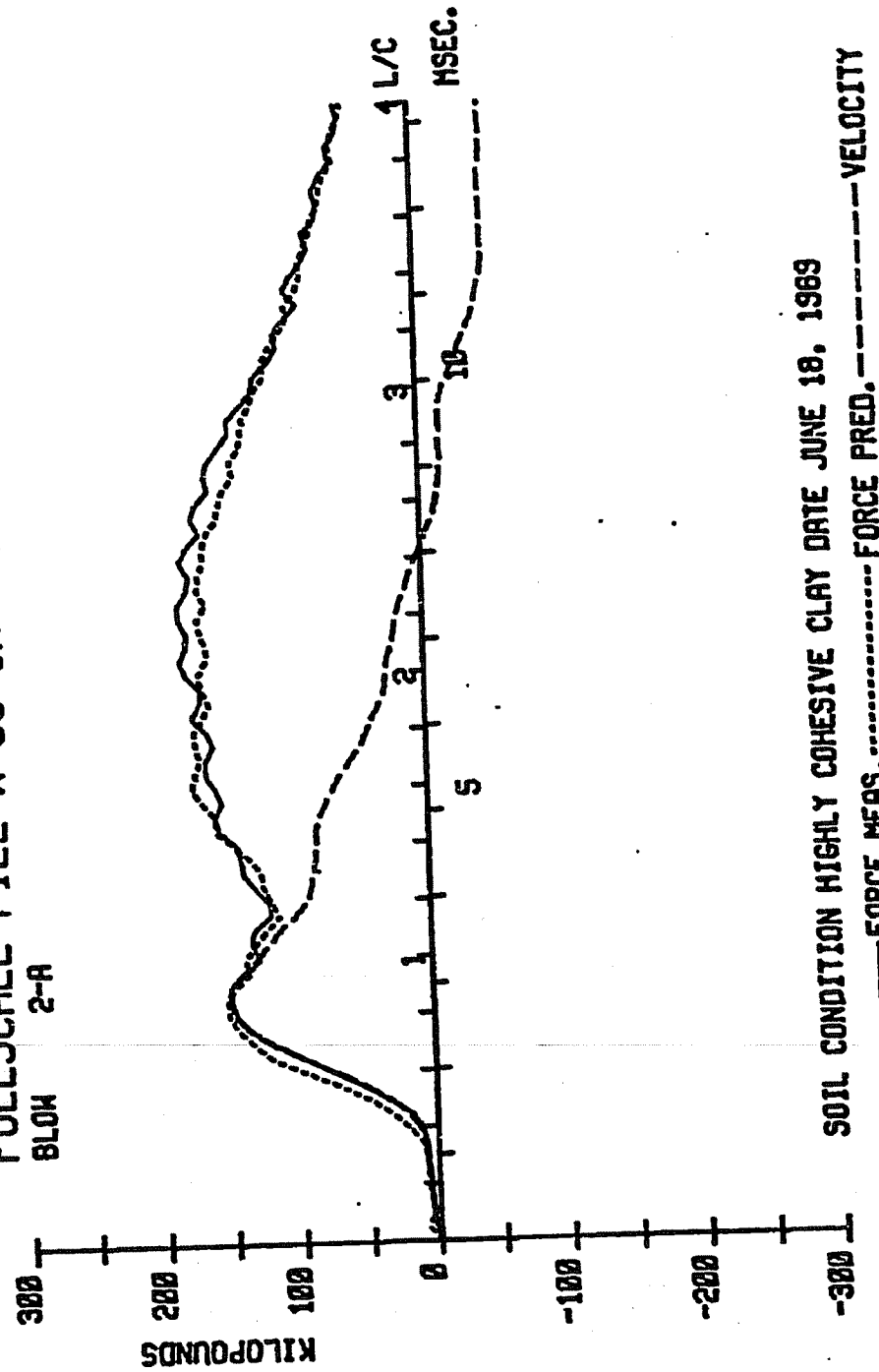

FIGURE 3.32: COMPARISON OF PREDICTED WITH MEASURED PILE TOP FORCE FOR DATA SET NO. 18

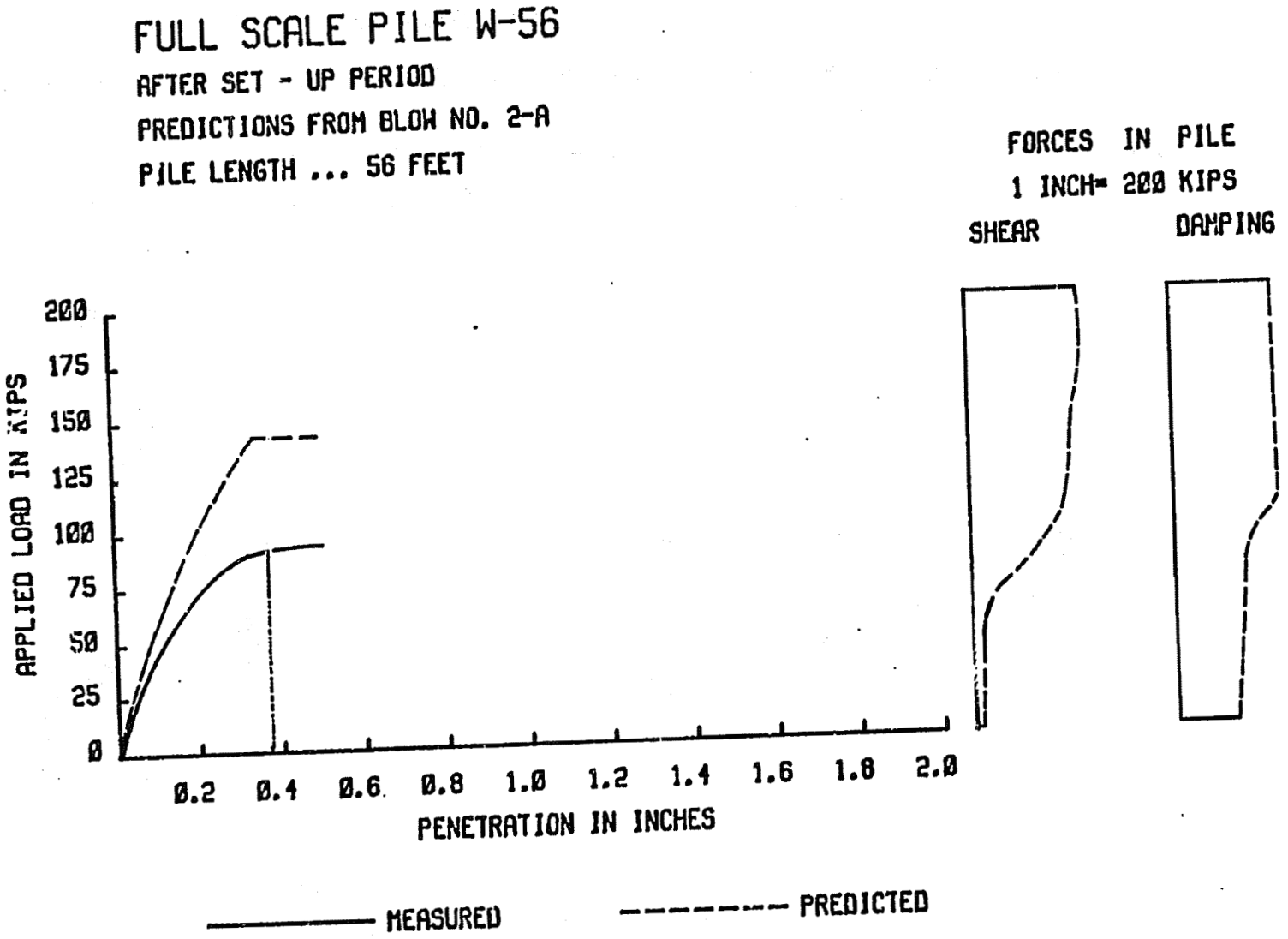

FIGURE 3.33: COMPARISON OF PREDICTED STATIC RESULTS WITH MEASURED LOAD TEST AND FORCES IN PILE

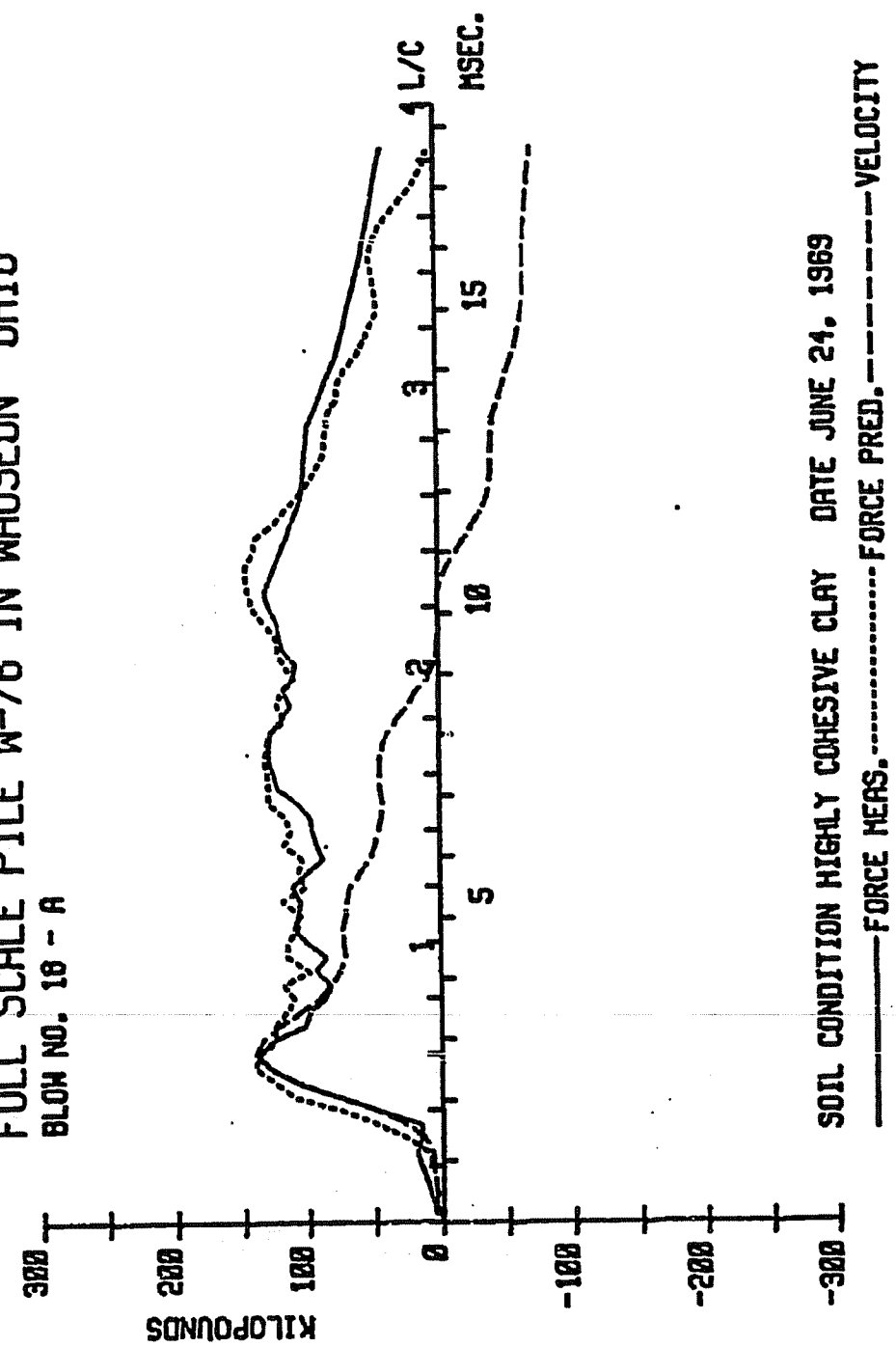

FIGURE 3.34: COMPARISON OF PREDICTED WITH MEASURED PILE TOP FORCE FOR DATA SET NO. 19

PREDICTION FROM AUTOMATED ROUTINE

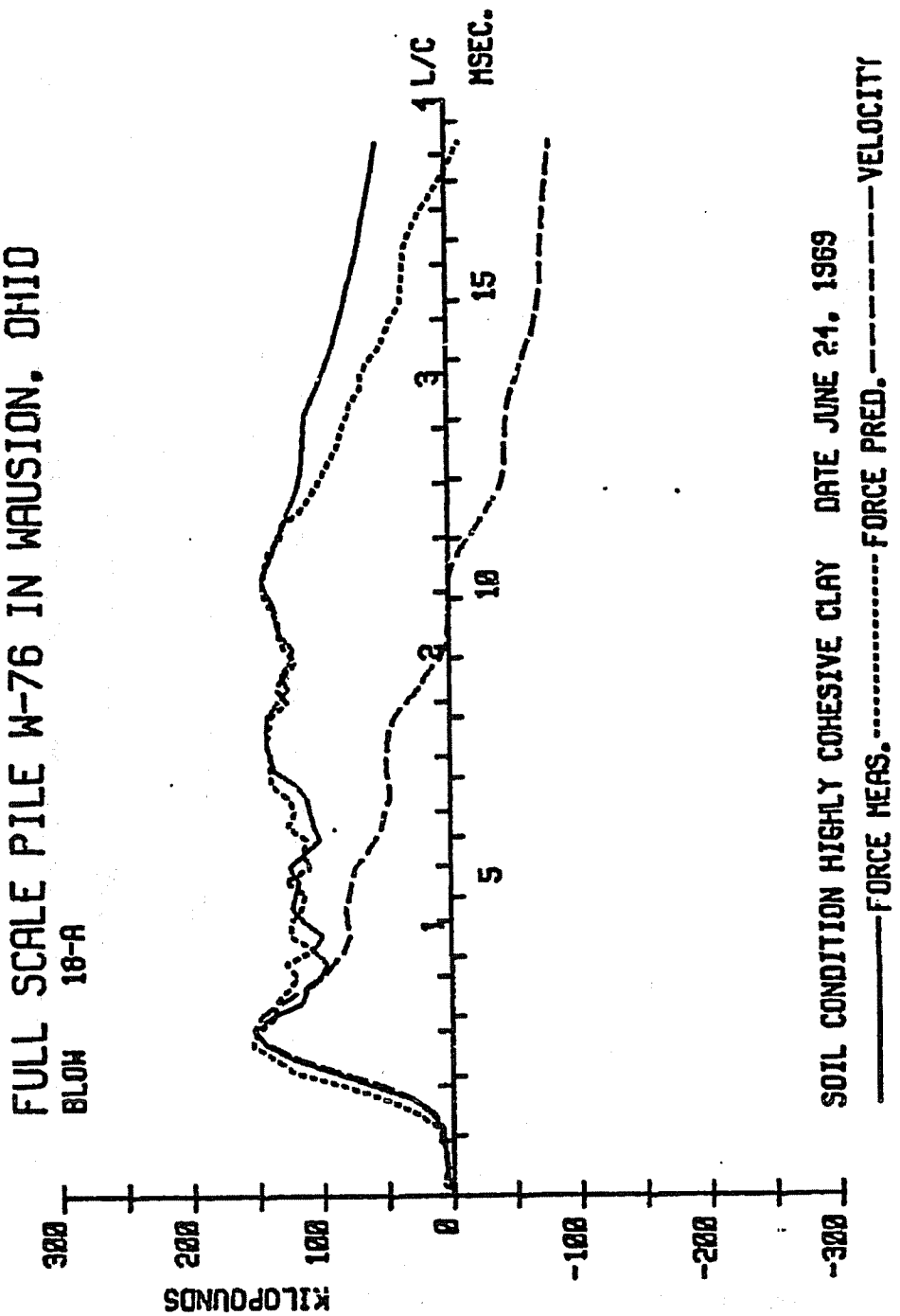

FIGURE 3.35: COMPARISON OF PREDICTED WITH MEASURED PILE TOP FORCE FOR DATA SET NO. 19

PREDICTION BY INSPECTION

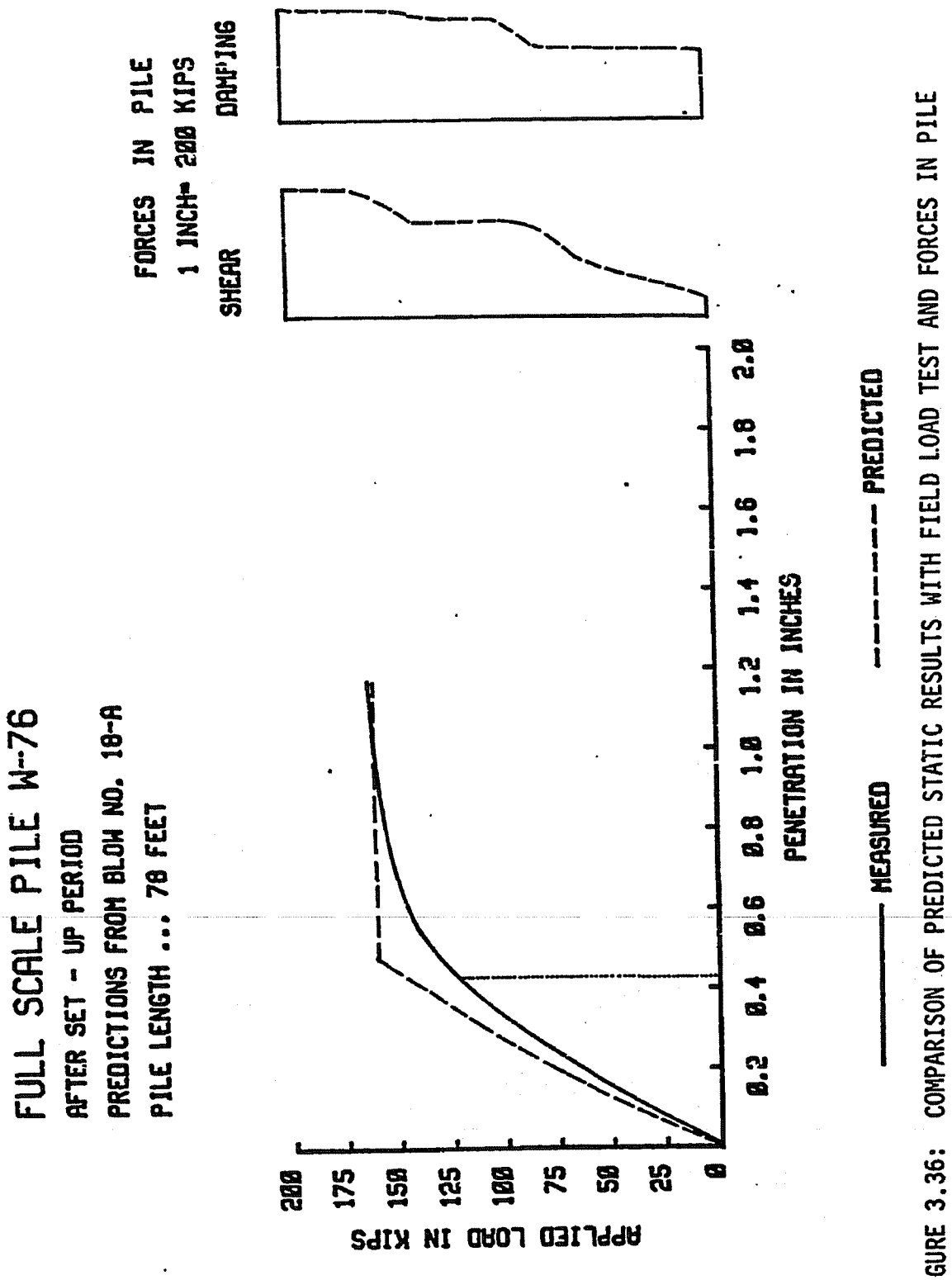

FIGURE 3.36: COMPARISON OF PREDICTED STATIC RESULTS WITH FIELD LOAD TEST AND FORCES IN PILE PREDICTIONS FROM COMPUTER ROUTINE

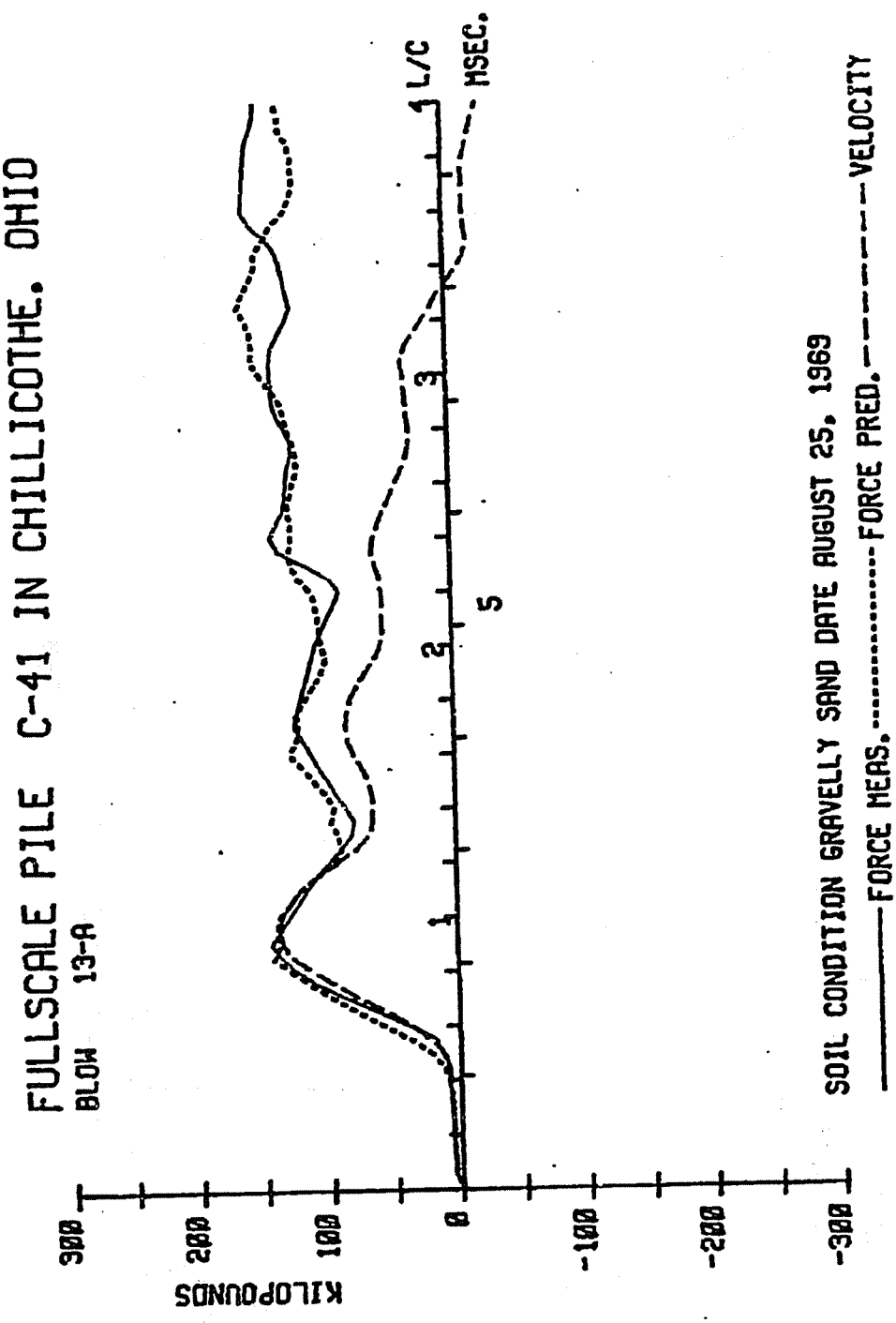

FIGURE 3.37: COMPARISON OF PREDICTED WITH MEASURED PILE TOP FORCE FOR DATA SET NO. 19

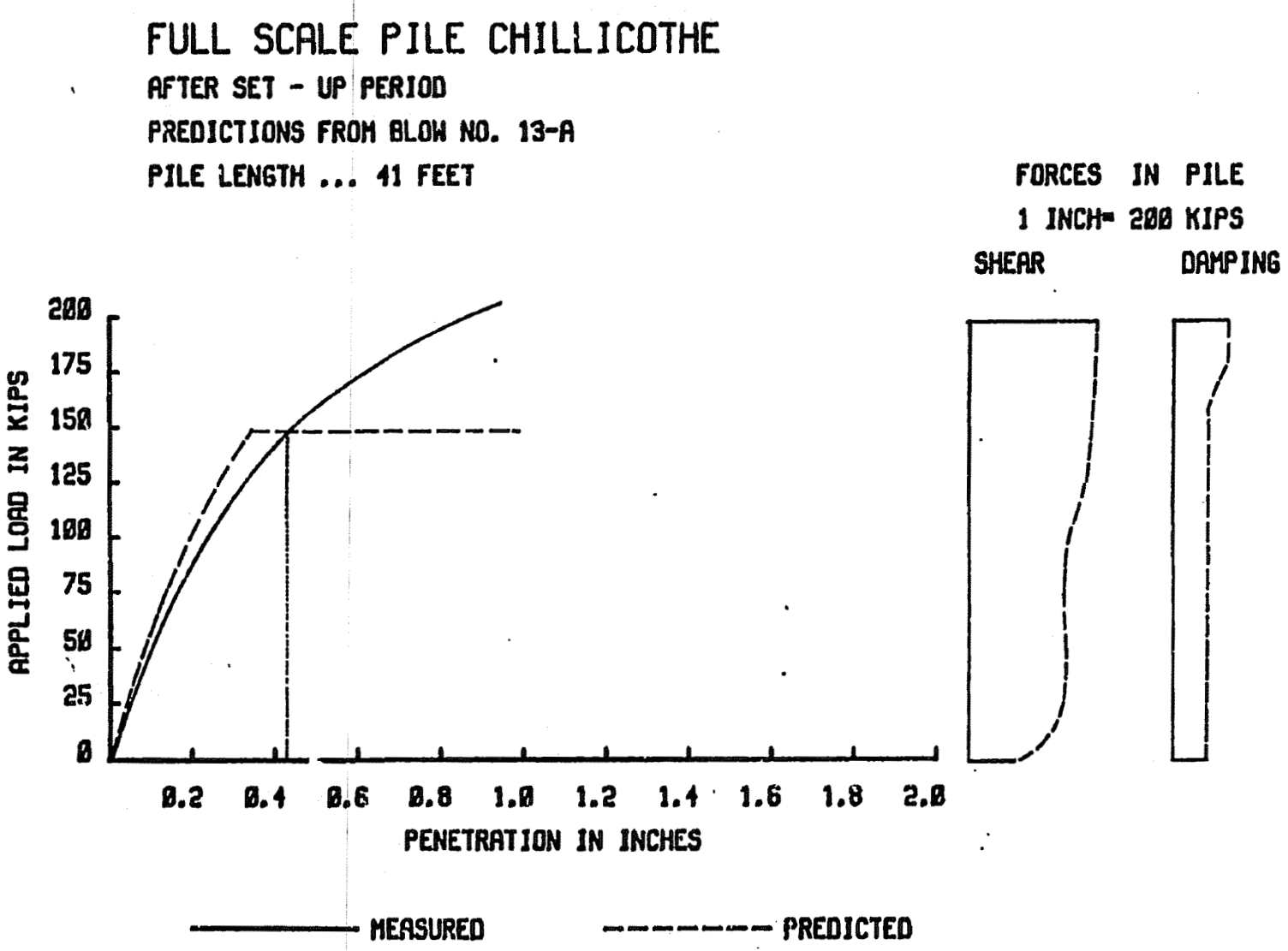

FIGURE 3.38: COMPARISON OF PREDICTED STATIC RESULTS WITH FIELD TEST AND FORCES IN PILE

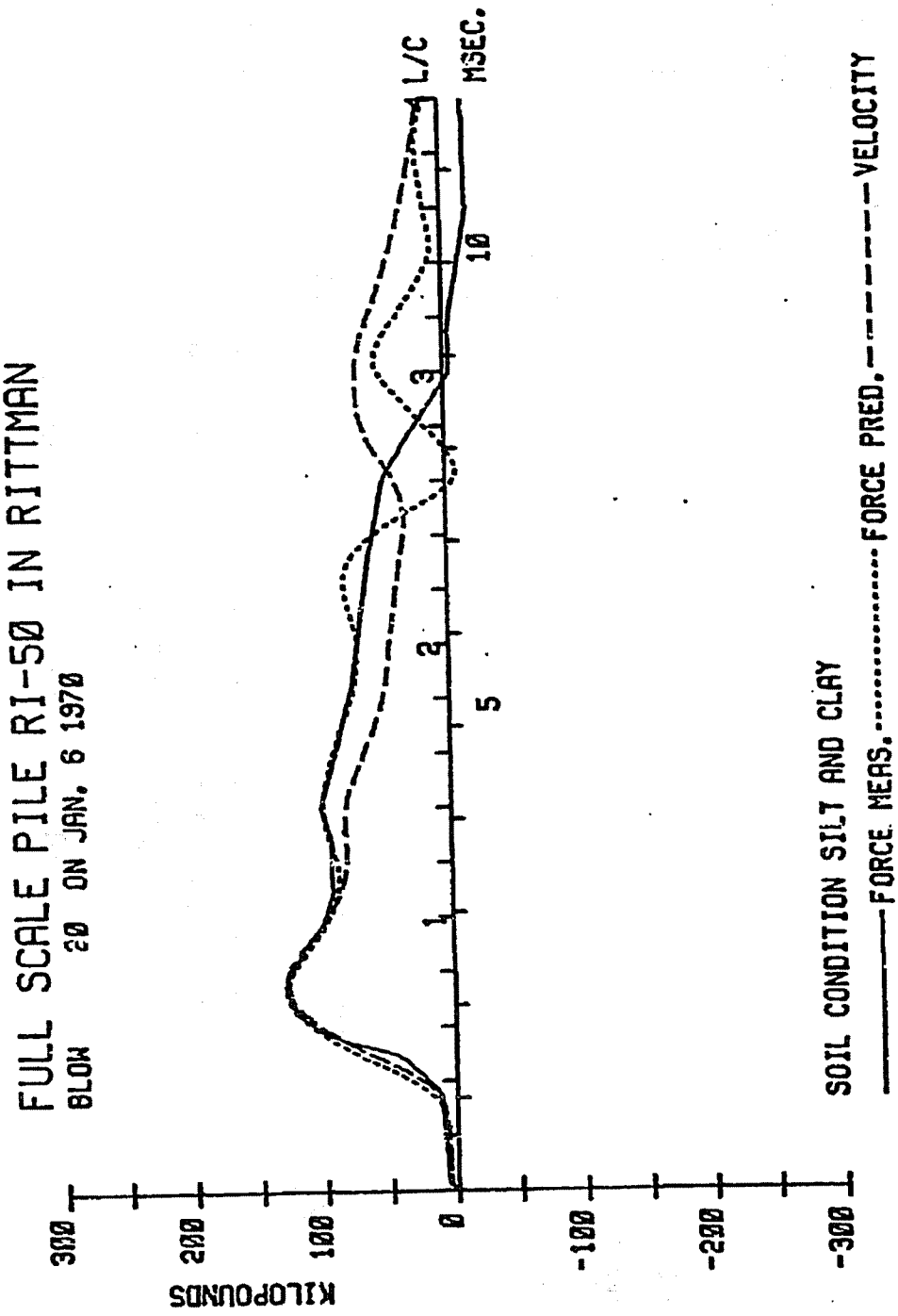

FIGURE 3.39: COMPARISON OF PREDICTED WITH MEASURED PILE TOP FORCE FOR DATA SET NO. 21

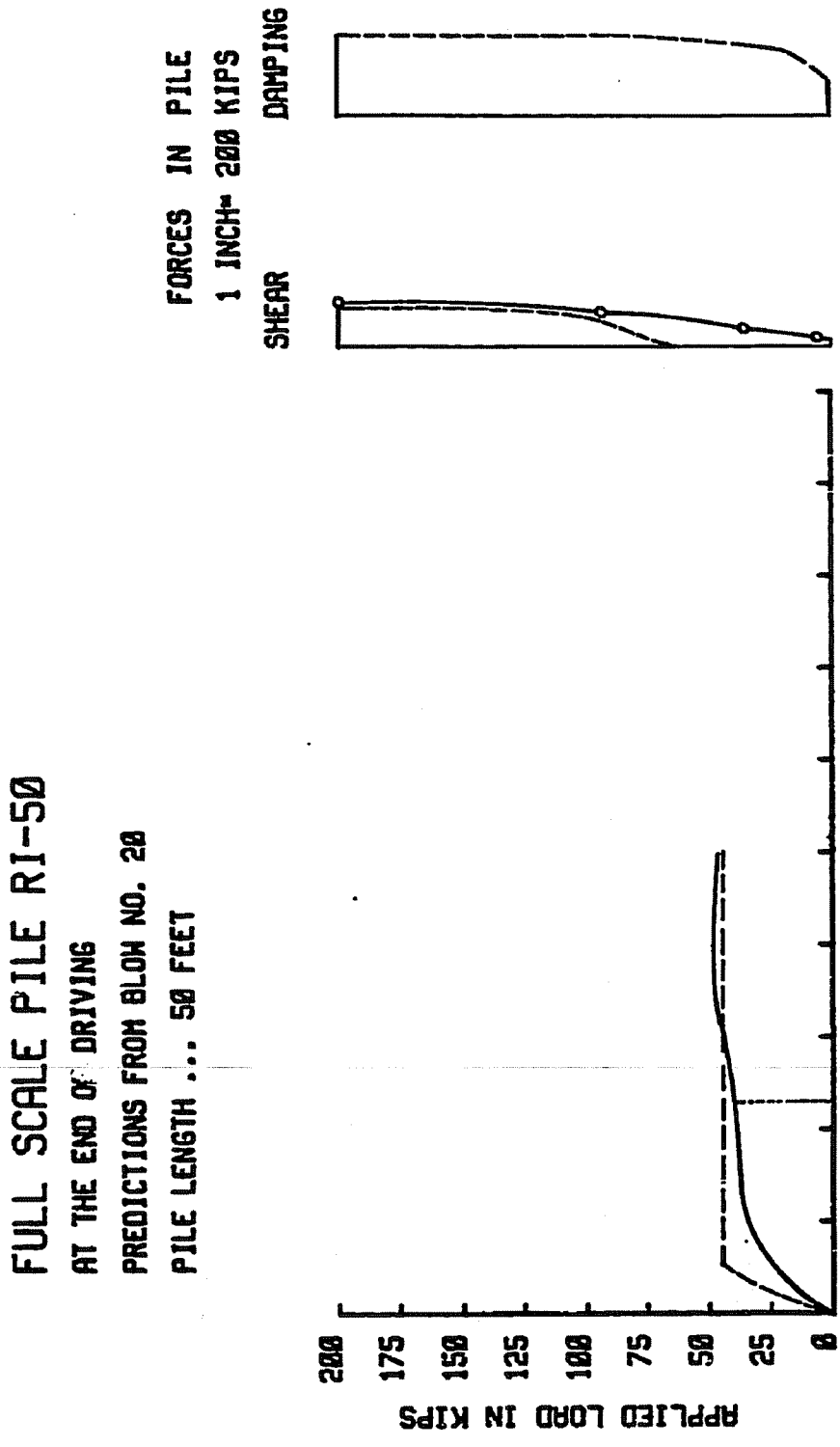

FIGURE 3.40: COMPARISON OF PREDICTED STATIC RESULTS WITH FIELD LOAD TEST AND FORCES IN PILE

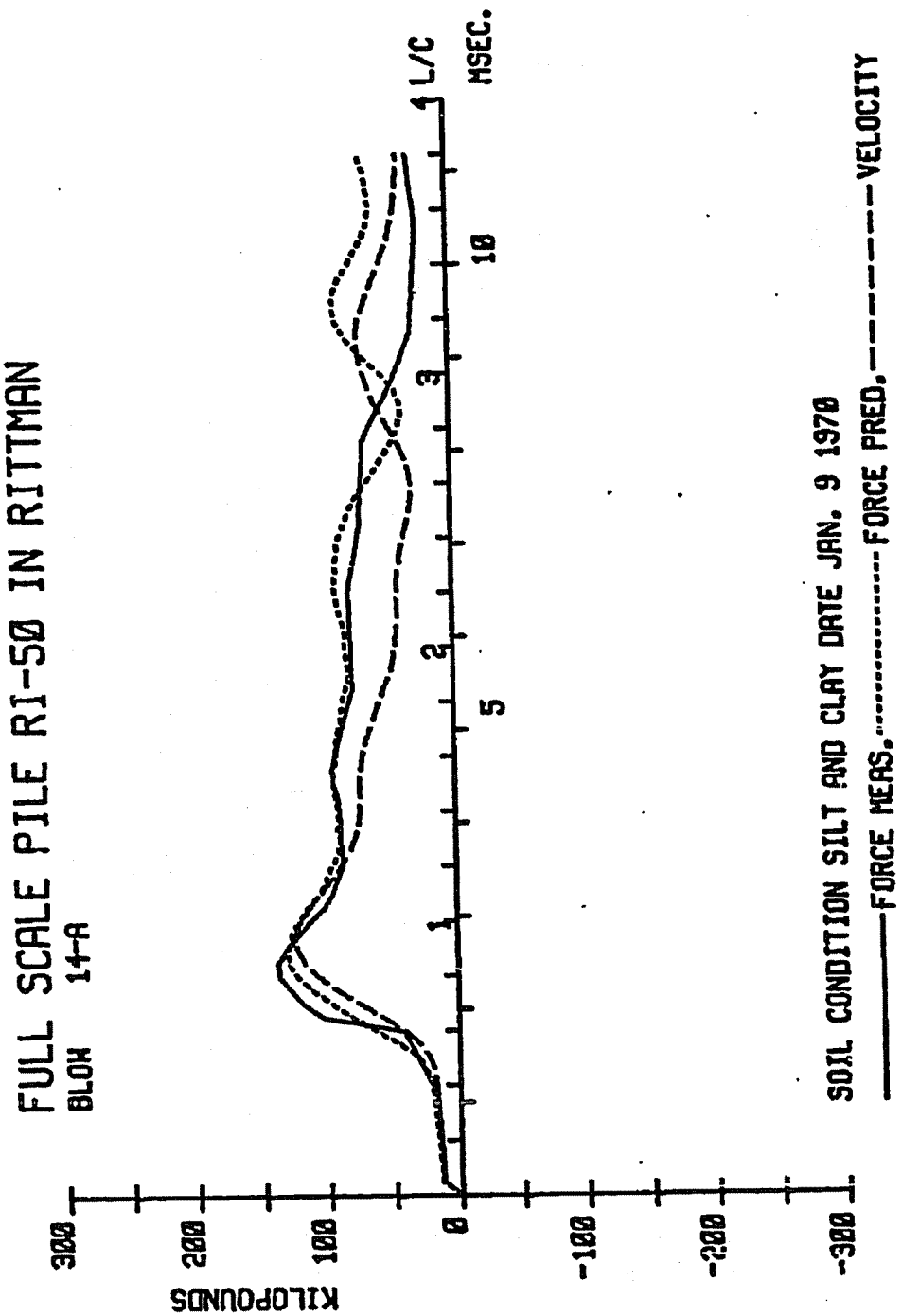

FIGURE 3.41: COMPARISON OF PREDICTED WITH MEASURED PILE TOP FORCE FOR DATA SET NO. 22

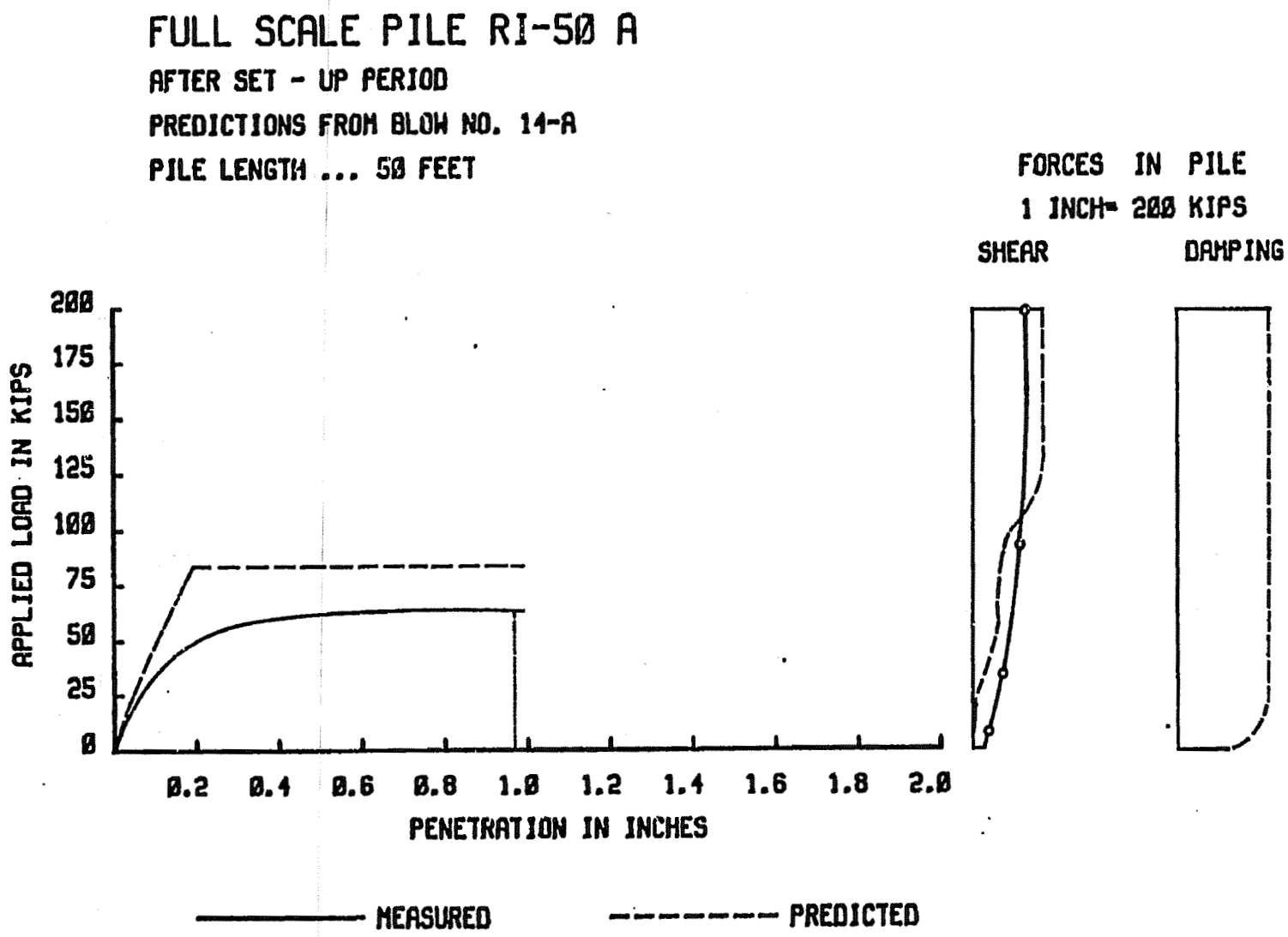

FIGURE 3.42: COMPARISON OF PREDICTED STATIC RESULTS WITH FIELD LOAD TEST AND FORCES IN PILE

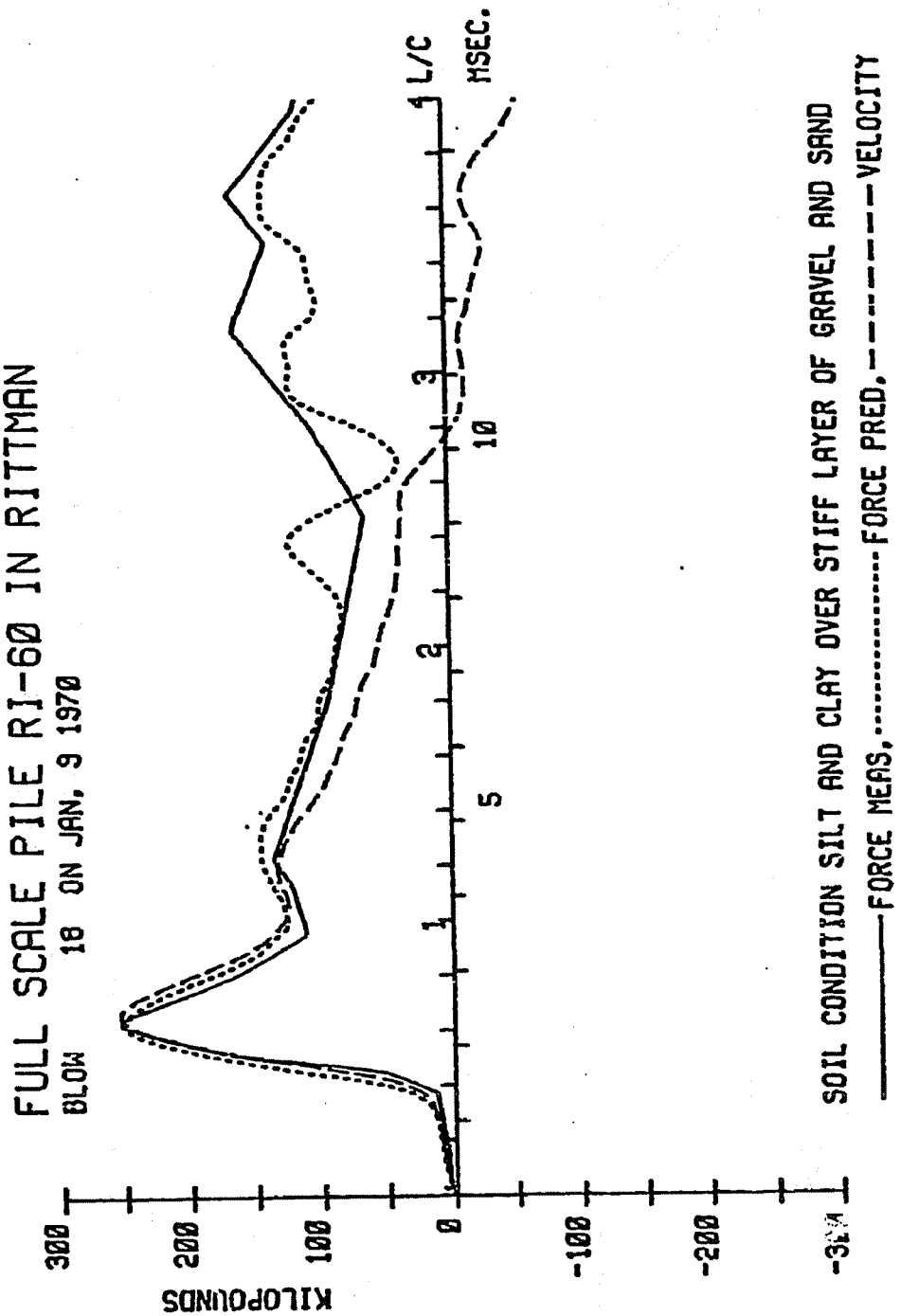

FIGURE 3.43: COMPARISON OF PREDICTED WITH MEASURED PILE TOP FORCE FOR DATA SET NO. 23

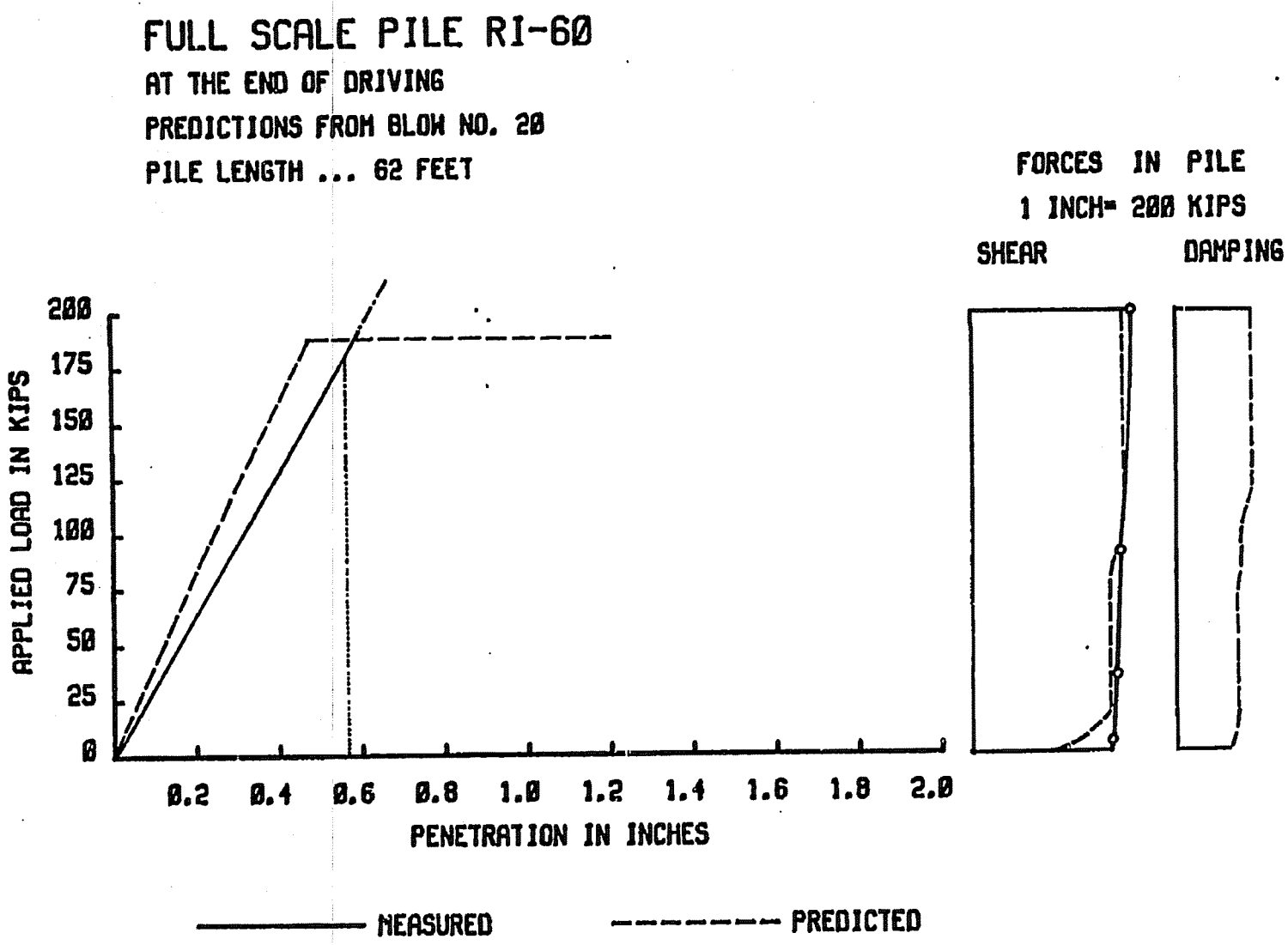

FIGURE 3.44: COMPARISON OF PREDICTED STATIC RESULTS WITH FIELD LOAD TEST AND FORCES IN PILE

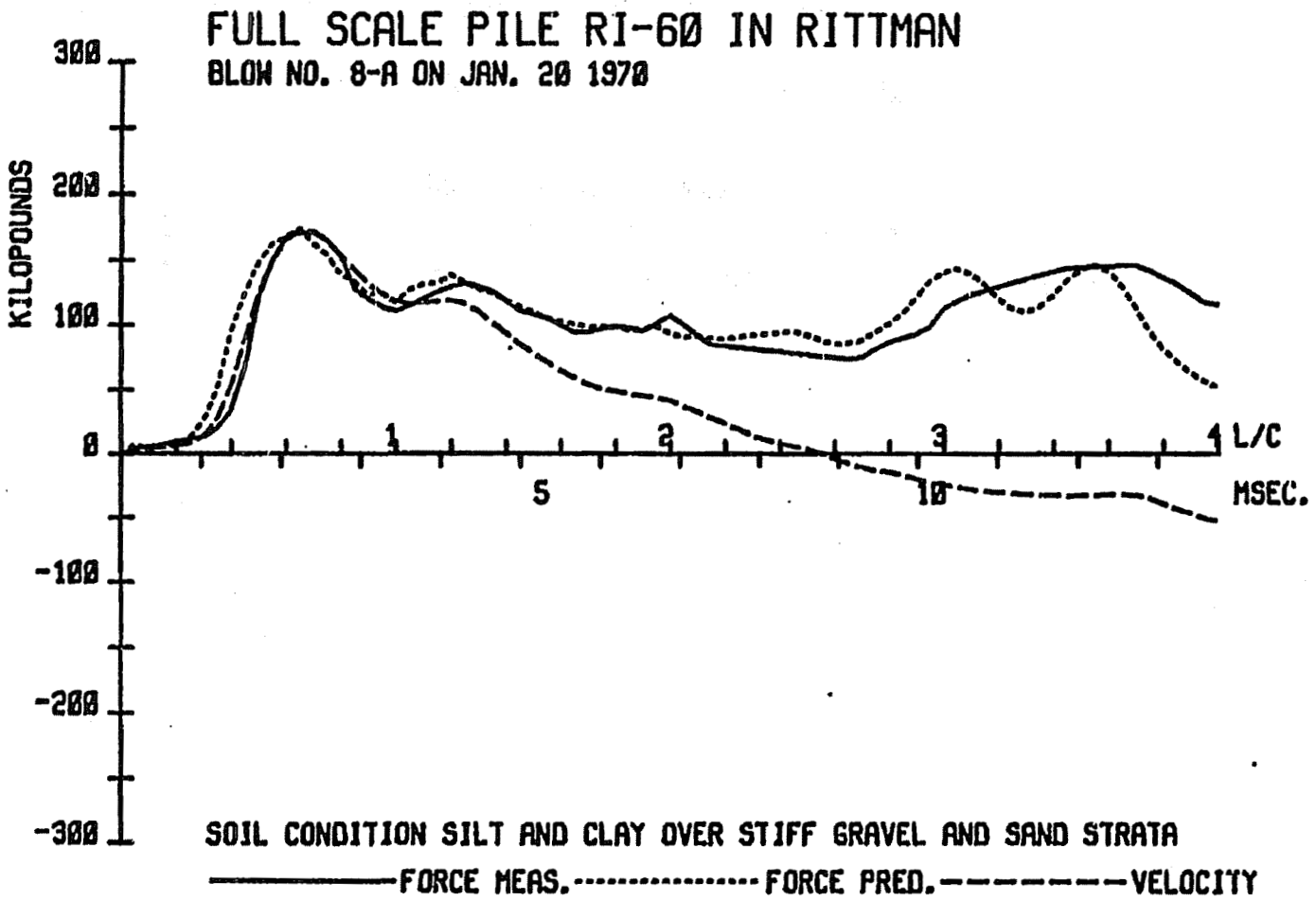

FIGURE 3.45: COMPARISON OF PREDICTED WITH MEASURED PILE TOP FORCE FOR DATA SET NO. 24

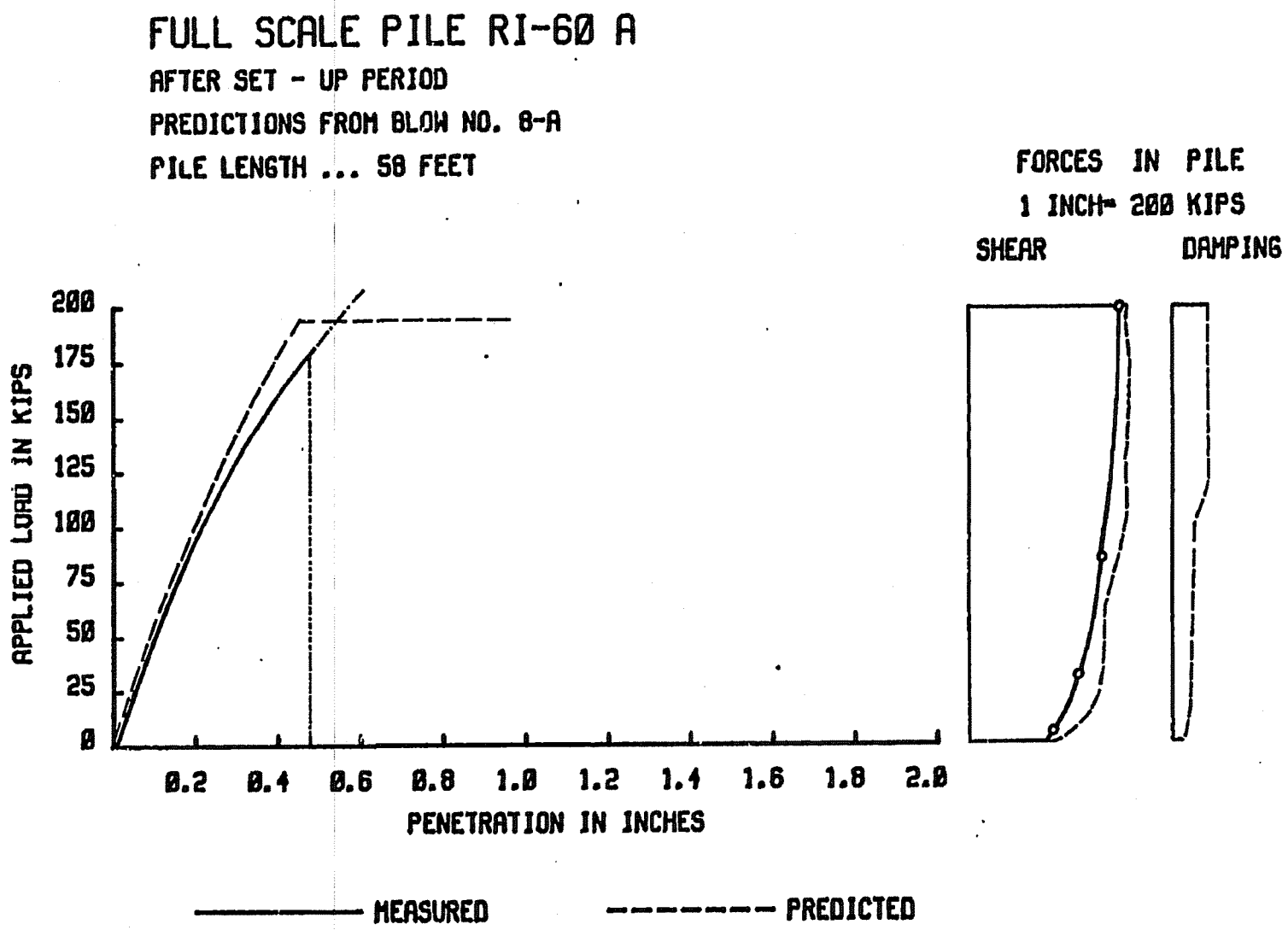

FIGURE 3.46: COMPARISON OF PREDICTED STATIC RESULTS WITH FIELD LOAD TEST AND FORCES IN PILE

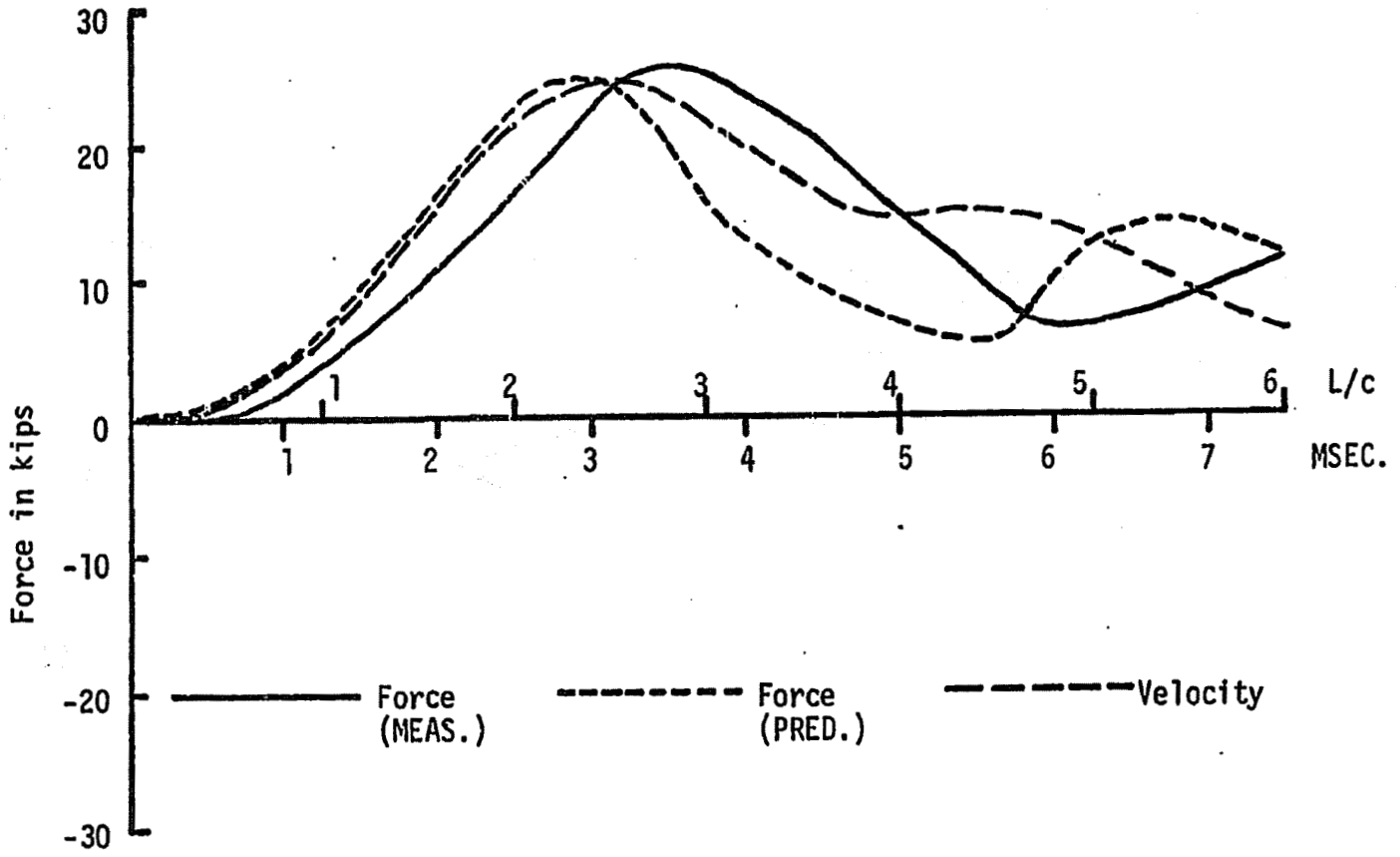

FIGURE 3.47: MEASURED FORCE AND VELOCITY AND PREDICTED PILE TOP FORCE FOR REDUCED SCALE Pile 3-R-20 (Data Set No. 12)

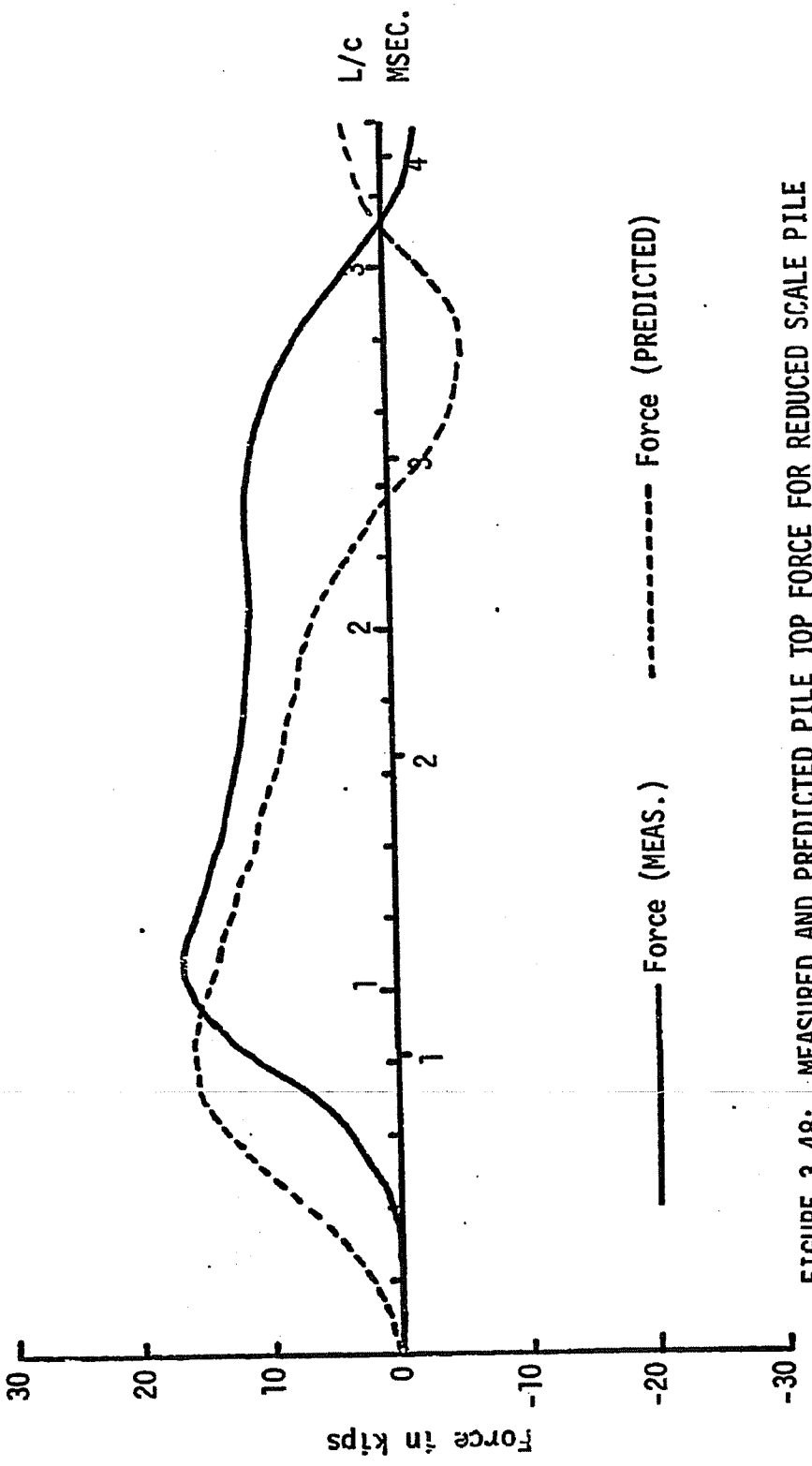

FIGURE 3.48: MEASURED AND PREDICTED PILE TOP FORCE FOR REDUCED SCALE PILE 6-T-15 (data Set No. 22)

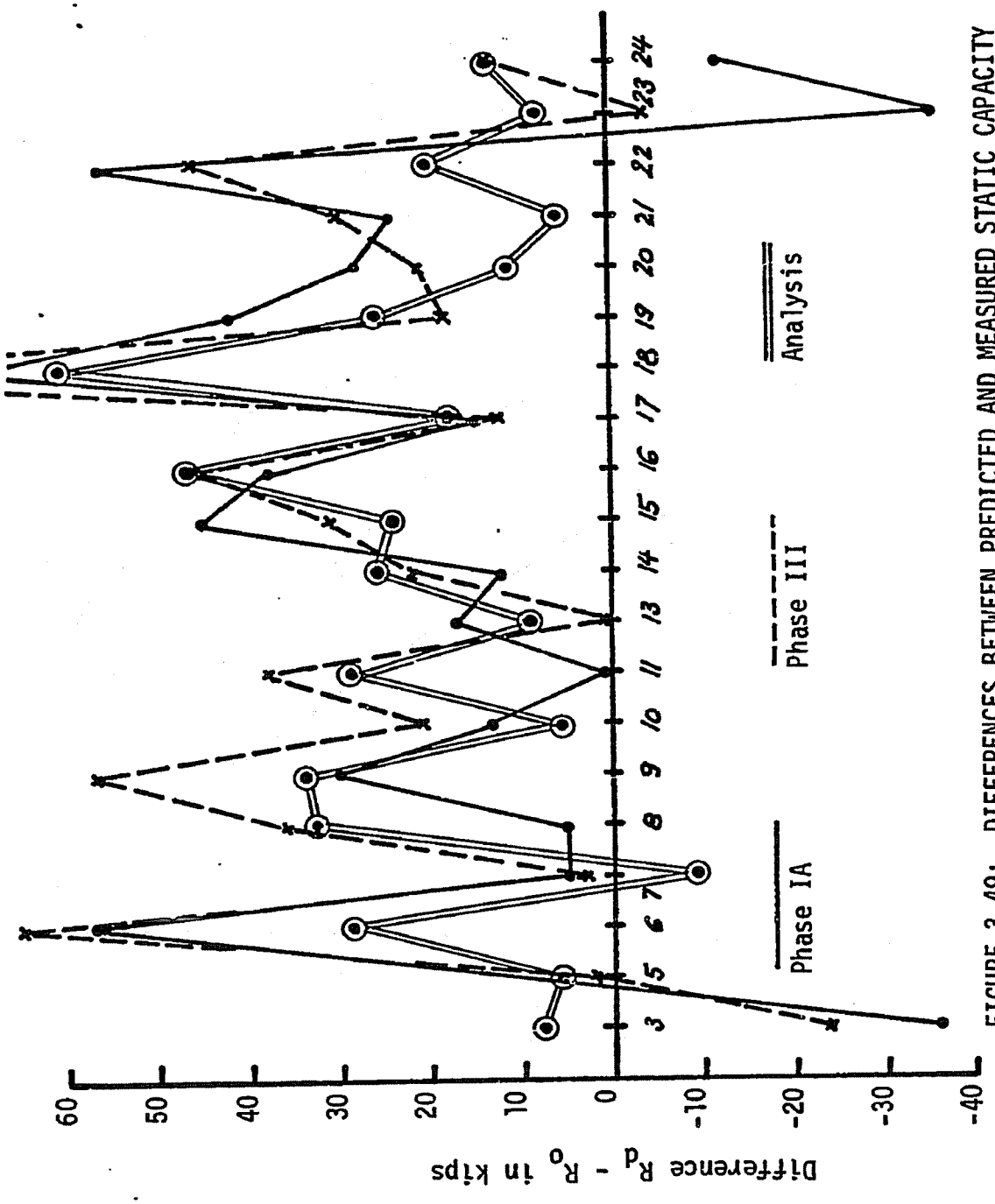

FIGURE 3.49: DIFFERENCES BETWEEN PREDICTED AND MEASURED STATIC CAPACITY

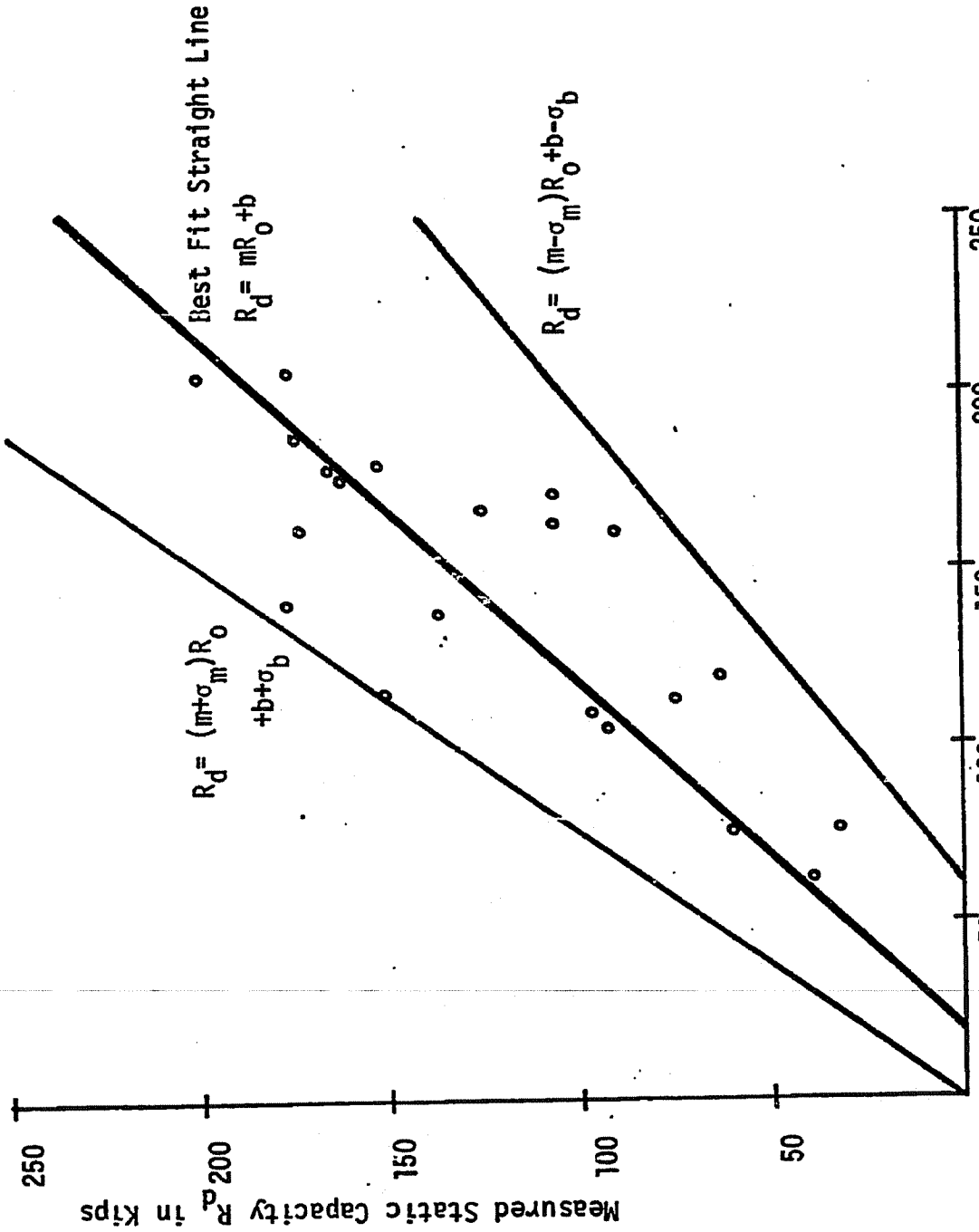

Figure 3.50 RESULTS FROM STATISTICAL ANALYSIS FOR PHASE IIA PREDICTION METHOD

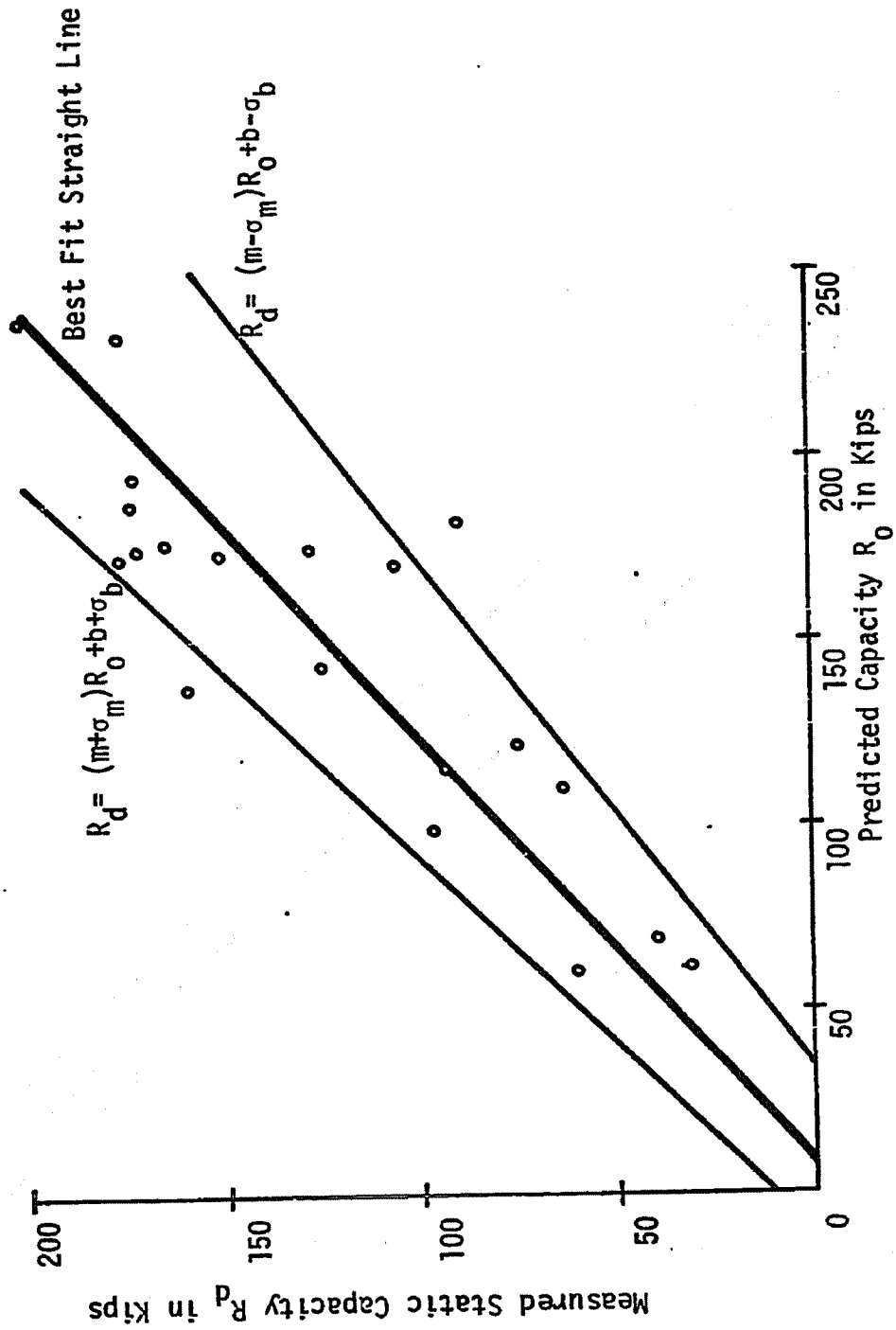

FIGURE 3.51: RESULTS FROM STATISTICAL ANALYSIS FOR PHASE III PREDICTION METHOD

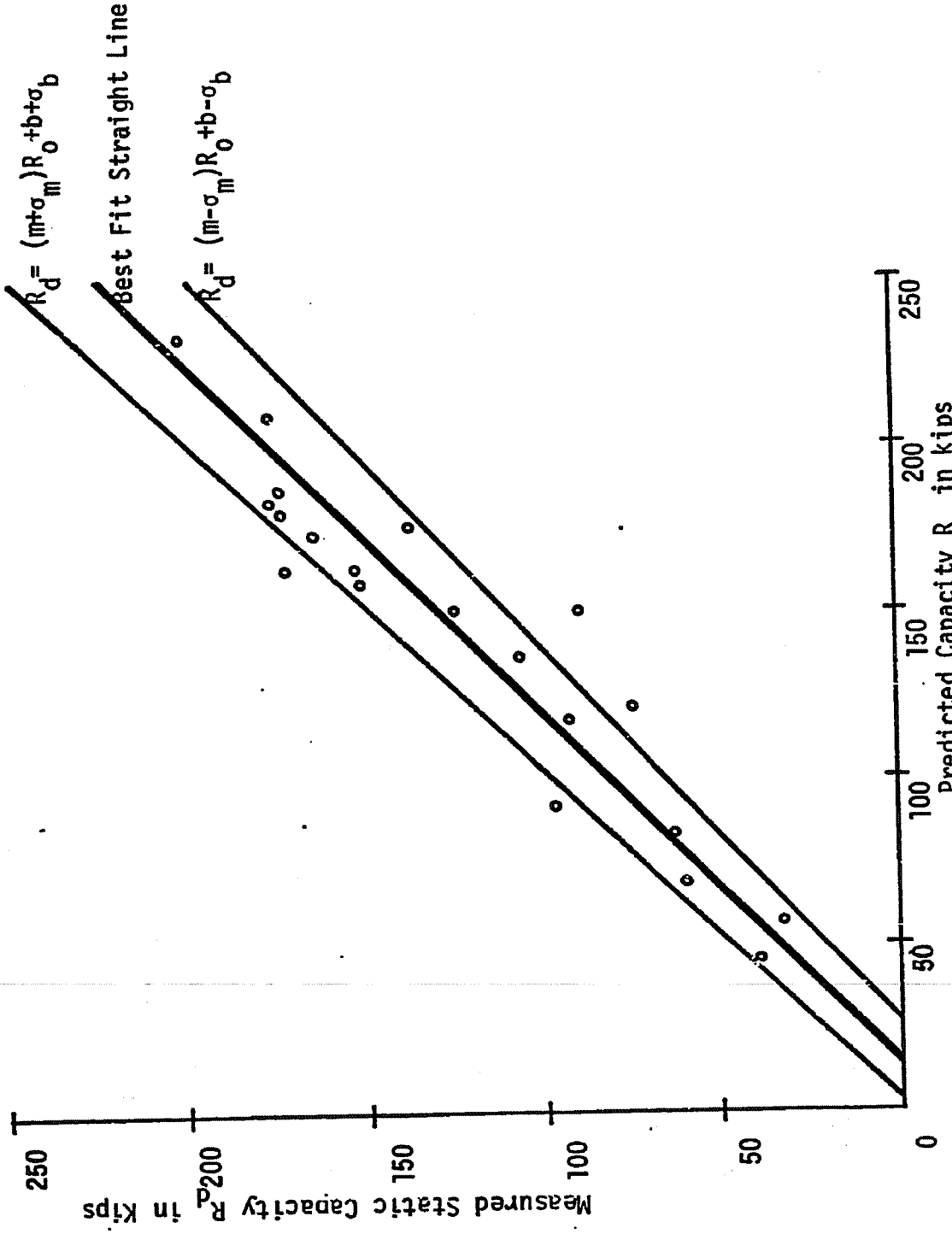

FIGURE 3.52: RESULTS FROM STATISTICAL ANALYSIS FOR PREDICTIONS FROM WAVE ANALYSIS

Ri-50 Blow No. 8-4

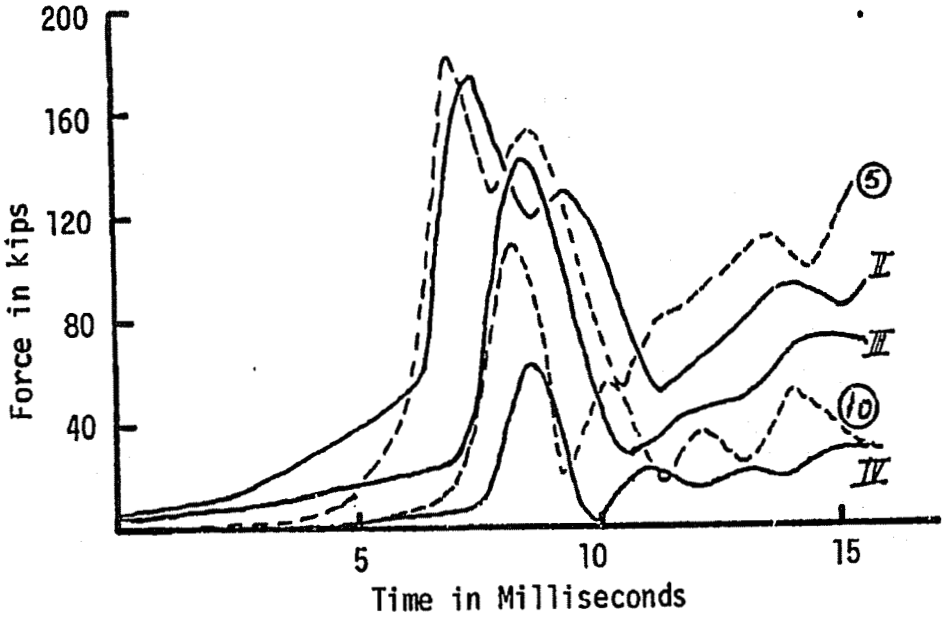

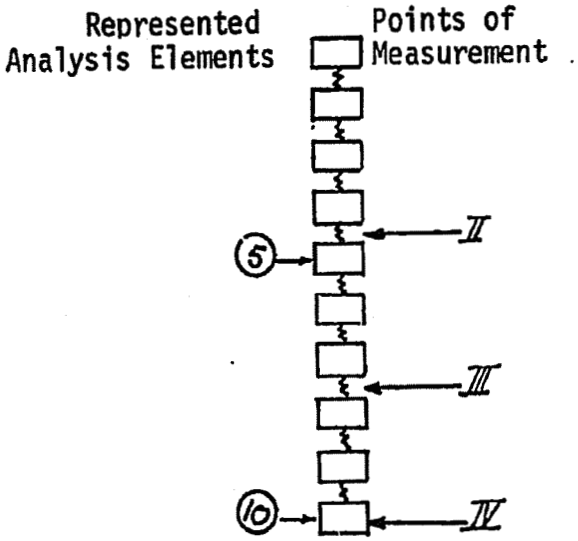

FIGURE 3.53: COMPARISON OF PREDICTED WITH MEASURED PILE FORCES DURING DRIVING

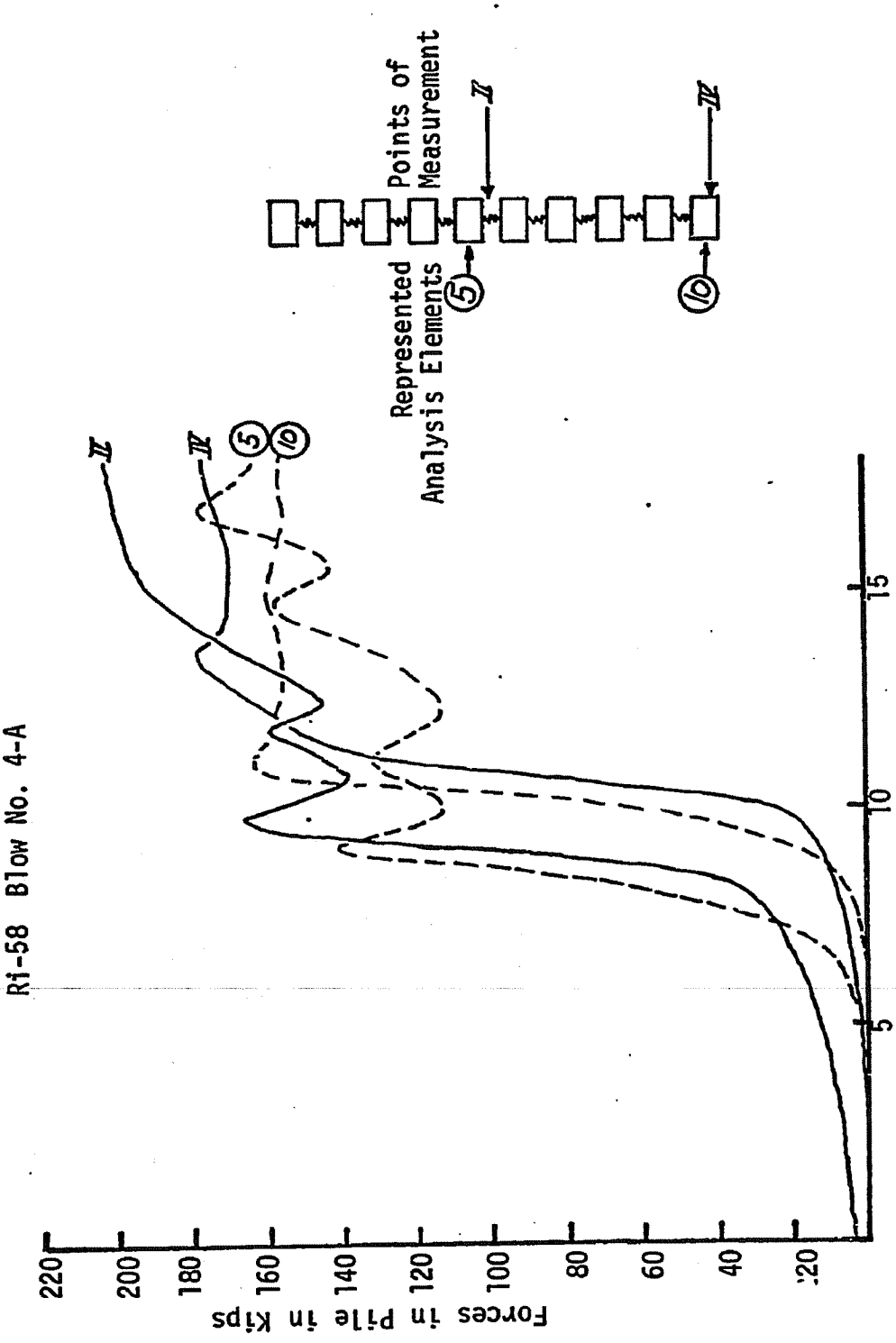

FIGURE 3.54: COMPARISON OF MEASURED WITH COMPUTED FORCES IN PILE DURING DRIVING

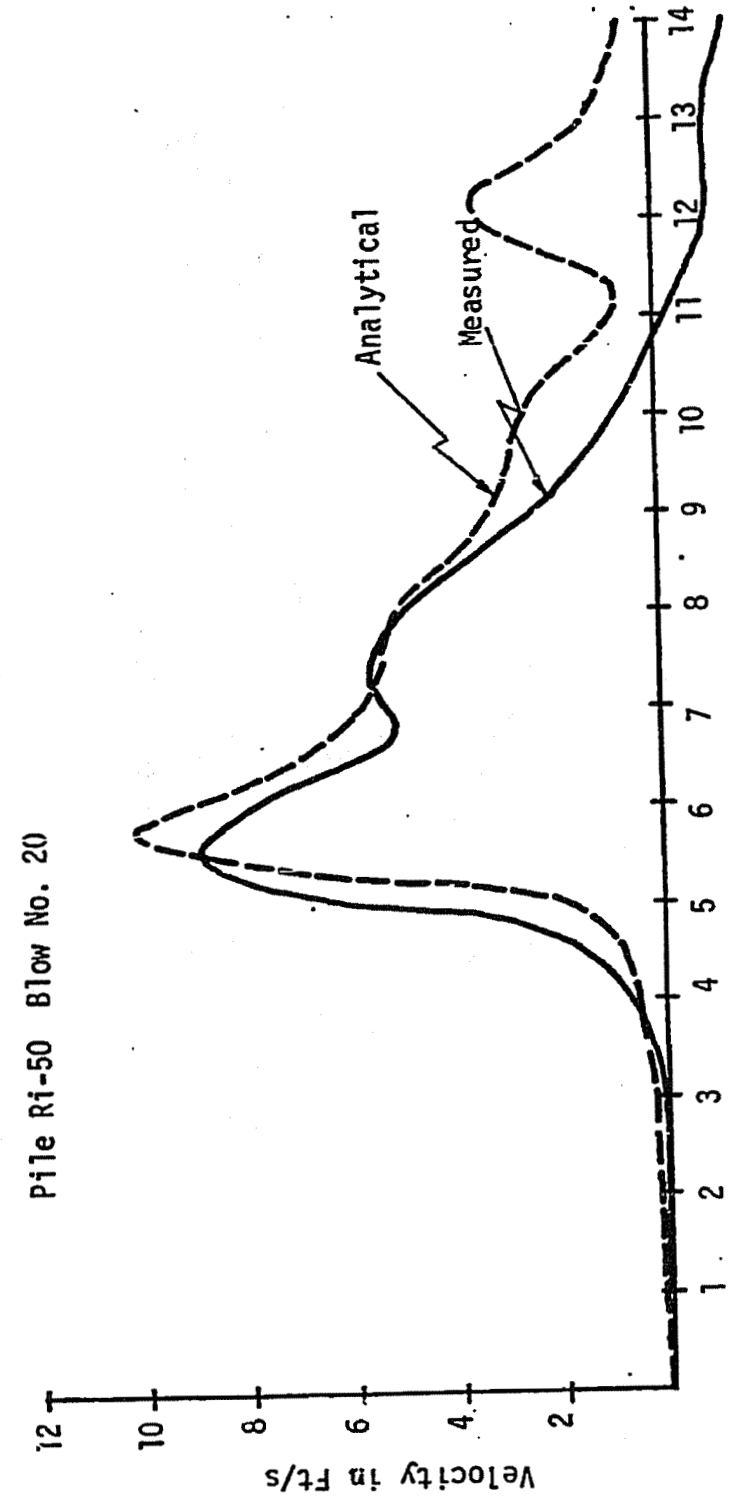

FIGURE 3.55: VELOCITY AT PILE TIP
COMPARISON BETWEEN MEASUREMENT AND ANALYSIS

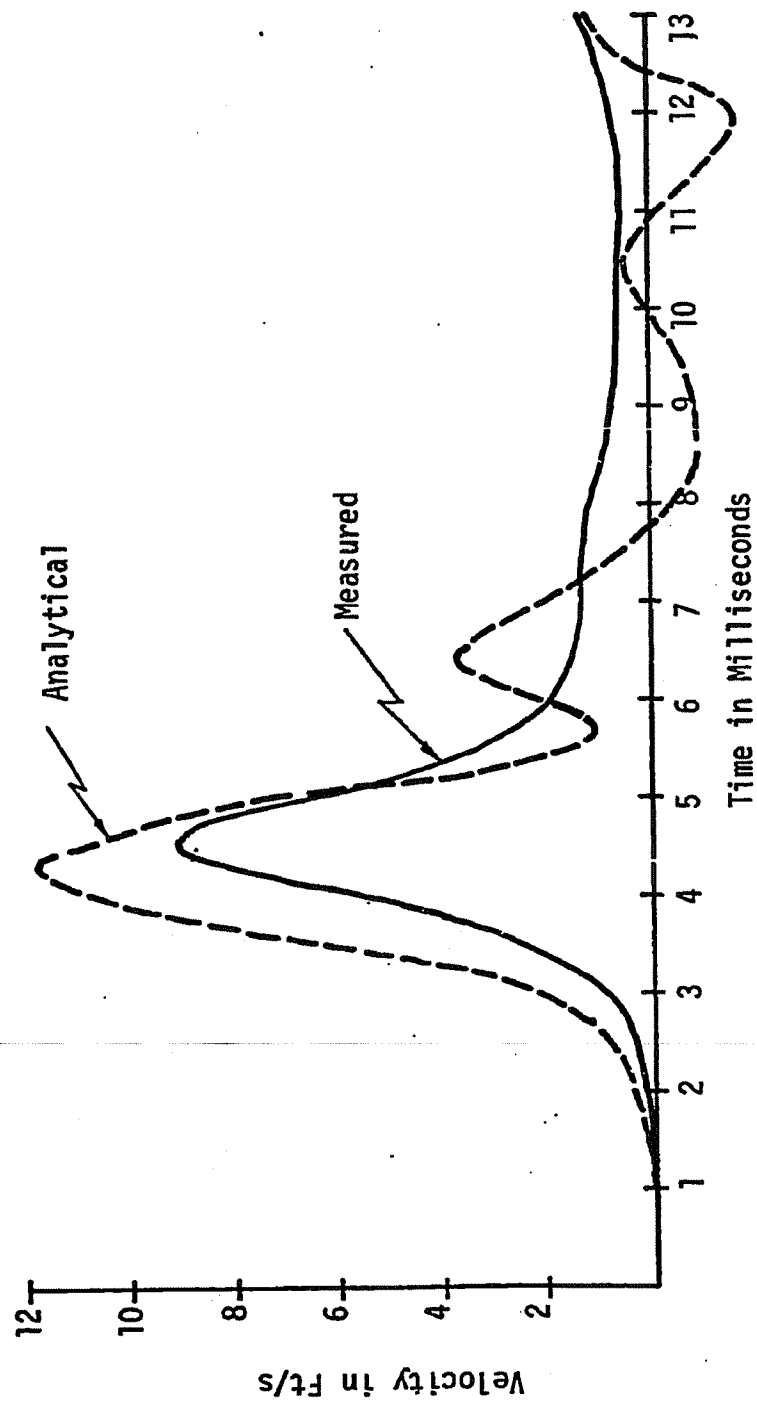

FIGURE 3.56: VELOCITY AT PILE TIP
COMPARISON BETWEEN MEASUREMENT AND ANALYSIS

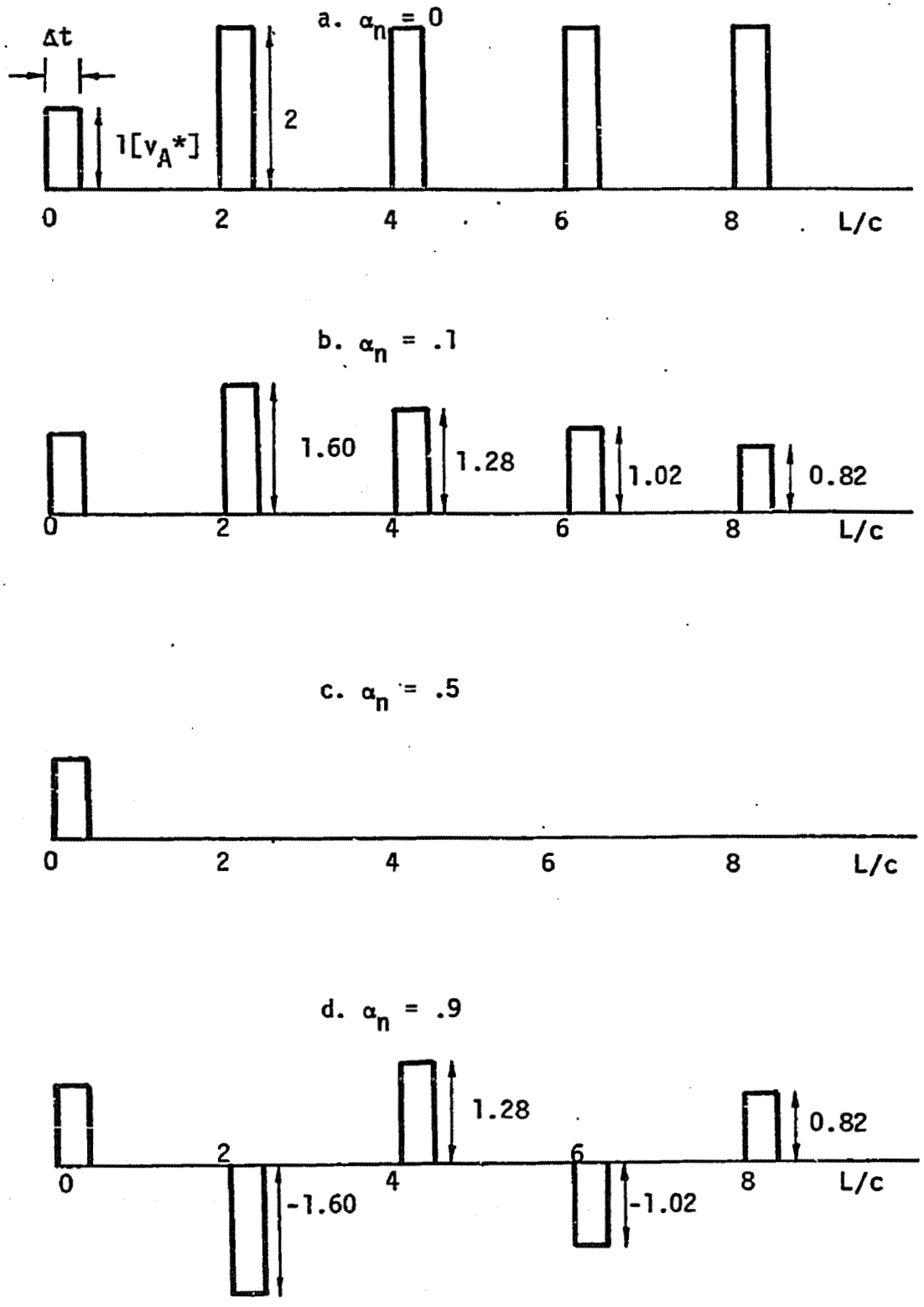

FIGURE 4.1: PILE TOP VELOCITY DUE TO A INPUT AT TIME t = 0 AND A DAMPER AT THE PILE BOTTOM

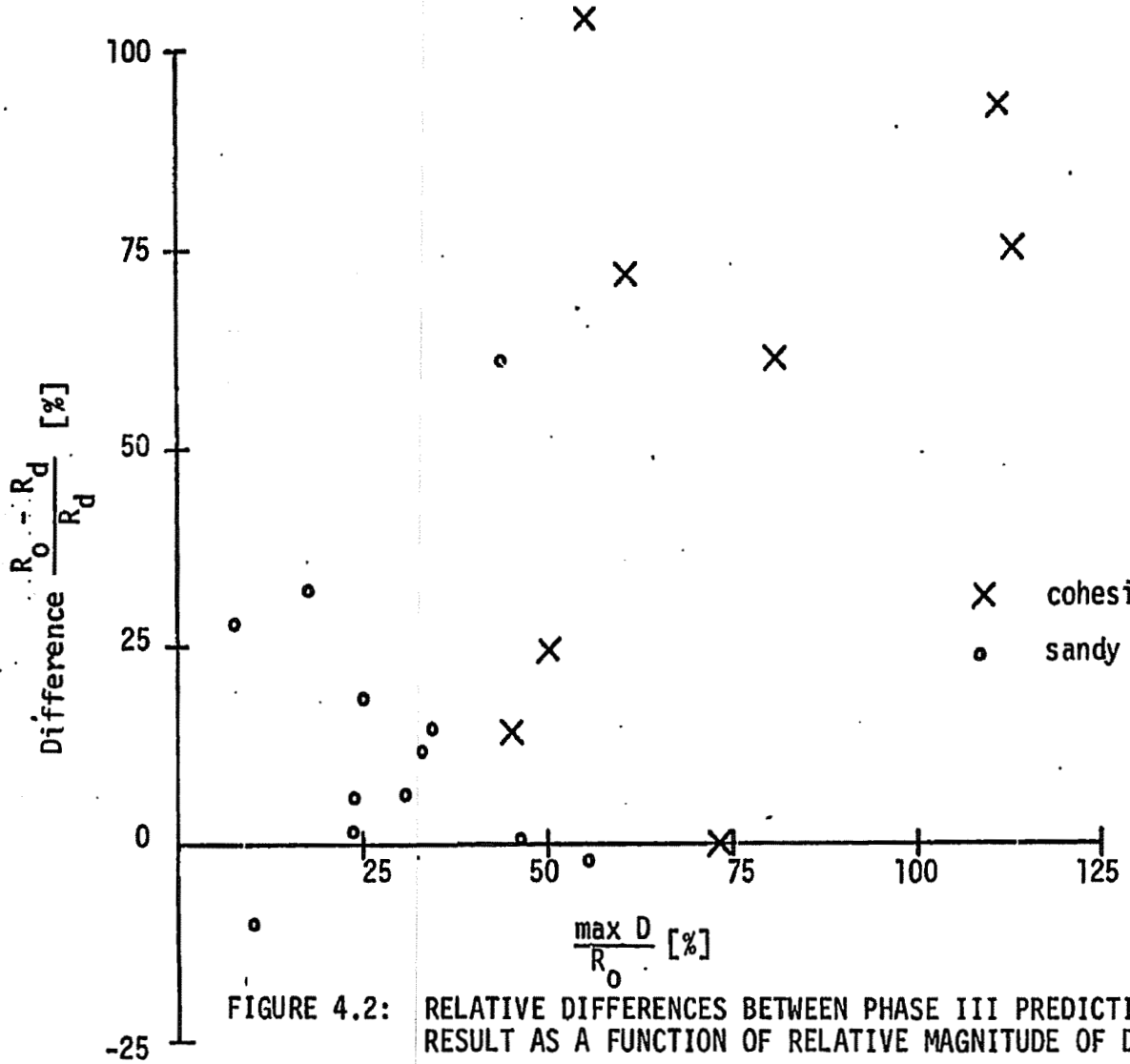

FIGURE 4.2: RELATIVE DIFFERENCES BETWEEN PHASE III PREDICTION AND STATIC LOAD TEST RESULT AS A FUNCTION OF RELATIVE MAGNITUDE OF DAMPING

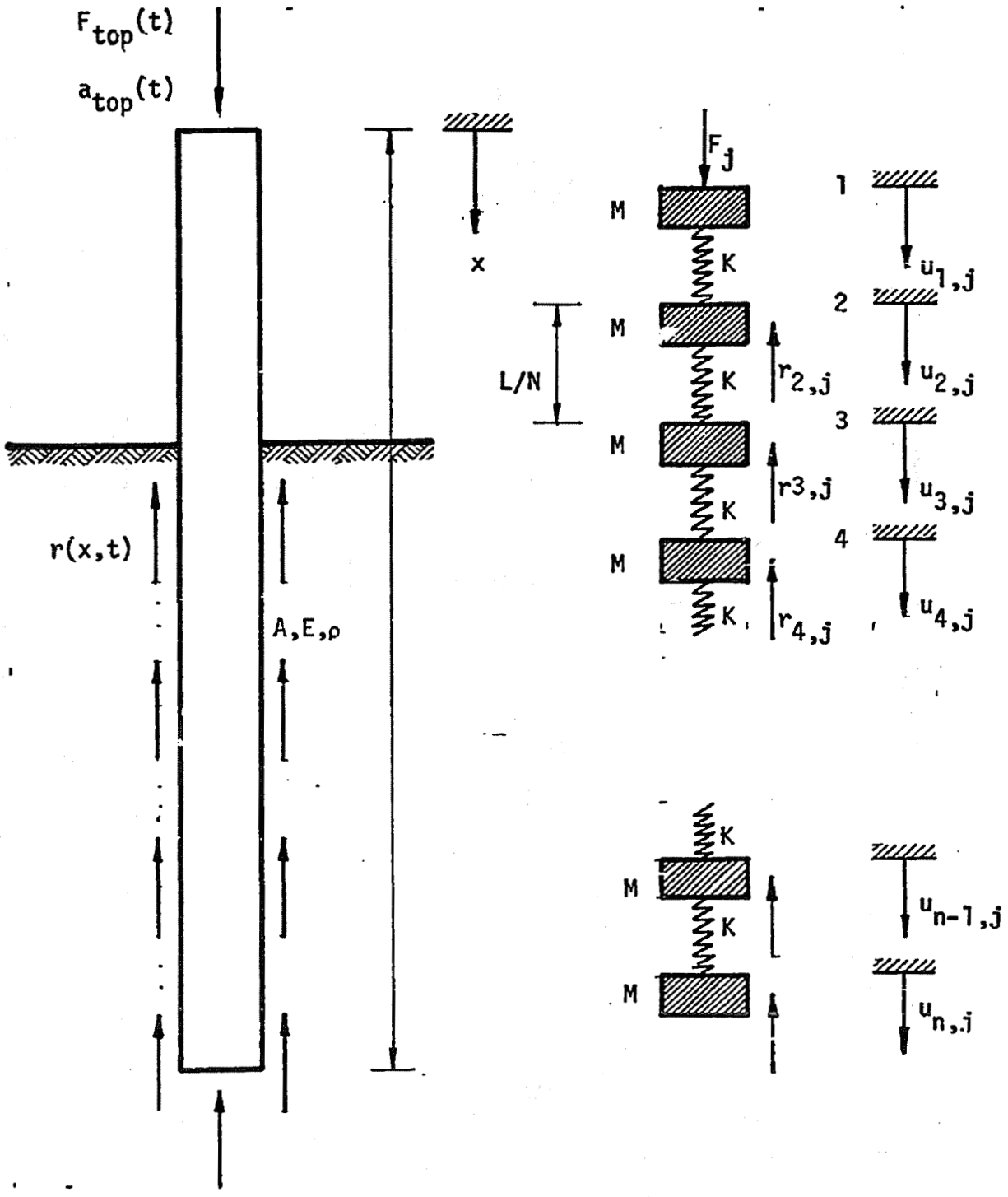

FIGURE A1.1: CONTINUOUS PILE AND SPRING-MASS MODEL

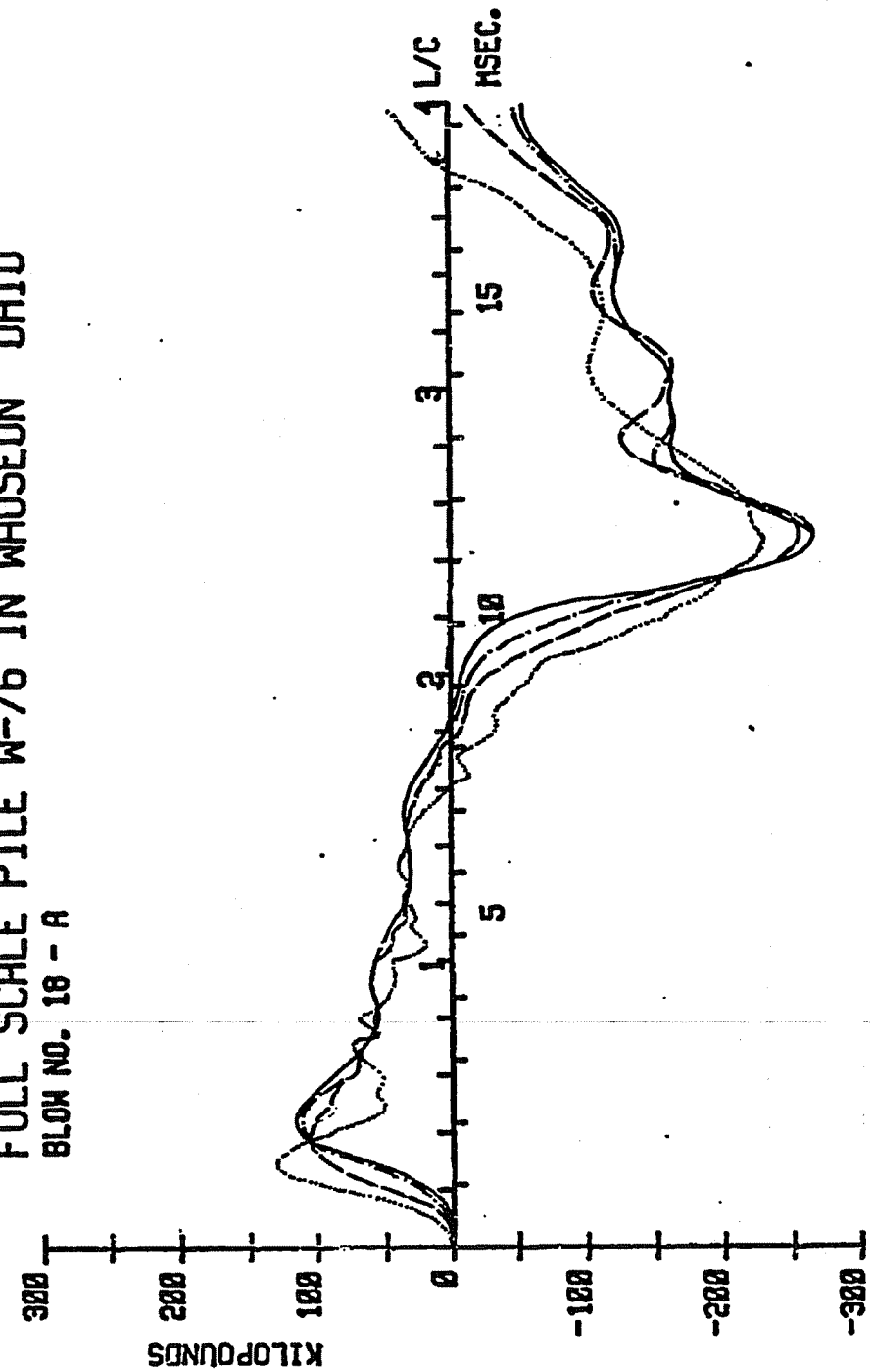

FIGURE A1.2: COMPARISON OF ANALYSIS RESULTS USING DIFFERENT NUMBERS OF ELEMENTS

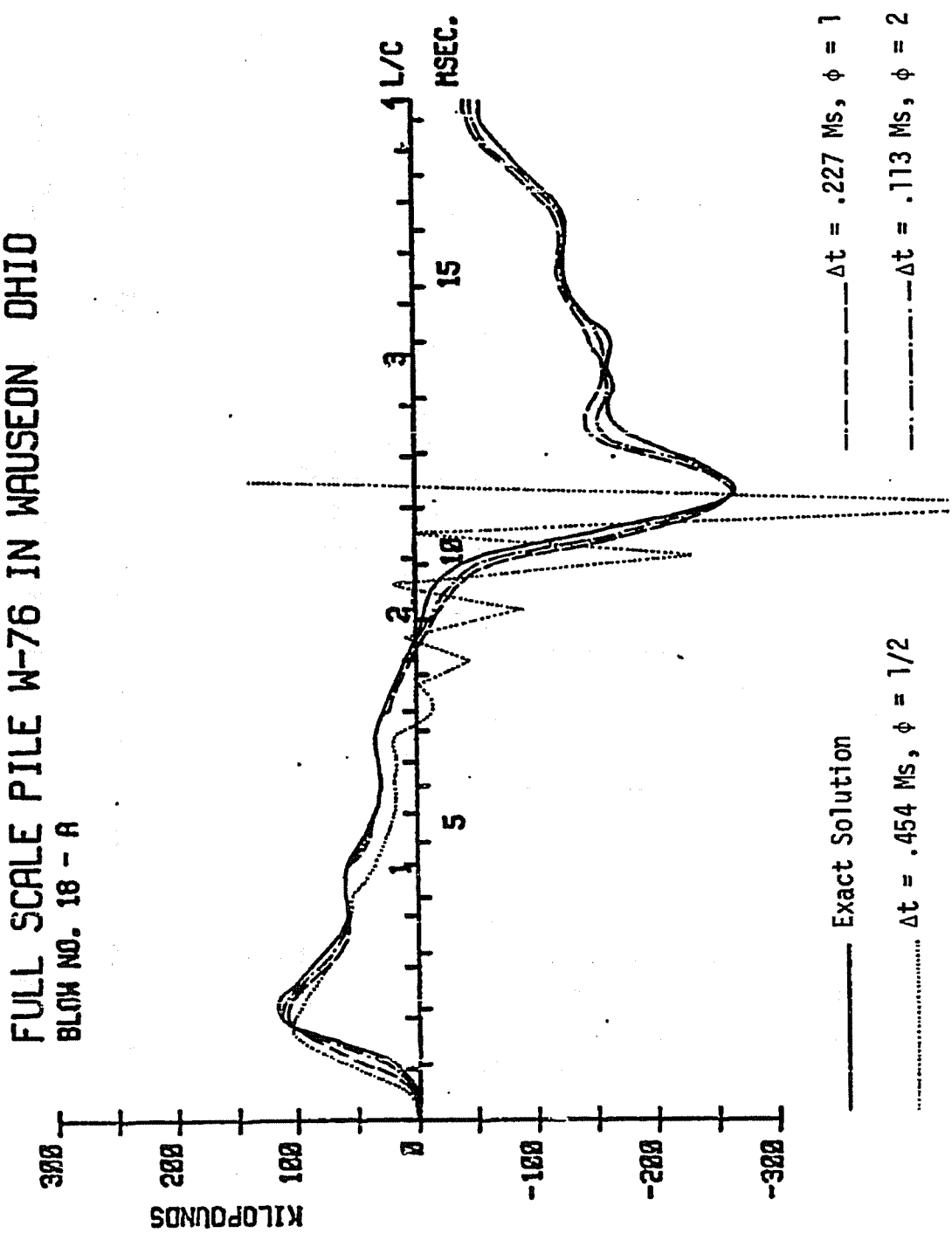

FIGURE A1.3: COMPARISON OF ANALYSIS RESULTS USING DIFFERENT TIME INCREMENTS, N = 20 and ε = .01

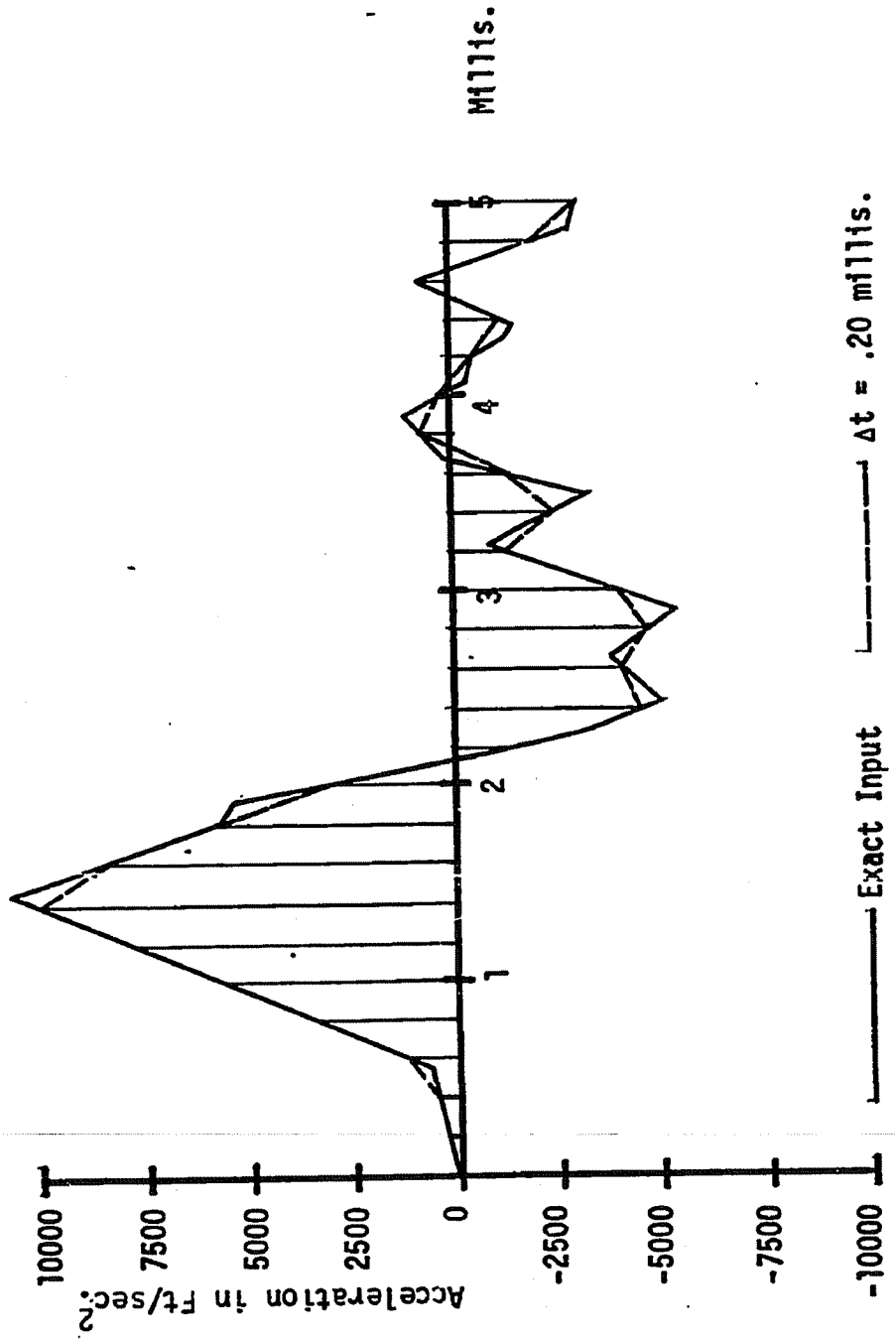

FIGURE A1.4: POSSIBLE DEVIATIONS FROM EXACT INPUT USING FINITE STEP SIZES

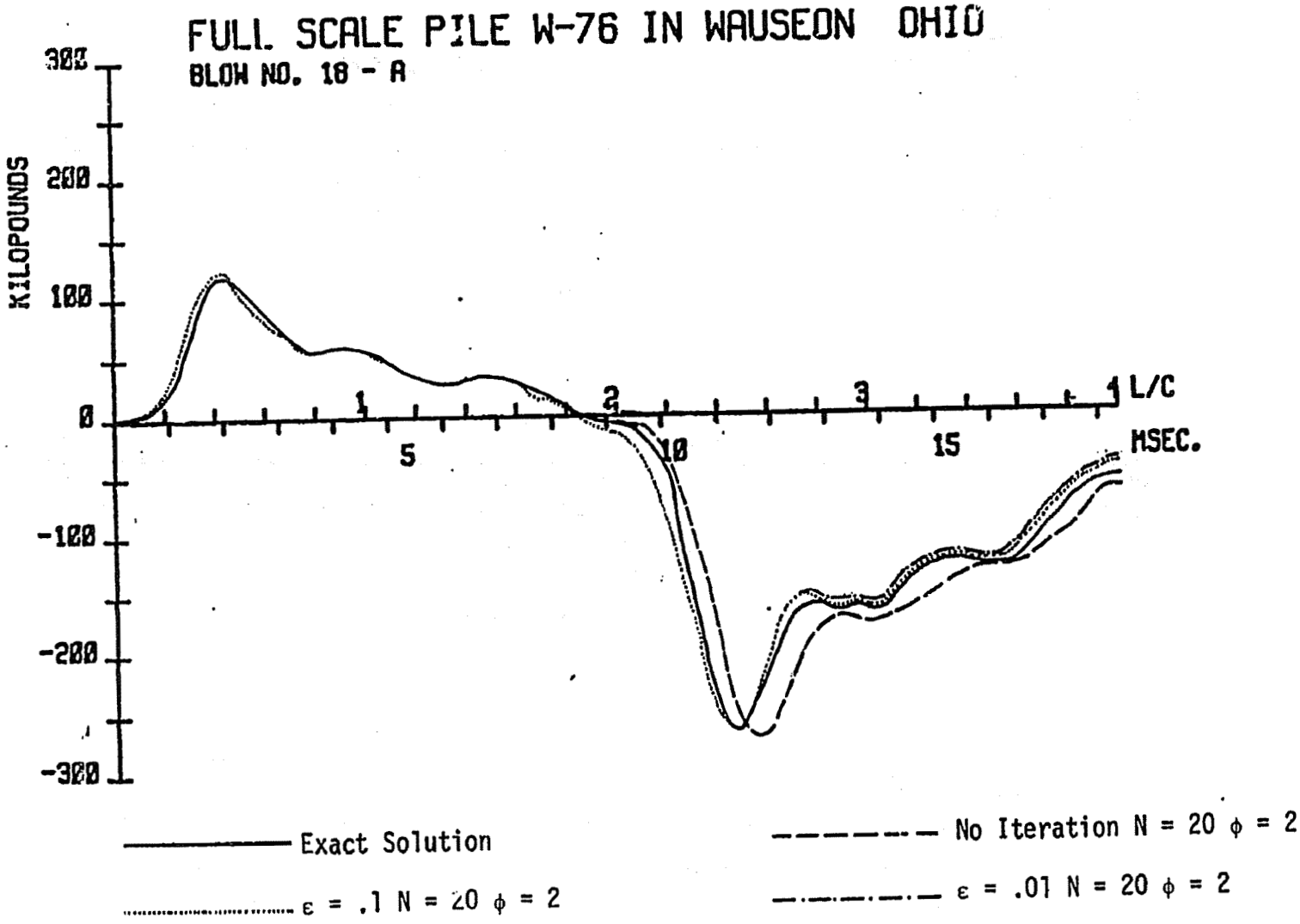

FIGURE A1.5: COMPARISON OF ANALYSIS RESULTS USING DIFFERENT CONVERGENCE CRITERIA

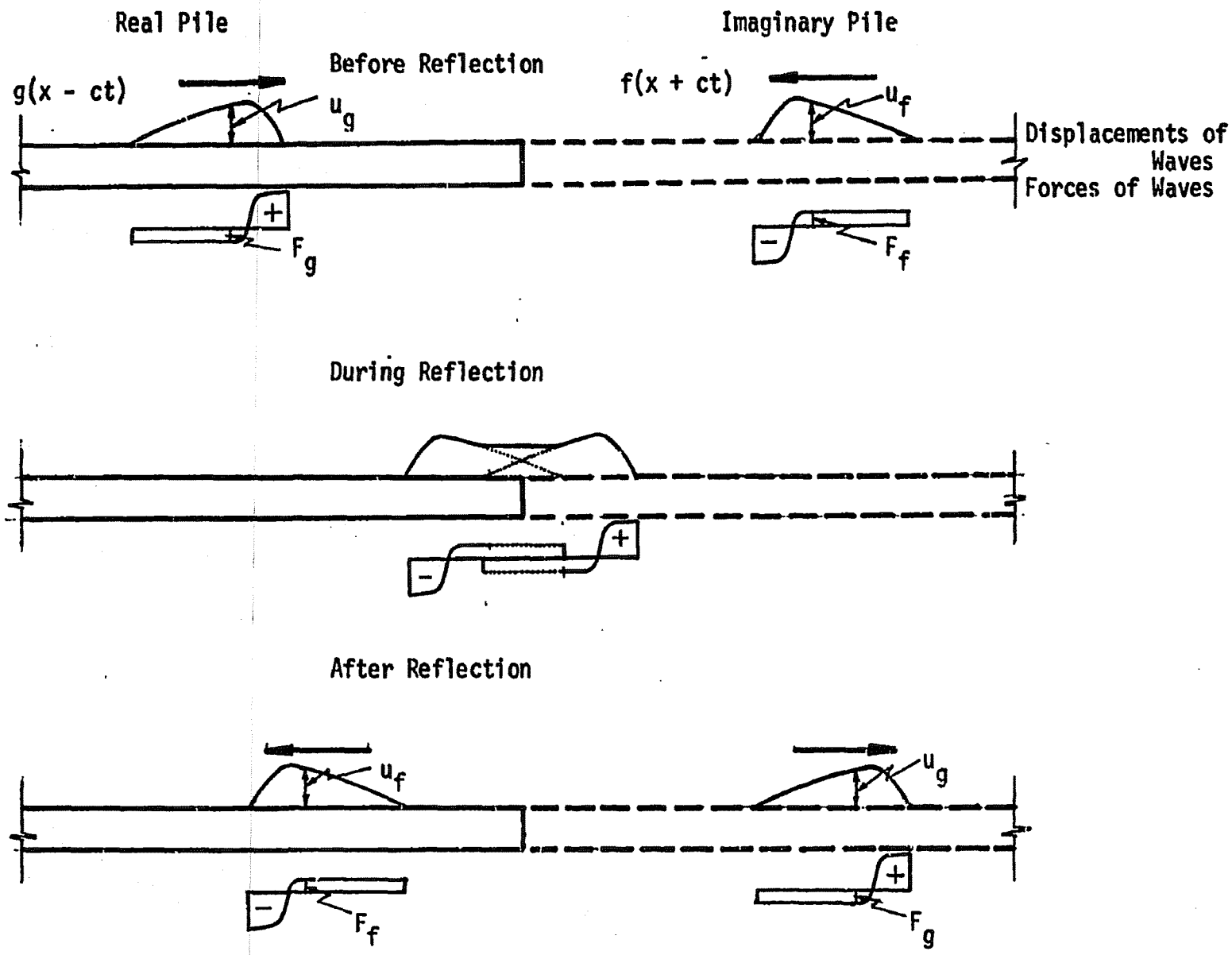

FIGURE A3.1: TREATMENT OF FREE END BOUNDARY CONDITION

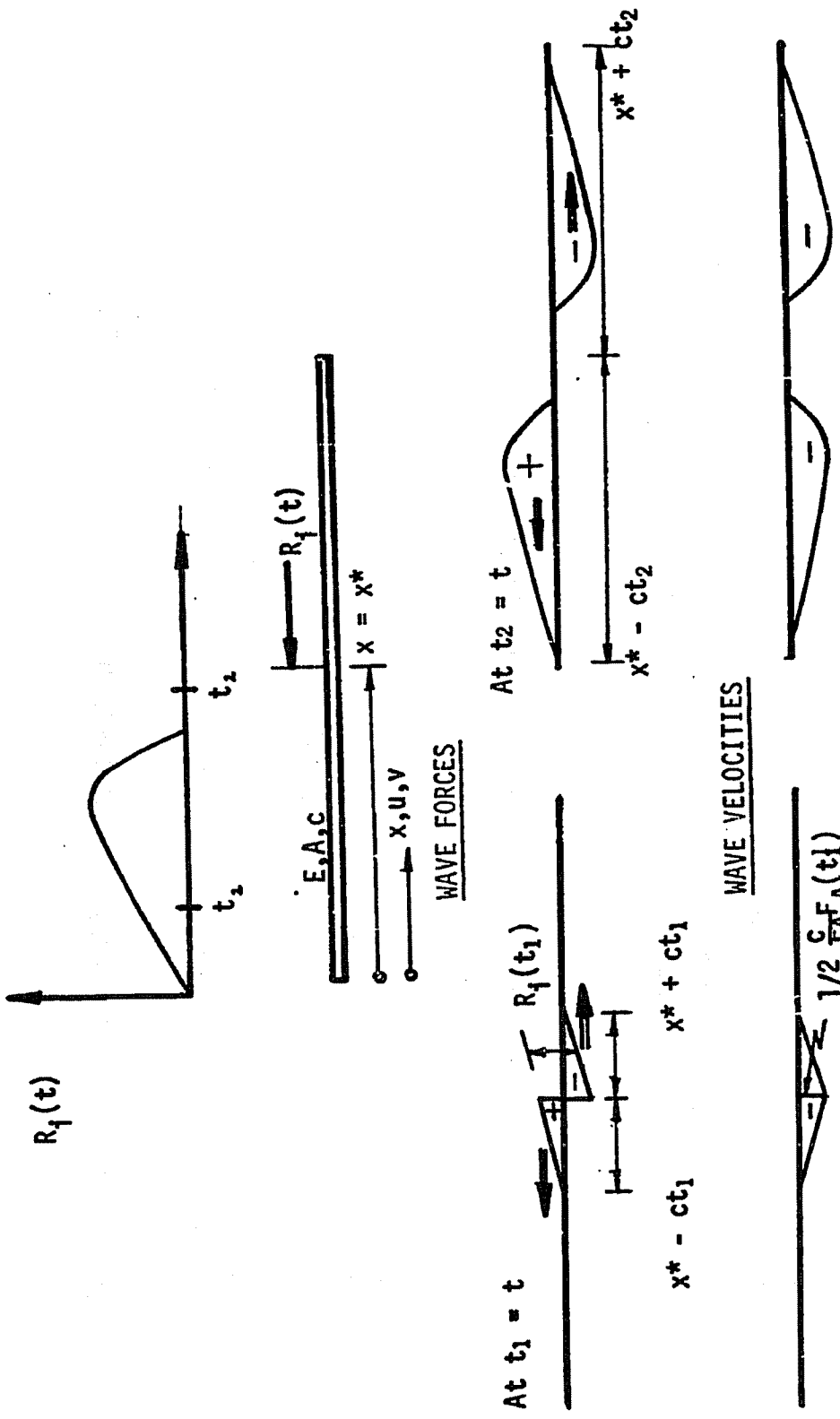

FIGURE A3.2: IMPACT FORCE APPLIED AT AN INTERMEDIATE POINT ALONG THE PILE

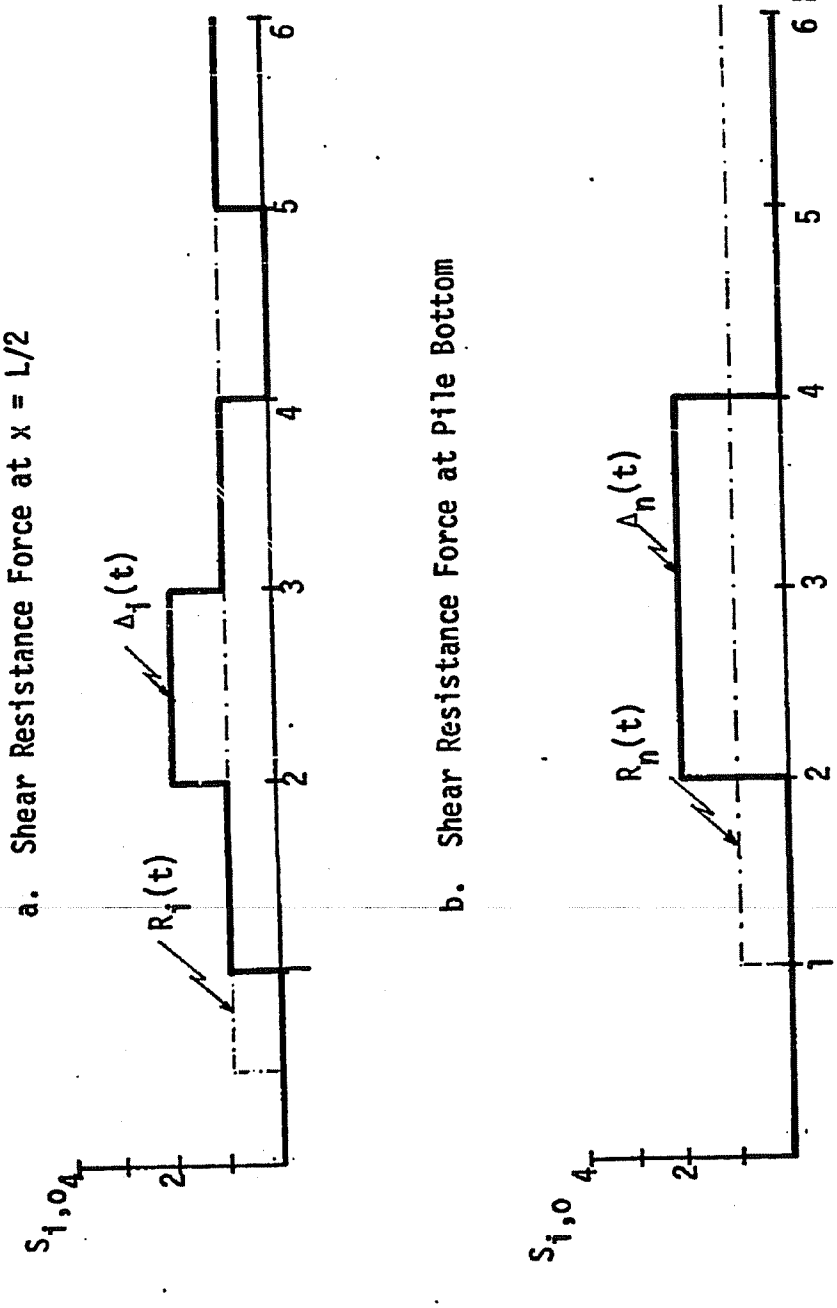

FIGURE A3.3: RESISTANCE DELTA CURVES FOR THEORETICAL SHEAR FORCES AT MIDDLE AND BOTTOM OF PILE

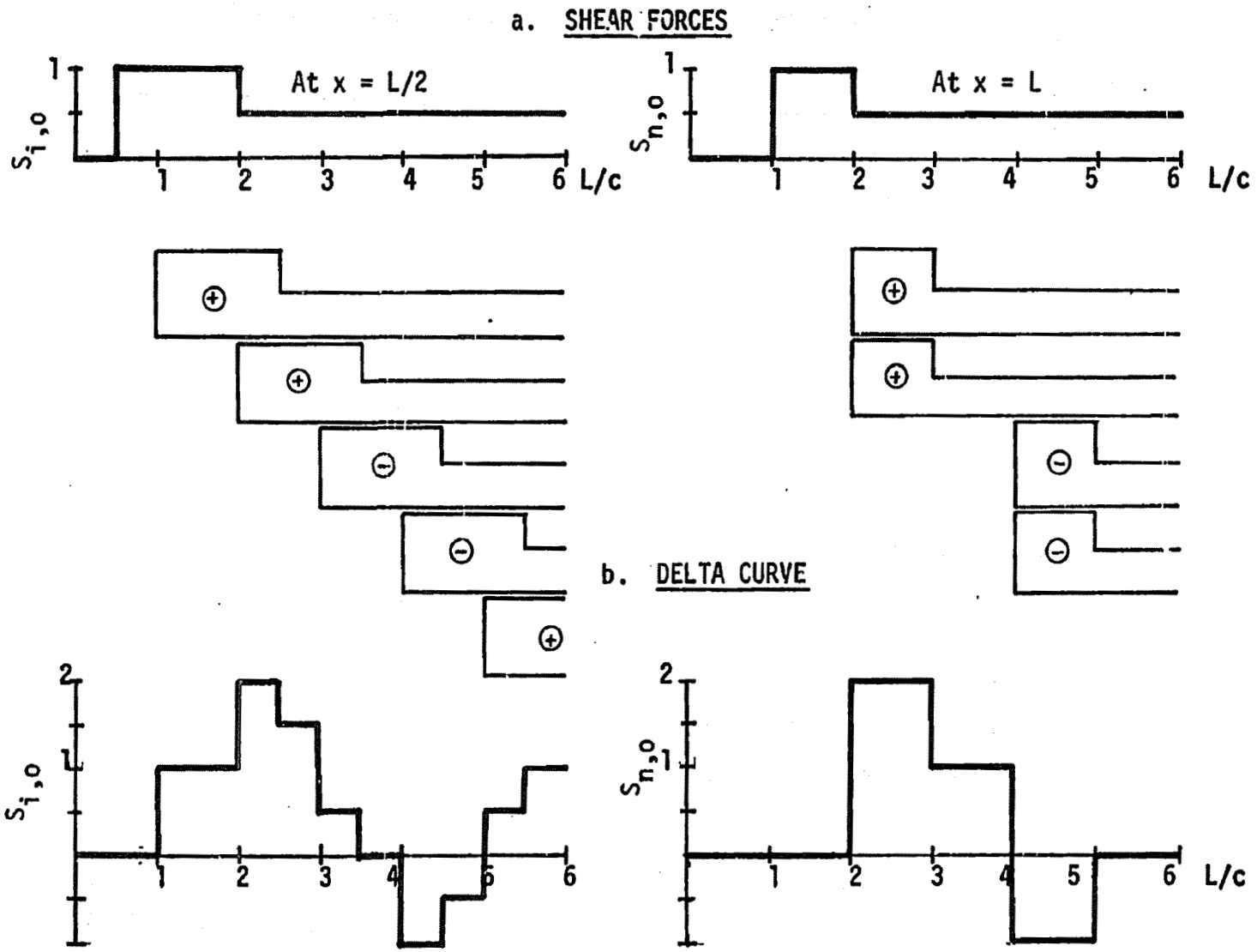

FIGURE A3.4: RESISTANCE DELTA CURVES FOR THEORETICAL SHEAR FORCES WITH UNLOADING

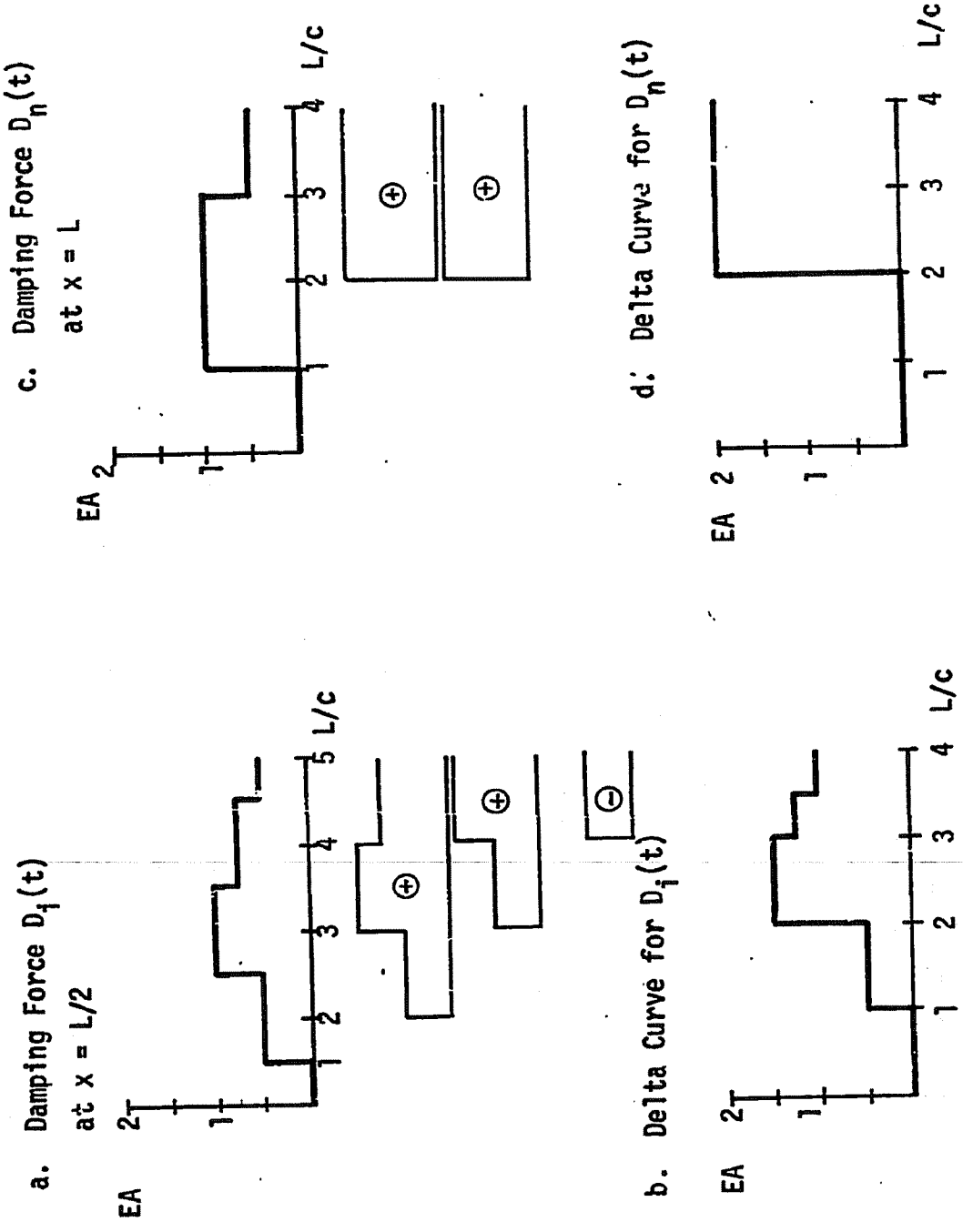

FIGURE A3.5: RESISTANCE DELTA CURVES FOR DAMPING WITH CONSTANT VELOCITY AT PILE TOP

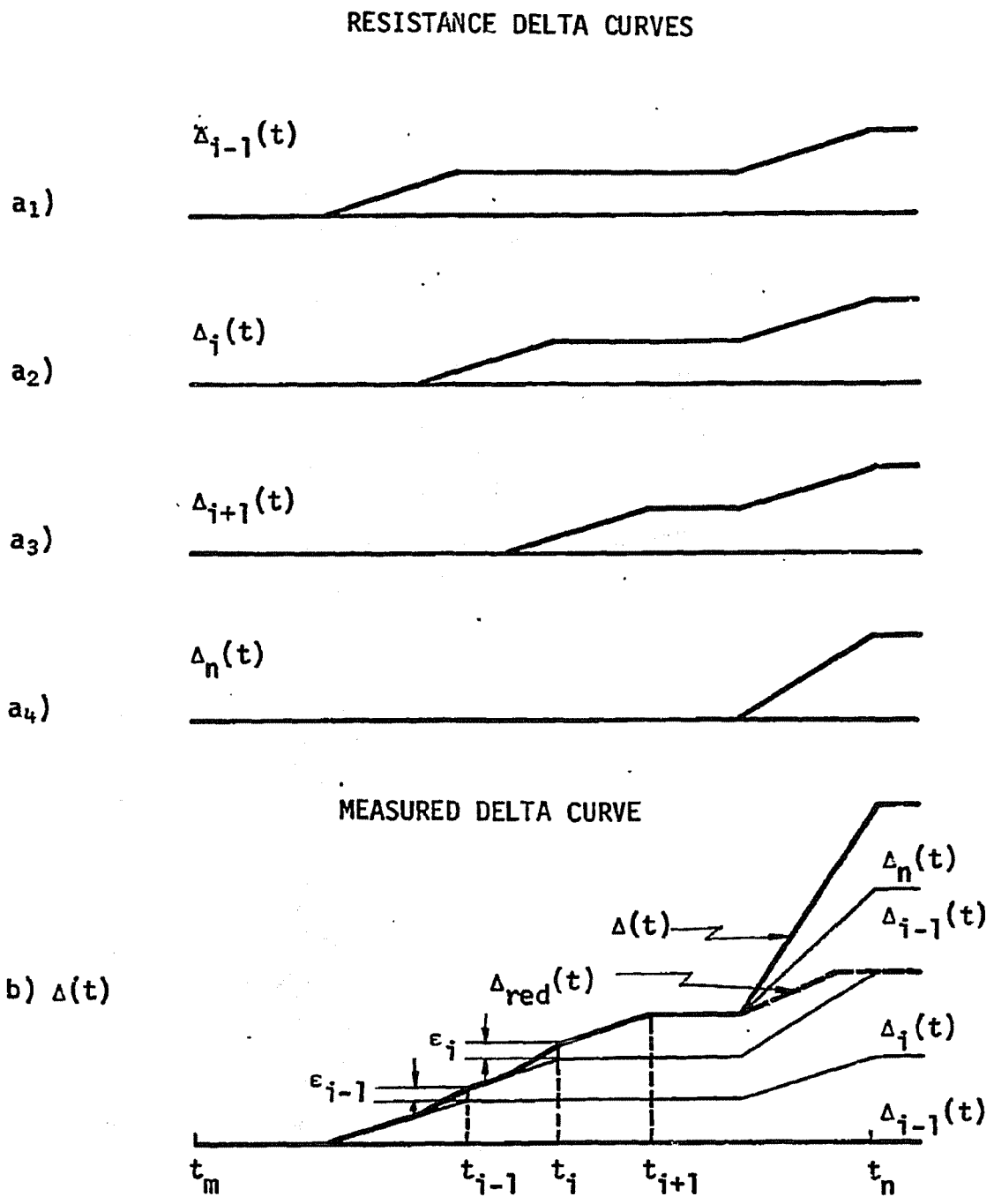

FIGURE A3.6: PREDICTION OF SHEAR RESISTANCE FORCES FROM MEASURED DELTA CURVE IN ABSENCE OF DAMPING FORCES

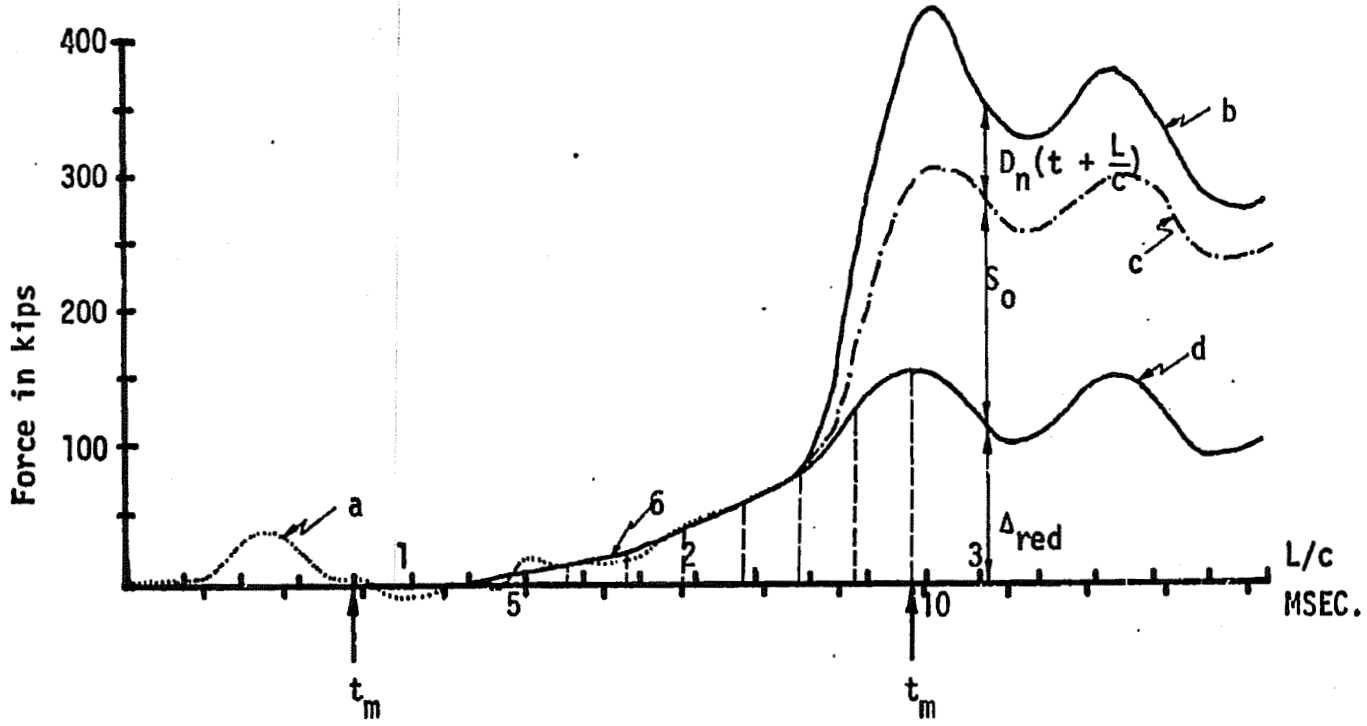

FIGURE A3.7: GRAPHICAL REPRESENTATION OF INITIAL PREDICTION SCHEME

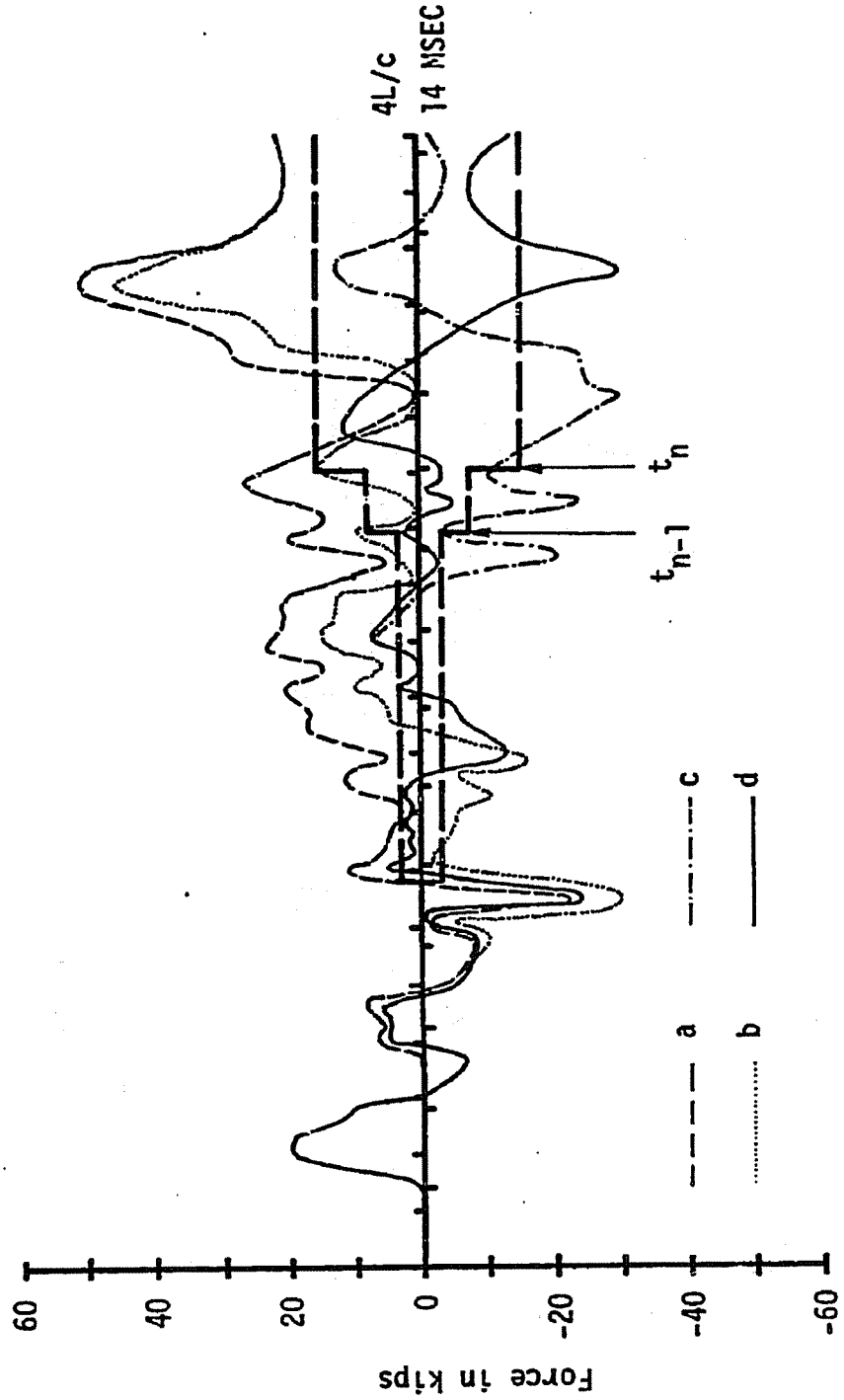

FIGURE A3.8: ERROR DELTA CURVES FROM PREDICTION PROCESS FOR DAMPER AT PILE TIP

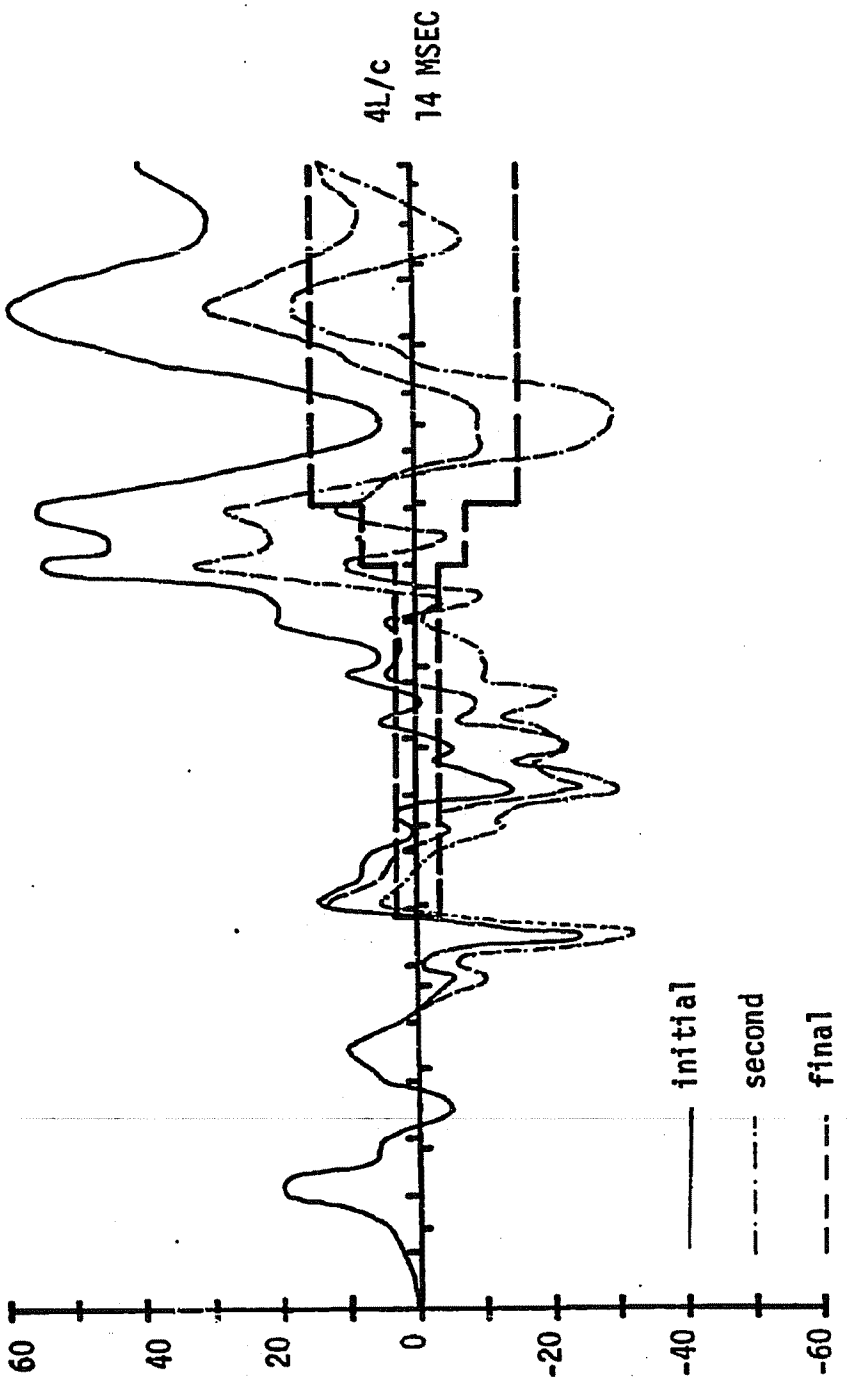

FIGURE A3.9: ERROR DELTA CURVES FROM PREDICTION PROCESS FOR DISTRIBUTED DAMPING

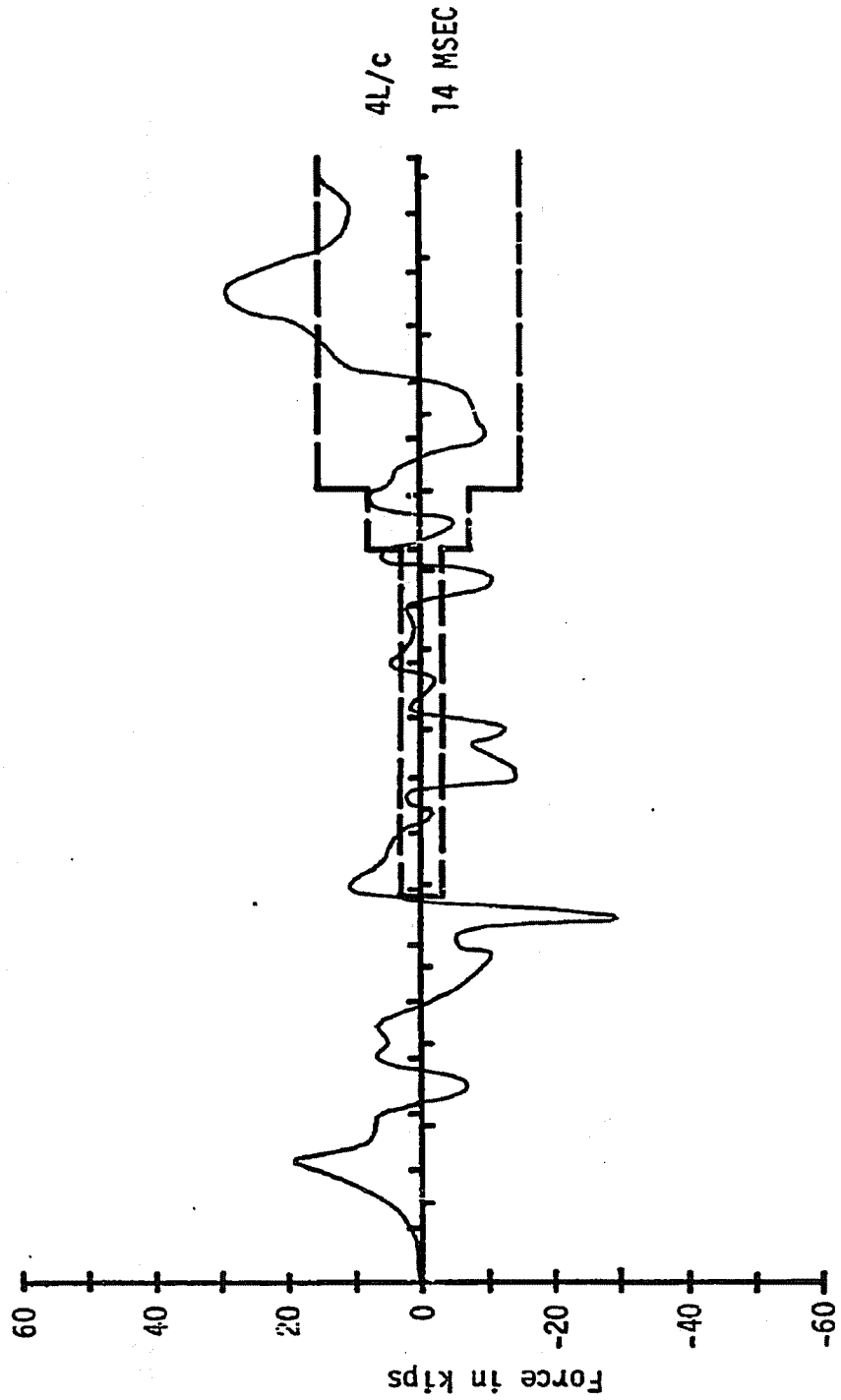

FIGURE A3.10: ERROR DELTA CURVE FOR ONE SKIN AND ONE TOE DAMPER

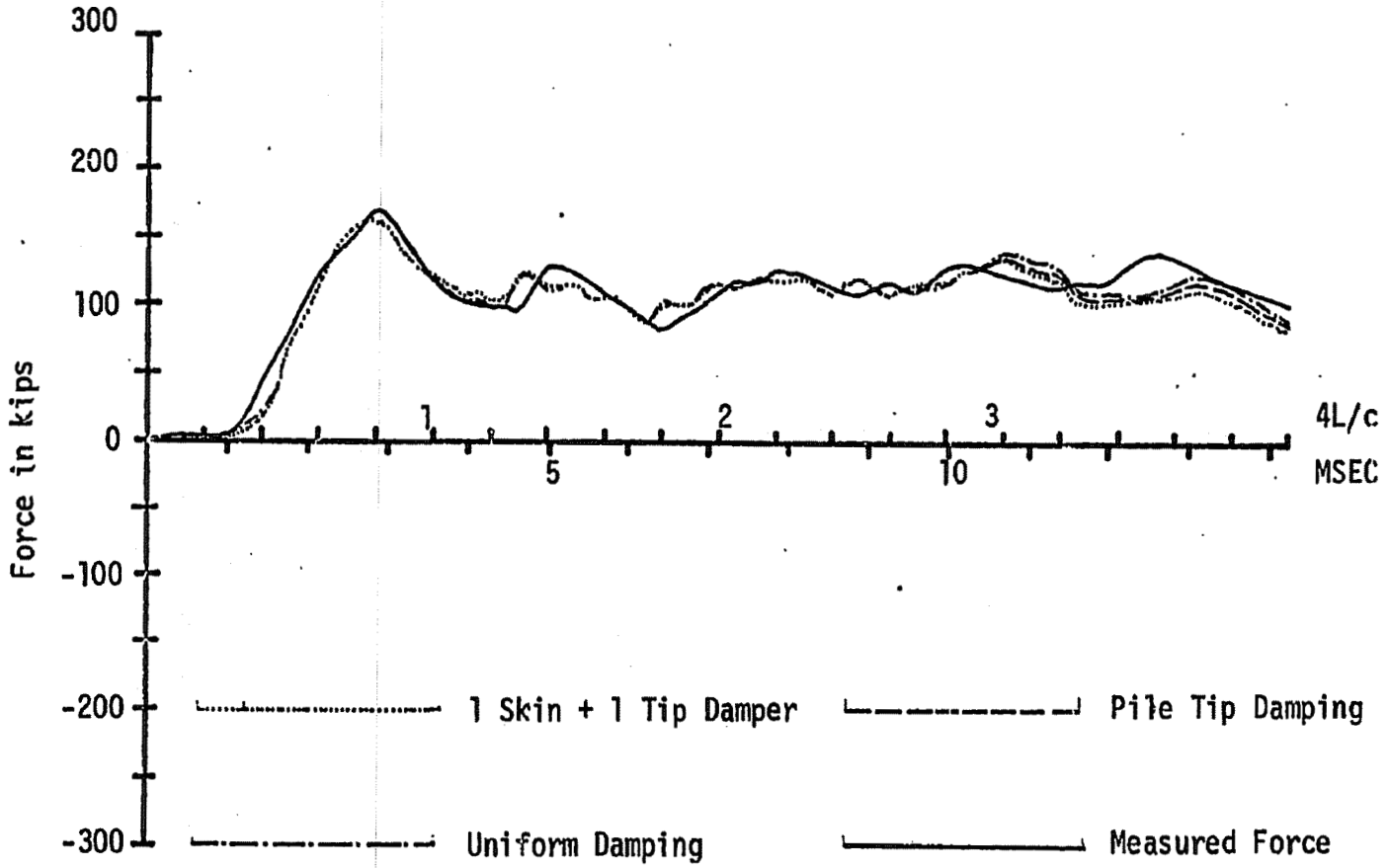

FIGURE A3.11: PREDICTED PILE TOP FORCE FOR THREE DIFFERENT DAMPING DISTRIBUTIONS COMPARED WITH MEASURED PILE TOP FORCE

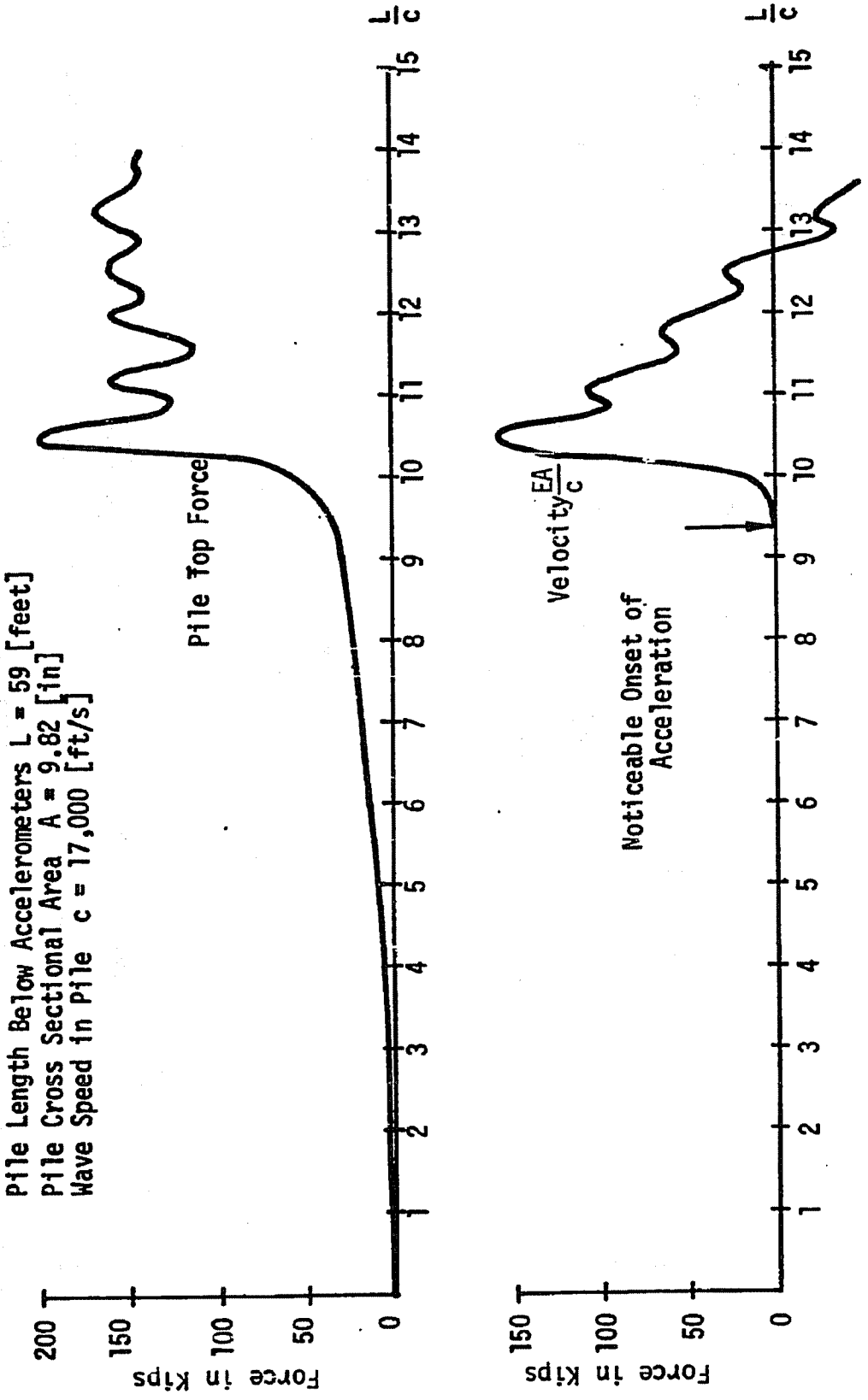

FIGURE B.1: MEASURED FORCE AND VELOCITY OF PILE F-60 NO. 26.A

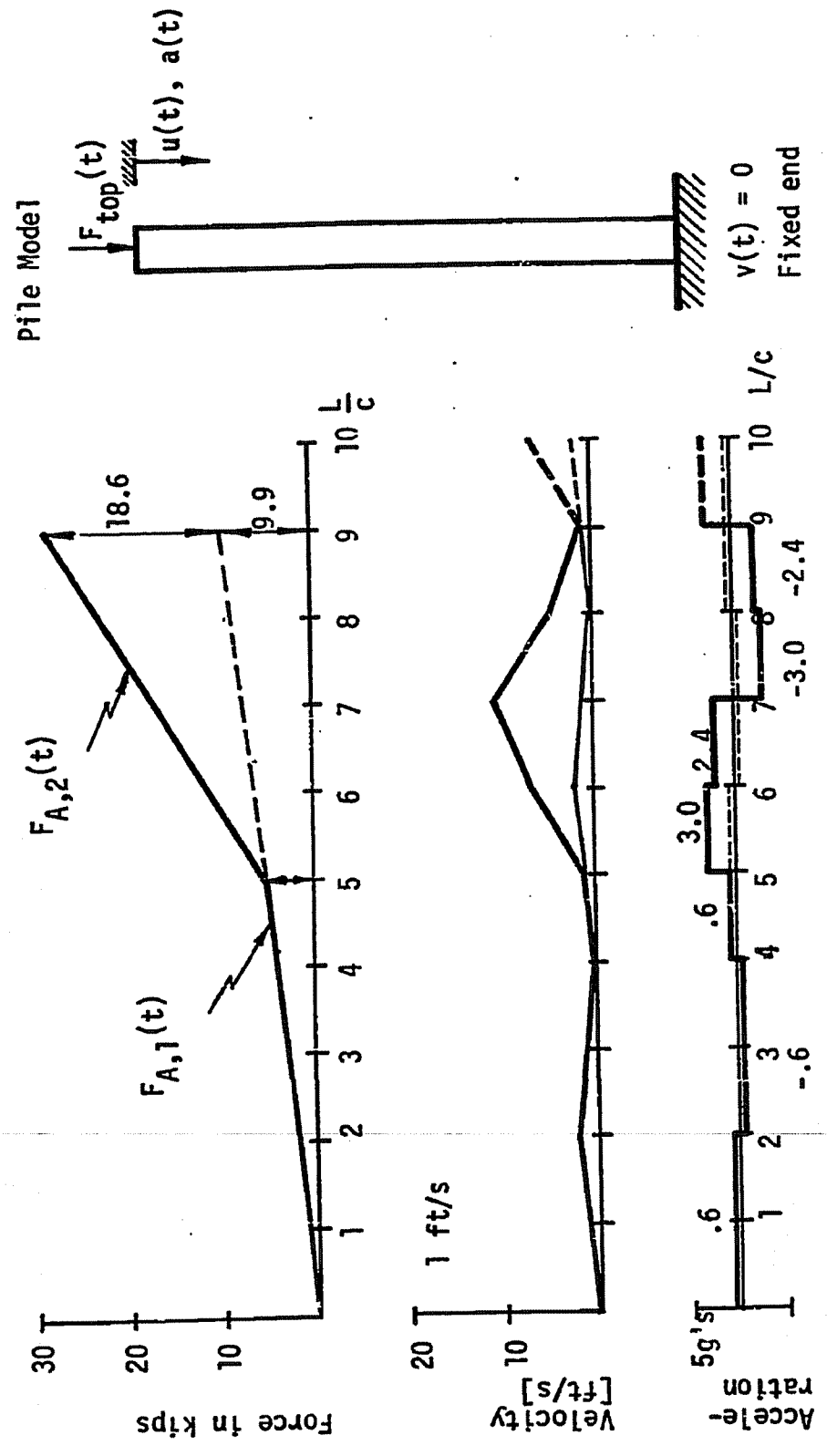

FIGURE B.2: VELOCITY AND ACCELERATION AS DERIVED FROM FORCE OVER INITIAL PORTION OF RECORD

Pile F-60 Blow No. 26-A

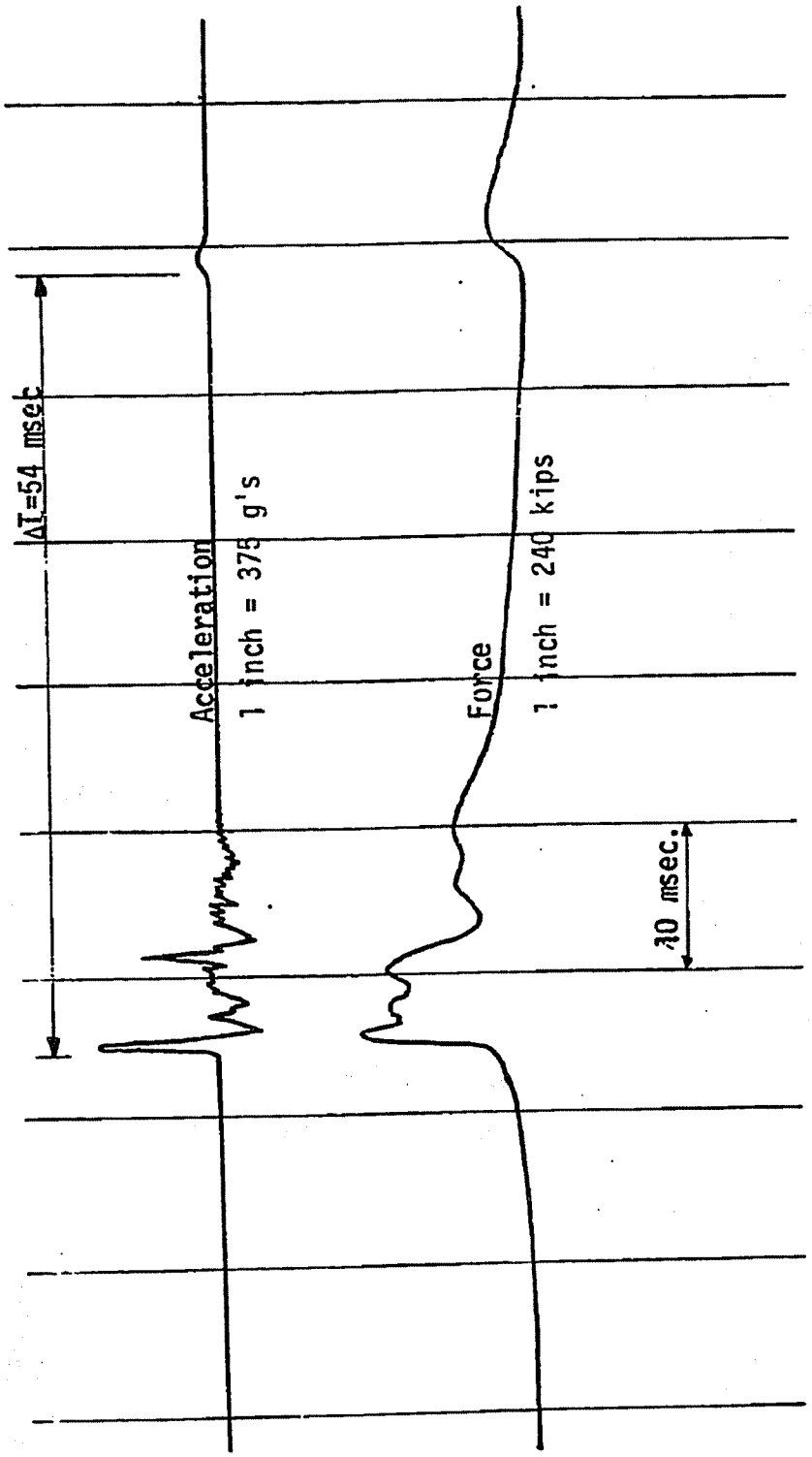

FIGURE B.3: FORCE AND ACCELERATION IN ORIGINAL SCALE

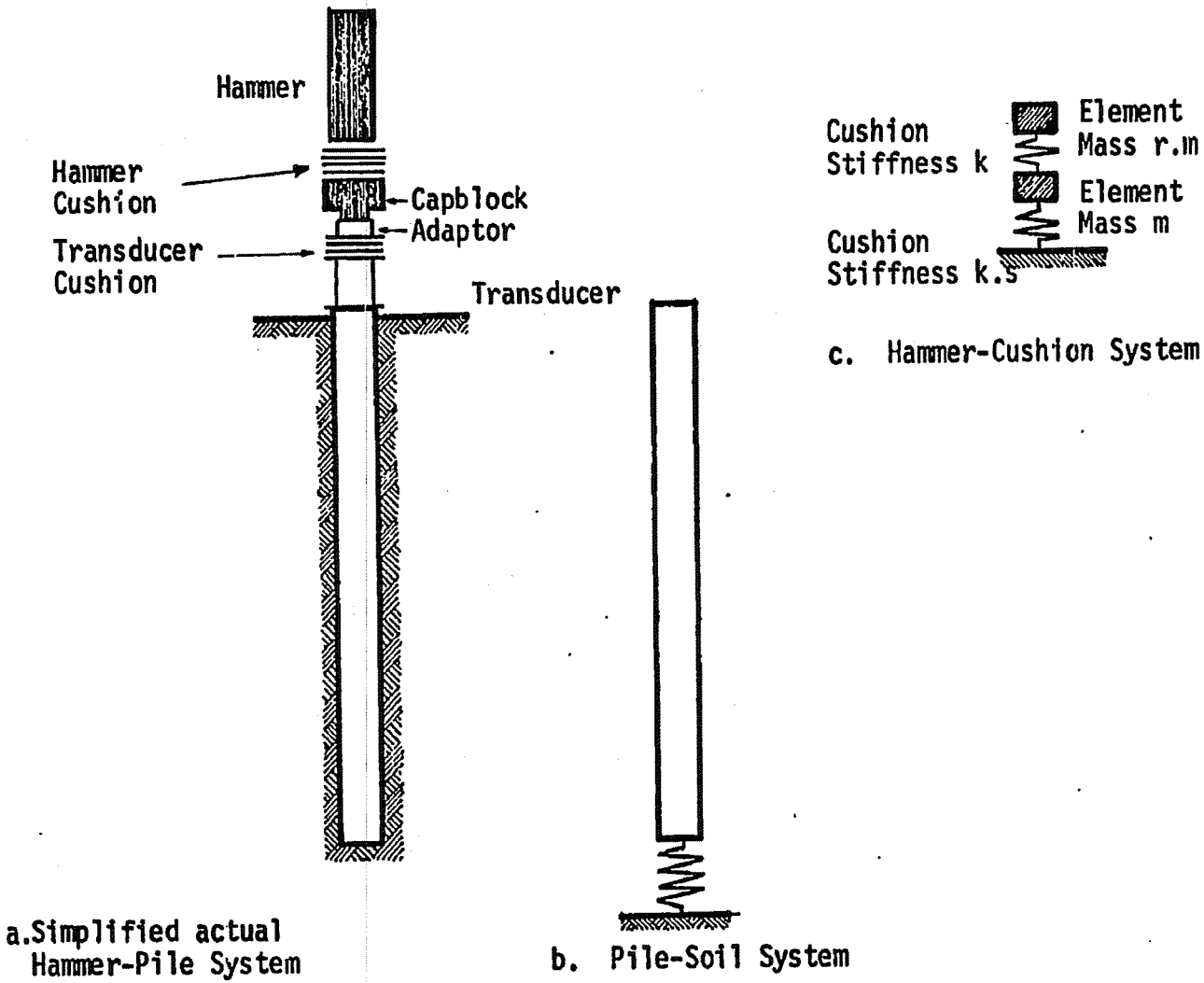

FIGURE B.4: SIMPLIFIED MODELS OF HAMMER PILE SYSTEMS

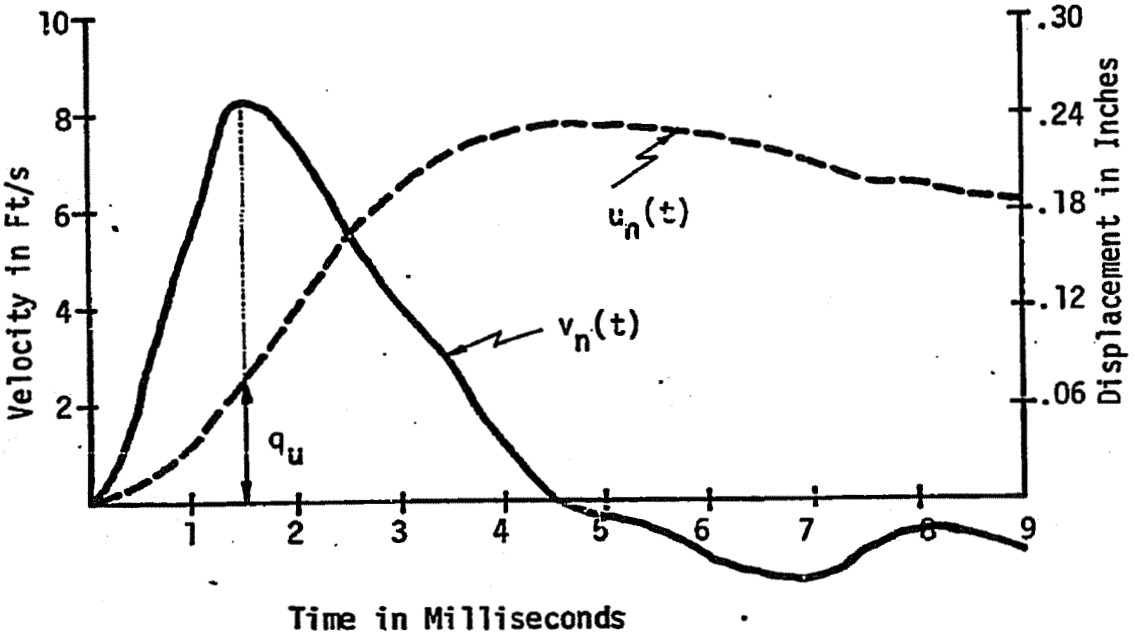

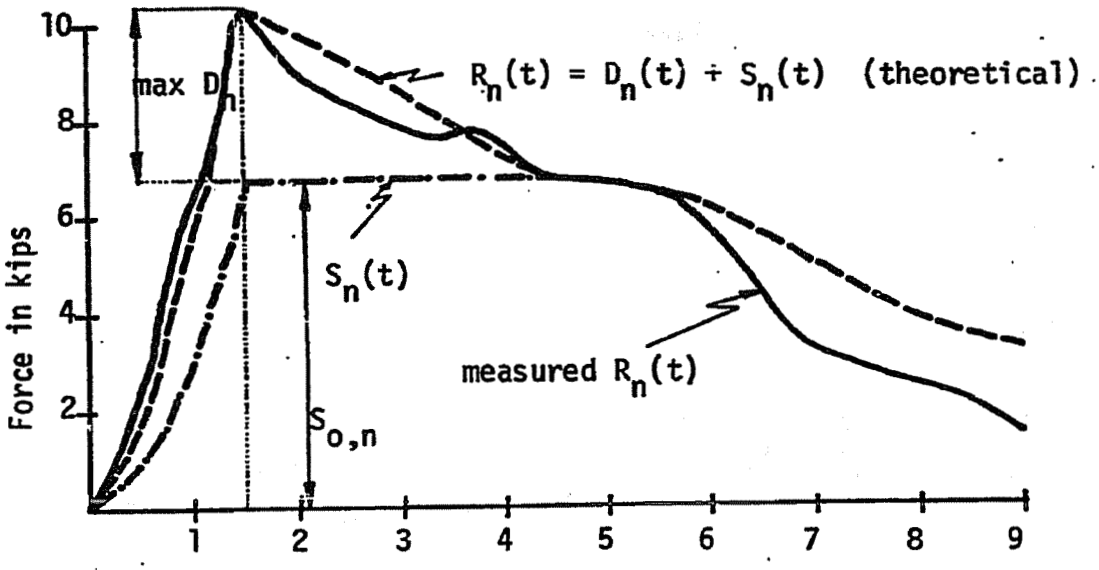

FIGURE C-1: SOIL RESISTANCE FORCES AT PILE TIP 6-T-20, BLOW NO. 1-A

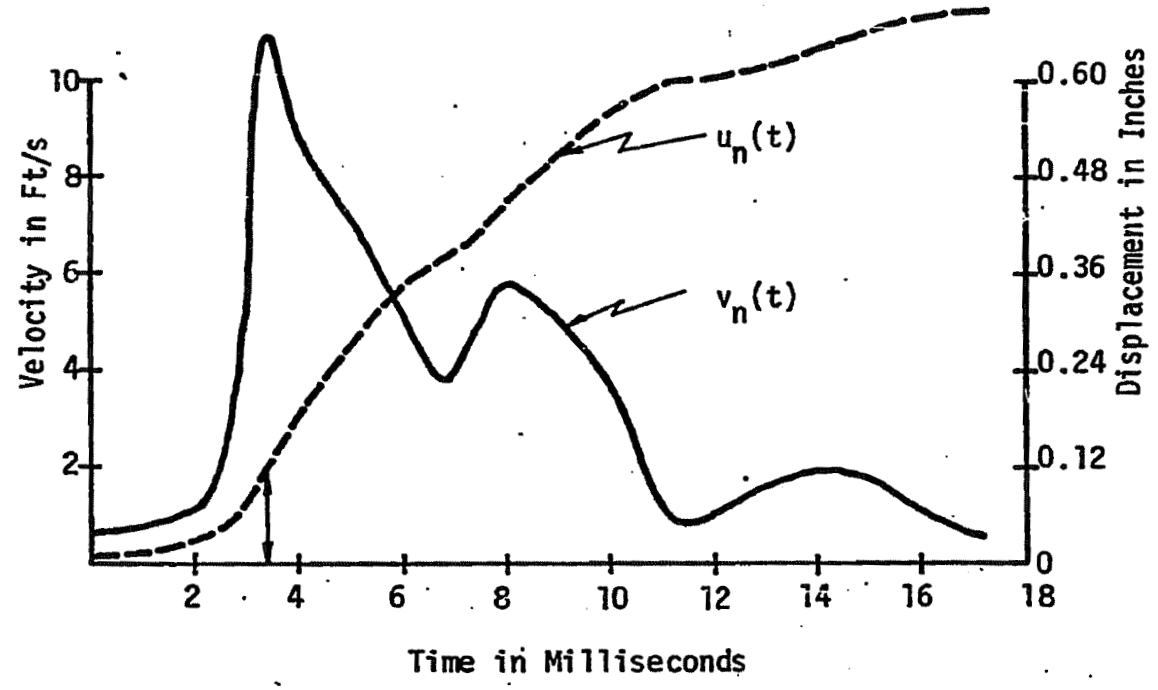

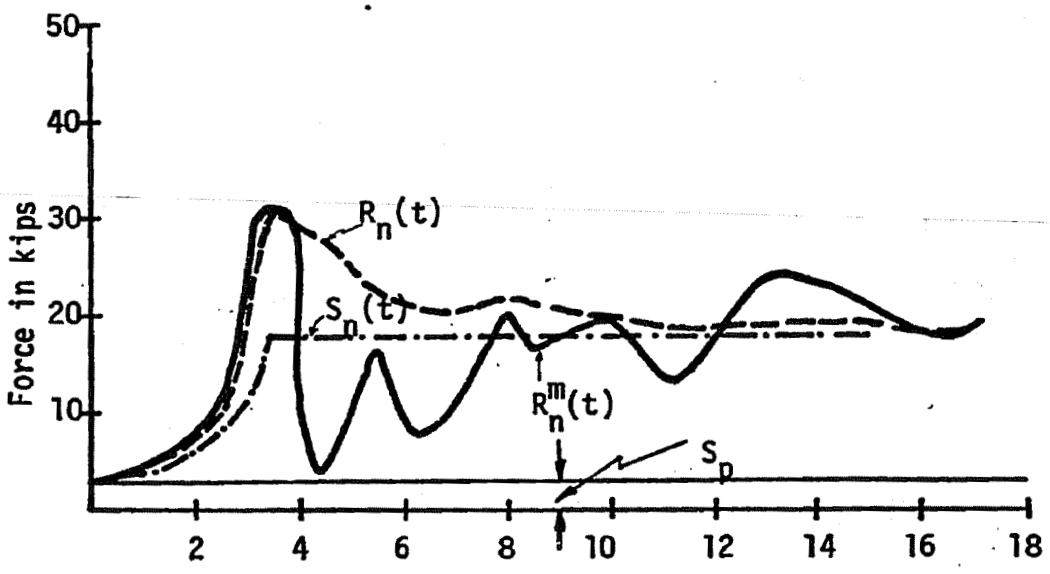

FIGURE C.2: SOIL RESISTANCE FORCES AT PILE TIP Ri-50, BLOW NO. 22

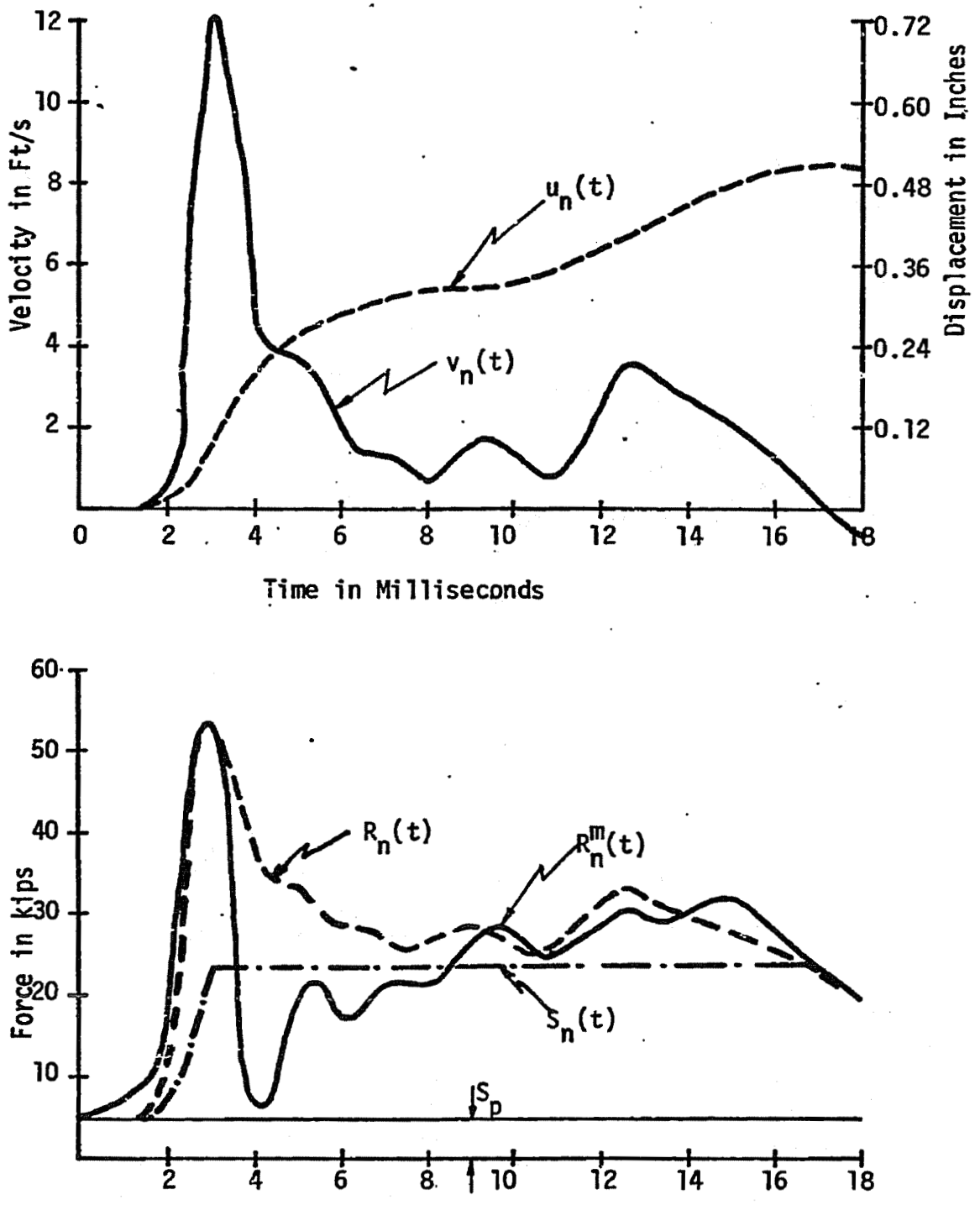

FIGURE C.3: SOIL RESISTANCE FORCES AT PILE TIP Ri-50 BLOW NO. 8-A.

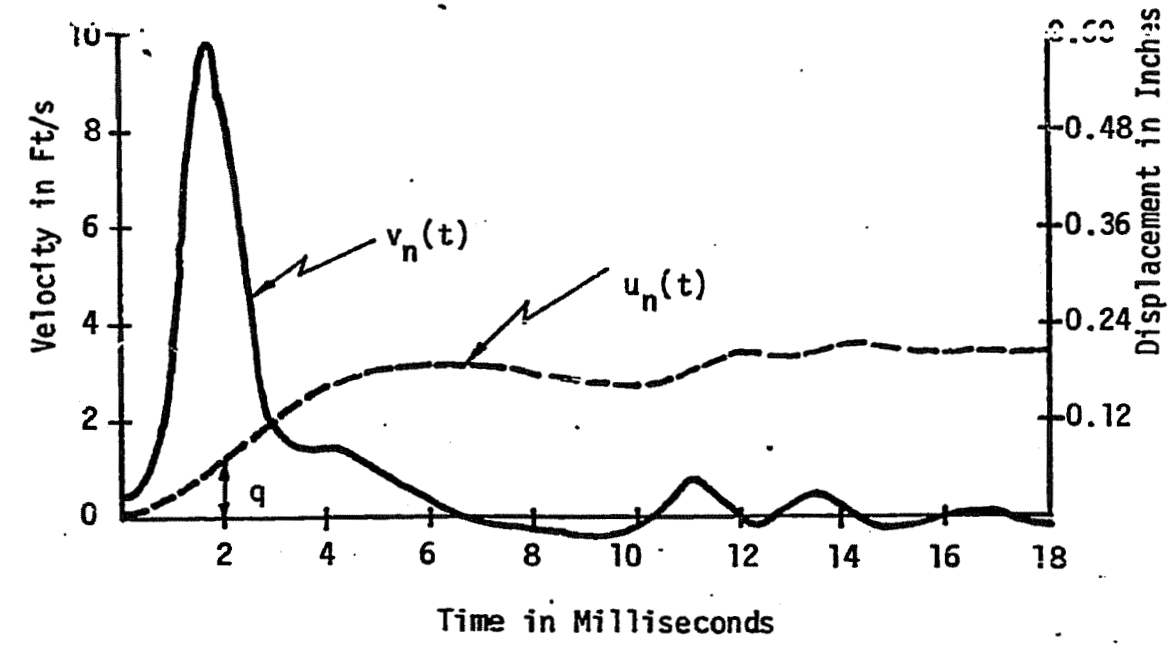

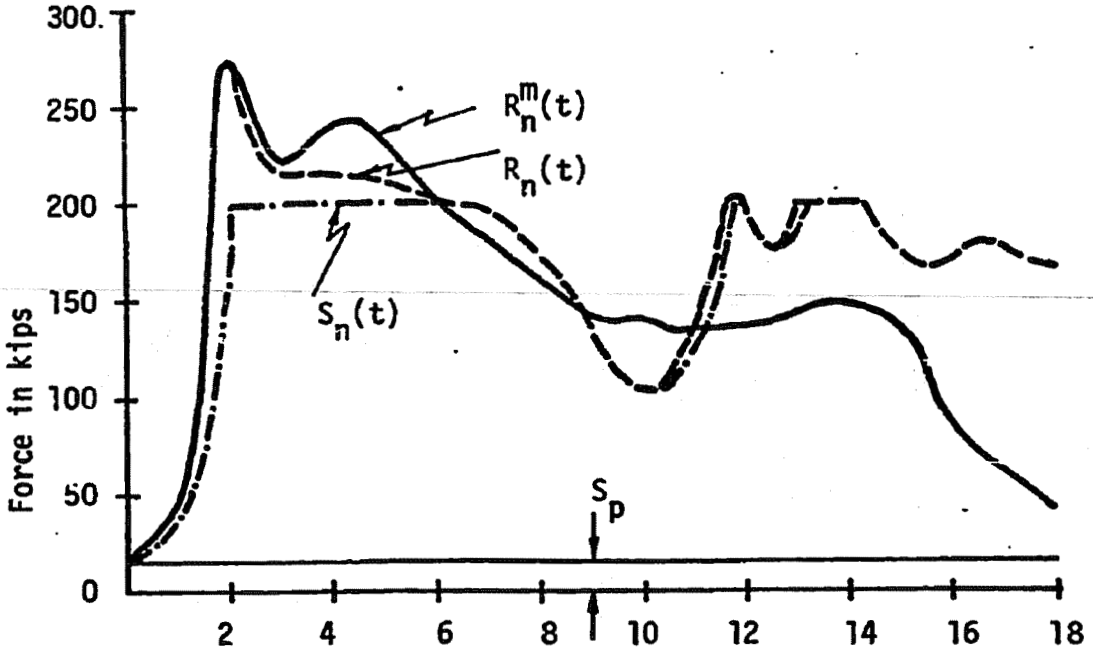

FIGURE C.4: SOIL RESISTANCE FORCES AT PILE TIP Ri-60, BLOW NO. 22

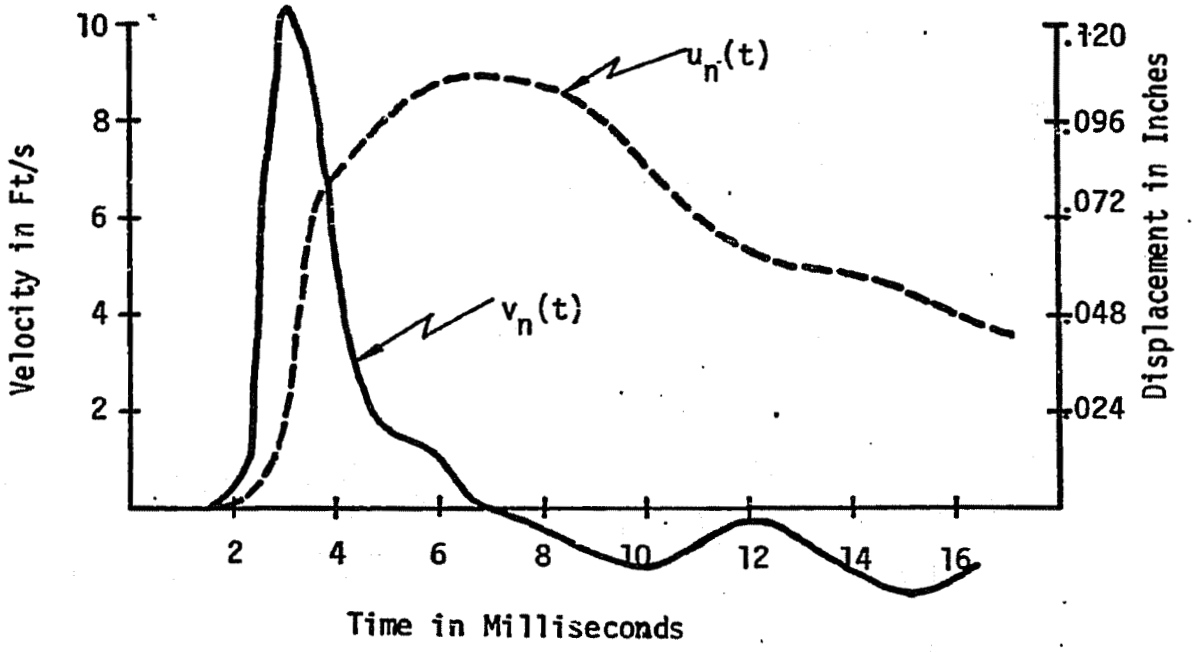

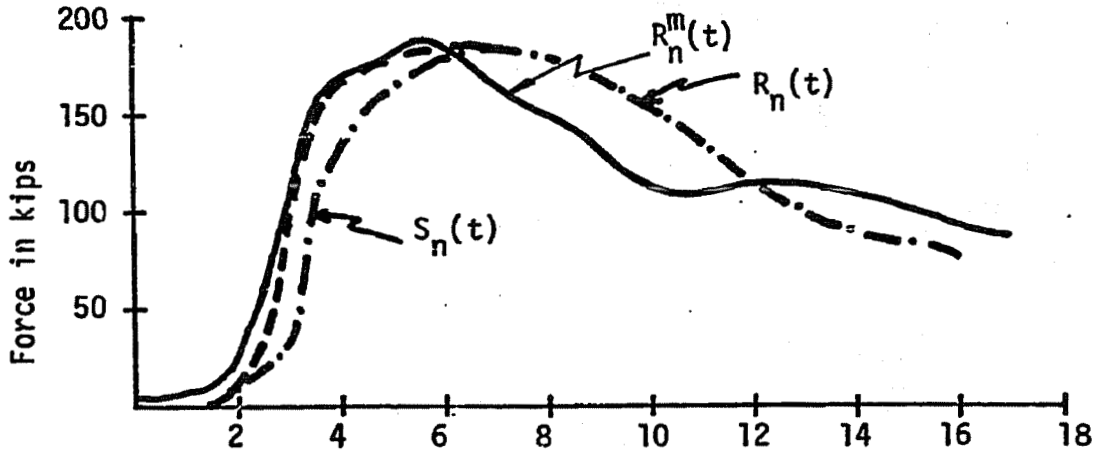

FIGURE C.5: SOIL RESISTANCE FORCES AT PILE TIP Ri-60, BLOW NO. 8-A

a) 6-T-20 Sand

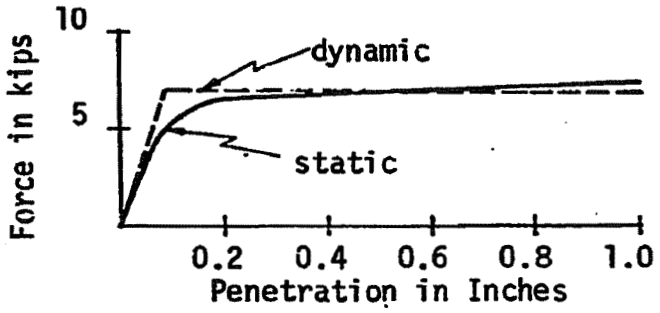

b) Ri-50 Silt and Clay

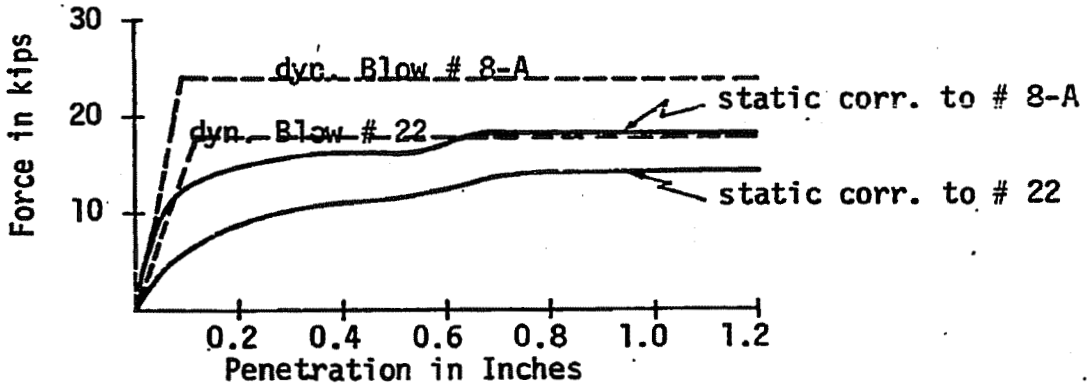

c) Ri-60 Granular Soil

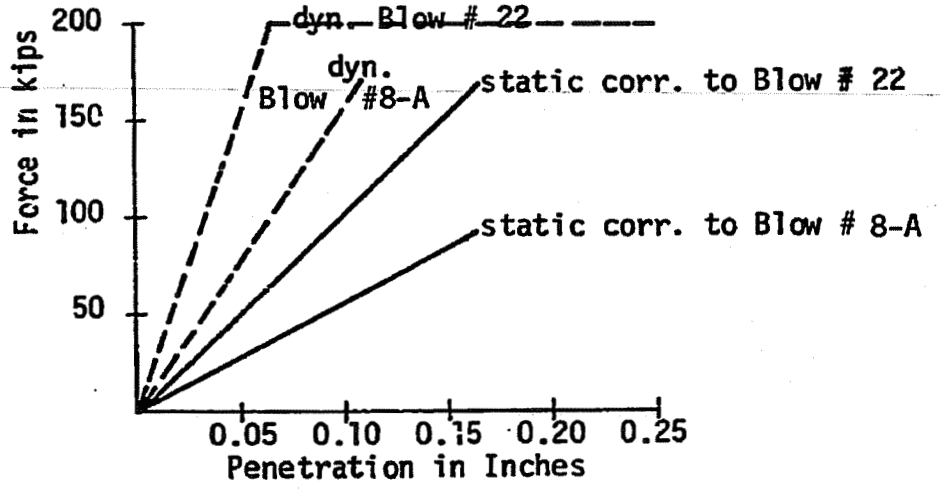

FIGURE C.6: RESULTS FROM STATIC AND DYNAMIC PILE TIP MEASUREMENTS

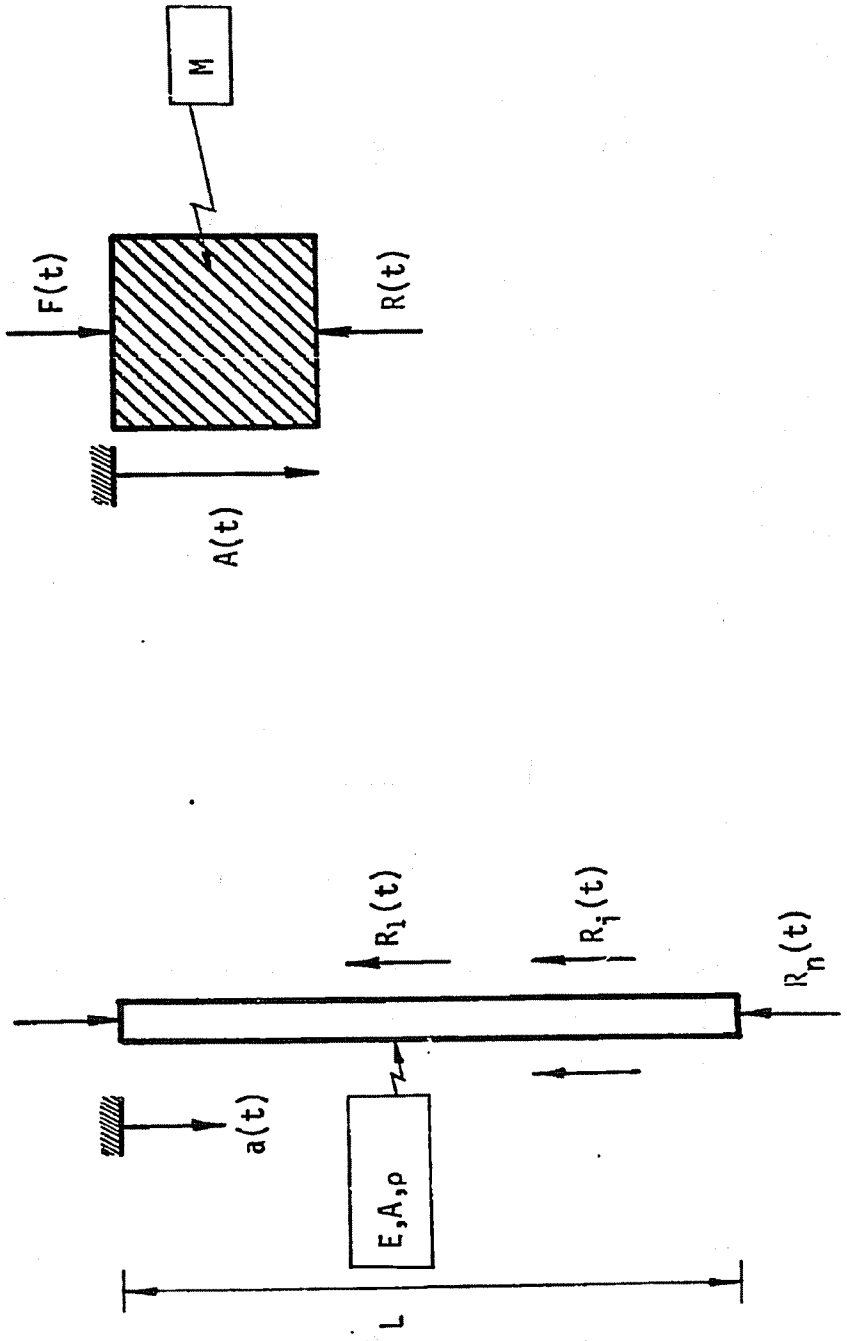

FIGURE D.1: REAL PILE AND RIGID BODY MODEL

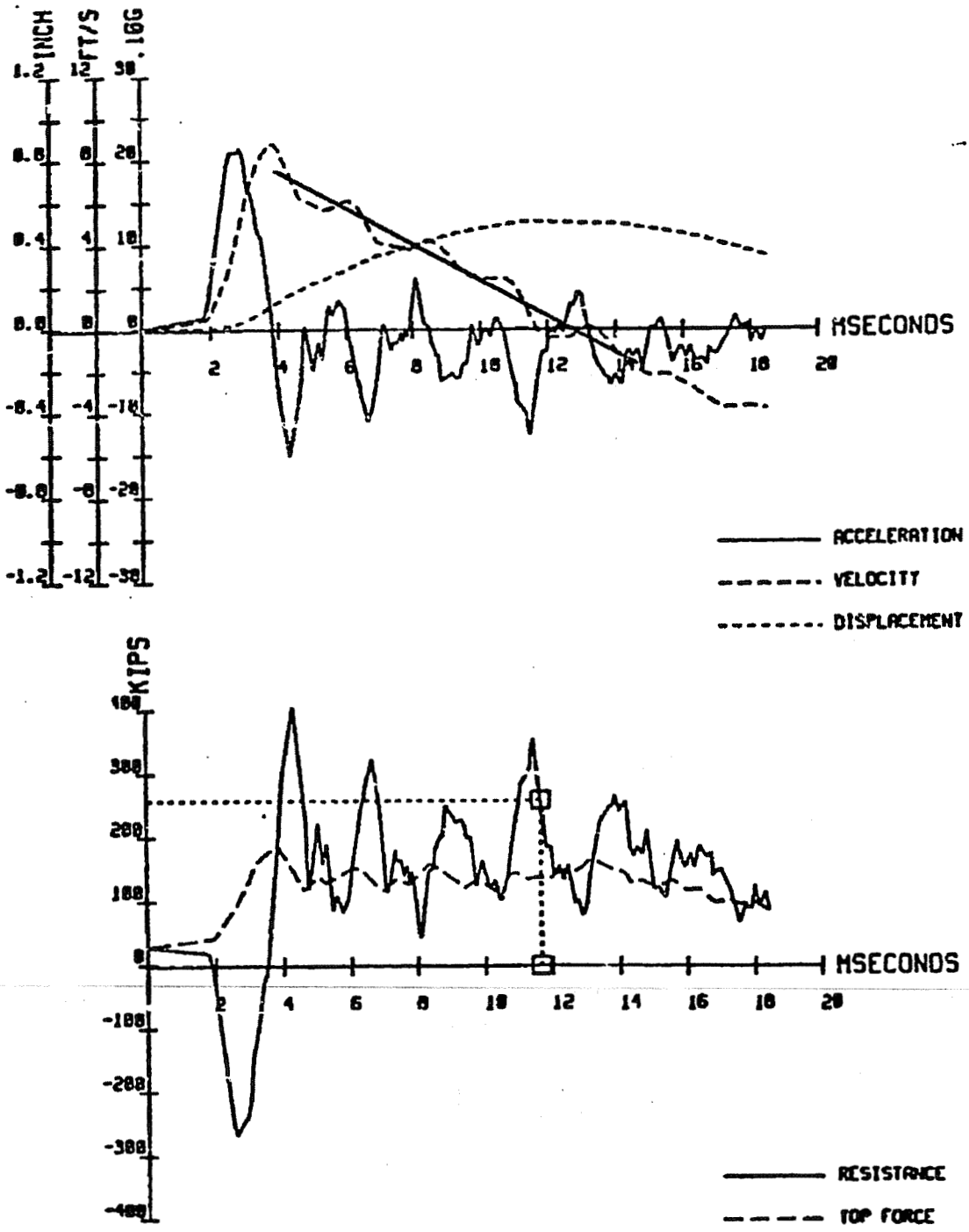

FIGURE D.2: DYNAMIC RESULTS OF PILE F-50 AFTER DRIVING (DATA SET NO. 7)

a. Shear at Bottom End

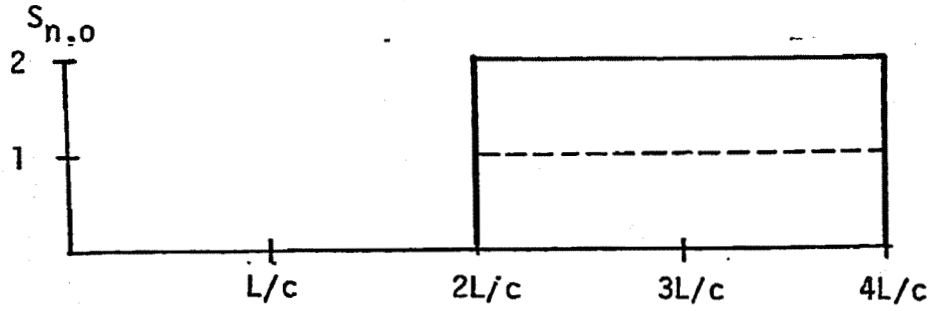

b. Shear at x = L/4

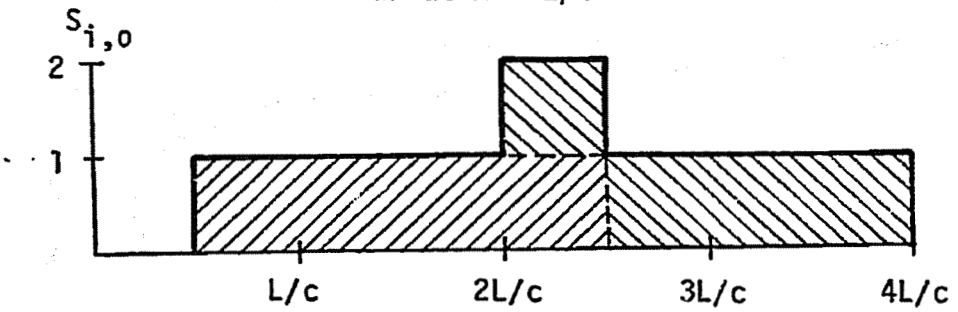

c. Modified Delta Curve

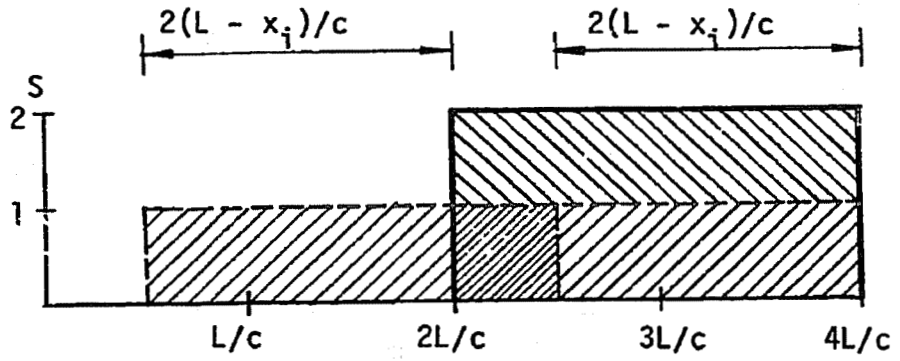

FIGURE D.3 MODIFICATION OF RESISTANCE DELTA CURVE FOR SKIN SHEAR FORCE TO PRODUCE EQUIVALENT DELTA CURVE FOR BOTTOM SHEAR FORCE

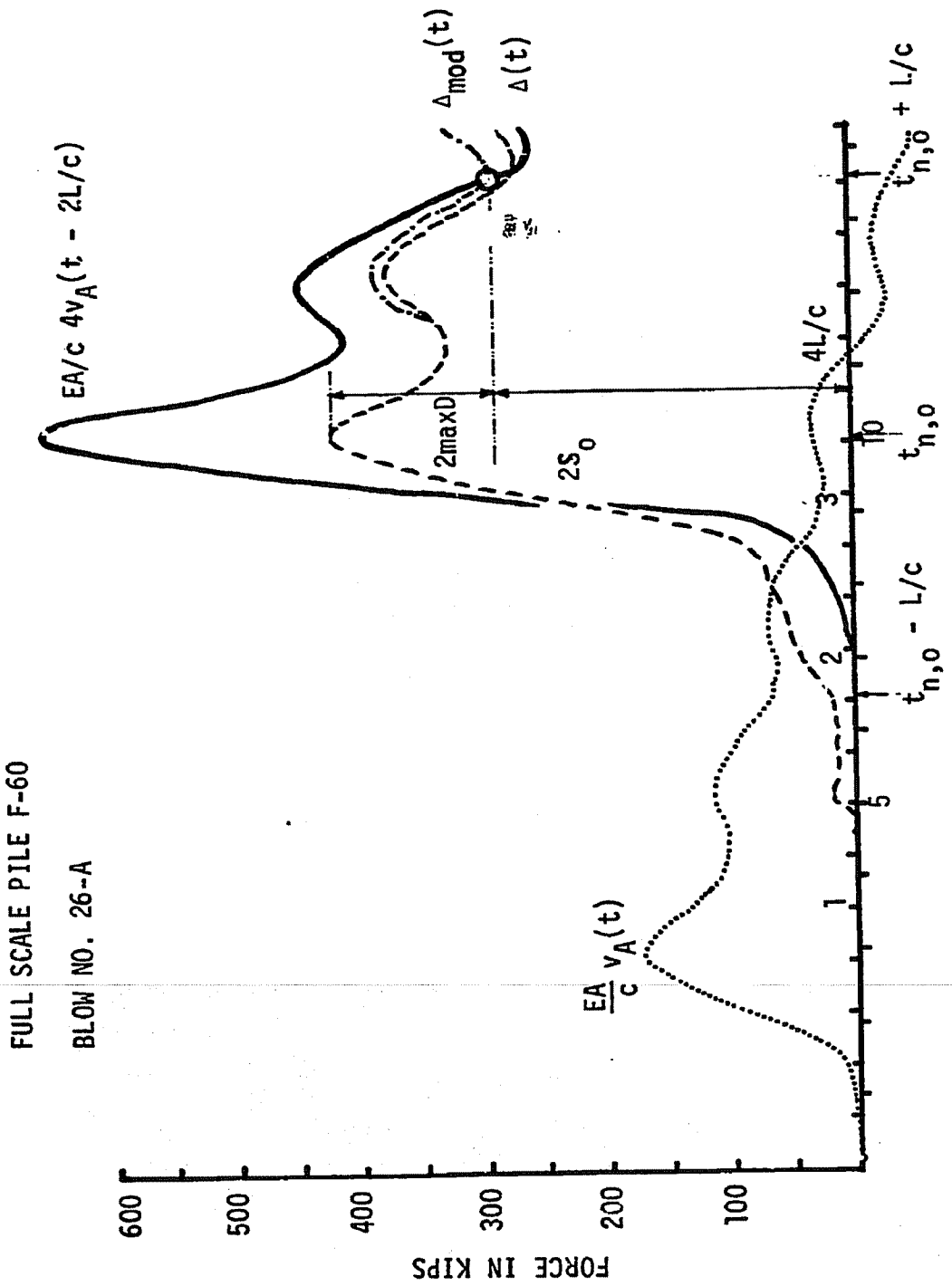

FIGURE D.4: ILLUSTRATION OF PHASE III PREDICTION SCHEME

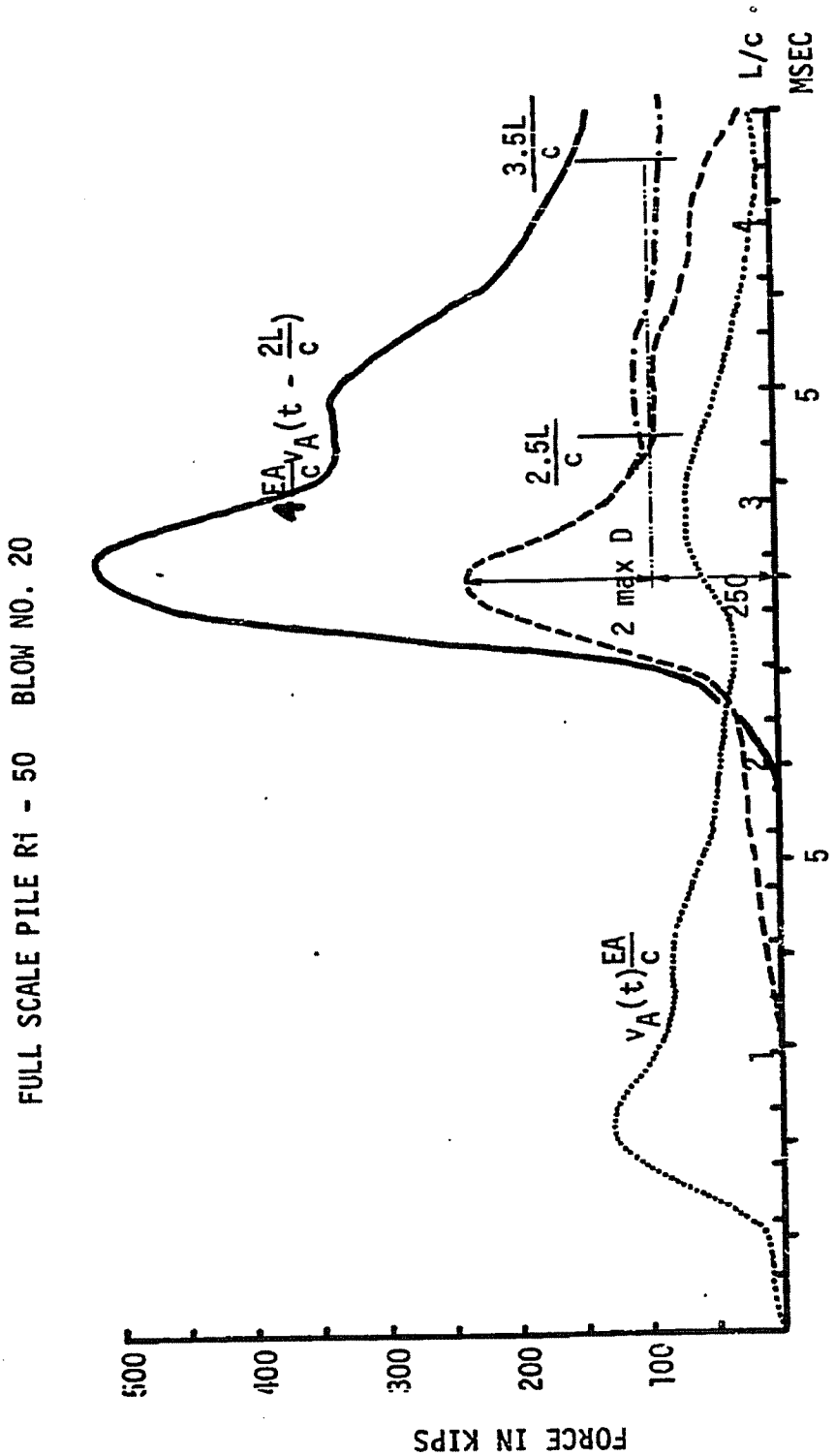

FIGURE D.5: ILLUSTRATION OF PHASE III PREDICTION SCHEME FOR LOW DRIVING RESISTANCE